TÉCNICO LISBOA

UNIVERSIDADE DE LISBOA
INSTITUTO SUPERIOR TÉCNICO

Digital Control System for Vertical Stability of the TCV Plasma

Nuno Sérgio Castelo Branco da Cruz

Supervisor: Doctor Carlos António Abreu Fonseca Varandas

Thesis approved in public session to obtain the PhD Degree in
Technological Physics Engineering

Jury final classification: Pass with Merit

Jury

Chairperson: Chairman of the IST Scientific Board

Members of the committee:

- Doctor Carlos António Abreu Fonseca Varandas
- Doctor Minh Quang Tran
- Doctor Bernardo Brotas de Carvalho
- Doctor Bruno Miguel Soares Gonçalves
- Doctor Rui Miguel Dias Alves Coelho
- Doctor Jean-Marc Moret

2014

TÉCNICO LISBOA

UNIVERSIDADE DE LISBOA
INSTITUTO SUPERIOR TÉCNICO

Digital Control System for Vertical Stability of the TCV Plasma

Nuno Sérgio Castelo Branco da Cruz

Supervisor: Doctor Carlos António Abreu Fonseca Varandas

Thesis approved in public session to obtain the PhD Degree in
Technological Physics Engineering

Jury final classification: Pass with Merit

Jury

Chairperson: Chairman of the IST Scientific Board

Members of the committee:

Doctor Carlos António Abreu Fonseca Varandas, Professor Catedrático Aposentado do Instituto Superior Técnico, da Universidade de Lisboa

Doctor Minh Quang Tran, Full Professor, École Polytechnique Fédérale de Lausanne, Suisse

Doctor Bernardo Brotas de Carvalho, Professor Auxiliar do Instituto Superior Técnico, da Universidade de Lisboa

Doctor Bruno Miguel Soares Gonçalves, Investigador Auxiliar (com Habilitação) do Instituto de Plasmas e Fusão Nuclear, do Instituto Superior Técnico, da Universidade de Lisboa

Doctor Rui Miguel Dias Alves Coelho, Investigador Auxiliar Convidado do Instituto de Plasmas e Fusão Nuclear, do Instituto Superior Técnico, da Universidade de Lisboa

Doctor Jean-Marc Moret, Senior Researcher, Centre de Recherche en Physique des Plasmas, École Polytechnique Fédérale de Lausanne, Suisse

2014

To my lovely wife Helena
and children Rui, António and Ana

Come, let us sing for joy to the Lord,
Let us shout joyfully to the rock of our salvation.
Let us come before His presence with thanksgiving,
Let us shout joyfully to Him with psalms.

Psalm 95

Abstract

In advanced mode operation of fusion devices, real time control plays a central role in achieving the desired plasma performance and minimizing the risk of disruptions. With the advances in digital technologies like Digital Signal Processors (DSPs), Field Programmable Gate Arrays (FPGAs) and standard commercial computer processors, the development of digital control systems to use in fusion experiments has spread to all modern tokamaks.

Tokamak à Configuration Variable (TCV) had limited control capabilities due to the utilization of an analogue control system. In the first part of the PhD Program an Advanced Plasma Control System (APCS), capable of improving the capacity of control of highly configurable plasma shapes, position, current and density by the introduction of nonlinear digital controllers, was designed, implemented and integrated in TCV.

Early tokamaks with circular cross-section plasmas were not prone to the vertical plasma column instability, an inherent problem arising in plasmas with vertically elongated cross sections, with benefits to the energy confinement time, increased plasma current and β. To overcome this problem, complex closed feedback loop control systems with a vertical position measurement, signal processing, control algorithm, power supplies and active actuating coils are used. In the second part of the PhD Program a predictive vertical stabilization non-linear digital controller was designed and implemented, with the help of a new mathematical simulator based on a rigid plasma model. The layout of a method to define controllable limits for the plasma position and velocity may be used for the design of new control systems. Evidence is presented of the TCV vertical stability enhancement using the implemented controller during experimental tokamak discharges.

Keywords

Control System, Real Time, Feedback Control, Optimal Control, Tokamak, Plasma Physics, Nuclear Fusion, Magnetic Confinement, Vertical Plasma Stability, Bang-bang Control.

Resumo

Nos modos avançados de operação de dispositivos de fusão, o controlo em tempo real realiza um papel central para atingir o desempenho desejado do plasma, minimizando o risco de disrupções. Com os avanços das tecnologias de Processadores Digitais de Sinal (DSPs), Matrizes de Portas Programáveis por Campo (FPGAs) e processadores de uso comercial, o desenvolvimento de sistemas de controlo digital propagou-se por todos os tokamaks modernos.

O *Tokamak à Configuration Variable* (TCV) tinha uma capacidade limitada de controlo devido ao seu sistema analógico. Na primeira parte deste trabalho foi desenhado, implementado e integrado no TCV um Sistema Avançado de Controlo do Plasma (APCS), para melhorar a capacidade de controlo de plasmas, da sua forma, posição, corrente e densidade, introduzindo a possibilidade de utilização de controladores digitais não lineares.

Inicialmente, tokamaks com secção de plasma circular eram verticalmente estáveis não estando sujeitos à instabilidade vertical que surge com o plasma elongado. Este conceito apresenta benefícios no tempo de confinamento, no aumento da corrente de plasma e β. Para minimizar os efeitos desta instabilidade, foram desenvolvidos complexos sistemas de controlo em malha fechada com medida da posição do plasma, processamento de sinal, algoritmo de controlo, fontes de tensão e bobines de actuação activa. Na segunda parte deste trabalho um controlador digital não linear foi desenhado e implementado, usando um novo simulador matemático baseado num modelo rígido de plasma. O desenvolvimento de um método que define zonas de controlabilidade do plasma pode ser utilizado para o desenho de novos sistemas de controlo. Neste documento é apresentada evidência do aumento de estabilidade vertical dos plasmas do TCV usando o novo controlador em descargas experimentais do TCV.

Palavras Chave

Sistema de Controlo, Tempo-real, Controlo em Malha Fechada, Controlo Óptimo, Tokamak, Física de Plasmas, Fusão Nuclear, Confinamento Magnético, Estabilidade Vertical do Plasma, Controlador Bang-bang.

Acknowledgments

My gratitude goes first to my supervisor, Professor Carlos Varandas, for the inspiring work and scientific leadership that he put in all his tasks during the many years as head of Instituto de Plasmas e Fusão Nuclear, and in each project he believes in. Without his competence and vision IPFN would not be the success research laboratory it is today. Moreover, I would like to extend my appreciation for the time and effort that Professor Varandas dedicated to the revision of this document.

I would like to thank Doctor António Pinto Rodrigues for the hardware development and design of the Advanced Plasma Control System, for his help on the design of the low level software functionality of the system and for being the IPFN head of the project during so many years. It is a pleasure to work with a friend with whom I share the memories of our early stays in Lausanne.

With out the scientific support and discussions with Doctor Jean-Marc Moret, Doctor Stefano Coda and Doctor Basil Duval from *Centre de Recherches en Physiques de Plasmas* this thesis would not be as reach. A profound gratitude goes to Doctor Jean-Marc Moret for the revision of Chapter 5 of this thesis and for his contribute in the improvement of the ambiguities left on the first version of the document. To the head of the TCV Operations, Doctor Stefano Coda, and all TCV Team, I would like to thank the machine time that permitted the tests of the APCS system, the controller and the results presented in this thesis. To the staff at CRPP for receiving me in the endless weeks of work at *Tokamak à Configuration Variables*, with special emphasis to the TCV Control Team, thank you all.

To Doctor Rui Coelho I would like to thank the multiple in depth comments made to improve the quality and clarity of the Thesis.

To the present head of IPFN Doctor Bruno Gonçalves I thank the opportunity that was given me to continue my research work under his leadership and wish him the best of success in implementing his ideas in this research unit.

To the other members of the Control and Data Acquisition Group working in Lisbon (Doctor Jorge Sousa, Doctor Bernardo Brotas, Doctor António Baptista) and Coimbra

(Doctor Rita Pereira, Doctor Ana Fernandes, Álvaro Combo, Bruno Santos, Miguel Correia and Paulo Ricardo), I would like to thank for the excellent friendship and professionalism that go hand in hand with group history and achievements, demanding the best from all of us.

To the Group of Electronics and Instrumentation of University of Coimbra I would like to thank the opportunity of sharing the knowledge, friendship and premises in special to Doctor João Cardoso and Professor Carlos Correia.

My gratitude also goes to Miguel Silva, Katharina Füglister and Tiago for receiving me in their home at Lausanne every time a hotel room seamed too lonely.

To my parents Rui e Céu for their unconditional love and support during all my life, *Obrigado! Gosto muito de vocês.*

For Rui Daniel, António Pedro and Ana Isabel, the hope that when something becomes really difficult to achieve, you will have someone to inspire you and never let you down, just like I had you and your mother...

The confidence that you had in my work and capacities, and the strength you always showed when you were left alone with the children (mostly when you gave birth to Ana in my absence) was the inspiration and strength I ever needed to stay on track on the most difficult phases of this work. I love you Helena.

I thank God for the miracle of life.

Coimbra, September 29th 2014.

Contents

List of Figures

List of Tables

List of Acronyms

AC	Alternating Current
ADC	Analogue to Digital Converter
APCC	Acquisition, Processing and Control Channel
APCS	Advanced Plasma Control System
API	Application Programming Interface
ASDEX-Upgrade	Axially Symmetric Diverter Experiment Upgrade
ASTRA	Automated System for TRansport Analysis
CPLD	Complex Programmable Logic Device
CREATE	Consorzio di Ricerca per l'Energia e le Applicazioni Tecnologiche dell'Elettromagnetismo
CRPP	Centre de Recherches en Physique des Plasmas
DAC	Digital to Analogue Converter
DC	Direct Current
DMA	Direct Memory Access
DMBUS	Data Mover Bus
DSP	Digital Signal Processor
ECCD	Electron Cyclotron Current Drive

EFIT	Equilibrium FITting
ELM	Edge Localized Mode
EPFL	École Polytechnique Fédérale de Lausanne
EU	European Union
FBT	Free Boundary Tokamak
FIFO	First In First Out
FIR	Finite Impulse Response
FPGA	Field Programmable Gate Array
FPS	Fast Power Supply
GC	Gravitational Confinement
IAEA	International Atomic Energy Agency
IC	Inertial Confinement
ICCD	Ion Cyclotron Current Drive
IIR	Infinite Impulse Response
IP	Plasma Current
IPCC	Intergovernmental Panel on Climate Change
IPFN	Instituto de Plasmas e Fusão Nuclear
IST	Instituto Superior Técnico
ISTTOK	IST Tokamak
ITER	International Thermonuclear Experimental Reactor
JET	Joint European Torus
JT-60	Japan Torus
LHCD	Lower Hybrid Current Drive

LIVVS	Laser In-Vessel Viewing System
LTI	Linear Time Invariant
MAST	Mega-Amp Spherical Tokamak
MC	Magnetic Confinement
MHD	Magnetohydrodynamics
MIMO	Multi Input Multi Output
MPI	Message Passing Interface
MPRu	Magnetic Proton Recoil Neutron Spectrometer Upgrade
MSPS	Mega Samples Per Second
NBI	Neutral Beam Injection
NIF	National Ignition Facility
OS	Operating System
PCS	Plant Control System
PCU	Plasma Control Upgrade
PF	Poloidal Field
PID	Proportional Integral Differential
SISO	Single Input Single Output
TCL	Tree Command Language
TCV	Tokamak à Configuration Variable
TDC	Time to Digital Converter
TDI	Tree Data Interface
TF	Toroidal Field
TF	Transfer Function (in Chapter 5)

TOFOR	Time-of-flight Neutron Spectrometer
TORE SUPRA	Tore Supraconducteur
TSC	Tokamak Simulation Code
VME	Versa Module Eurocard
VS	Vertical Stabilization

Part I

Research Context

1

Introduction

Contents

"We will now discuss in a little more detail the Struggle for Existence."
Charles Darwin (The Origin of Species)

1.1 Nuclear Fusion

1.1.1 The Need for Nuclear Fusion

As it is very well known today, during the twentieth century energy has become essential for modern society lifestyle. A great variety of technologies that are used everyday depend on different types of energy. Moreover, with the big economic growth of high population density countries in Asia and Africa, as well as with the increase of life quality in developed countries, energy has become a precious resource for nations and mankind in the modern world.

At the current rate of energy consumption growth, it is predicted that the fossil fuels such as oil and natural gas will be exhausted before the end of this century. Coal is predicted to last longer[1], however it is the worth option due to the environmental consequences of its use. Figure 1.1 plots the difference between the world energy needs and the available fossil fuels energy [2]. Figure 1.2 shows that the oil production in the USA has already reached the peak production in 1973 and is now declining, according to data from the Energy Information Administration [3]. Nevertheles, it is important to make reference to the change this trend has suffered during the last 4 years (figure 1.3).

As a result of the increase in energy consumption, enormous quantities of fossil fuels are burned everyday for electricity production, transports and heating, with severe consequences to the environment, due to the emission of carbon dioxide to the atmosphere. Figures 1.4 and 1.5 depict the evolution of CO_2 concentrations in the atmosphere through the last 50 years and in the last four ice ages, showing a significant rise since the beginning of the industrial revolution [4][5].

The data from figure 1.4 (Keeling Curve[2]) is plotted at the right of figure 1.5 showing the recent increase in atmospheric carbon dioxide outside the pattern of the natural cycle.

The way how the increase of greenhouse gases affects the temperature has been a field of study and the process has been explained and worldwide accepted by the scientific community. However, if any doubt might still arise about the fact that the increase of

[1]The predicted year for the 90% world coal exhaustion varies between 2070 and 2095 [1].

[2] The Keeling Curve is named after Charles David Keeling plots the concentration of carbon dioxide evolution in Earth's atmosphere since 1958, based on continuous measurements taken at the Mauna Loa Observatory in Hawaii

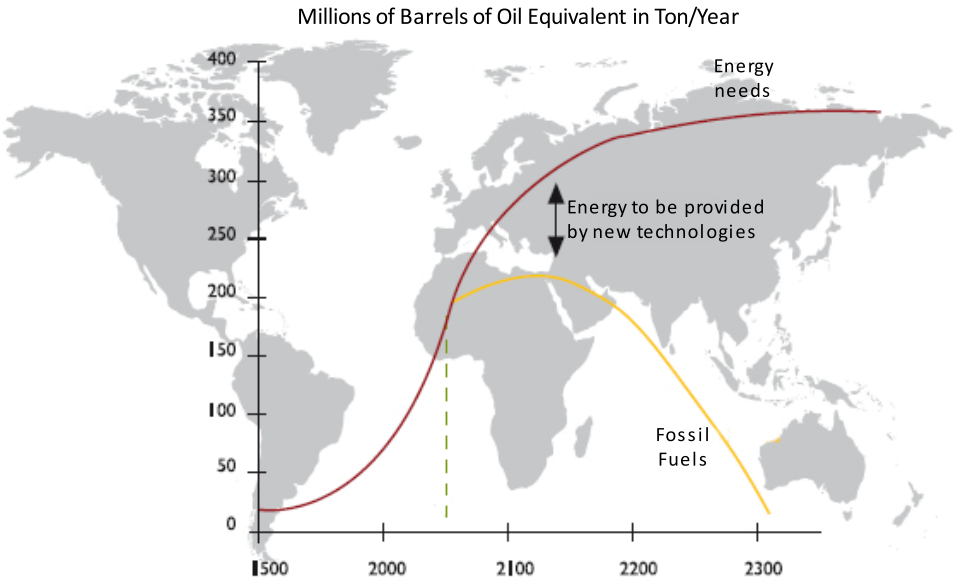

Figure 1.1: Evolution of the energy needs and the availability of fossil fuels to fulfill the energy demands [2].

carbon dioxide is closely related to the air temperature, the work published on Nature in 1999 by J. R. Petit [5] showed a clear match between both. Figure 1.6 presents the evolution of these quantities over the past 450 thousand years.

The Intergovernmental Panel on Climate Change [3] (IPCC) presented a report in 2007 [6] with important data on research and simulations for recent years. There is a statement on the unequivocal warming of the climate, *evident from observations of increases in global average air and ocean temperatures, widespread melting of snow and ice and rising global average sea level* [6]. The causes of these changes are also assessed. The Panel concluded that the main reason for climate changes is the emissions of greenhouse gases due to human activities, which have grown since 1750 and more significantly from 1970 where there was a 70% increase. The impact and consequences of climate changes is reported with studies of the influence throughout different regions in several systems and sectors, like, for instance: ecosystems, food, coasts, industry, settlements and society, health and water.

Figure 1.7 shows the rise of temperature in different continents and at global scale given by simulations of climate models using either natural or both natural and anthropogenic causes.

[3]The Intergovernmental Panel on Climate Change is a scientific panel that works under the United Nations supervision aiming at reviewing and assessing relevant scientific, technical and socio-economic information to the understanding of climate changes, its causes and consequences.

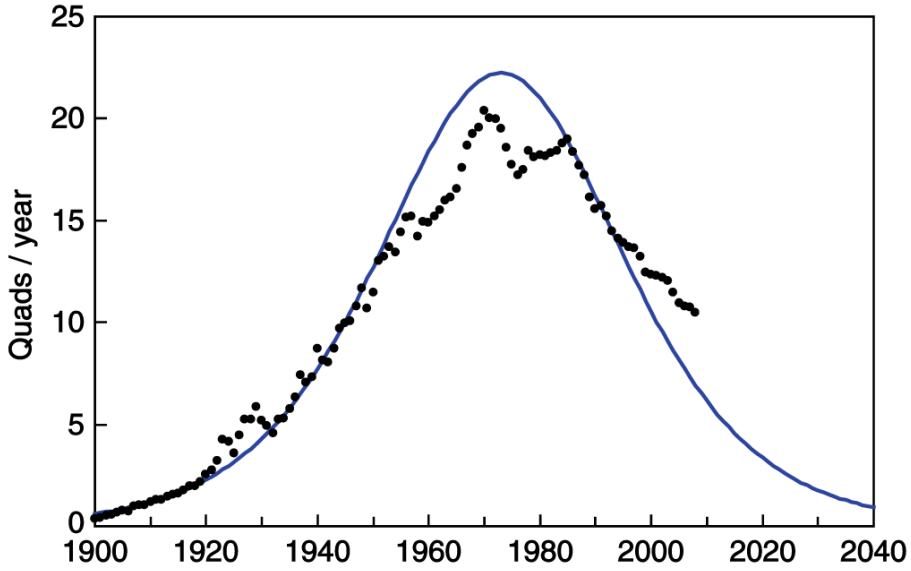

Figure 1.2: Production of oil data in the USA (dots) fitted to a Hubbert curve (line) using data from the Energy Information Administration website [3].

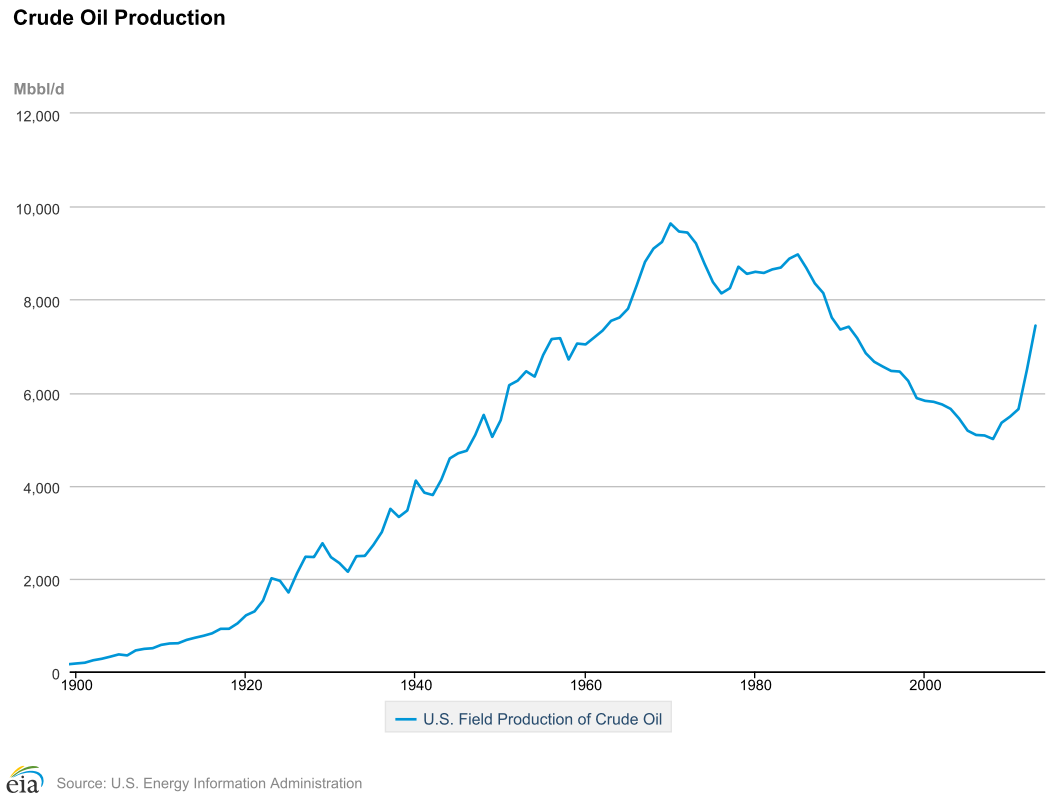

Figure 1.3: Recent trend on the production of oil data in the USA according to the US Energy Information Administration.

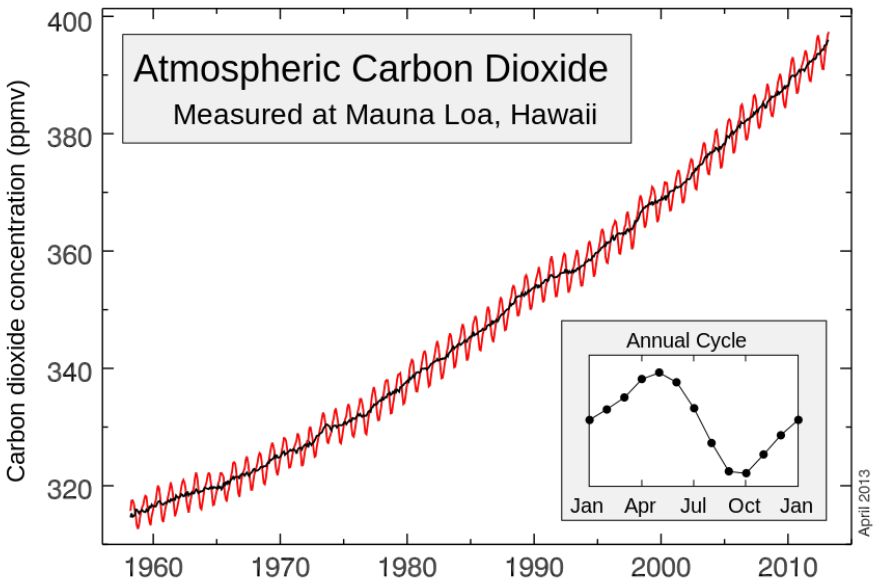

Figure 1.4: Evolution of the carbon dioxide concentration in the atmosphere during the last 50 years [4], updated to 2013 data.

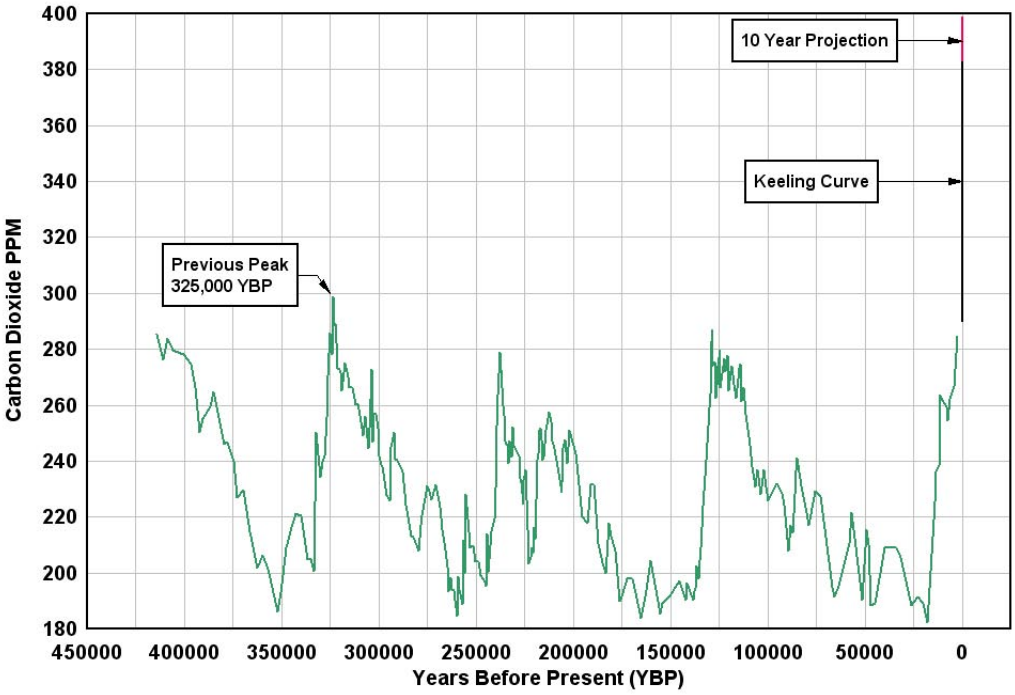

Figure 1.5: Evolution of the carbon dioxide concentration in the atmosphere during the last four ice ages [5].

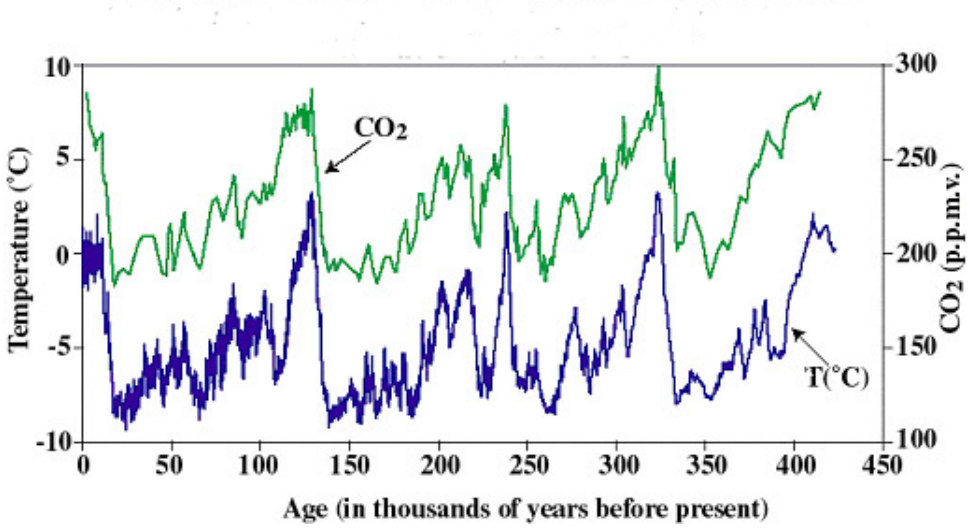

Figure 1.6: Comparison of the evolution of carbon dioxide concentration in the atmosphere with air temperature over the years [5].

To overcome the environmental problems and the scarcity of fossil fuels [4], important research efforts and investments have been made to increase fossil fuels burning efficiency and to use renewable energy sources like solar, wind, hydro, geothermal and biofuels [2]. Significant efforts have also been made to decrease energy consumption by increasing thermal insulation and improving combustion engine performance, as well as by changing some consumption habits of our society [2]. Although all these measures have given very important contributions to diminish the problem, they have proven to be of limited effect and none of them present a complete solution for the future energy needs of mankind.

An enormous worldwide research effort is also being made to develop an alternative for the world energy production that is inexhaustible, environment friendly (without greenhouse gas emission), inherently safety, sustainable and economically attractive. At the present stage of scientific and technology knowledge, nuclear fusion is a very strong potential candidate to fulfill these requirements.

Nuclear fusion has been the most important and most used energy source on Earth, coming from the Sun in the form of light and heat, assuring sustainable life in our planet

[4]According to the European Environment Agency [7], fossil fuels will remain the most important energy source until 2030, with the growth of oil, gas and coal use. Although coal is not scarce, it is problematic for pollution and climate change reasons. The costs of oil production will rise with the expanding difficulty of exploitation in deeper sea waters.

Nevertheless, fossil fuel reserves are concentrated in a small number of countries, with 80% of the coal reserves located in just six countries. European Union (EU) has just 4% of the global total. The EU share of the world's gas reserves decreased from 4.6 % in 1980 to 1.3 % in 2009 and these reserves are expected to be exhausted before 2030 [7].

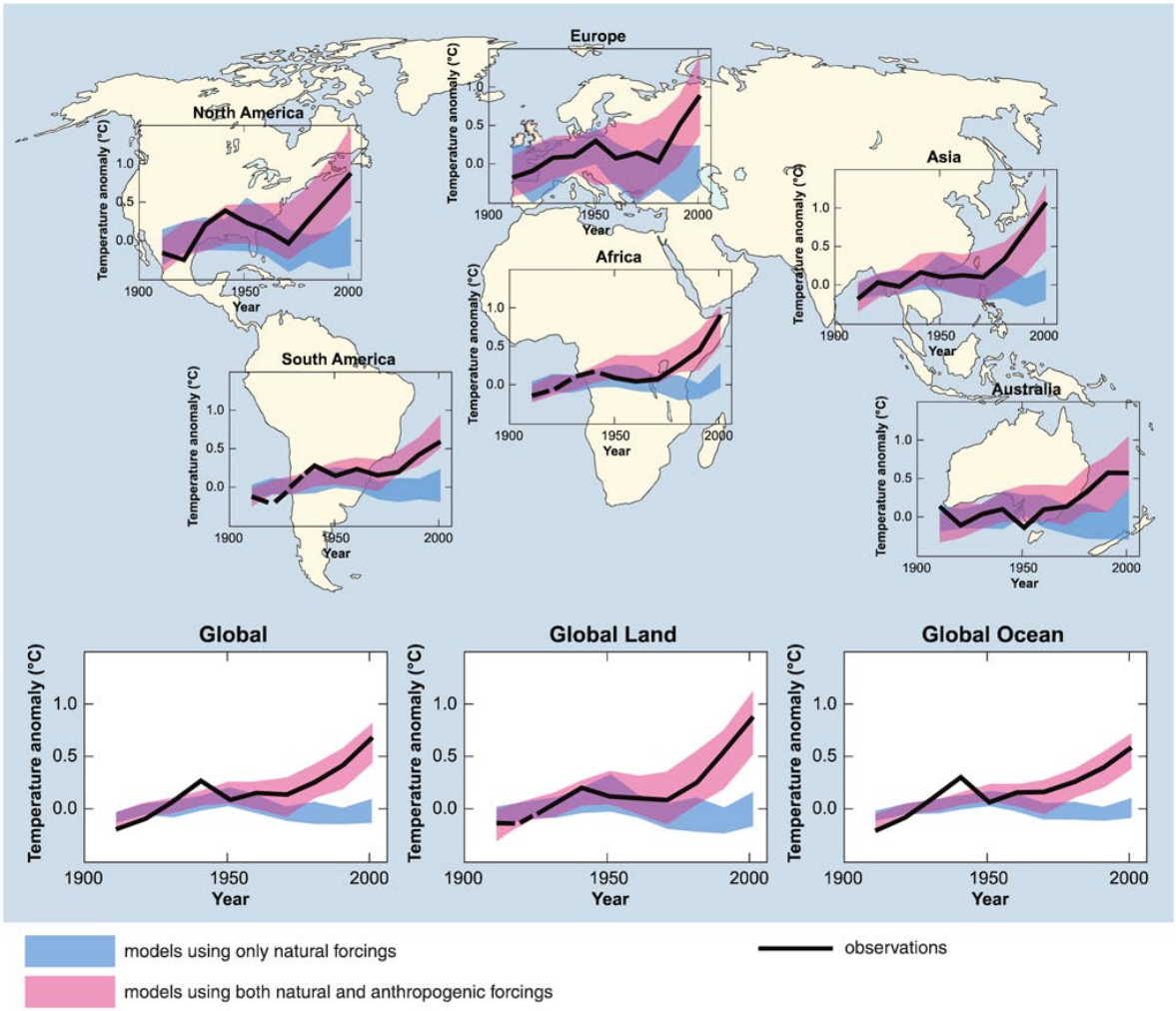

Figure 1.7: Comparison of observed continental and global-scale changes in surface temperature with results simulated by climate models using either natural or both natural and anthropogenic forcings [6].

since its beginning [8]. Another energy source of relevant importance that has been used to minimize the energy and environment problems is nuclear fission. In both cases, energy is produced when a nuclear reaction takes place, leading to a more stable nucleus[5] with reduction of the mass of the reaction products, and to the release of energy accordingly with the famous Einstein equation $E = mc^2$. The energy released in the process comes as kinetic energy of the reaction products. While in fission this is achieved by breaking a heavy nucleus into smaller ones, in fusion lighter nucleus are fused to form a heavier nucleus, which is lighter than the sum of the masses of the initial nuclei.

[5] As a general rule, the binding energy per nucleon increases with increasing size, up to the more stable elements iron and nickel, and then decreases for heavier nuclei.

Although nuclear fission and nuclear fusion are based on the same fundamental equation and neither of them directly cause any air pollution or greenhouse gases[6], there are some important differences between these two nuclear techniques that give electricity production by nuclear fission some important disadvantages when compared to nuclear fusion:

- The risk of serious nuclear accidents;
- Production of significant quantities of long-term radioactive waste;
- The misuse of fission technology and fuel for the production of nuclear weapons;
- The quantity of available fuels.

On the opposite side, nuclear fusion has relevant advantages on similar matters. Indeed, nuclear fusion is:

- *Inherently safe* due to absence of chain reactions that can become out of control. Accidents like Chernobyl or Fukushima would not happen in a fusion reactor;
- *Environment friendly* with neither emission of greenhouse gases nor production of long life toxic radioactive products;
- *Efficient* since it generates more energy per mass unit than any other known energy source;
- *Sustainable* as it will use raw fuels (water and lithium) that are abundant on Earth, allowing to produce during thousands of years the energy needed for mankind.

This thesis tries to give a small contribution to the research and development activities on a solution of the energy problems by making the production of controllable fusion power on Earth a reality.

1.1.2 Nuclear Fusion Reactions

The three lightest elements of the periodic table (and their isotopes) are used to achieve nuclear fusion on Earth: directly, (i) Hydrogen and its heavier isotopes Deuterium (D) and Tritium (T) and (ii) Helium (He^3 and He^4); and indirectly, (iii) Lithium (Li^6 and Li^7) is used inside the fusion reactor to produce Tritium [8].

The reactions

$$H + H \rightarrow D + e^+ + \nu_e + 0.42\ MeV \tag{1.1}$$

[6]However the operation of a nuclear power plant produces small amounts of air pollution and greenhouse gases due to the energy needed for the running, transport and preparation of the fuels currently used in these power plants.

$$D + H \rightarrow He^3 + \gamma + 5.49\ MeV \tag{1.2}$$

are very common in the center of the stars but, due to their very small cross sections, these reactions can not be used on Earth since they have a very small probability of occurring. In our planet these reactions are replaced by heavier elements reactions such as D-D and D-T with bigger cross sections, favoring the probability of these reactions to happen.

The D-D, D-T and D-He reactions are presented by the following equations:

$$D + D \rightarrow T(1.01MeV) + p(3.03\ MeV) \tag{1.3}$$

$$D + D \rightarrow He^3(0.82MeV) + n(2.45\ MeV) \tag{1.4}$$

$$D + T \rightarrow He^4(3.52MeV) + n(14.06\ MeV) \tag{1.5}$$

$$D + He^3 \rightarrow He^4(3.67MeV) + p(14.67\ MeV) \tag{1.6}$$

where the kinetic energy of the products is presented between parenthesis and represent the energy released by one nuclear reaction.

The most favorable reactions in terms of energy production are D-T and D-He^3. This last reaction would also be preferable because it does not produce any neutron. However this reaction has two main disadvantages: He^3 is not available on Earth and it occurs at higher temperature since the maximum of its cross section is at about 200 keV. For these reasons, the D-T reaction (figure 1.8) is expected to be used in the first fusion power plants.

Deuterium is extracted from water and Tritium is produced inside the fusion reactor from the Lithium blanket using the neutrons that are released from D-T reactions[7].

$$Li^6 + n \rightarrow T + He^4 + 4.8\ MeV \tag{1.7}$$

$$Li^7 + n(2.5\ MeV) \rightarrow T + He^4 + n \tag{1.8}$$

Since water and Lithium can be found in abundance on Earth, the fuels for D-T

[7]The tritium that is necessary to start the reactions is produced in a type of fission reactors.

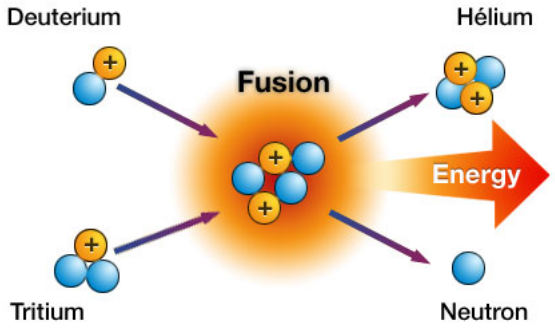

Figure 1.8: Nuclear fusion reaction between hydrogen isotopes deuterium and tritium.

reactions will allow electricity production that can last for more than a million years.

The fusion of Deuterium and Tritium nucleus implies a big increase of their energies, aiming at overcoming the repulsion force between two charged particles of the same signal. Because the cross sections of the D-T reaction has a maximum for energies of about 50 keV (figure 1.9), the fuels should be heated to temperatures of about 10-20 keV. At these very high temperatures, the fuels are in the fourth state of matter: plasma.

1.1.3 Plasma: the Fourth State of Matter

The term plasma comes from the Greek, meaning "moldable substance", and it is used to describe an ionized gas, quasi neutral and with collective behavior. It was first used by Irving Langmuir, when studying the tungsten filament in light bulbs. The idea behind the name comes from the similarity between the blood plasma carrying its components and the electrified fluid carrying charged particles (ions and electrons)[9].

In the three best known states of matter (solid, liquid and gaseous), the positive charged nucleus of the atom is surrounded by the negative charged electrons, being the atom neutral. Although at room temperature these three states are the most common on Earth, most matter of the universe is not in any of these states. When temperature is raised above the ionization temperature of the atoms (typically 10^4 K), the electrons are ripped off from the atom, making a transition to the fourth state of matter called plasma state. This state of the matter is composed of free charged particles (electrons and ions) that give to the plasma state some important and unique characteristics that differ from the gaseous state [8] :

[8]The plasma state has also some similarities with the gaseous state such as a deformable shape and variable volume.

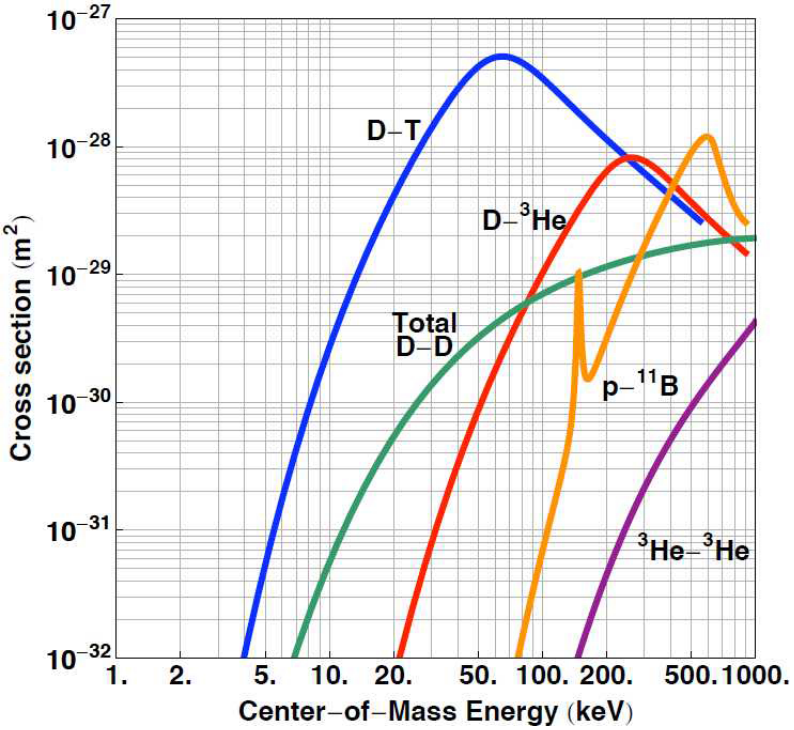

Figure 1.9: Nuclear fusion reactions cross sections vs kinetic energy (or temperature) (http://iec.neep.wisc.edu/).

- Electrical conductivity;
- Possibility of production of magnetic fields by electrical currents, generated by electric fields;
- Actively respond to electromagnetic fields, thus permitting to shape its form and control its position.

Plasmas can be found in our daily life in fluorescent and neon lights, plasma TV, electric sparks, laboratory experiments, several industrial production processes and in nature around the Earth in the ionosphere, lightnings and the Sun. Moreover, most matter in the Universe is in the plasma state in stars (high density plasmas) and in interstellar plasma (low density plasmas).

Langmuir research started a new area of studies called plasma physics that is applied in different areas of science and technology, such as Radio Broadcasting; Astrophysics; Hydrogen Bomb; Magnetic Confinement Nuclear Fusion; Laser Plasma Physics; Inertial Confinement Nuclear Fusion and Production of Modern Integrated Circuits.

1.1.4 Confinement

1.1.4.1 Introduction

There are several basic problems that have to be solved aiming at achieving successful operation of a fusion device. They can be summarized as follows:

- How to heat the plasma up to the very high temperatures that are needed for the occurrence of fusion reactions;
- The plasma has to be confined to a space region in order to allow the fusion reactions to occur and to take advantage of the released energy. Moreover, in a Laboratory the plasma can not contact with the vessel wall since it can melt, the plasma temperature decreases and impurities are generated, which increase the losses of energy and diminish the stability of the plasma;
- When an ion core transformer or a central solenoid are used, non-inductive current drive methods have to be utilized aiming at producing long duration plasma discharges, since the magnetic flux created by these two components saturates after some time;
- A lot of physics and technologies problems, in which real-time plasma control and plasma stability are included, have to be addressed in order to avoid plasma disruptions that will stop the plasma discharge and could damage the vessel wall.

There are three ways to solve the second problem, called plasma confinement: Gravitational Confinement (GC), Inertial Confinement (IC) and Magnetic Confinement (MC) [8].

1.1.4.2 Gravitational Confinement

Long before the studies on nuclear energy, it was already known that the stars would contain a huge unknown source of energy. Calculation based on the known chemical energy sources were not compatible with the long duration of the formation of the Earth predicted by geologists.

Even with the dawn of nuclear energy with the radioactivity discovery, it was not immediately found the relation between this energy and the Sun. The evolution of nuclear physics, Einstein's special theory of relativity and the astronomy studies on the interior of stars, led to the explanation, in 1929, of the nuclear fusion energy source that took place inside the stars [10].

Robert Atkinson and Fritz Houtermans showed that in the interior of the stars exist the necessary conditions of high temperature and high density for sustaining nuclear fusion

reactions. Due to its huge mass the Sun creates a strong gravitational field, capable of sustaining a very hot and dense plasma of hydrogen atoms that fuse together, forming helium. This nuclear reaction releases a big quantity of energy with a low consumption of mass, explaining the sustainability of the emission of big quantities of energy during billions of years.

This work was then continued by H. A. Bethe, that a decade later published a more complete work on the explanation of energy production in stars [11].

1.1.4.3 Inertial Confinement

This concept is based on the compression and heating of a small pellet of deuterium and tritium, of approximately one millimeter, by a set of very powerful lasers up to thermonuclear temperatures. The use of lasers [9] comes from the fact that they are easily focused on very small pellets and its large radiation intensity that can be used to exchange large quantities of energy to the pellet in a very short time.

The process of direct driven inertial fusion using lasers can be roughly described as a four step process (Figure 1.10):

- *Energy absorption* A set of powerful laser beams are focused on a pellet of fusion fuel. The pellet absorbs the energy, heating to temperatures near the Sun temperatures.
- *Energy transport and compression* The heated shell propagates its energy producing very high pressure over the fusion fuel in the centre of the pellet.
- *Nuclear fusion reactions* The high temperature, highly compressed begins the fusion reactions from the centre of the pellet.
- *Energy release* The energy from the center fusion reactions propagates outwards, propagating and amplifying the energy received from the laser beams.

Another approach is known as indirect drive, where the D-T targets are surrounded by a small metal cylinder which is irradiated by the laser beams. The lasers are focussed on the inner side of the cylinder, heating it to a super hot plasma which radiates mostly in X-rays. This electromagnetic radiation is then absorbed by the target surface, imploding it in the same way as was previously described for the direct driven approach.

The largest inertial fusion experiment in operation is the National Ignition Facility (NIF) at the Lawrence Livermore National Laboratory [12]. NIF has 192 laser beams and achieved ignition some months ago[10] [13]. Another important experiment is the Laser

[9] Instead of lasers, very powerfull X-ray or heavy ion beams can also be used.
[10] Please see section 1.1.5

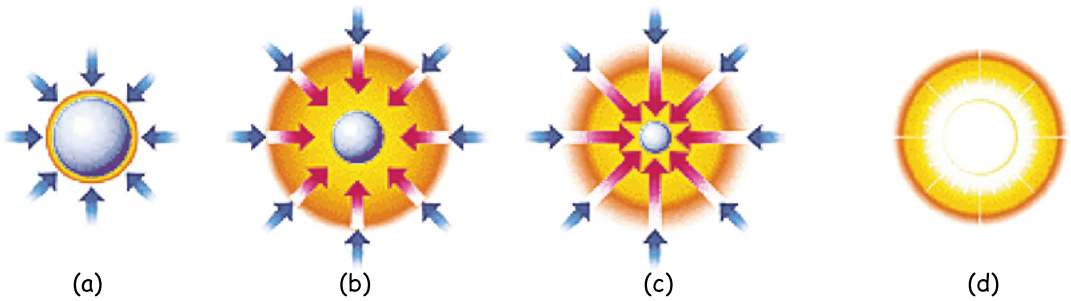

Figure 1.10: Four stages process of a fusion reaction chain in an inertial confinement capsule: (a) Energy absorption; (b) Energy transport and compression; (c) Nuclear fusion reactions; (d) Energy release [8].

Mega Joule, a French project located in Bordeaux [14].

1.1.4.4 Magnetic Confinement

Magnetic confinement is presently the most promising research option to build a sustained way of energy production for the future based on nuclear fusion reactions. This concept is based on guiding centre orbits of charged particles in a magnetic field (B) with a radius given by

$$r = \frac{vm}{qB} \tag{1.9}$$

where q and m are the charge and the mass of the charged particle, and v is its velocity in the plane perpendicular to $\vec{B}$. The analysis of this formula allows to conclude that strong magnetic fields ($\geq 1\,Tesla$) confine the plasma to a narrow space zone, avoiding contact of the plasma with its vessel.

After the initial linear configurations, fusion devices rapidly evolved to toroidal magnetic configurations, which have several advantages (only axial confinement is needed and allow an electric toroidal current that is used not only to heat the plasma up to around 1 keV[11], but also to contribute to the stabilization of the plasma column) and a major drawback: the plasma column moves outward the vacuum vessel wall. Indeed, due to the existence of a gradient of B ($\vec{\nabla}B$) perpendicular to $\vec{B}$, there is a force that moves the plasma charged particles in opposite directions to the top and bottom of the plasma column, creating an electric field. This field and the toroidal magnetic field creates another force that moves the plasma electrons and ions to the region of low B-field.

[11] When the electron temperature increases, the plasma resistivity decreases, being approximately zero for $T_e \approx 1\,keV$. This means that the ohmic heating has finished.

Three main toroidal magnetic configurations have been developed: the Tokamak, the Stellerator and the Reversed Field Pinch. The main difference between these types of devices is the way how the plasma column is stabilized. The twisted shape of the magnetic field lines, necessary for the stabilization of the plasma column, is obtained:

- In a *tokamak* using a series of coils evenly spaced around the torus, to create the toroidal field, while the poloidal field is produced by the plasma current and by two sets of toroidal coils that create the so called vertical and horizontal magnetic fields.
- In a *stellerator* using external coils that might be non-plane and with non-linear axis (Figure 1.11).
- In a *reversed field pinch* using a much stronger plasma current compared to a tokamak with similar toroidal field, where the set up of the magnetic fields is such that the direction of the toroidal field is reversed, although toroidal and poloidal fields are created in the same way as in tokamaks.

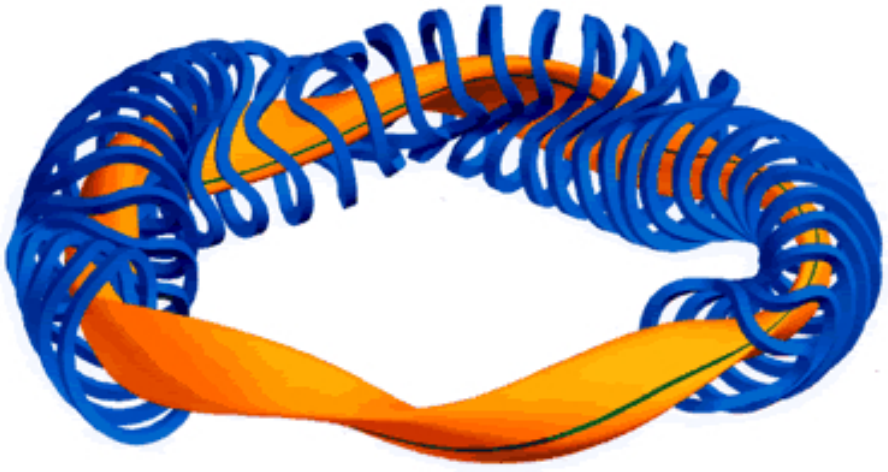

Figure 1.11: Schematic view of the stellerator Wendelstein 7-X [15].

1.1.5 Ignition

There are two main power sources involved in the operation of a fusion device: (i) the power fed from outside the device (P_{ext}), necessary for the plasma creation, maintenance and heating; and (ii) the power generated inside the device by the fusion reactions (P_f).

At low plasma densities (n_0) and temperatures (T_i), P_{ext} is much greater than P_f. When n_0 and T_i increase, P_f also rises, being used one part for additional plasma heating

(alpha-particle heating) (P_α) and the other to heat the wall of the vacuum chamber in order to produce electricity (P_e) like in any thermal power plant.

The power amplification factor (Q) is given by

$$Q = \frac{P_e}{P_{ext}} \tag{1.10}$$

When $P_e = P_{ext}$, the device reaches the break-even, where $Q = 1$.

Preliminary studies about the operation of a nuclear fusion reactor plant show that, from the economic point of view, a fusion reactor is attractive only if $Q > 20$.

Ignition occurs when the energy created by fusion reactions in a plasma is enough to maintain the rate of fusion reactions, without the need of external heating[12]. When stable ignition state is achieved, it is only necessary to keep the plasma burning by feeding in the fuel to receive the energy that comes out of the plasma.

The energy that is used for electricity production comes from the particles that escape from the plasma and hit the vessel wall. These are mainly the non charged particles like neutrons that can not be confined by the magnetic field. These particles heat the walls of the vessel making the process of energy production similar to the other energy production power plants.

1.1.6 Lawson Criterion

The Lawson Criterion [16] defines minimal conditions to achieve fusion ignition based on the triple product of electron density n_e by the ion temperature T_i and the energy confinement time τ_E:

$$n_e T_i \tau_E \geq 3 \times 10^{21}\, m^{-3}.keV.s \tag{1.11}$$

When applied to D-T reactions at $T_i \approx 20\, keV$, this product has a minimum value to reach ignition that is represented by the following equation:

$$n_e \tau_E \geq 1.5 \times 10^{20}\, m^{-3}.s \tag{1.12}$$

From this equation, it is possible to foresee two approaches to achieve ignition state: (i) high density plasmas or (ii) high confinement times plasmas. The first approach is

[12]For the magnetic confinement fusion community, ignition means $Q = \infty$. Sometimes on inertial confinement fusion, the term ignition is used when the fusion power is greater than the absorbed power.

pursued by inertial confinement where high density plasmas are obtained at the cost of the confinement time [13]. The second approach is pursued by magnetic confinement[14].

Figure 1.12 shows an impressive increase of the fusion triple product since the beginning of the research and development activities in magnetic confinement nuclear fusion. The Joint European Torus (JET) [17] and the Japan Torus (JT-60) [18] tokamaks were able to create plasmas in which the energy released from the plasma was very near the energy that was used to heat the plasma. The condition for ignition state is represented in red and it might be achieved in the ITER tokamak [19].

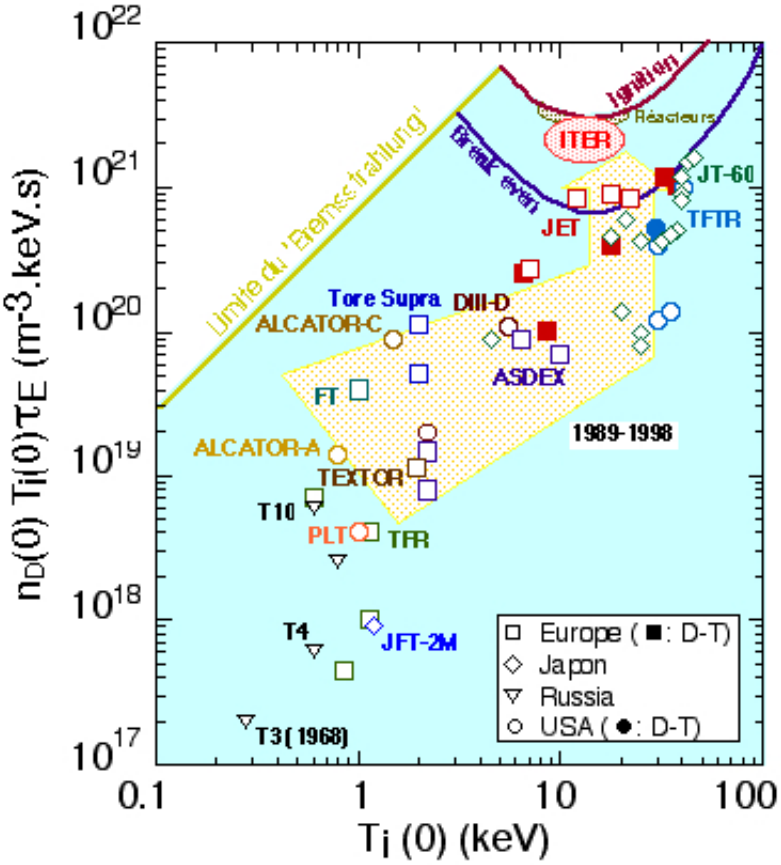

Figure 1.12: Diagram representing the path to ignition domain - achieved triple product for different magnetic confinement devices (http://www-fusion-magnetique.cea.fr/).

[13] Inertial fusion is also known as fast nuclear fusion
[14] Magnetic fusion is also known as slow nuclear fusion

1.2 Controlled Nuclear Fusion and Tokamaks

1.2.1 Tokamak Concept

The best experimental results for the fusion triple product have been obtained until now in tokamaks [20], a concept presented in 1950 by two Russian scientists Igor Yevgenyevich Tamm and Andrei Sakharov.

Figure 1.13 presents a schematic drawing of a tokamak. The plasma current is created by a toroidal induced electric field, generated by a transformer[15][16] in which the plasma acts as the secondary. This plasma current is used to heat the plasma up to ion and electron temperatures of about 1 keV. Additional heating to achieve typical temperatures needed for fusion reactions (10 to 20 keV) is provided by injection of either neutral beams or electromagnetic waves. In the first case, the beam energy is directly transferred by collisions to the plasma electrons or ions, while in the second method the energy is transferred to plasma charged particles using resonances of the system: Electron Cyclotron, Ion Cyclotron or Lower Hybrid Frequency.

The tokamak operation is pulsed due to either the saturation of the transformer iron core or the limit of the magnetic flux that can be stored in the central solenoid[17][18]. The discharge duration can be increased by reversing the current in the primary before the saturation (AC operation) [22][23][19] or generating the current by non-inductive methods:

- Neutral Beam Injection (NBI);
- Electron Cyclotron Current Drive (ECCD);
- Ion Cyclotron Current Drive (ICCD);
- Lower Hybrid Current Drive (LHCD).

Aiming at obtaining the necessary temperature and energy confinement time to achieve ignition, large plasma currents must be produced. Since the plasma current increases with the tokamak size, bigger experiments have to be built. JET, the largest tokamak currently

[15] The transformer can have an iron core, like on ISTTOK, TORE SUPRA and JET, or an air core, like on ITER, ASDEX-Upgrade, MAST and TCV.

[16] The primary circuit is the central solenoid while the plasma acts as the secondary circuit.

[17] The variation in time of this flux drive the electromotive force that is responsible for the "'loop voltage"' that creates the toroidal induced electric field (Faraday Law) that in turn is connected to the ohmic component of the plasma current. When all the accumulated magnetic flux was spent, the discharge must inevitably end, unless the plasma current is generated by other non-inductive methods, like the injection of high power beams of radiofrequency waves or neutral particles.

[18] It is also due to this flux expenditure that when the plasma is heated with external sources, it becomes a better conductor and as such the same amount of plasma current can be inductively generated, spending less flux in the primary circuit and therefore the discharge lasts longer.

[19] Although this solution is only adequate for small-size tokamaks.

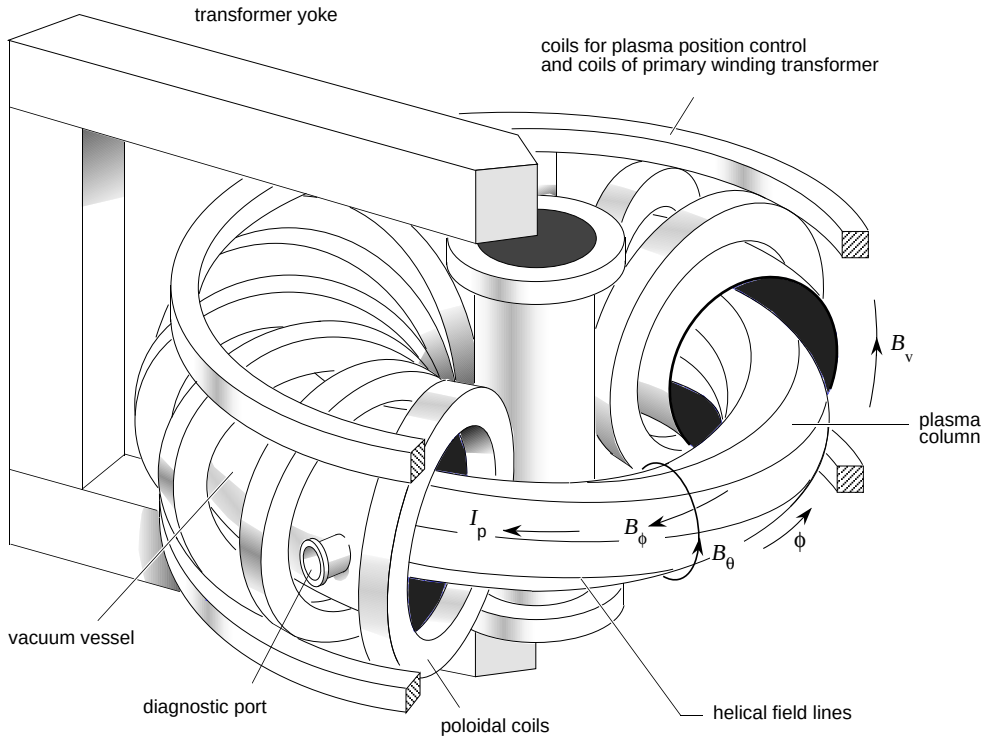

Figure 1.13: Schematic diagram of the main parts of a general tokamak [21].

in operation and the only fusion device that can operate with mixes of Deuterium and Tritium, has plasma currents up to 7 MA [24]. ITER, the first fusion experimental reactor currently being built in the South of France, was designed for plasma currents up to 15 MA [25].

Figure 1.14 contains the schematic drawings of JET and ITER, at the same scale. Besides the difference in size of both devices, ITER will have higher toroidal magnetic field (5.3 T instead of 4 T) and plasma current (15 MA instead of 7 MA) as well as longer duration discharges. ITER has been designed for D-T operation and for testing of Test Blanket Modules. The main ITER components are contained in a cryogenic system for adequate cooling.

Table 1.1 depicts the main parameters of several important tokamaks.

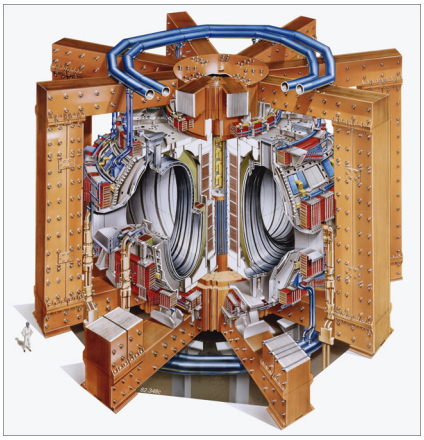

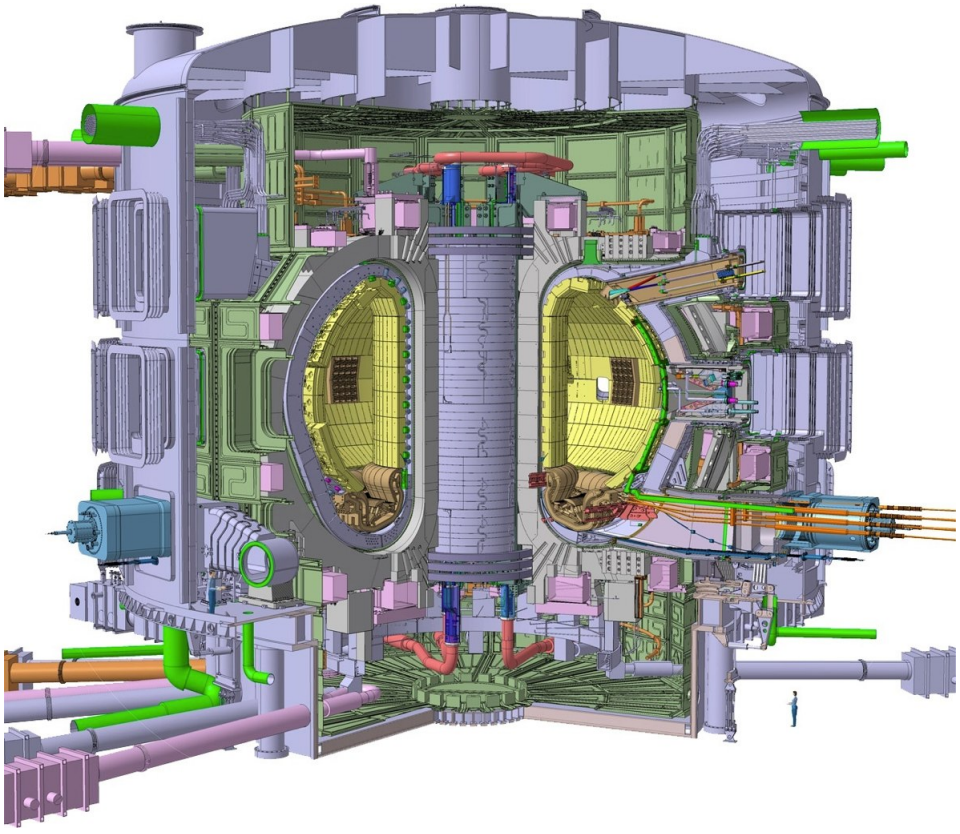

Figure 1.14: The JET tokamak in Culham Science Centre (top) [26] and the ITER tokamak currently being built in the south of France (bottom) [27].

Parameter	TCV	Tore Supra	Asdex-U	DIII-D	TFTR	JT-60U	JET	ITER
R[(1)]	0.88	2.25	1.65	1.66	2.4	3	2.96	6.2
a[(2)]	0.25	0.7	0.8	0.67	0.8	1	0.96	2.0
x95[(3)]	2.8						1.6	1.7
TF [(4)]	1.4	4.5	3.9	2.2	6	4.5	4	5.3
IP [(5)]	1.2	2	1.4	3	3	2.7	7	15
ECRH[(6)]	4.5	2.4	4	6	-	-	-	20
ICRH[(7)]	-	9	6	5	11.4	5	12	20(40)
NBI[(8)]	-	1.7	20	20	39.5	20	24	33(50)
LH [(9)]	-	5	-	-	-	10	7	0(40)

Table 1.1: Main parameters, characteristics and achievements of relevant tokamaks for controlled fusion research: (1) Major radius (m); (2) Minor radius (m); (3) Vertical elongation; (4) Toroidal field (Tesla); (5) Plasma current (MA); (6) Electron Cyclotron Resonance Heating Power (MW); (7) Ion Cyclotron Resonance Heating Power (MW); (8) Neutral Beam Injection Power (MW), (9) Lower Hybrid Power (MW).

1.2.2 TCV Tokamak

The *Tokamak à Configuration Variable* (TCV) is a medium size, air core transformer, magnetic fusion device with a standard aspect ratio $1/\epsilon = R/a \approx 3.5$ exploited by *Centre de Recherches en Physique des Plasmas* (CRPP) at *École Polytechnique Fédérale de Lausanne* (EPFL) [28]. It was designed to study the influence of the shape poloidal cross section in the plasma stability and confinement. Figure 1.15 presents several different plasma configurations and shapes that can be studied on TCV [28].

The importance of plasma shape comes from the fact that plasma columns with different shapes means that the stability of the plasma edge is different. Higher stability permits higher plasma density. The research on plasma shapes and stability is therefore a very important study that aims at improving fusion power performance.

Figure 1.16 shows a TCV drawing. The primary circuit of the transformer is composed by 9 ohmic coils around the central column (A). The 16 poloidal field coils (B) are used to create the toroidal magnetic field. To permit the different plasma shapes and high elongated plasmas, the vacuum vessel itself (C) presents a vertical elongated cross section. The shaping of the plasma is achieved by the use of the 16 independently powered toroidal coils (D). To diagnose the plasma parameters several measurement equipment must access the inside of the vessel using the diagnostic windows (E). To vertically stabilize the elongated plasma the in-vessel toroidal coils are used (F).

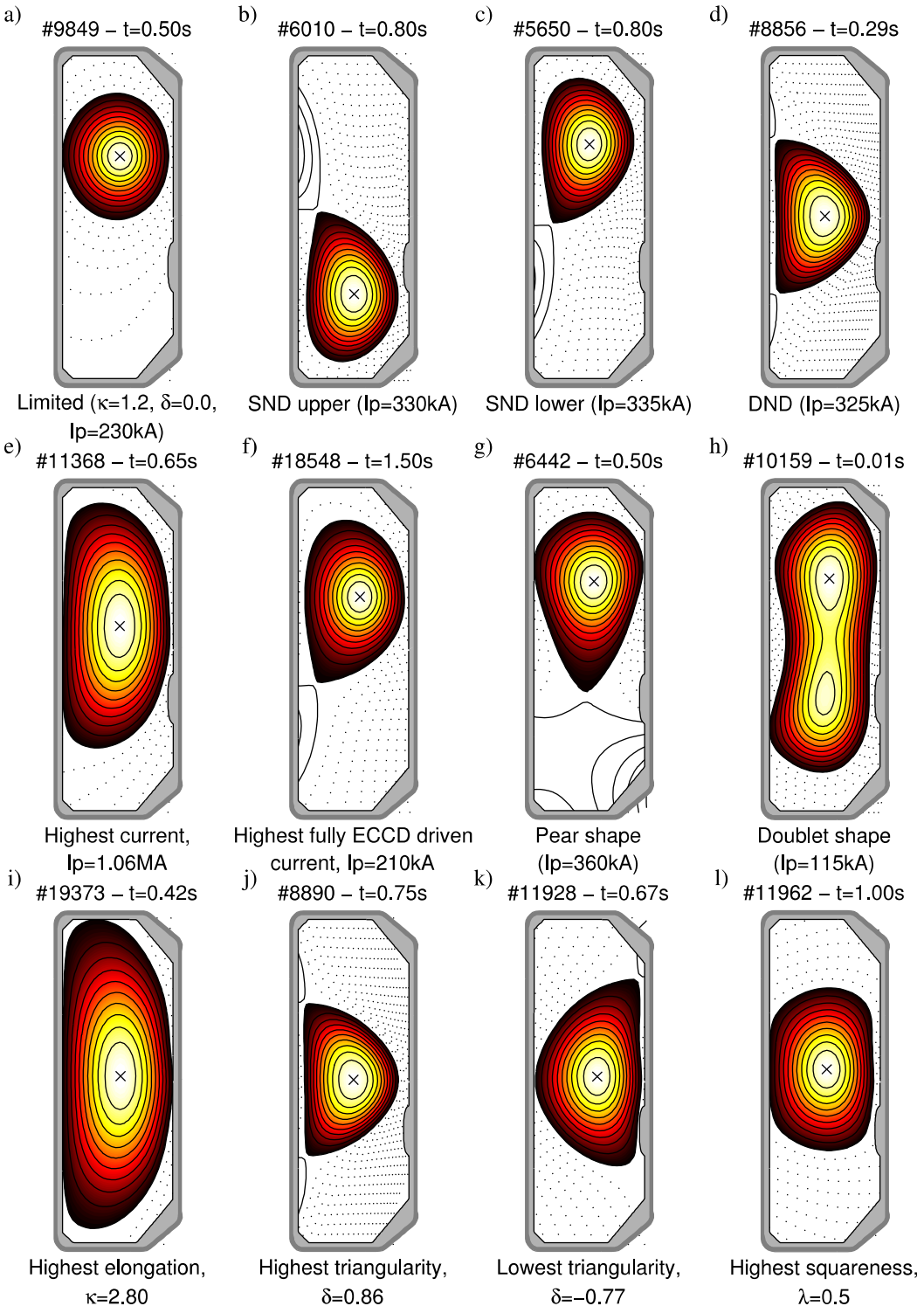

Figure 1.15: Several plasma shapes achieved at TCV, representing important goals of the tokamak.

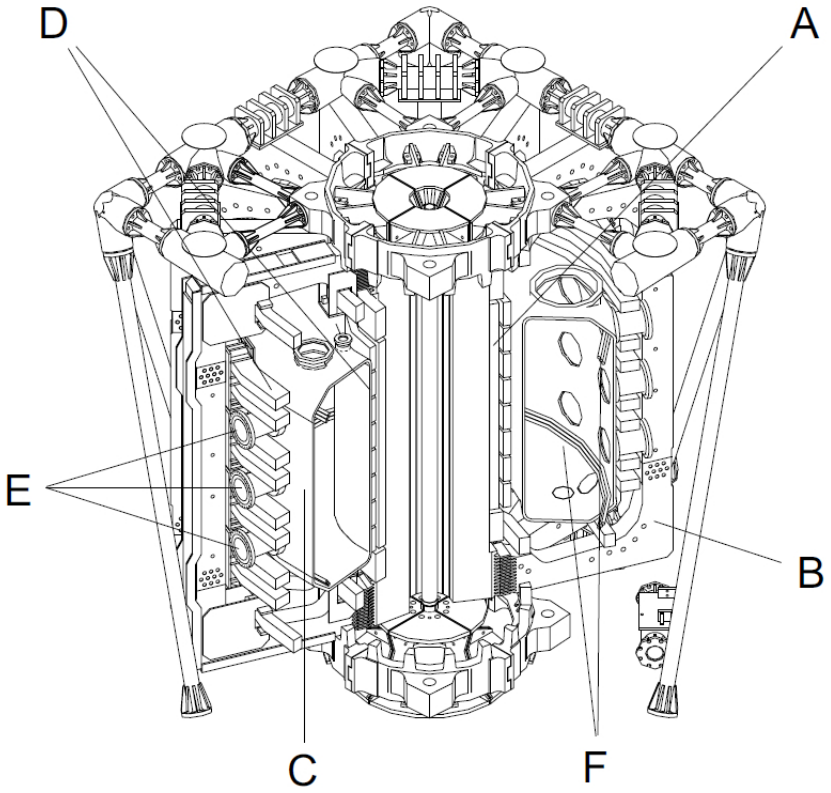

Figure 1.16: TCV mechanical structure schematic representation: (A) Ohmic coils to induce plasma current; (B) Poloidal coils to produce a the toroidal magnetic field; (C) Vacuum vessel; (D) Shaping coils; (E) Windows for the diagnostics to access the vacuum vessel; (F) Toroidal coils for elongated plasmas stabilization.

1.3 Motivation

1.3.1 Introduction

The advances on fusion research have led to the progressive replacement of the initial analogue control systems by digital control tools and, more recently, to the implementation of real-time control. These changes have occurred due to the improvement of the information technologies, the specialization of the fusion research programmes, the operation in new parameter windows and the need of a new paradigm for data acquisition since the increase of the discharge duration as well as of the number of plasma diagnostics do not permit to store all data provided by the sensors, detectors and diagnostics of a fusion device.

The new faster and more complex digital systems for fusion control demand evolutions

not only in the hardware but also in the algorithms development and programming tools that must be available for the physicists to work in an user-friendly manner.

1.3.2 Advanced Plasma Control System

Real-time is a requirement even more important in a device like TCV, which was specially designed for the study of the plasma control and stability in different configurations of the cross section of the plasma column, with different elongations and triangularities.

TCV has extensive plasma control capabilities due to an extremely flexible set of actuators composed of 16 independent powered poloidal field coils, gas valves and electron cyclotron power supplies and launchers.

Therefore, after an initial and very successful phase of TCV operation, CRPP has decided to use programmable real-time systems not only to control the tokamak operation but also to garantee the safe and efficient operation of the new plasma diagnostics. In this context, CRPP and Instituto Superior Técnico (IST) have agreed to carry out a working programme aiming at developing a real-time pulse height analysis X-ray diagnostic [29], based on a very powerful Digital Signal Processor (DSP), parallel processing, VME module [30]. Later it was decided to use this module in the implementation of an Advanced Plasma Control System (APCS) for the improvement of the control capabilities of TCV and in particular the vertical stability of the TCV plasma.

The TCV control system was firstly based on analogue/digital controllers, which depend on analogue input/output (I/O) and digital coefficients provided by digital to analogue converters. Control was achieved using predetermined waveforms which have low programming capability. This system has used only Proportional Integral Differential (PID) controllers.

The new digital control systems has been developed aiming at allowing:

- Larger flexibility and higher performance for controlling the TCV plasma shape, position, current and density;
- Use of other types of controllers than the classic PIDs, including non-linear controllers;
- Easy change of algorithms and parameters;
- Use of modern hardware technologies and programming techniques;
- Use of faster control cycles;
- Use of large bandwidth systems (at least 100 kHz).

1.3.3 Vertical Plasma Stability Improvement

Modern tokamaks have been designed in order to permit elongated cross section shaped plasma columns, aiming at increasing the energy storage in the plasma. However, high elongation also leeds to the instability of the plasma column vertical position, which has to be stabilized using a feedback control system.

The vertical instability problem has been tackled in several tokamaks with the improvement of their vertical stabilization controllers. The JET Plasma Control Upgrade (PCU) Project aiming at increasing the capabilities of the Vertical Stabilization (VS) System [31] developed with an important contribution from "Instituto de Plasmas e Fusão Nuclear", is a reference for the innovative work on the new hardware platform [32][33], the real time software implementation [34][35], the modeling and simulation capabilities [36], as well as the testing functionality in a wide range of scenarios before going online, reducing the development and maintenance costs, improving system performance and reliability [37][38]. The contribution to the PCU Test-Bench [37][38] also gave to the author of this PhD. thesis expertise in real time plasma control that was important for the work presented in this document.

TCV uses in-vessel poloidal field coils driven by a pair of fast switching power supplies, which require bandwidth of 100 kHz, to achieve highly elongated plasmas vertical stabilization.

The algorithms of the analogue control system were limited to a PID controllers with out the possibility of running optimal non-linear algorithms. APCS permits the development of vertical stabilization non-linear digital controller, aiming at improving the performance of the stabilization of the vertical position of the plasma column using the same power supplies and in-vessel coils.

1.4 Thesis Outline

This thesis describes part of the work performed in the frame of the research and development programme, jointly carried out by IST and CRPP aiming at developing a new digital advanced plasma control system for TCV. This system has been used to improve the plasma vertical stability by applying the theory of optimal control to the mathematical model that describes the TCV plasma and system hardware. The innovative contributions from the author of this thesis are presented in section 6.2.

This thesis is organized as follows: *Chapter 1, Introduction*, presents an introduction

of the developed work, its context and motivations. *Chapter 2, Modern Control Theory for Plasma Control in Tokamaks*, contains an overview of the basis on control theory that was used through the development of the work presented in this thesis. This chapter also presents a study of the mathematical tools and concepts necessary for the understanding and development of the plasma vertical stability optimal controller. *Chapter 3, Plasma Control in Tokamaks* depicts the background knowledge and state of the art control methods and techniques used in modern tokamak control. *Chapter 4, Advanced Plasma Control System*, gives an overview of the TCV hybrid control system, as an introduction to the need of evolution of this very well designed control system. After this introduction, this chapter presents a complete description and development of the digital Advanced Plasma Control System, including its design, implementation, integration and tests. *Chapter 5, Improving the Plasma Vertical Stability*, describes the implementation of a new controller for TCV plasma vertical stabilization based on optimal control theory. The controller was completely redesigned from the observer, modelization of the system and control theory application. This chapter presents a complete description of the mathematical treatment, control method, plasma and device models used, simulation and results. Finally, *Chapter 6, Conclusions and Future Work* contains a short summary of the main achievements, underlines the original contributions from the author of this thesis and presents some ideas regarding the work that can be carried out for further improvements of the digital control system as well as of the plasma vertical stabilization.

Part II

Control Theory

2

Modern Control Theory

Contents

"It is not the strongest of the species that survives, nor the most intelligent, but the one most responsive to change."

Charles Darwin

2.1 Modern Control Engineering

2.1.1 Introduction

The history of control theory comes back to 150 years ago, when the behavior of mechanical governors were studied mathematically aiming at an automation of the control of simple processes. From the amazing evolution of this field of science, some selected historical steps may be referenced as major breakthroughs to the evolution of control system development [39].

- *XVIII Century*
  - James Watt develops the steam engine and the centrifugal governor connected to steam regulator valve to maintain the machine at constant speed. The steam engine marks the beginning of industrial revolution and permits the development of mechanization, a technology preceding automation.
  - The concept of interchangeable parts in manufacturing shown for the production of muskets by Eli Whitney. This concept is the precursor of mass production.
- *XIX Century*
  - J. C. Maxwell formulates a mathematical model for the governor control of a steam engine.
- *XX Century*
  - Henry Ford introduces a mechanized assembly machine for automobile production.
  - H. S. Black and H. W. Bode propose and analyze the negative feedback amplifier.
  - H. Nyquist develops a method for analyzing the stability of a system.
  - The first anti-aircraft gun with active control is created during World War II.
  - Numerical control is developed for control of machine-tool axes.
  - George Devol develops "programmed article transfer" - the first industrial robot design.
  - The begin of Space Age leads to miniaturization of computers and advances in automatic control theory.
  - The state-variable models and optimal control are developed.
  - Robust control system design is widely studied.

  - Introduction of the personal computer and control design software brought the tools of design to the engineer's desktop.
  - Industry and manufacturing companies emphasize automation.
  - Automobile industry demands reliable, robust systems in manufacturing.
  - Feedback control is widely used in automobiles.
  - First ever autonomous rover vehicle explores the Martian surface.
- *XXI Century*
  - Advances in nanotechnology permit the creation of the first intelligent micromachines as well as the first nanomachines.

The aim of modern control engineering is to control the evolution of one or more system properties (variables) over the time. Controllers are demanded to maintain both transient or steady-state behavior according to a reference signal that the system must follow as accurately as possible.

Modern control theory and engineering is a mix of three other branches of science: (i) the theory of servomechanisms; (ii) the mathematical theory of variations and differential equations; and (iii) the application and development of computer sciences algorithms, communication and processing hardware.

This section provides the basis of the theory that was used throughout the work of this thesis.

2.1.2 Open-loop, Closed-loop and Digital Control

An open-loop control system uses a pre-established signal to control the actuators driving the system to the desired set point. This type of controller is very limited as any unpredictable occurrence can not be corrected by the controller that has no way of measuring the current state of the controlled system.

In the presence of unpredictable and unstable disturbances, as well as model uncertainties, the original open-loop or feed-forward control is replaced by a more robust type of control called feedback control. This concept uses a sensor to measure the control variable, while the error signal defined as the difference between the reference signal and the measured value is used to correct the system behavior.

Figure 2.1 depicts the difference between open and closed loop control systems.

Analogue systems were initially used to manipulate the error signal and produce the controller signal. With the advent of modern digital processors, analogue to digital and digital to analogue converters, a new type of control system were introduced. The in-

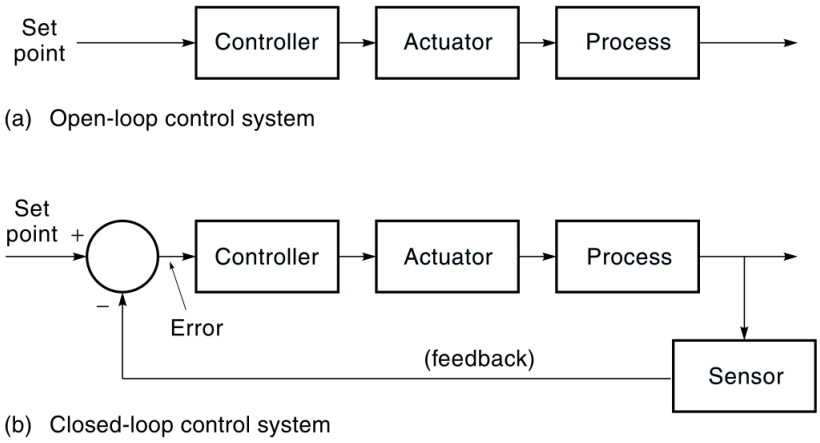

Figure 2.1: (a) Open-loop control system and (b) closed loop or feedback control system diagrams.

troduction on the control chain of digital devices that process the control signal is called digital control. Figure 2.2 presents the feedback control diagram with a digital controller.

Digital controllers have progressively replaced most of the analogue controllers due to the evolution and advantages of some important technologies and processes:

- *Flexibility* The difficulty to modify and redesign a controller after it is implemented in an analogue hardware is one of the major drawbacks digital controllers were able to overcome. A new controller algorithm can be applied to a digital controller by updating the firmware or software running on the same hardware. On the other hand, the update of some parameters in an analogue controller may need the substitution of some hardware parts.
- *Reliability* Digital systems have become more and more reliable with the massive use of the technology in different areas of application. This reliability permitted the application of digital control system in vital areas where expensive devices and human life may be at risk.
- *Evolution* The speed of a digital control system is related to the speed of the computational system used. With the fast increase of computational speed, it is easy to conclude that digital controllers performance have improved very fast during the last decades.
- *Cost* The price of digital systems has decreased significantly with the evolution of technology and production processes. On the other hand precision analogue components become more expensive when compared to high performance digital systems.

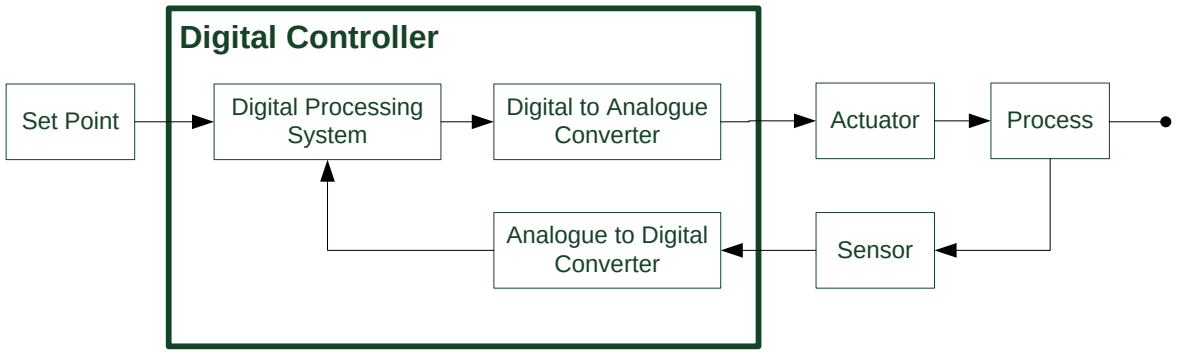

Figure 2.2: Introduction of a digital controller in the feedback control diagram: digital control diagram.

2.1.3 MIMO and SISO Systems

The diagrams presented in the previous section represent control systems with one reference or error input and one control output. These types of system are called Single Input Single Output (SISO) systems. The control of more complex systems requires to control simultaneously several related variables. Since these variables are not independent from each other, the control can not be accomplished by using several independent SISO systems. One Multi Input Multi Output (MIMO) system is necessary to optimize the behavior of the process. Figure 2.3 shows the diagram of a MIMO system.

2.1.4 State Space Model

A MIMO system may have complex relations between the different input and output systems. The analysis of such systems may become too difficult or impossible to analyze based on transfer function conventional control theory. With this limitation in mind modern control theory bases the system description in vector and matrices of differential equations. Using vector-matrix representation the mathematical complexity of increasing the number of state variables, inputs and outputs is minimized becoming only slightly more complex than a classical SISO system.

While classical control theory uses frequency domain to study Linear Time Invariant (LTI) SISO systems, modern control theory adopt the time domain applied to MIMO systems that may be nonlinear and time varying. To accomplish the correct system description, some important definitions are adopted like state, state variables, state vector,

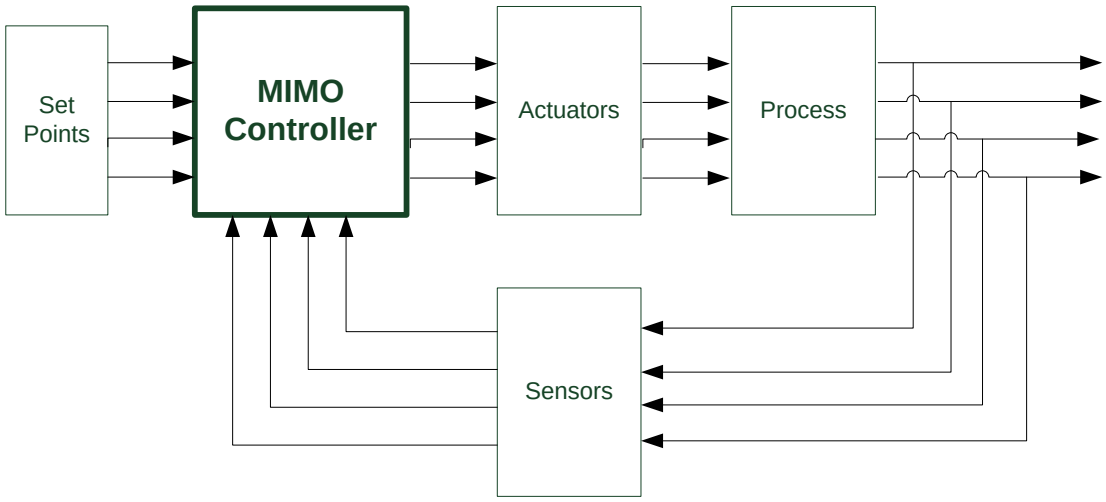

Figure 2.3: Diagram of a MIMO system.

state space and state space equations:

- *State* of a system is defined by a vector with a set of variables that describe the system in a certain moment in time.
- *State Variables* are the smallest set of variables necessary to describe a system in a certain moment. The state variables are not necessarily physically meaningful or measurable. In these cases, they are non observable variables. They can be chosen to facilitate some calculations, but observable variables are preferable when possible to ease implementation of the control system. State variables are used to define the present state of a system. Together with the description of the system given by the system matrices representing its dynamics, and the control inputs, it is possible to determine the future state and behavior of the system.
- *State Vector* is the vector that contains the state variables.
- *State Space* is the n-dimensional space that can be defined by the n state variables in the state vector. The state of the system at any time is a point in the state space.
- *State Space Equations* The modeling of dynamic systems using state space analysis uses state variables, input variables and output variables. The set of equations that describe a dynamic system are not unique depending on the state variables that were chosen. However for a set of state variables, a unique set of equations relate the input, output and state variables according to the description that will briefly follow in this section.

  Considering an LTI system described by n state variables, r input variables and m

output variables, the state equations and the output equations can be written in matrix format as the following simplified equations, where the dot above a quantity represents its time derivative[1]:

$$\dot{x}_{[n]} = A_{[n,n]}x_{[n]} + B_{[n,r]}u_{[r]} \tag{2.1}$$
$$y_{[m]} = C_{[m,n]}x_{[n]} + D_{[m,r]}u_{[r]} \tag{2.2}$$

The matrices coefficients are given by the state equations:

$$\dot{x}_1 = a_{11}x_1 + a_{12}x_2 + ... + a_{1n}x_n + b_{11}u_1 + b_{12}u_2 + ... + b_{1r}u_r \tag{2.3}$$
$$\dot{x}_2 = a_{21}x_1 + a_{22}x_2 + ... + a_{2n}x_n + b_{21}u_1 + b_{22}u_2 + ... + b_{2r}u_r \tag{2.4}$$
$$... \tag{2.5}$$
$$\dot{x}_n = a_{n1}x_1 + a_{n2}x_2 + ... + a_{nn}x_n + b_{n1}u_1 + b_{n2}u_2 + ... + b_{nr}u_r \tag{2.6}$$

and the output equations:

$$y_1 = c_{11}x_1 + c_{12}x_2 + ... + c_{1n}x_n + d_{11}u_1 + d_{12}u_2 + ... + d_{1r}u_r \tag{2.7}$$
$$y_2 = c_{21}x_1 + c_{22}x_2 + ... + c_{2n}x_n + d_{21}u_1 + d_{22}u_2 + ... + d_{2r}u_r \tag{2.8}$$
$$... \tag{2.9}$$
$$y_m = c_{m1}x_1 + c_{m2}x_2 + ... + c_{mn}x_n + d_{m1}u_1 + d_{m2}u_2 + ... + d_{mr}u_r \tag{2.10}$$

The names of the matrices presented are related to its function on equations 2.1 and 2.2:

- *State matrix* using the above equations is given by:

$$A = \begin{bmatrix} a_{11} & a_{12} & \cdots & a_{1n} \\ a_{21} & a_{22} & \cdots & a_{2n} \\ \vdots & \vdots & \ddots & \vdots \\ a_{n1} & a_{n2} & \cdots & a_{nn} \end{bmatrix} \tag{2.11}$$

[1]This notation will be used throughout this chapter

- *Input matrix* using the above equations is given by:

$$B = \begin{bmatrix} b_{11} & b_{12} & \cdots & b_{1r} \\ b_{21} & b_{22} & \cdots & b_{2r} \\ \vdots & \vdots & \ddots & \vdots \\ b_{n1} & b_{n2} & \cdots & b_{nr} \end{bmatrix} \tag{2.12}$$

- *Output matrix* using the above equations is given by:

$$C = \begin{bmatrix} c_{11} & c_{12} & \cdots & c_{1n} \\ c_{21} & c_{22} & \cdots & c_{2n} \\ \vdots & \vdots & \ddots & \vdots \\ c_{m1} & c_{m2} & \cdots & c_{mn} \end{bmatrix} \tag{2.13}$$

- *Direct transmission matrix* (or *feed forward matrix*) using the above equations is given by:

$$D = \begin{bmatrix} d_{11} & d_{12} & \cdots & d_{1r} \\ d_{21} & d_{22} & \cdots & d_{2r} \\ \vdots & \vdots & \ddots & \vdots \\ d_{m1} & d_{m2} & \cdots & d_{mr} \end{bmatrix} \tag{2.14}$$

The vectors also take their names from the function they play in the same equations:

- *State vector* given by the coefficients in the state and output equations:

$$x = \begin{bmatrix} x_1 \\ x_2 \\ \vdots \\ x_n \end{bmatrix} \tag{2.15}$$

- *Input vector* given by the coefficients in the state and output equations:

$$u = \begin{bmatrix} u_1 \\ u_2 \\ \vdots \\ u_r \end{bmatrix} \tag{2.16}$$

- *Output vector* given by the coefficients in the state and output equations:

$$y = \begin{bmatrix} y_1 \\ y_2 \\ \vdots \\ y_m \end{bmatrix} \tag{2.17}$$

Figure 2.4 depicts the block diagram of the graphical representation of state and output equations.

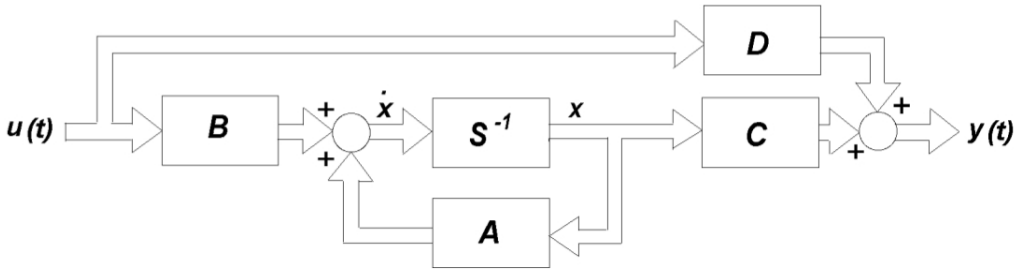

Figure 2.4: Block diagram describing the operations and matrices of an LTI system in state-space. Besides the matrices A, B, C and D and the signal vectors $u(t)$, $x(t)$ and $y(t)$ already defined, the block S^{-1} represents the time integration operator.

2.2 Optimal Control

2.2.1 Introduction

When designing a control system, a set of requirements must be met to improve or satisfy the performance of a system regarding a set of parameters. Using classical methods, as the ones presented in the previous section, the requirements are presented to the systems engineer as a range of acceptable measures to be met by the controller. These requirements can be given in time or frequency domain and usually include parameters such as maximum overshoot, settling time, gain margins, phase margins and steady state error. The need for simultaneously satisfy several of these requirements makes the design process difficult and many times an empirical trial and error task is used. These empirical trial and error tasks may be acceptable and satisfactory when treating SISO systems,

but becomes impossible to adopt when dealing with more complex and multiple variables dependent MIMO systems.

Optimal control theory tries to solve this problem by obtaining the best possible design (optimal control) with reference to one particular performance index that is defined a-priori. Optimal control design replaces the conventional parameters (overshoot, settling time, gain-margin, phase-margin, steady-state error) by one performance index. This gives a high importance to the choice of the correct performance index, because all the design will be based on optimizing this unique parameter.

2.2.2 Optimal Control Problem

The beginning of an optimal control problem is thus to find the path of a system from one state to another, minimizing (or maximizing) the performance index. Examples of performance indexes in a control system include the quantity of energy spent, the tracking error, the controller effort, the amount of time to reach the set point, (or in economy and management) sales of a product, advertising campaign spendings, overall earnings, etc. For the optimal control problem focused in this thesis the performance index that was specially taken into consideration and was minimized was the amount of time to reach a set point.

Depending on the type of problem to be solved, a different performance index can be chosen to optimize the control design. This choice will also imply what variables are free to optimize the performance index. For the formulation and solving of the optimal control problem a set of requirements must be met:

- The system mathematical model;
- The performance index to be optimized;
- The boundary conditions and constraints to be met by states and controls during the process;
- The variables that are left free to optimize the performance index.

2.2.3 Dynamic Programming

2.2.3.1 Introduction

After the performance index is found, a method is used to determine the controller that optimizes this criterion. The Dynamic Programming developed by R. E. Bellman [40][41] and the Pontryagin's Minimum Principle [42] are the methods used to find the optimal

control law that minimizes the performance index. Both methods are presented in this chapter.

Pontryagin's Minimum Principle tries to solve a nonlinear problem to find the optimal control law, while *Dynamic Programming* uses a functional equation that is solved by a digital computer algorithm.

2.2.3.2 Optimality Principle

The principle of dynamic programming is based on the fact that any part of an optimal trajectory has to be also an optimal path. This is called the *Optimality Principle*.

The intuitive conclusion presented in the optimality principle can be applied to the decision making that is necessary when searching for the control law that optimizes a certain path. Considering all the possible paths resulting from the decision of a certain control action that takes the system from one state to the set point, the optimal path is the one that minimizes the cost function.

2.2.3.3 Optimality Principle Application

An example can be considered to illustrate the application of the principle of optimality.

A process in the start state a has several paths resulting from the control decisions that are possible. Considering three possible control decisions the resulting states are b, c and d. Taking the optimal paths from b, c and d to the set point e as J^*_{be}, J^*_{ce} and J^*_{de}, the optimality principle implies that if the initial segments are the optimal paths between ab, ac and ad, the optimal trajectory between a and e is the one that minimizes the cost:

$$C^*_{abe} = J_{ab} + J^*_{be} \tag{2.18}$$

$$C^*_{ace} = J_{ac} + J^*_{ce} \tag{2.19}$$

$$C^*_{ade} = J_{ad} + J^*_{de} \tag{2.20}$$

Dynamic programming is a computer technique that uses the principle of optimality to make sequences of decisions that define the optimal trajectory.

2.2.3.4 Dynamic Programming Example

Let us consider a routing problem, which is a useful example to investigate an algorithm that can be implemented in a computational system. A system in position a must go to the set point position f using an optimal path (figure 2.5).

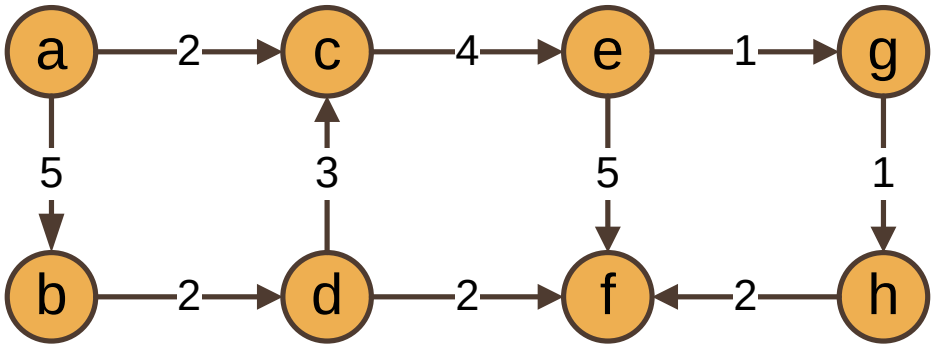

Figure 2.5: A route map for finding the optimal path from any state to the final state f. The number in the path is the postulated cost function and the system can move only to states that respect the direction of the arrows.

The simplest algorithm would be to apply a brute force method to calculate the cost of all allowable paths between a and f. A more efficient algorithm can be used based on the principle presented. At state a two decisions can be made to go to b or c. The optimal path is given by the minimum of two cost functions:

$$C^*_{abf} = J_{ab} + J^*_{bf} \tag{2.21}$$

$$C^*_{acf} = J_{ac} + J^*_{cf} \tag{2.22}$$

where C^*_{xyz} represents the minimum cost from x to z through y, J_{xy} is the cost from x to y and J^*_{xy} is the minimum cost from x to y using any possible path.

The same procedure must then be applied to making the following decisions, minimizing the cost functions:

$$J^*_{bf} = J_{bd} + J^*_{df} \tag{2.23}$$

$$J^*_{cf} = J_{ce} + J^*_{ef} \tag{2.24}$$

The same procedure must continue until the set point is reached. To gain performance when applying the algorithm, the cost of each path should be calculated previously, by "walking" backward from the set point. This is also necessary because the minimum cost to reach the set point from a certain state must be previously calculated to apply the algorithm. Table 2.1 is used for the application of the algorithm to the current example.

Current State	Control Decision	Next State	Minimum Cost Through State	Minimum Cost to Set Point	Optimal Control Decision
α	u_n	x_n	$J_{\alpha x_n} + J^*_{x_n f} = C^*_{\alpha x_n f}$	$J_{\alpha f}$	$u^*(\alpha)$
h	Left	f	2	2	Left
g	Down	h	$1 + 2 = 3$	3	Down
e	Down	f	5	5	
	Right	g	$1 + 3 = 4$	4	Right
c	Right	e	$4 + 4 = 8$	8	Right
d	Right	f	2	2	Right
	Up	c	$3 + 8 = 11$		
b	Right	d	$2 + 2 = 4$	4	Right
a	Right	c	$2 + 8 = 10$		
	Down	b	$5 + 4 = 9$	9	Down

Table 2.1: Application of Dynamic Programming for the control decision of a routing problem.

Table 2.1 gives the minimum cost to reach the set point from any state and, moreover, it gives the optimal decision that optimizes the path to the set point. For example, from state a to reach the set point f the path to follow is not ac (Right) with a cost function of 2, but go to b (Down) with an initial cost function of 5 that is compensated by the cost of the remaining path from b to f.

2.2.3.5 Generalization of Dynamic Programming

The dynamic programming method can be applied to a general system described by a first order differential equation [44]. Consider the system described by the equation:

$$\dot{x}(t) = ax(t) + bu(t) \tag{2.25}$$

where $x(t)$ is the state variable, $u(t)$ the control variable, a and b are constants.

Let the performance measure cost to be minimized be given by:

$$J = x^2(T) + \lambda \int_0^T u^2(t)dt \tag{2.26}$$

For the proper computational treatment, the system equation and cost function must be discretized:

$$x(k+1) = [1 + a\Delta t]x(k) + b\Delta t u(k) \tag{2.27}$$

$$J = x^2(N) + \lambda\Delta t \sum_{k=0}^{N-1} u^2(k) \tag{2.28}$$

with $k = 0, 1, ..., N-1$.

Let $a = 0$, $b = 1$, $\lambda = 2$, $T = 2$ and $\delta t = 1$. In this case $N = 2$ and the system is described by the equation:

$$x(k+1) = x(k) + u(k) \qquad k = 0, 1 \tag{2.29}$$

The performance measure used to minimize the cost and make the decision for the control $u(0)$ or $u(1)$ is:

$$J = x^2(2) + 2u^2(0) + 2u^2(1) \tag{2.30}$$

Let the state and the control variables be subject to the following constraints:

$$0 \leq x(k) \leq 1.5 \qquad k = 0, 1, 2 \tag{2.31}$$

$$-1 \leq u(k) \leq 1 \qquad k = 0, 1 \tag{2.32}$$

To make the calculation suitable for a computer algorithm the possible state and control values must be quantized. The algorithm to find the optimal path from the set point backward is

1. Start from a selected value of k=1 and one of the quantized values of $x(k)$. Try all values of $u(1)$ to calculate the trajectory and cost value. The minimum cost value gives the optimal control.
2. Repeat the same procedure for all the discretized values of $x(k)$, building a table similar to table 2.1.
3. Consider the next stage (always from the set point backward) and repeat steps 1 and 2 for k=0.
4. Repeat the procedure until all stages are covered and all possible states are in the table.

This algorithm can be expressed mathematically by the *Functional Equation of Dy-*

namic Programming [44]:

$$C^*_{kN}(x(k), u(k)) = J_{k,k+1}(x(k), u(k)) + J^*_{k+1,N}(x(k+1)) \tag{2.33}$$

$$J^*_{kN}(x(k)) = min_{u(k)} \left[C^*_{kN}(x(k), u(k))\right] \tag{2.34}$$

2.2.4 Calculus of Variations and Pontryagin's Minimum Principle

2.2.4.1 Introduction

The calculus of variations is an extremely useful tool for solving optimization problems. Sir Isaac Newton began the use of this branch of mathematics to determine the body shape that offers the least air resistance, although some bases to calculus of variations had already been laid in ancient Greece [44].

The aim of optimal control is to find the function that minimizes a functional that is defined as the performance measure. This procedure has an analogous in calculus when the minimum or maximum value of a function is determined.

2.2.4.2 Calculus of Variations

The definition of function is a rule that assigns each value of its domain a value of its range. The definition of functional is analogous to the definition of function. A functional is a rule that assigns to each function f of its space of functions ω, also called domain of the functional, a unique real number. Similar to the function, the set of real numbers that results from the calculation of a functional for the domain elements is the range.

In a practical sense the functional can be seen as a function of functions. For example, $J(x)$ is a functional that represents the area under a function $x(t)$ between t_0 and t_f, given by:

$$J(x) = \int_{t_0}^{t_f} x(t)dt \tag{2.35}$$

The properties usually attributed to functions can also be analysed in terms of a functional. Consider, as an example, the concept of linearity of a function applied to the functional. J is a linear functional if it satisfies the linearity equations for all x in Ω (the principles of homogeneity and additivity):

$$J(\alpha x) = \alpha J(x) \tag{2.36}$$

$$J(x_1 + x_2) = J(x_1) + J(x_2) \tag{2.37}$$

Similar properties may also be extrapolated from the calculus to the mathematics of functional: (i) the norm of a function (analogous to the norm of a real value), (ii) the increment of a functional (analogous to the increment of a function); (iii) the variation of a functional (analogous to the differential of a function); (iv) the maximum and minimum of functional (analogous to the maximum and minimum of functions).

The fundamental theorem of the calculus of variations is the analogous for the theorem of finding extreme values of functions. The necessary condition for the existence of the extreme of a continuous function is that the differential of the function is zero at that point. The corresponding rule for the functional is that the variation must be zero on the extreme of the curve when no bounds are imposed. The formal presentation and proof of the fundamental theorem of the calculus of variations can be found on [44].

A consequence of the theorem is the fundamental lemma of the calculus of variations [45] that states that if:

$$\int_{t_0}^{t_f} h(t)\delta x(t)dt = 0 \tag{2.38}$$

and $h(t)$ is a continuous function, then $h(t)$ must be zero in the interval $[t_0, t_f]$. The reason for this consequence comes from the fact that for the integral to be zero for any arbitrary variation of $x(t)$ ($\delta x(t)$), $h(t)$ must be zero. The application of this lemma is used to find a function x^* that make the functional $J(x)$ have a relative extreme, with $J(x)$ given by [44]:

$$J(x) = \int_{t_0}^{t_f} g(x(t), \dot{x}(t), t)dt \tag{2.39}$$

The necessary condition for x^* to be an extreme is

$$\frac{\partial g}{\partial x}(x^*(t), \dot{x}^*(t), t) - \frac{d}{dt}\left[\frac{\partial g}{\partial x}(x^*(t), \dot{x}^*(t), t)\right] = 0 \tag{2.40}$$

This equation is known as the *Euler Equation*. It is used as an evaluator for finding the function that minimizes or maximizes a functional.

2.2.4.3 Minimization of Functionals Under Constraints Lagrange Multiplier Method for Functionals

This section introduces the *Lagrange Multiplier Method* applied to the minimization of functionals in a more generic case, in which the functional is constrained by a vector of functions that must be satisfied.

Given the functional of the form

$$J(\mathbf{w}) = \int_{t_0}^{t_f} g(\mathbf{w}(t), \dot{\mathbf{w}}(t), t)dt \tag{2.41}$$

with $\mathbf{w}$ a $(n+m) \times 1$ vector of functions that must satisfy n relations:

$$f_i(\mathbf{w}(t), t) = 0 \qquad i = 1, 2, ..., n \tag{2.42}$$

let us find the conditions for a function $\mathbf{w}^*$ to be an extreme of the functional. The n *point constraints* defined have the consequence that only m components of $\mathbf{w}$ are independent.

The Lagrange Multipliers Method can be used to solve this problem. The Lagrange functional is calculated by adjoining the constraining functions:

$$\begin{aligned} J_a(\mathbf{w}, \mathbf{p}) = \int_{t_0}^{t_f} & g(\mathbf{w}(t), \dot{\mathbf{w}}(t), t) \\ & + p_1(t)\left[f_1(\mathbf{w}(t), t)\right] + p_2(t)\left[f_2(\mathbf{w}(t), t)\right] + ... + p_n(t)\left[f_n(\mathbf{w}(t), t)\right] dt \end{aligned} \tag{2.43}$$

where p_1, p_1, ..., p_n are the Lagrange multipliers, which in the case of functionals are functions of t. The equation can be reduced using matrix notation:

$$J_a(\mathbf{w}, \mathbf{p}) = \int_{t_0}^{t_f} \left[g(\mathbf{w}(t), \dot{\mathbf{w}}(t), t) + \mathbf{p}^T(t)\left[\mathbf{f}(\mathbf{w}(t), t)\right]\right] dt \tag{2.44}$$

The variation of the functional is given by

$$\begin{aligned} \delta J_a(\mathbf{w}, \delta\mathbf{w}, \mathbf{p}, \delta\mathbf{p}) = \int_{t_0}^{t_f} & \left[\frac{\partial g^T}{\partial \mathbf{w}}(\mathbf{w}(t), \dot{\mathbf{w}}(t), t) + \mathbf{p}^T(t)\left[\frac{\partial \mathbf{f}}{\partial \mathbf{w}}(\mathbf{w}(t), t)\right]\right] \delta\mathbf{w}(t) \\ & + \left[\frac{\partial g^T}{\partial \dot{\mathbf{w}}}(\mathbf{w}(t), \dot{\mathbf{w}}(t), t)\right] \delta\dot{\mathbf{w}}(t) + \left[\mathbf{f}^T(\mathbf{w}(t), t)\right] \delta\mathbf{p}(t) dt \end{aligned} \tag{2.45}$$

The extremal demands that the following variations and coefficients in the previous

equations are zero:

$$\delta J_a(\mathbf{w}^*, \mathbf{p}) = 0 \tag{2.46}$$

$$\mathbf{f}(\mathbf{w}^*(t), t) = 0 \tag{2.47}$$

$$\delta \mathbf{p}(t) = 0 \tag{2.48}$$

The Lagrange multipliers can be selected arbitrarily and the remaining coefficients of $\delta\mathbf{w}(t)$ become independent. By choosing the Lagrange multipliers that make their components of $\delta\mathbf{w}(t) = 0$ in the interval $[t_0, t_f]$, the following equations must also be satisfied:

$$\frac{\partial g}{\partial \mathbf{w}}(\mathbf{w}^*(t), \dot{\mathbf{w}}^*(t), t) + \left[\frac{\partial \mathbf{f}}{\partial \mathbf{w}}(\mathbf{w}^*(t), t)\right]^T \mathbf{p}^*(t) - \frac{\partial}{\partial t}\left[\frac{\partial g}{\partial \dot{\mathbf{w}}}(\mathbf{w}^*(t), \dot{\mathbf{w}}^*(t), t)\right] = 0 \tag{2.49}$$

Finally an augmented integrand function is defined, including the Lagrange multipliers:

$$g_a(\mathbf{w}(t), \dot{\mathbf{w}}(t), \mathbf{p}(t), t) \equiv g(\mathbf{w}(t), \dot{\mathbf{w}}(t), t) + \mathbf{p}^T(t)\left[\mathbf{f}(\mathbf{w}(t), t)\right] \tag{2.50}$$

The Lagragian method applied to the functionals defines the set of differential equations (2.51) and constraining relations (2.52) that constitute the set of necessary conditions to find the extremal $\mathbf{w}^*$:

$$\frac{\partial g_a}{\partial \mathbf{w}}(\mathbf{w}^*(t), \dot{\mathbf{w}}^*(t), \mathbf{p}(t), t) + \left[\frac{\partial \mathbf{f}}{\partial \mathbf{w}}(\mathbf{w}^*(t), t)\right]^T \mathbf{p}^*(t) - \frac{\partial}{\partial t}\left[\frac{\partial g}{\partial \dot{\mathbf{w}}}(\mathbf{w}^*(t), \dot{\mathbf{w}}^*(t), t)\right] = 0 \tag{2.51}$$

$$\mathbf{f}(\mathbf{w}^*(t), t) = 0 \tag{2.52}$$

2.2.4.4 Optimal Control Law

According to what has been presented, the optimal control law is the function $u(t)$ that drives a system from one state to the desired set point through an optimal path, that minimizes a cost function. This section explains the application of the calculus of variations

that was depicted in the previous section to the optimal control of a dynamic system.

Consider the function $u(t)$ that minimizes the value of the functional:

$$I_{x_i}(u) = \int_{t_i}^{t_f} F(x(t), u(t), t)dt \tag{2.53}$$

Let x be the unique solution of the differential equation

$$\dot{x}(t) = f(x(t), u(t)) \qquad t_i \leq t \leq t_f \qquad x_i = x(t_i) \tag{2.54}$$

Equation 2.54 is the "constrain equation" to be included in the augmented function with the Lagrange multipliers. The augmented functional integrand is given by:

$$F(x(t), u(t), t) + p(t)(f(x(t), u(t)) - \dot{x}(t)) \tag{2.55}$$

Suppose both $F(x(t), u(t), t)$ and $f(x(t), u(t))$ are continuous and differentiable functions and u^* is the optimal control for the functional I_{x_i} defined by equation 2.53 and x is the unique solution of the differential equation 2.54. In this case, for a x^* that is the state corresponding to input u^*, there is a lagragian multiplier p^* that satisfies the following equations:

$$\frac{\partial F(x^*(t), u^*(t), t)}{\partial x} + p^*(t)\frac{\partial f(x^*(t), u^*(t))}{\partial x} = -\dot{p}^*(t) \qquad t_i \leq t \leq t_f \qquad p^*(t_f) = 0 \tag{2.56}$$

$$\frac{\partial F(x^*(t), u^*(t), t)}{\partial u} + p^*(t)\frac{\partial f(x^*(t), u^*(t))}{\partial u} = 0 \qquad t_i \leq t \leq t_f \tag{2.57}$$

This result provides the necessary condition for optimal control, however not every u^* that satisfies the condition must be the optimal solution. A solution of this type is called a critical control. If there is only one critical control and there is an optimal solution, then the critical control must be the optimal solution.

2.2.4.5 The Pontryagin Minimum Principle

The development in this section reformulates the notation of the previous section. Let us define the Hamiltonian $\mathcal{H}$ as:

$$\mathcal{H}(p, x, u, t) = F(x, u, t) + pf(x, u) \tag{2.58}$$

Let $F(x, u, t)$ and $f(x, u)$ be continuously differentiable functions. If u^* is an optimal control of the functional:

$$I_{x_i}(u) = \int_{t_i}^{t_f} F(x(t), u(t), t)dt \tag{2.59}$$

and x is the unique solution of the differential equation:

$$\dot{x}(t) = f(x(t), u(t)) \qquad t_i \leq t \leq t_f \qquad x_i = x(t_i) \tag{2.60}$$

and if x^* is the solution state, then there is a p^* such that

$$\frac{\partial \mathcal{H}(p^*(t), x^*(t), u^*(t), t)}{\partial x} = -\dot{p}^*(t) \qquad t_i \leq t \leq t_f \qquad p^*(t_f) = 0 \tag{2.61}$$

$$\frac{\partial \mathcal{H}(p^*(t), x^*(t), u^*(t), t)}{\partial u} = 0 \qquad t_i \leq t \leq t_f \tag{2.62}$$

We can also express the differential equation $\dot{x}(t) = f(x(t), u(t))$ with $x_i = x(t_i)$ as

$$\frac{\partial \mathcal{H}(p^*(t), x^*(t), u^*(t), t)}{\partial p} = \dot{x}^*(t) \qquad t_i \leq t \leq t_f \qquad x_i = x(t_i) \tag{2.63}$$

These equations are the *Hamilton differential system.* The function $p^*(t)$ is called the co-state and equation 2.61 is the *adjoint differential equation.* The analogy with Hamiltonian mechanics motivated Pontryagin research that led to the *Pontryagin Minimum Principle* [43][44]. This principle was formulated in 1956 by the Russian mathematician Lev Semenovich Pontryagin and is used in optimal control theory to build the optimal control law of a system.

The Pontryagin minimum principle states that if $F(x, u, t)$ and $f(x, u)$ are continuously differentiable functions and u^* is an optimal control to the functional

$$I_{x_i}(u) = \int_{t_i}^{t_f} F(x(t), u(t), t)dt \tag{2.64}$$

subject to the differential equation

$$\dot{x}(t) = f(x(t), u(t)) \qquad t_i \leq t \leq t_f \qquad x_i = x(t_i) \tag{2.65}$$

and if x^* is the solution state, then there is a co-state p^* such that

$$\frac{\partial \mathcal{H}(p^*(t), x^*(t), u^*(t), t)}{\partial x} = -\dot{p}^*(t) \qquad t_i \leq t \leq t_f \qquad \dot{p}^*(t_f) = 0 \tag{2.66}$$

and for all t in $t_i \leq t \leq t_f$

$$\mathcal{H}(p^*(t), x^*(t), u(t), t) \geq \mathcal{H}(p^*(t), x^*(t), u^*(t), t) \tag{2.67}$$

The complete derivation and examples of use of Pontryagin principle can be found in the literature [44][46][47][48].

2.2.4.6 The Minimum Time Problem

This section considers the problem of transferring a system from an initial state to a specified set state in the minimum time possible [44].

The set point is denoted by $S(t)$ and the minimum time to reach the set point by t^*.

Let the system be described by the equation:

$$\dot{x}(t) = a(x(t), u(t), t) \tag{2.68}$$

The initial state is X_0 and the function to minimize is

$$J(u) = \int_{t_0}^{t_f} dt = t_f - t_0 \tag{2.69}$$

The control variables are usually constrained by power or other requirements, expressed mathematically by

$$|u_i(t)| \leq 1 \qquad j = 1, 2, ..., m \qquad t_0 \leq t \leq t^* \tag{2.70}$$

Let us consider the example of a controlled missile that travels in the direction of a moving target. For simplicity the movement is in one dimension only. The missile initial position is $x = 0$ and the target is $x = a$. Moreover, the target movement is given by the equation of motion:

$$x_{Target} = a + 0.1t^3 \tag{2.71}$$

This equation defines also the set point $S(t)$ that the missile must reach.

If the missile mass is unity the missile motion is described by:

$$\ddot{x} = u(t) \tag{2.72}$$

Using the equivalent variables ($x_1(t) \equiv x(t)$; $x_2(t) \equiv \dot{x}(t)$), we can use the state form:

$$\dot{x_1} = x_2(t) \tag{2.73}$$

$$\dot{x_2} = u(t) \tag{2.74}$$

The thrust must be constrained to a maximum. Let the following relationship define that maximum:

$$|u(t)| \leq 1 \tag{2.75}$$

A trivial example can be considered. The optimal strategy for the control of the missile is to accelerate with the maximum thrust in the positive direction ($u^*(t) = 1$) until it hits the target at t^*. The value of t^* can be determined by solving the equation:

$$\frac{1}{2}(t^*)^2 = a + 0.1(t^*)^3 \tag{2.76}$$

If this equation has no positive solution it means that the target is initially far enough so it can escape from the missile. For $a > 1.85$ this is the situation, while for $a = 1.85$ the minimum time is $t^* = 3.33$.

A1though this is an extremely simplified example, it already illustrates very important characteristics that are relevant for minimum time problems:

- It may happen that for certain initial conditions the time optimal control does not exist;
- The optimal time control, if exists, is the maximum effort during the total time control interval.

2.2.4.7 Minimum Time Control of a Linear Time Invariant System

Let us consider the minimum principle to determine the optimal control of the Linear Time Invariant (LTI) System of order n with m controls, given by:

$$\dot{\mathbf{x}}(t) = \mathbf{A}\mathbf{x}(t) + \mathbf{B}\mathbf{u}(t) \tag{2.77}$$

Consider the system is controllable and the control vector is constrained to

$$|u_i(t)| \leq 1 \qquad i = 1, 2, ..., m \tag{2.78}$$

We want to find the control that takes the system from an arbitrary initial state (x_0)

to the final state ($x(t_f) = 0$) in the minimum time. This problem is usually called in the literature as *stationary linear regulator minimum time problem.*

Let us assume some important consequences of the Pontryagin Principle when applied to the minimum time control of an LTI system [44]:

- The optimal time control of an LTI system is a bang-bang controller.
- Optimal control to take the system from any initial state to origin (or any other set point properly defined) exists if all eigenvalues of $\mathbf{A}$ have nonpositive real parts.
- If the optimal control exists, it is unique.
- If all eigenvalues of $\mathbf{A}$ are real and time optimal control exists, the number of switches for each control component is at most $(n-1)$.

Let us consider the example of a simple system, given by:

$$\dot{x}_1(t) = x_2(t) \tag{2.79}$$

$$\dot{x}_2(t) = u(t) \tag{2.80}$$

which we want to take from an initial state x_0 to the origin in the minimum time possible. Note that matrices $\mathbf{A}$ and $\mathbf{B}$ are given by:

$$\mathbf{A} = \begin{bmatrix} 0 & 1 \\ 0 & 0 \end{bmatrix} \tag{2.81}$$

$$\mathbf{B} = \begin{bmatrix} 0 \\ 1 \end{bmatrix} \tag{2.82}$$

The eigenvalues of A are both zero. In consequence of this and the Pontryagin Principle, we can already conclude that an optimal control exists, is unique, and has one switching at most.

The Hamiltonian is given by:

$$\mathcal{H}(x(t), u(t), p(t)) = 1 + p_1(t)x_2(t) + p_2(t)u(t) \tag{2.83}$$

The minimum principle requires that the optimal control must satisfy:

$$p_2^*(t)u^*(t) \leq p_2^*(t)u(t) \tag{2.84}$$

for all $u(t)$ in the interval $[t_0, t_f]$.

The optimal control law is then given by:

$$u^*(t) = \left\{ \begin{array}{ll} -1 & \leftarrow p_2^*(t) > 0 \\ +1 & \leftarrow p_2^*(t) < 0 \end{array} \right\} \tag{2.85}$$

The Hamiltonian costate equations are

$$\dot{p_1^*}(t) = 0 \tag{2.86}$$

$$\dot{p_2^*}(t) = 0 - p_1^*(t) \tag{2.87}$$

Which lead to the following solutions:

$$p_1^*(t) = c_1 \tag{2.88}$$

$$p_2^*(t) = -c_1 t + c_2 \tag{2.89}$$

with c_1 and c_2 constants of integration. Equation 2.89 is the equation of a straight line that changes sign only once. As a consequence u^* also changes sign at most once, which confirms that the optimal control has at most one switch.

The optimal control law $u^*(t)$ is given by one of the following expressions, depending on the initial state:

- $+1 \leftarrow t \in [t_0, t_f]$
- $-1 \leftarrow t \in [t_0, t_f]$
- $+1 \leftarrow t \in [t_0, t_s[$ and $-1 \leftarrow t \in [t_s, t_f]$
- $-1 \leftarrow t \in [t_0, t_s[$ and $+1 \leftarrow t \in [t_s, t_f]$

with t_f the time to reach the set point and t_s the switch control time.

The optimal trajectories can be calculated integrating the state equations, given the optimal control $u = \pm 1$:

$$x_2(t) = \pm t + c_3 \tag{2.90}$$

$$x_1(t) = \pm \frac{1}{2} t^2 + c_3 t + c_4 \tag{2.91}$$

where c_3 and c_4 are constants of integration and the sign correspond to $u = \pm 1$. The system is solved to eliminate the variable of time to obtain the state-space trajectories:

$$x_1(t) = \frac{1}{2} x_2^2(t) + c_5 \qquad \leftarrow \qquad u = +1 \tag{2.92}$$

$$x_1(t) = -\frac{1}{2}x_2^2(t) + c_6 \qquad \leftarrow \qquad u = -1 \tag{2.93}$$

These equations define the possible paths in the state-space for the maximum control (positive or negative) applied to the system. Figure 2.6 shows several possible such trajectories.

Let us now consider several initial states A_0 to A_5 in figure 2.7. The state space diagram shows the time optimal trajectories from the initial states to the origin, as well as the location of the control switch for each trajectory.

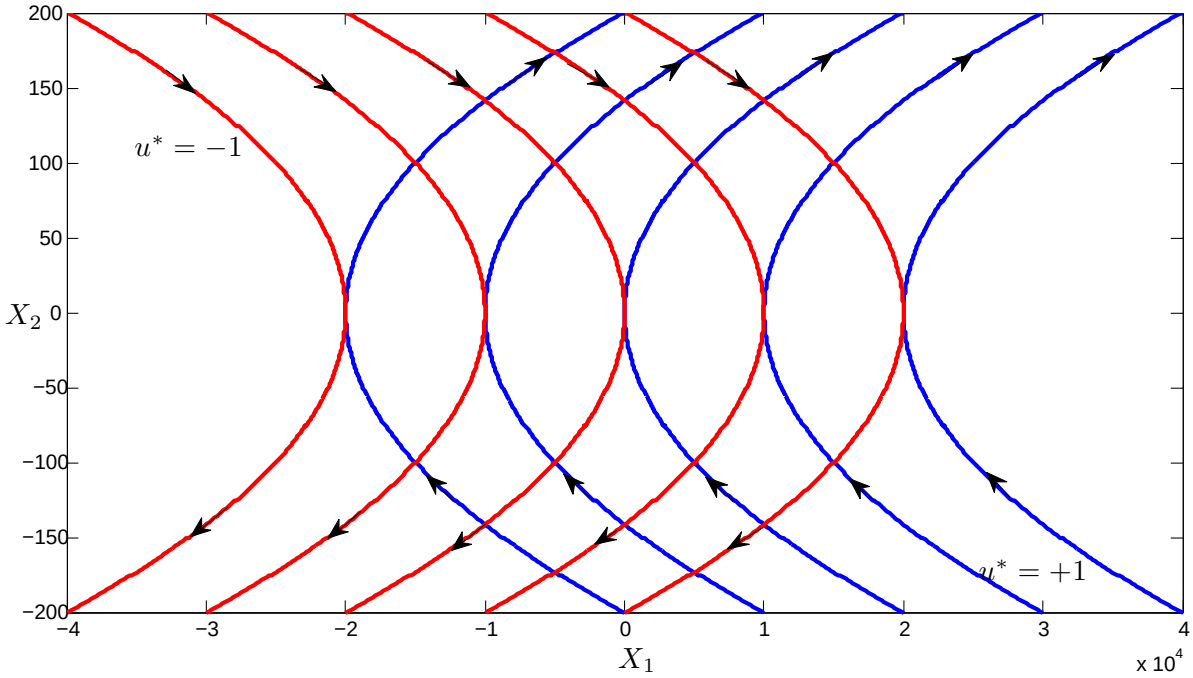

Figure 2.6: A set of possible trajectories for $u = +1$ in blue and $u = -1$ in red. The arrows point in the direction of increasing time.

Depending on the initial state, the optimal trajectory has a different control switch position:

- State positions A_0 and A_1 are in the segments of optimal trajectories without the need of control switching. These positions define the switching curve $A_0 - 0 - A_1$. Equation 2.94 describes that switching curve:

$$x_1(t) = -\frac{1}{2}x_2(t)|x_2(t)| \tag{2.94}$$

- State positions A_2 and A_3 are "under" the switching curve. The initial optimal control

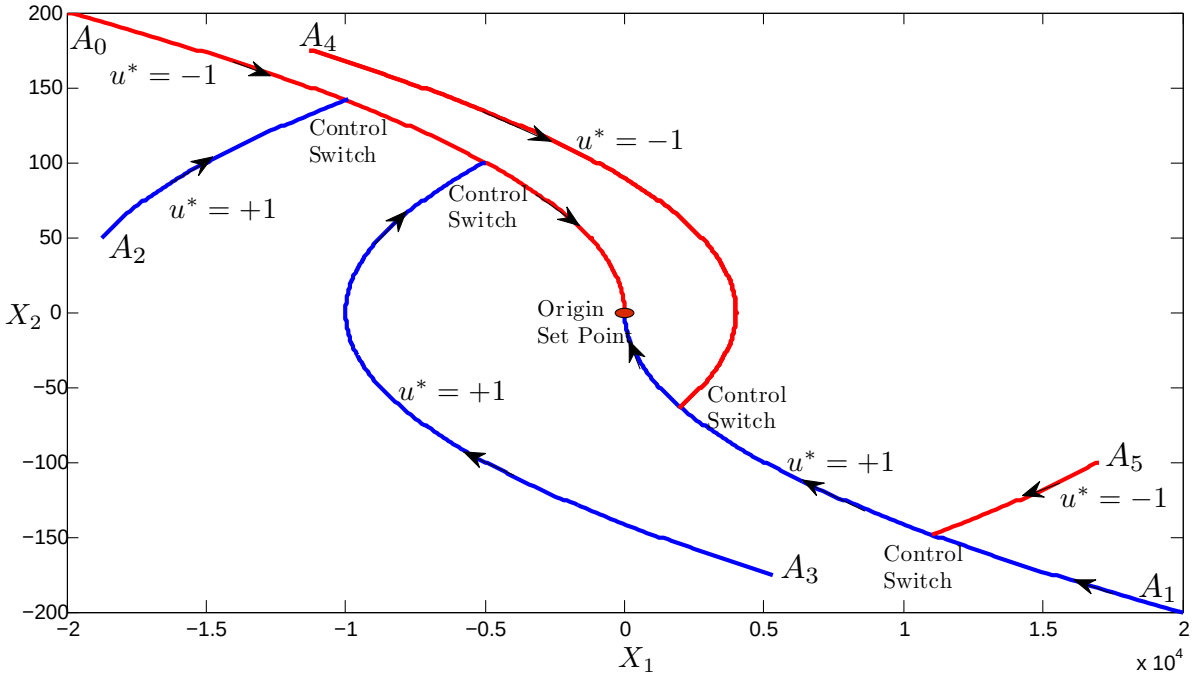

Figure 2.7: Switching curve and optimal trajectories for different initial state values.

is $u^* = +1$ until the system crosses the switching curve, where the optimal control switches to $u^* = -1$.

- State positions A_4 and A_5 are "above" the switching curve. The initial optimal control is $u^* = -1$ until the system crosses the switching curve, where the optimal control switches to $u^* = +1$.

The optimal control law can be described mathematically as a function of the system state $x(t)$ using the *switching function* $S(x(t))$:

$$S(x(t)) = x_1(t) + \frac{1}{2}x_2(t)|x_2(t)| \tag{2.95}$$

The optimal control law is thus given by:

$$u^*(t) = \left\{ \begin{array}{cc} -1 & \leftarrow S(x(t)) > 0 \\ +1 & \leftarrow S(x(t)) < 0 \\ -1 & \leftarrow S(x(t)) = 0 \text{ and } x_2(t) > 0 \\ +1 & \leftarrow S(x(t)) = 0 \text{ and } x_2(t) < 0 \\ 0 & \leftarrow S(x(t)) = 0 \text{ and } x_2(t) = 0 \end{array} \right\} \tag{2.96}$$

2.2.5 Conclusions on the Time Optimal Control

The minimum time control of an LTI system has some important properties and some conclusions that may be referenced as the base for the application of optimal control theory to the vertical plasma stabilization. The problem discussed lays the foundations to the one presented in chapter 5 of this thesis to find the time optimal controller to take the vertical plasma position to the origin or the desired set point in the minimum time.

The main conclusions to retain from this section are:

- Time optimal control for a large class of systems is one that switches between its maximum and minimum admissible values (bang-bang control).
- The procedure for finding the time optimal control law for an LTI systems was presented for a simple second-order system.

The procedure is conceptually simple with no serious limitations, but some constraints can be already pointed:

- Higher-order systems (n $>$ 3) present analytical expressions for the switching surface that are difficult or impossible to obtain .
- Implementation of the control law expression may be too complex leading to suboptimal, easier to implement solutions.
- The procedure is not valid for nonlinear systems in general, due to the difficulty of integrating the differential equations analytically .

3

Plasma Control in Tokamaks

Contents

"The beautiful thing about learning is that nobody can take it away from you."
B.B. King

3.1 Tokamak Control

3.1.1 Introduction

A tokamak is a very complex device with many different components that are built together to fulfill the purpose of creating and maintaining a very hot plasma with the ultimate goal of achieving fusion reactions. The pursue of understanding the interaction between the device and the plasma as well as the need of improving the plasma performance and stability have led to an increasing interest in the application of modern control theory and innovative methods to the control of tokamak plasmas. A clear example of this interest is the number of PhD thesis in this area ([49], [50], [51], [52], [53], [54])[1], the number of papers published on relevant scientific journals and presented in some important conferences as well as the special issues that have been published on this matter[2]. This thesis is also a small contribution towards the goal of improving the control and stability of tokamak plasmas.

This chapter tries to highlight the physics and control theory necessary for the application to the control of tokamak plasmas, the physics and engineering involved in the processes, as well as the main models and codes that have been developed for simulation, data analysis and tokamak control. The work presented here is not a full review of the research work developed in the area, but it is meant to be a summary of the knowledge that has been acquired and used in the course of the research and development work that has led to this Ph.D. thesis.

3.1.2 Plasma Vertical Stabilization Control

A vertically elongated plasma has several important advantages since it allows the creation of divertor plasmas, the increase of the plasma current and density limit as well as it provides better plasma stability (see section 5.1).

[1]References [49], [50] and [51] are important contributions to the hardware and software technologies used for plasma control, while references [52], [53] and [54] are strong improvements to the plasma modeling and tokamak control theory.

[2]Two important examples of this type of publications are the IEEE Control Systems Magazine on Control of Tokamak Plasmas (October 2005) and Fusion Engineering Design Special Issue on "Design and implementation of real-time systems for magnetic confined fusion devices" (March 2014).

However, an elongated plasma is unstable due to the forces that pull the plasma column upward or downward respectively on its top and bottom. The result of these forces is a plasma configuration that tends to be pushed up or down depending on the initial displacement disturbance. For example, a small displacement downwards results in the lower poloidal field coils pulling the plasma down, with increased strength as the plasma gets further from the equilibrium position. To compensate this instability, feedback controllers have been designed to correct the vertical position displacement [31][32][55][56][57].

The design of vertical stabilization feedback controllers has been based in simple models, resulting in experimentally tuned Single Input Single Output (SISO), Proportional Integral and Derivative (PID) regulators. This procedure requires an in-depth experimental treatment that is time consuming and demands a big number of experimental discharges to obtain the necessary optimization of the controller gains.

The typical way to address the vertical stabilization problem is to independently control the vertical plasma position from the plasma current and shape controllers [58] (figure 3.1), which are designed on the basis that the system is vertically stable due to the controller already implemented. This double loop arrangement simplifies the design of the controllers, based on the assumption and later confirmation that the controllers act on different time scales. Diverse frequencies in the controllers permit the treatment of some parameters as disturbances to the next stage of the global controller.

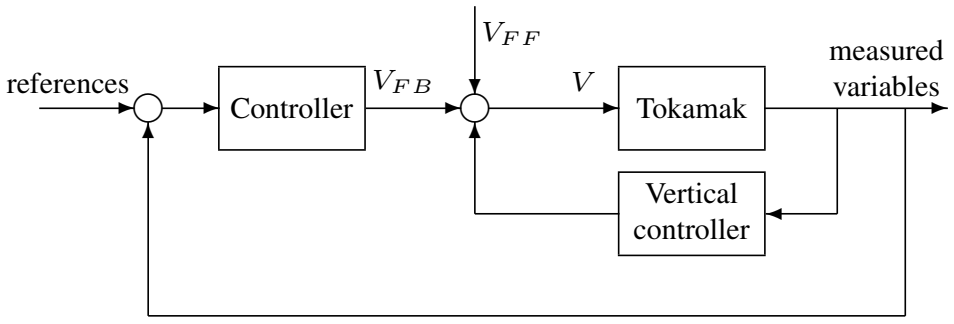

Figure 3.1: A simplified controller scheme that reflects the possibility of separating the vertical stabilization control from the rest of the plasma control [58]. The V_{FB} and V_{FF} are the input signal voltage for Feed Back and Feed Forward Control respectively.

3.1.3 Discharge Concept

A tokamak is a device that is operated in a pulsed mode due to the saturation of its transformer iron core and/or the consumption of the Volt-seconds available in its central solenoid (inductive operation) as well as due to technical constrains of the auxiliary equipment used for non-inductive plasma current drive[3]. Each tokamak discharge can be divided into the following phases [59]:

- *Breakdown*, where the gas inside the vacuum vessel is transformed into a plasma. This phase does not require feedback control. The plasma is created based on feed forward control with pre-established control signals.
- *Ramp up*, where all quantities that were set for the desired type of plasma are linearly ramped until they reach the set points. Special attention is given to the control of the rise of the plasma current as well as of the radial position of the plasma column in the vacuum vessel while the plasma volume grows. Usually the plasma has circular cross section during this segment of the discharge aiming at avoiding vertical instability.
- *Flat top*, which is the main part of the discharge, where all plasma parameters shall be maintained stable and constant, by appropriate control. It is during this phase that fusion reactors will produce energy, and control efforts must be made to maintain the plasma avoiding any events that may cause its collapse.
- *Ramp down* where the plasma is finished in normal operation[4] by reducing the plasma current to zero and gradually reducing the plasma volume.

Control of different plasma parameters must be applied during all the discharge. However, the phase of interest concerning the vertical instability feedback control is the flat top, because it is when the plasma becomes not only more elongated in order to improve its performance, but also more vertically unstable.

[3] A problem for the operation of a tokamak based fusion reactor is how to transform pulsed operation into continuous energy production. Two solutions are envisaged: to use either energy storage or two tokamak operating alternately.

[4] Sometimes the tokamak discharges are abruptly interrupted by disruptions caused by instabilities generated inside the plasma. These disruptions might be very dangerous since large amounts of energy go from the plasma to the vacuum vessel wall.

3.2 Physics for Plasma Modeling

3.2.1 The Ideal Magnetohydrodynamics Equations

Magnetohydrodynamics (MHD) is one of the theories that describe the behavior of a magnetic confined plasma[5]. This theory considers the plasma as a neutral fluid that conducts electrical currents. The MHD equations are given by the Maxwell Equations and Ohm Law, which take into account the electromagnetic properties of the plasma, as well as the flow and mass conservation continuity equations that take into account the fluid nature of the plasma. This set of equations govern the plasma behavior and interactions, when the plasma is considered as a single fluid with mass density ρ_m with a ratio of specific heats γ, plasma velocity v, plasma pressure p, charge density ρ, current density j, electrical conductivity σ, vacuum electric permittivity ϵ_0, exposed to an electric field E and to a magnetic field B :

Faraday Law

$$\nabla \times E = -\frac{\partial B}{\partial t} \tag{3.1}$$

Ampere Law

$$\nabla \times B = \mu_0 j + \mu_0 \epsilon_0 \frac{\partial E}{\partial t} \tag{3.2}$$

Gauss Law (electric field)

$$\nabla . E = -\frac{\rho}{\epsilon_0} \tag{3.3}$$

Gauss Law (magnetic field)

$$\nabla . B = 0 \tag{3.4}$$

Ohm Law

$$E + v \times B = \frac{j}{\sigma} \tag{3.5}$$

Flow Equation

$$\rho_m \frac{\partial v}{\partial t} = j \times B - \nabla p \tag{3.6}$$

[5]A magnetic confined plasma can also be described by the kinetic theory.

Adiabatic Energy Equation

$$\frac{d}{dt}\left(\frac{p}{\rho_m^{\gamma}}\right) = 0 \tag{3.7}$$

Continuity Equation

$$\frac{\partial \rho_m}{\partial t} + \nabla.(\rho_m v) = 0 \tag{3.8}$$

Taking into consideration the quasi-static approximation, $\rho \approx 0$, Gauss and Ampere Laws can be simplified. Moreover, considering an ideal MHD flow with negligible plasma velocity, one obtains:

$$\frac{\partial \rho_m}{\partial t} = 0 \tag{3.9}$$

$$\frac{\partial B}{\partial t} = 0 \tag{3.10}$$

The mass density and magnetic field are constant in time and equilibrium implies that Lorentz forces compensate plasma kinetic pressure:

$$\nabla p = j \times B \tag{3.11}$$

This equation is used with the Gauss Law and simplified Ampere Law to form the ideal MHD description of a tokamak plasma under equilibrium conditions:

$$\nabla.B = 0 \tag{3.12}$$

$$\nabla \times B = \mu_0 j \tag{3.13}$$

3.2.2 The Grad-Shafranov Equation

The given ideal MHD equations are better applied when expressed in terms of a different notation that emphasizes the axysymetric geometry of the toroidal vessel (figure 3.2), assuming that there are no variations along the toroidal angle Φ.

Using the cylindrical coordinates described in figure 3.2, the equilibrium equations can be expressed by the Grad-Shafranov equilibrium Equation [61][62]:

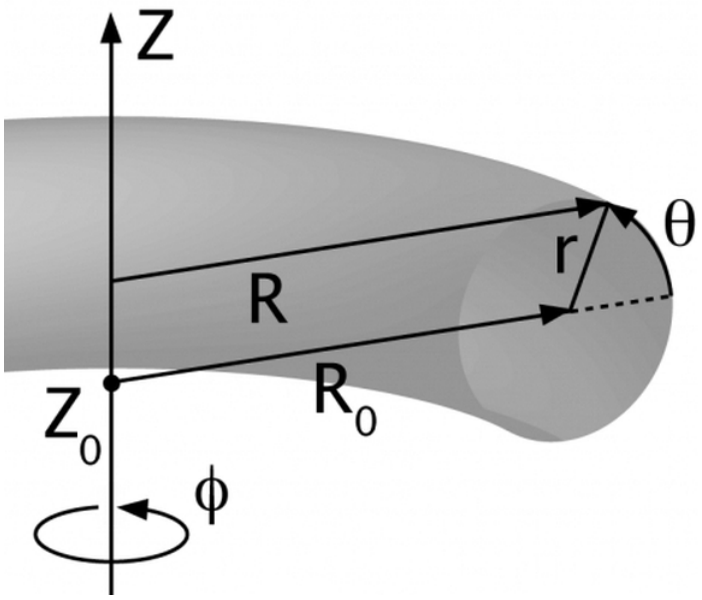

Figure 3.2: Polar coordinates (r,θ) of a circular plasma poloidal section defined by the axis (R_0, Z_0) in general cylindrical coordinates (R, Φ, Z).

$$\Delta^* \psi = -\mu_0 R^2 \frac{dp}{d\psi} - F\frac{dF}{d\psi} \tag{3.14}$$

where the elliptic operator Δ^* is given by:

$$\Delta^* \equiv R^2 \nabla \cdot \left(\frac{1}{R^2}\nabla\right) = R\frac{\partial}{\partial R}\left(\frac{1}{R}\frac{\partial}{\partial R}\right) + \frac{\partial^2}{\partial Z^2} \tag{3.15}$$

In this equation the functions toroidal flux $F(\psi)$ and pressure $p(\psi)$ are both dependent of the poloidal flux ψ, which is simultaneously a dependent and independent variable of the equation.

The complete explanation and deduction of Grad-Shafranov equation can be found in the original papers by Shafranov [61][62] but also in more recent descriptions [52][63][64].

3.2.3 Transport Equations

The solution of the Grad-Shafranov equation can be used together with transport equations [65][66] to simulate the time evolution of the plasma. The computational algorithm used in the simulations follows the steps [67]:

- Initial equilibrium calculation using initial values of ψ, p and F;
- Using the transport equations, the algorithm calculates the new parameters after a

small time evolution δt, with the algorithm typically tracking the time evolution of the functionals $N(\psi)$, $T(\psi)$ and ψ ;

- A new equilibrium is calculated for the new time t.

Some of the most used transport equations are more accurate for small time intervals, because of errors due to the difficulty of attaining deep physical understanding of all the involved processes. By maintaining small time intervals between equilibrium reconstructions, more computational power and time are necessary, but the error is kept small enough to provide valid calculations of plasma equilibrium over time. Moreover, using small time steps is necessary due to the (i) convergence of the numerical solvers used; (ii) avoidance of convergence loops at every time step, as they are necessary in each time step only if the equilibrium changes and needs to be recalculated.

Some transport equations used in less complex simulation codes [67] are:

- *The magnetic field diffusion equation* describing the magnetic field evolution in the conduction fluid.
$$\frac{\partial B}{\partial t} = \nabla \times (v \times B) + \eta_0 \nabla^2 B \tag{3.16}$$
where $\eta_0 = \frac{1}{\mu_0 \sigma}$ is the magnetic diffusion factor.
- *The particle density equation* valid for electrons and ions in a plasma, where the index p should me replaced for e or i accordingly.
$$\frac{\partial n_p}{\partial t} + \nabla.(n_p.v_p) = S_p \tag{3.17}$$
where S_p is the source term[6] and n_p is the particle density [65].
- *The energy balance equation* describes the evolution of the ion and electron pressure of the plasma.
$$\frac{3}{2}\frac{\partial p_p}{\partial t} + \nabla.(\frac{3}{2}p_p.v_p) + p_p \nabla.v_p + \nabla.q_p = Q_p \tag{3.18}$$
where q_p is the heat flux and Q_p is the heat generated in the plasma.

3.2.4 Plasma Models for Tokamak Control Physics

The tokamak plasma control aims at maintaining the plasma shape, current and position during the flat top part of a discharge. Given the reference signals and the measures from the plasma diagnostics, the controller is designed to minimize these errors, even in the

[6]The source term includes variation of density due to the production or annihilation of particles, as well as any particles being injected into the plasma.

presence of disturbances. The aim of the controller is to recover the plasma parameters from the perturbations occurring in the required range for the different specifications (settling time, maximum displacement, plasma current and shape).

It is important to note that the controller must be designed according to the resources available in each device. Special attention is usually given to the modelization of all coil currents and voltages that are limited by design to lower its production costs and due to the maximum power available in the plant for use in feedback control.

The modeling of a tokamak plasma demands very complex mathematical calculation, in depth physical knowledge and very high computational power for numerical calculation during the simulation phase. Different paths and approaches have been tried to accomplish this mission.

The simpler models consider the plasma as a filament or non-deformable matrix of conducting filaments. The more complex models include nonlinear codes featuring a full domain plasma transport code coupled to free boundary equilibrium codes with feedback control element, which permit the simulation of nonlinear behaviors such as large vertical position displacements.

These are some of the most important plasma models and reconstruction codes already developed by different research teams[7] [67]:

- *PET* is a free boundary plasma equilibrium evolution code developed at the Efremov Scientific Research Institute, St. Petersburg [68].
- *ASTRA* [69] (Automated System for TRansport Analysis) is a code to solve a set of transport equations in toroidal geometry. This code is presently used to make transport simulations of tokamak and stellarator plasmas. The first version of ASTRA was implemented at the Kurchatov Institute in Moscow, but an international community continues to develop the code and new features are regularly added to its functionality.
- *TSC* (Tokamak Simulation Code) was originally developed by S. C. Jardin at Plasma Physics Laboratory, Princeton University for free boundary 2D transport [70].
- *EFIT* (Equilibrium FITting) is a code developed to perform magnetic and kinetic-magnetic analysis for Doublet-III, at General Atomics. EFIT takes the measurements from plasma diagnostics and calculates relevant plasma properties such as geometry, stored energy and current profiles. Although it is a very fast computational code, it

[7]The difference between a plasma model and a plasma reconstruction code can be expressed in the following concepts: (i) The plasma model is used to predict the evolution of the plasma parameters, based on plasma measurements or on previous model calculations; (ii) The plasma reconstruction code is a computer algorithm that uses plasma measurements to calculate other relevant indirect plasma properties such as shape, position or current profile.

lacks the accuracy of other more computational intensive algorithms[8] [71].

- *FBT* (Free Boundary Tokamak) is a code originally developed by F. Hofmann at Centre de Recherches en Physique des Plasmas, École Polytechnique Fédérale de Lausanne. FBT allows the computation of arbitrarily shaped tokamak equilibrium specially dedicated to highly shaped and elongated plasmas [72][73].
- *PROTEUS* is a nonlinear tokamak simulation code that solves the Grad-Shafranov equation by an iterative finite element method. This code is used to simulate the evolution of a tokamak plasma for a fixed plasma current [74].
- *CREATE-L* is a linearized plasma equilibrium response model in view of the plasma current, position and shape control in tokamaks [75][76]. The origin of this code's name is the consortium where it was originally developed, the *Consorzio di Ricerca per l' Energia e le Applicazioni Tecnologiche dell'Elettromagnetismo* (CREATE).
- *DINA* is a tokamak plasma axis symmetric, time-dependent, resistive MHD simulation code and a free boundary equilibrium solver developed at the RRC Kurchatov and TRINITI institutes in Moscow [77].
- *RZIP* is a rigid plasma model that predicts the plasma current, as well as the radial and the vertical plasma positions, used at Centre de Recherches en Physique des Plasmas, Lausanne [78].

Some of these codes are accurate for plasma simulation and reconstruction but due to its complex structure they require extra effort to ensure robustness, numerical stability/convergence for any plasma scenario and some of them are too CPU intensive for real time plasma control. The design of the control system is based on simpler linear models that ensure the stability, robustness and performance of the controller, provided that the states are not too far from equilibrium. Controllers are thus usually designed based on the linear model of the flat top phase, achieving good performance through the whole discharge due to its robustness.

Linear models for control design purposes use electric circuit equations to calculate the time evolution of the plasma current, as well as the current on the control coils and passive conductors. Equations of the type [76]:

$$\frac{d\Psi}{dt} + \mathbf{RI} = \mathbf{V} \tag{3.19}$$

[8] Although it should be emphasized that an intensive computational algorithm alone is not enough to achieve accuracy. Rather all the physics model, the limitations and simplifications assumed as well as the diagnostics precision contribute for the final accuracy of the plasma properties.

are used, where Ψ is the vector of fluxes for each conductor, $\mathbf{R}$ is the resistance matrix, $\mathbf{I}$ is the vector of conductor currents and $\mathbf{V}$ is the vector of applied voltages.

Two examples of linear models are the CREATE-L and the RZIP. While the first considers the plasma deformation through the calculation of the plasma current distribution equilibrium, the second is an enhanced non deformable model that permits the variation of the vertical and radial position, as well as the total plasma current. RZIP was used for the design of the controller presented in chapter 5, where more details on the RZIP implementation for TCV are presented.

3.3 Diagnostics and Actuators

3.3.1 Introduction

Precise control of the plasma parameters in a magnetic fusion device implies accurate measurements of relevant plasma properties as well as appropriate and carefully design and implementation of the actuators aiming at correcting the variables that drift from the desired set points.

3.3.2 Diagnostics

3.3.2.1 Introduction

Plasma diagnostics are used to measure and/or to calculate information about at least one plasma parameter, from the analysis of physic processes or its effects occurring in the plasma. Many times it is necessary to define a complex chain of deduction, only possible from the deep understanding of the involved physics processes, in order to make some of these measurements or to evaluate indirectly the plasma parameter. For instance, plasma shape and position can not be measured with accuracy directly based on magnetic measurements and other diagnostics are envisaged to improve the measurement precision[9]

The so-called magnetic diagnostics are still today the main tools that provide information for real-time plasma control. However, several limitations of these diagnostics, particularly in ITER[10], have led to the increase use in real-time plasma control of other

[9] Although plasma shape is determined mainly by magnetic measurements, plasma position can also be determined by other diagnostics such as X-ray tomography or reflectometry [79].

[10] The ITER radiation could damage the magnetic diagnostics, specially those that are in the inside part of the vacuum vessel.

diagnostic techniques. Some examples of these techniques are microwave reflectometry, X-ray spectroscopy and Thomson scattering.

3.3.2.2 Magnetic Diagnostics

Figure 3.3 depicts the main types of magnetic diagnostic techniques used for real-time plasma control.

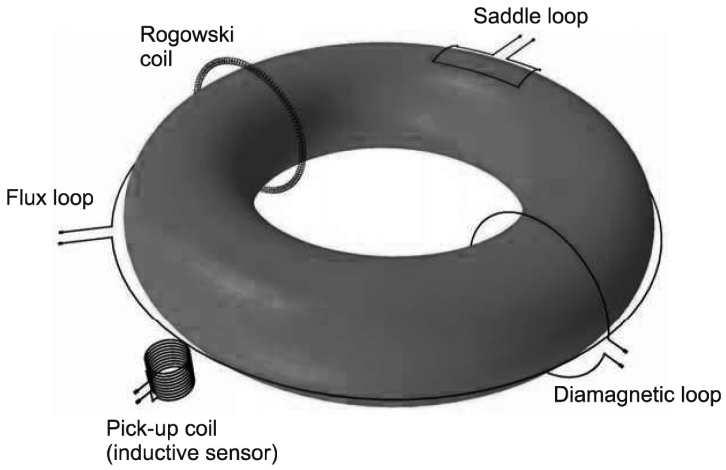

Figure 3.3: Basic magnetic diagnostics for a tokamak plasma.

The voltage applied to create the plasma current is measured by means of the flux loop parallel to the plasma column. The plasma current (I_p) is measured by integrating the signal from the Rogowski coil[11]. The poloidal magnetic field (B_θ) and the radial magnetic field (B_r) used for plasma position control are measured using a set of magnetic pick-up coils[12]. The energy in the plasma, the normalized pressure (β_N) and the energy confinement time (τ_E) are determined from the diamagnetic flux loop.

Table 3.1 presents a summary of some magnetic sensors with information on the quantities that are measured and the purpose of the diagnostic.

An in-depth description of magnetic diagnostics is presented in [80]. The reminding part of this section briefly gives the basic concepts for the most important measurements of plasma parameters using this class of diagnostics.

[11]The plasma resistivity is calculated dividing the voltage by the plasma current.
[12]The simplest cpnfiguration of this diagnostic is the Sin-Cos coils used in small tokamaks, like ISTTOK.

Type of sensor	Measured quantity	Purpose
Flux loop	ψ (poloidal flux)	Equilibrium reconstruction and plasma control
Rogowski coil	I_p (plasma current) I_c (coils current)	Equilibrium reconstruction and plasma control
Diamagnetic loop	$\Delta\Phi_D$ (diamagnetic flux)	Equilibrium reconstruction and plasma control
Saddle loop	B_r (radial field) δB_r (nonaxisymmetric B_r)	Equilibrium reconstruction, plasma control and MHD modes
Magnetic probe	B_θ (poloidal field) B_ϕ (toroidal field) dB_p/dt (B_p time derivative) δB_ϕ (nonaxisymmetric B_ϕ) δB_θ (nonaxisymmetric B_θ)	Equilibrium reconstruction, plasma control and MHD modes

Table 3.1: Summary of magnetic sensors used for plasma diagnostics.

A. Flux Loop

The flux loop is an axisymmetric conducting loop in the horizontal plane of the plasma column. This diagnostic is used to obtain the poloidal flux (ψ) at the plasma boundary. ψ is constant on the plasma surface and it is related to the magnetic poloidal field (B_θ) by the equation [81]:

$$B_\theta = \frac{\nabla\psi}{R} \times \nabla\phi \tag{3.20}$$

where R is the tokamak major radius and ϕ is the toroidal angle.

The total flux through the loop is given by $\Psi = 2\pi\psi$. The total flux is related to the voltage measured at the terminal ends of the flux loop (V) by the equation:

$$V = \frac{d\Psi}{dt} \tag{3.21}$$

B. Magnetic (pick-up) Coils

The magnetic coil is the simplest and oldest magnetic sensor, operating on the basis of the fundamental induction represented by the Faraday's law. The output voltage of the sensor is given by

$$V = n\frac{d\phi}{dt} = nA\frac{dB}{dt} \tag{3.22}$$

where ϕ is the magnetic flux through the coil section, A is the area enclosed by the coil, n is the number turns of the coil. Although the operating principle is very simple, a considerable experience and knowledge is necessary to achieve precision measurements.

C. Rogowski Coil

The Rogowski Coil (RC) is a very important tool to measure very high intensity electric currents. It is an helical coil of wire uniformly wound along a non-magnetic circular strip; the lead from one end returns through the center to the opposite end, putting both ends together (figure 3.4).

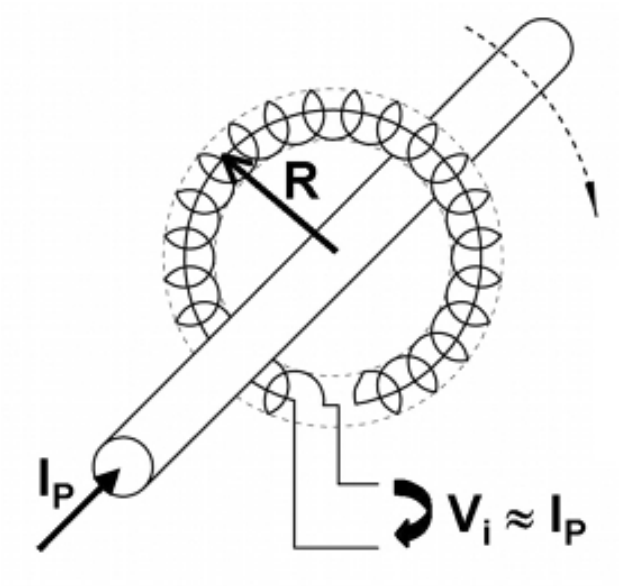

Figure 3.4: Rogowski coil scheme.

The voltage measured from the Rogowski coil is given by

$$V_i = \frac{d\Phi}{dt} = nA\mu\frac{dI_p}{dt} \tag{3.23}$$

where Φ is the total flux, n is the number of turns per unit length, A is the coil uniform cross section area, μ is the magnetic permeability of the medium in the solenoid and I_p is the total current going through the encircled space.

The electric current I_p is obtained by:

$$I_p = \frac{1}{nA\mu}\int V_i dt \tag{3.24}$$

In a tokamak, Rogowski coils can be used to measure the plasma current and the currents in the control coils. For the first purpose, the RC is inserted surrounding the plasma column in a poloidal section, either inside or outside the vacuum vessel.

D. Saddle Flux Loops

The saddle flux loop aims at measuring the radial magnetic field to control the radial plasma position. It is a large rectangular coil mounted near or on the vacuum vessel wall. The flux ϕ is given by

$$\phi = nAB_{\perp} \tag{3.25}$$

where n is the number of windings, A is the loop area and $B_{\perp}$ is the average magnetic field component normal to the surface, on which the loop is mounted.

3.3.3 Actuators

3.3.3.1 Introduction

The actuators for plasma position and shape control in a tokamak are tools that create electric and magnetic signals for interaction with the plasma, aiming at bringing some plasma parameters to the desired values and/or to control some undesired events like, for instance, plasma instabilities.

Since it is easier to create magnetic signals, the main actuators for real-time plasma control are poloidal field coils implemented outside the tokamak vacuum vessel. More recently, aiming at improving the efficiency of the control systems both for ELM mitigation and vertical stability, new type of coils have been designed for implementation inside the vacuum vessel[82][83][84][85][86].

3.3.3.2 Poloidal Field Coils

The Poloidal Field (PF) coils are the actuators that drive the position and shape of the tokamak plasma, maintaining the plasma equilibrium. The internal poloidal magnetic field (B-field), generated by the plasma current, is combined with the external poloidal B-field aiming at controlling the plasma vertical and radial positions. Moreover, the PF coils are also used to control the different plasma shapes by controlling the surface defined by the field lines, through the adjustment of the current distribution in the PF coils, that can be independently controlled from the plasma position.

The use of poloidal B-field to control the plasma shape and position is relevant for tokamak operation due to the following main reasons:

- Prevent the plasma from touching the vessel walls by controlling the position;
- Prevent the last closed flux surface to intersect the wall by controlling the plasma shape;
- Permit the coupling with auxiliary heating systems;
- Improve the particle and energy confinement time by controlling the plasma shape;
- Correctly place the strike point in diverted plasmas for scenario, confinement or impurity transport optimization and, eventually, to avoid energy deposition in dangerous places or certain overexposed divertor tiles.

Figure 3.5 depicts a 3-dimensional diagram of the JET poloidal field coils according to the original tokamak design. Figure 3.6 details its TCV counterpart with a larger number of outer coils and the introduction of the in-vessel coils on the top and bottom for vertical stabilization of elongated plasmas.

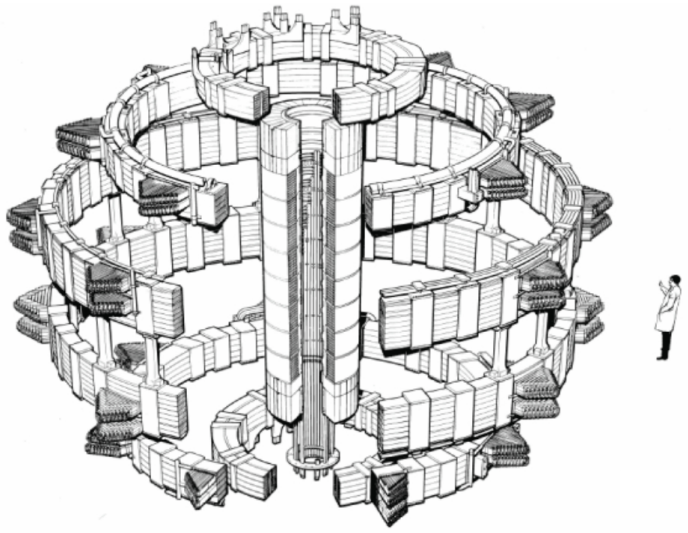

Figure 3.5: JET schematic diagram of the original poloidal field coils (Image courtesy of EFDA-JET).

3.4 TCV Magnetic Diagnostics and Actuators

The TCV magnetic diagnostics include 61 flux loops, 4 arrays of 38 magnetic probes, 24 saddle flux loops and a diamagnetic flux loop. The TCV plasma shaping and position control is made using in-vessel fast vertical stabilization coils and poloidal field coils. Figure 3.7 depicts the cross-section of the TCV tokamak where it is possible to see:

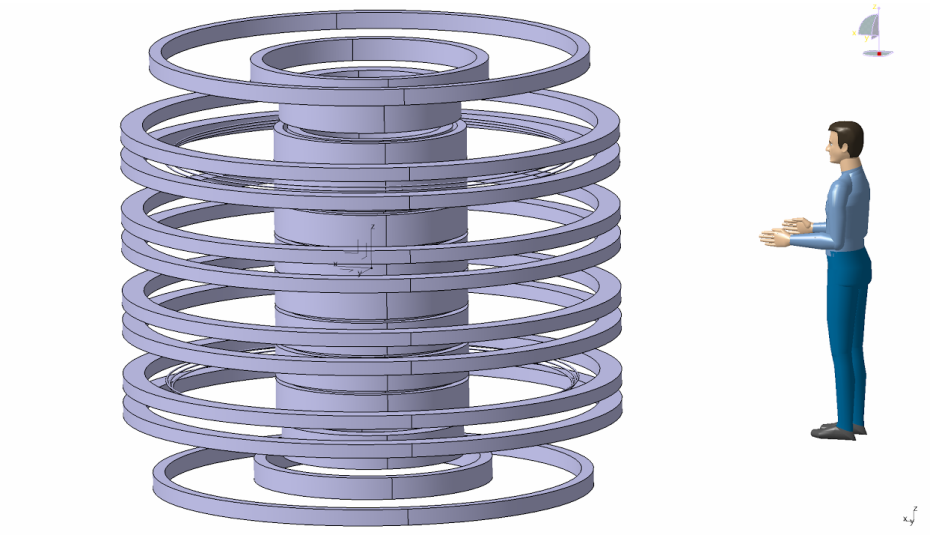

Figure 3.6: TCV schematic diagram of the poloidal field coils (Image courtesy of J.-D. Landis, CRPP).

- The vacuum vessel;
- The 6 fast stabilization coils inside the vessel (G1-G3 at the bottom and G4-G6 at the top outer corners), which are controlled by the same power supply;
- The 16 independently controlled poloidal field shaping coils (the inboard E1-E8 and outboard F1-F8 stacks of 8 coils each);
- The 54 flux loops (marked x);
- The 38 magnetic probes around the vessel contour (marked inside the tiles).

The total plasma current in TCV is estimated from the poloidal magnetic field probes signals, since no continuous Rogowsky coil has been installed around the vacuum vessel. This decision has the disadvantage of less precision in the measurement and bigger sensitivity to currents in the coils and vessel eddy currents.

A detailed description of the TCV magnetic diagnostics can be found in [87] and [88].

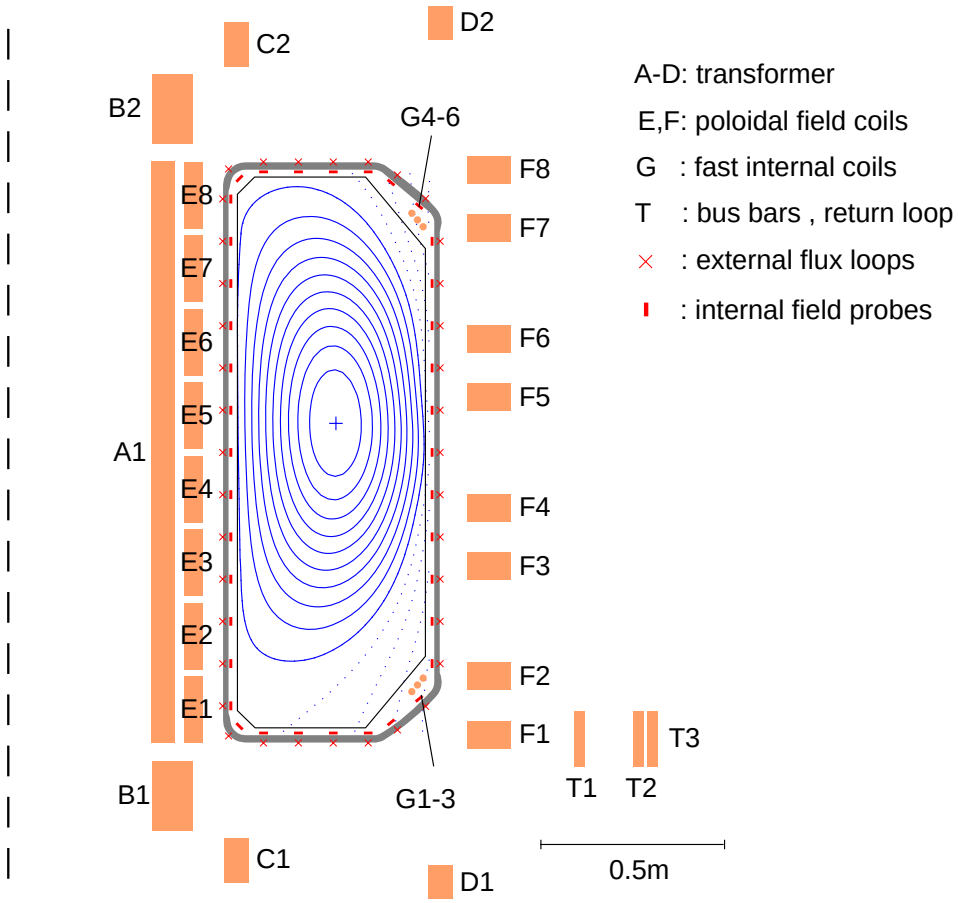

Figure 3.7: TCV cross-section with the magnetic probes, flux-loops and plasma shape and position control coils. Not shown are the Toroidal Field (TF) coils

Part III

Control Engineering

4

Advanced Plasma Control System

Contents

"So many people today seem to me like someone who has seen thousands of trees but has never seen a forest."

Albert Einstein (In a letter to Robert Thorton)

4.1 Introduction

TCV has presently a mix of different control systems that can be used in parallel. During the preparation of the plasma discharge, a choice is made of which system will be used, being also possible to utilize a mix of different controllers by separating the control variables of each system. A set of digitally pre-programmed switches will route the control signals for the desired plasma actuators.

One of these systems is the initial TCV control system [89][90]: an analog/digital hybrid controller. Although this system is extremely reliable, confirmed by the several years of use and achievements in TCV, it is very limited concerning the change of algorithms and parameters.

For these reasons, a new real-time digital feedback control system was developed and installed to allow larger flexibility and enhanced performance controlling the TCV plasma shape, position, current and density.

This chapter presents an overview of the TCV Hybrid Control System and the development of the digital Advanced Plasma Control System (APCS), including its design, implementation, integration into the TCV plant control system and the tests performed during system commissioning and validation.

4.2 TCV Hybrid Control System

4.2.1 General Description

The TCV Hybrid Control System is composed by several analogue matrix multipliers that can be programmed before each plasma discharge. Although the multipliers use analogue electronics, they are digitally programmed and can change over time during a TCV discharge. All programable matrix values must be calculated before the discharge. Then they are programmed in a digital memory that is converted into an analogue signal to set the multiplication factor. In short, the hybrid system is a pure analogue system under digital control, limited to the fixed calculation of matrix multiplication.

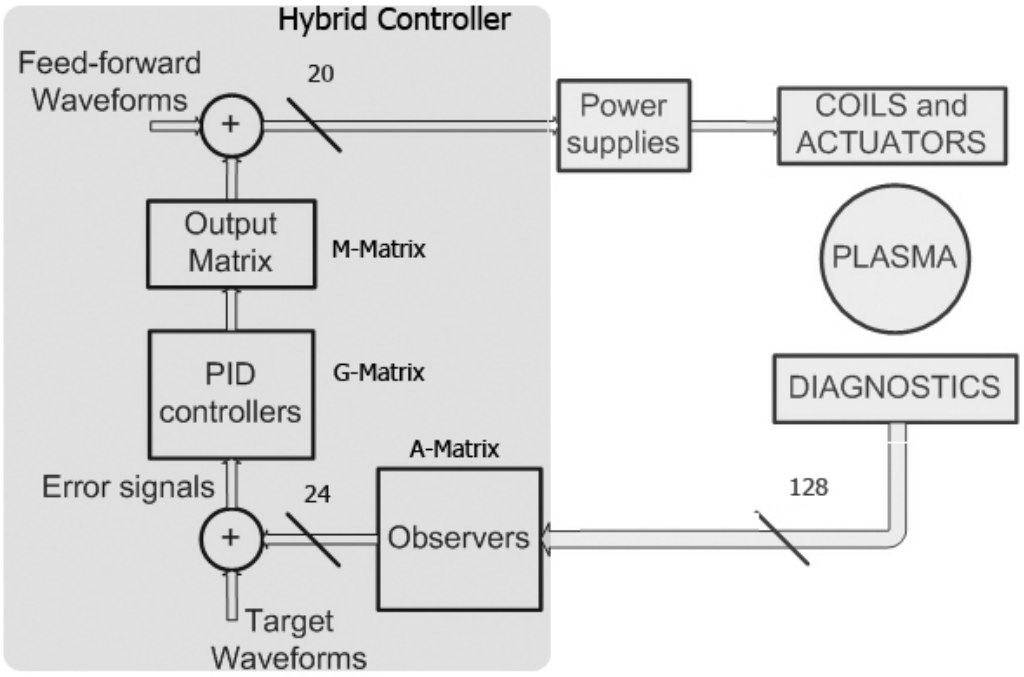

Figure 4.1: A simplified schematic overview of the TCV Hybrid Control System.

Figure 4.1 depicts a simple schematic of the Hybrid Control System and its interface with the plasma diagnostics and actuators. This figure also shows the controller implementation limited to PID algorithm that is possible to use. Figure 4.2 presents a more detailed design of the hybrid controller. Three major blocks should be referenced due to their importance and role in the control system:

- A-Matrix
- PID and G-Matrix
- M-Block

The role of each of these matrices is described in the next subsections. References [89] and [90] present a complete description of the TCV Hybrid control system.

4.2.2 A-Matrix

The A-Matrix has 128 inputs and 24 outputs (see figures 4.1 and 4.2 for schematic details).

The inputs are connected to the diagnostic signals that are used for the real-time plasma control. These signals are used to create the estimation signals of the physical variables (observers) to be controlled, according to preprogrammed weights of the inputs. The observers are thus linear combination of the diagnostic signals.

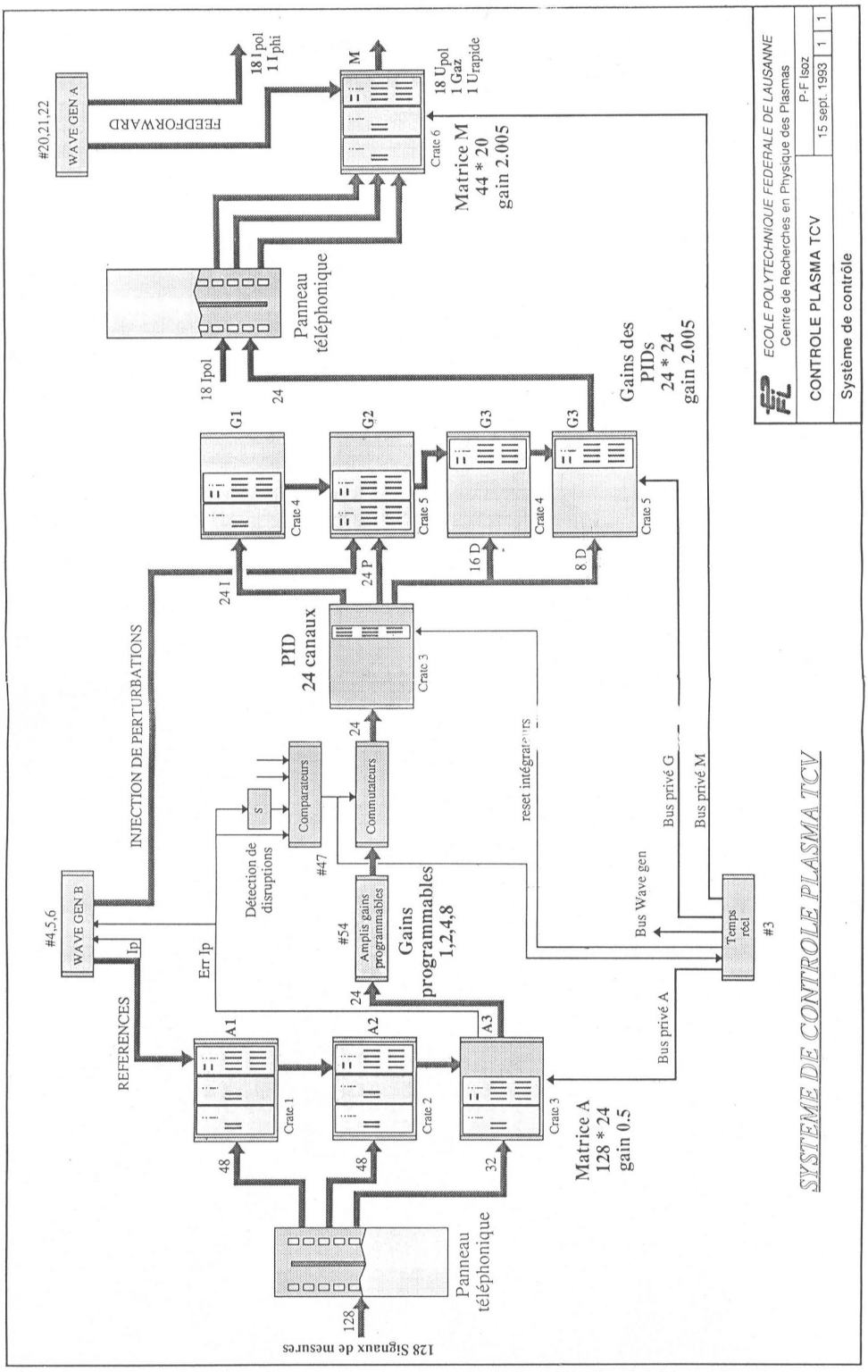

Figure 4.2: A schematic overview of the design of the TCV Hybrid Control System. This figure was kept in French because it is the original picture of the Hybrid Control System design. The design has never been translated from the original.

The diagnostic signals and observers currently available at TCV include:

- *Diagnostic inputs*
  - 38 integrated magnetic probe signals
  - 20 non-integrated magnetic probe signals
  - 38 flux loops
  - 20 coil current transducers on rectifiers
  - OH1-OH2 current difference
  - FIR interferometer fringe counter
  - 1 mm interferometer fringe counter
  - Non-integrated signal from innermost flux loop
- *Observer outputs*
  - E1-E8 currents
  - F1-F8 currents
  - Current difference between 2 Ohmic coils
  - Radial position
  - Plasma current
  - Vertical position (for slow vertical control)
  - Density
  - Elongation
  - Vertical position (for fast vertical feedback control)
  - Vertical velocity (for fast vertical feedback control)

After the linear calculation, the observers are subtracted to the reference signals generated as feed-forward waveform signals, to create the control error signals that are the inputs to the next control stage.

4.2.3 PID and G-Matrix

The output errors that come from the A-Matrix are fed into the PIDs and afterwards to the G-Matrix (see figures 4.1 and 4.2).

The G-Matrix is composed of 3 sub matrices (G_1, G_2 and G_3) of 24 inputs and 24 outputs each. Each of these matrices performs the sum of proportional, integrator or differentiator functions sequentially with the outputs being added to create the actuator signals.

The G-Matrix sums the PID outputs for each signal and also enables the introduction of different gains at the output. The PID gains are programmed before each TCV

discharge in each of the matrices.

4.2.4 M-Block

The actuator signals are finally fed through the M-Block aiming at decoupling the mutual inductances and compensating the resistive voltage of the coils (see figures 4.1 and 4.2).

The M-Block allows different programmable connections between the output of the G-Matrix and the output of the control system that feeds the actuators. The M-Matrix is designed specifically to introduce corrections for mutual coil inductances (M) and coil resistances (R). The coil currents measurements (I) are used together with G-Matrix outputs to calculate the voltage control signal (V) according to the equation:

$$V = RI + M\frac{dI}{dt} \tag{4.1}$$

4.3 Advanced Plasma Control System

4.3.1 Design Requirements

The Advanced Plasma Control System (APCS) was designed to fulfill the general requirements mentioned in the first chapter, as well as the following specific goals:

- Duration of the fast control cycle: 5 μs;
- Duration of the slow control cycle: 50 μs;
- Input signals: 34 at 10 MHz;
- Output signals: 34 at 10 MHz;
- The data from the input signal, the output signal and one processed value must be shared among the algorithms of all processes in each control cycle.

The APCS is required to control the following list of 34 actuators in real-time:

- 18 Shaping coils, ohmic transformer and toroidal field power supplies;
- 2 Internal coils driven by a fast power supply (FPS);
- 3 Gyrotron power: 2 X2 clusters and 1 X3 cluster;
- 7 ECH launcher mirrors: 6 X2 launchers and 1 X3 launcher;
- 4 Gas valves.

The requirements on the control cycle time, the number of inputs and outputs for the system to handle and the algorithms to be used are summarized in table 4.1

System	Time	Size I/O	Algorithms
Vertical Position	5 μs	2 x 2	IIR or FPS direct control
Plasma shape and current	1 ms	18 x 18	non linear + IIR
Gas injection	10 ms	4 x 4	IIR
ECH power	0.1 ms	3 x 3	non linear + envelope
ECH launching	20 ms	7 x 7	non linear + convolution

Table 4.1: Control requirements for different TCV control subsystems.

A decision was made to use a digital system using a DSP-based, parallel processing Versa Module Eurocard (VME) module, that has been developed by IST for a TCV real-time pulse height analysis X-ray diagnostic.

The intelligent module has four Acquisition, Processing and Control Channels (APCC), each one with one analogue input channel (ADC), one analogue output channel (DAC) and one Digital Signal Processor (DSP). Each APCC can be connected to the other three APCCs of the same module or to any other APCC of another module connected to the same VME crate, using an in-house developed proprietary bus.

4.3.2 Hardware Architecture

The TCV Digital Advanced Plasma Control System is composed by

- One Versa Module Eurocard (VME) host CPU module with a standard Intel processor running Fedora Core Linux;
- Nine VME bus intelligent modules with 4 APCCs each, eight for slow control and one for fast control;
- A backplane Data Mover bus for fast data transaction between the 8 modules in the slow control cycle;
- An XIO module for digital input/output and LED monitoring in the front panel.

The 32 DSPs in the 8 slow control cycle modules process the signals that were acquired and digitized by the corresponding analogue inputs (12 bits). The modules share their acquisition and processed data with the other modules in the chain, enabling the inclusion of data from any DSP in the algorithm of any other DSP. Each DSP can run a different algorithm over the acquired data, including Infinite Impulse Response (IIR), Finite Impulse Response (FIR), IIR + non-linear or another custom made algorithm. Every 25 μs (slow control cycle) all the analogue outputs (14 bits) are simultaneously updated with the processing result from each DSP.

The analogue output and the analogue input as well as other software values programmed are broadcasted to all DSPs of the eight modules in one VME crate. This procedure was implemented replacing the external event bus by the DMBUS. A passive bus board is connected to the rear of the P2 connector of the VME bus using the VME bus custom pins. Although module control and interface of the new DMBUS are based on the same electronic hardware as the external event bus, the control signals were redefined and the interface bus control in the Complex Programmable Logic Device (CPLD) was reprogrammed.

The four DSPs of the ninth module process, using PID algorithms, the acquired and digitized signals from the analogue inputs, update their analogue outputs and broadcast the results among them every 5 μs (fast control cycle) through the intercommunication buses among DSPs in the same module.

A digital input/output board (XIO) was developed in order to permit digital signals of the DMBUS to be input and output via the front panel of the crate. These signals are used to provide external and internal synchronization of the DSPs as well as to monitor plasma control process status.

Figure 4.3 depicts the complete system hardware block diagram with the input/output front end in the right and the DMBUS for data communication between the modules in the left. The internal structure of each module with the APCCs connected to the global bus and to each other through the DSP dedicated ports is presented in the top of this figure. The VME controller with the host CPU, HDD, SDRAM and Ethernet connection is in the bottom of figure 4.3. Just above is the XIO module for digital I/O.

Figure 4.4 shows the APCS hardware that was installed in TCV, showing one VME module on the left and the complete VME crate on the right.

4.3.3 Intelligent Hardware Module

The power of Digital Signal Processors (DSPs) and Field Programmable Gate Arrays (FPGAs) for digital control have been employed in a variety of systems due to their high processing capability together with low power consumption and low price. To increase the performance and to cope with distributed processing systems (like the APCS), complex parallel systems have been developed in several scientific areas [91]. The APCS is a high performance distributed system composed of several VME bus intelligent modules based on DSP technology.

The hardware of each intelligent module is 6U, A32/D32 VME bus printed circuit

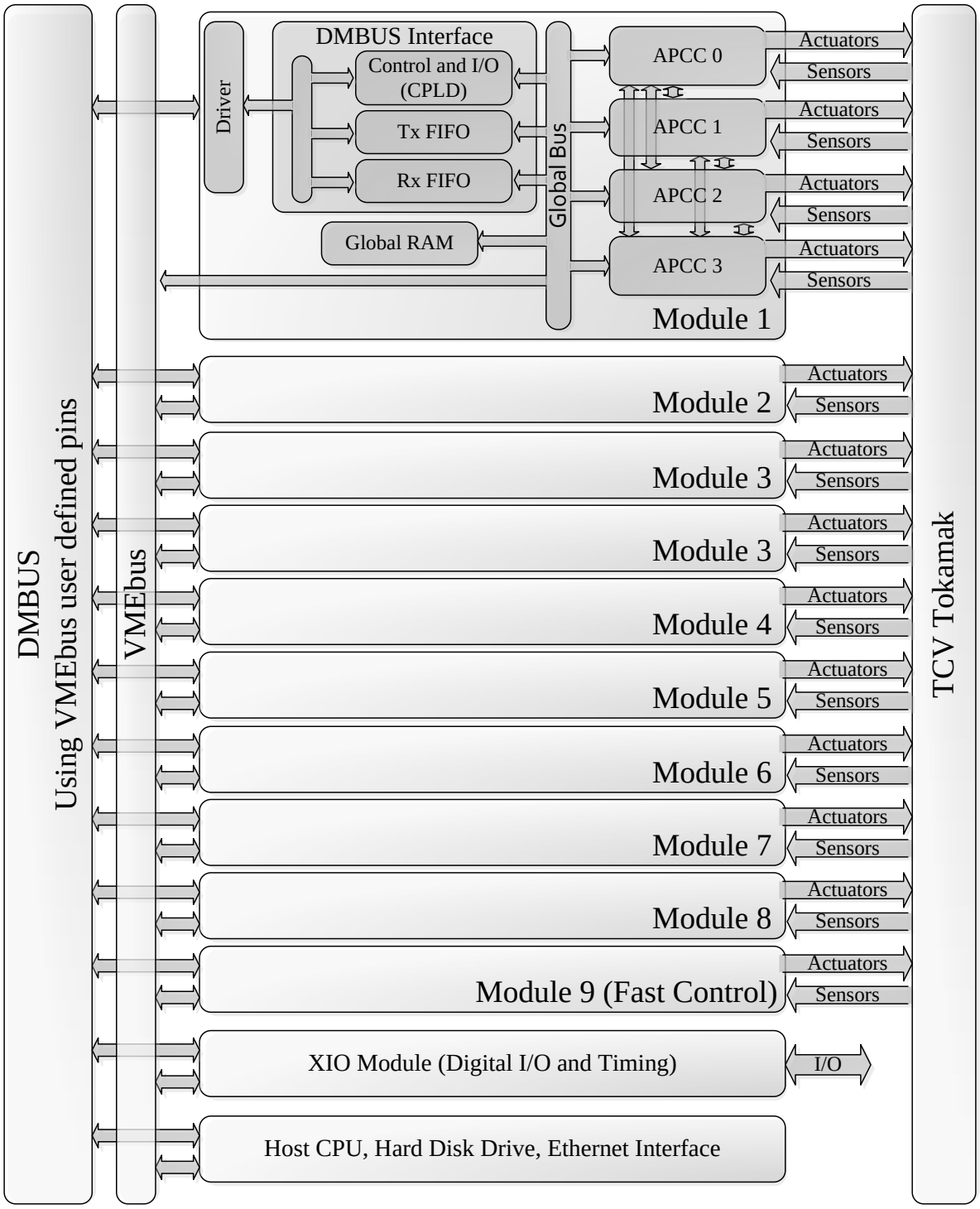

Figure 4.3: Advanced Plasma Control System architecture.

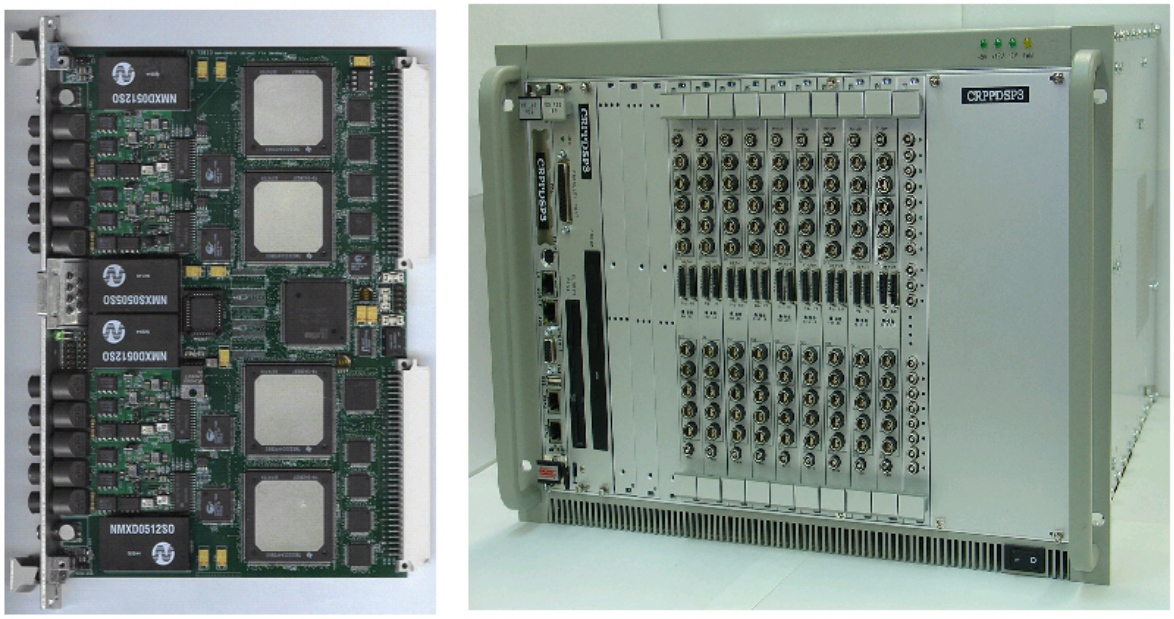

Figure 4.4: The Advanced Plasma Control System hardware: (i) On the left a VME module with 4 APCC channels with one DSP, one analogue input and one analogue output each; (ii) On the right the complete APCS VME crate with nine modules, the bus controller and digital I/O module.

board, with four Acquisition Processing and Control Channels (APCC), each one composed of an analogue input, a floating point DSP and an analogue output. The DSPs in the module share several resources through the module asynchronous global bus to store and transfer data, like FLASH memory, DRAM and SRAM. Figure 4.5 depicts the APCC block diagram.

Each APCC is composed of:

- One analogue differential input for data acquisition with 12-bit resolution, +/- 5 V voltage range, independent software programmable sampling rate of up to 40 MSPS, and a first in first out (FIFO) memory of up to 32 kword;
- One 32-bit floating point digital signal processor (DSP) (TMS320C44) that can process up to 80 MFLOPS;
- Up to 128 kword 32-bit wide SRAM for DSP program and data;
- One analogue output for control with 14-bit resolution, +/-5 V voltage range, independent software programmable update rate of up to 100 MSPS and a FIFO memory of up to 32 kword.

The DSPs of all APCCs are synchronized using a common external clock and can directly interchange data among each other for parallel processing, thus increasing the

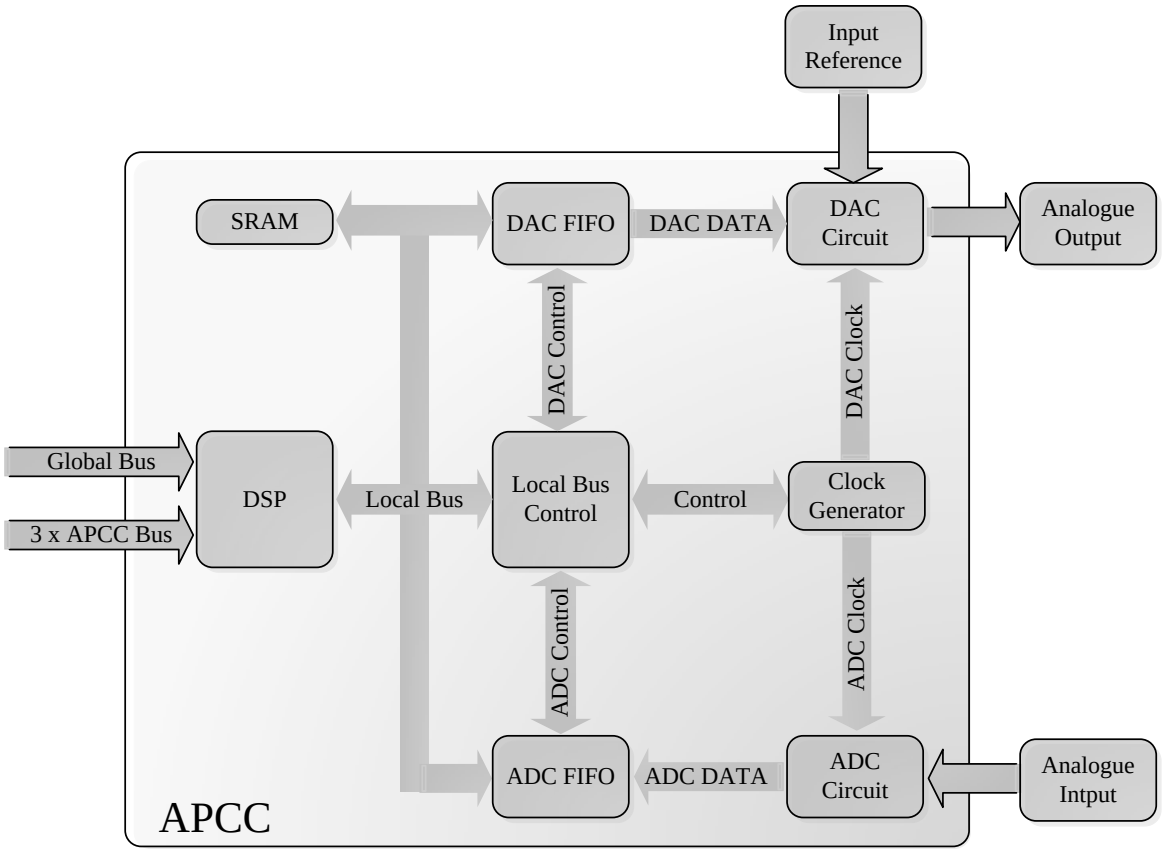

Figure 4.5: Acquisition Processing and Control Channels (APCC) block diagram.

processing capacity of the module by means of parallel processing. To permit this feature all DSPs in one board are interconnected via independent parallel buses. Each module has front panel connections that permit to cascade connections between modules, permitting that two DSPs in a module can directly interchange data with two DSPs in two other modules. This procedure enables the direct interconnection of DSPs of up to two times the maximum number of modules in a VME crate and also between different VME crates.

Figure 4.6 presents the complete intelligent module block diagram, composed of four APCC blocks.

The module can use a common block of DRAM to keep acquired data. This memory is also shared with the VME HOST and may be used as a memory buffer between the data acquisition and the VME bus or to exchange data between DSPs.

The module has programmable digital input/output ports, both with optical inter-

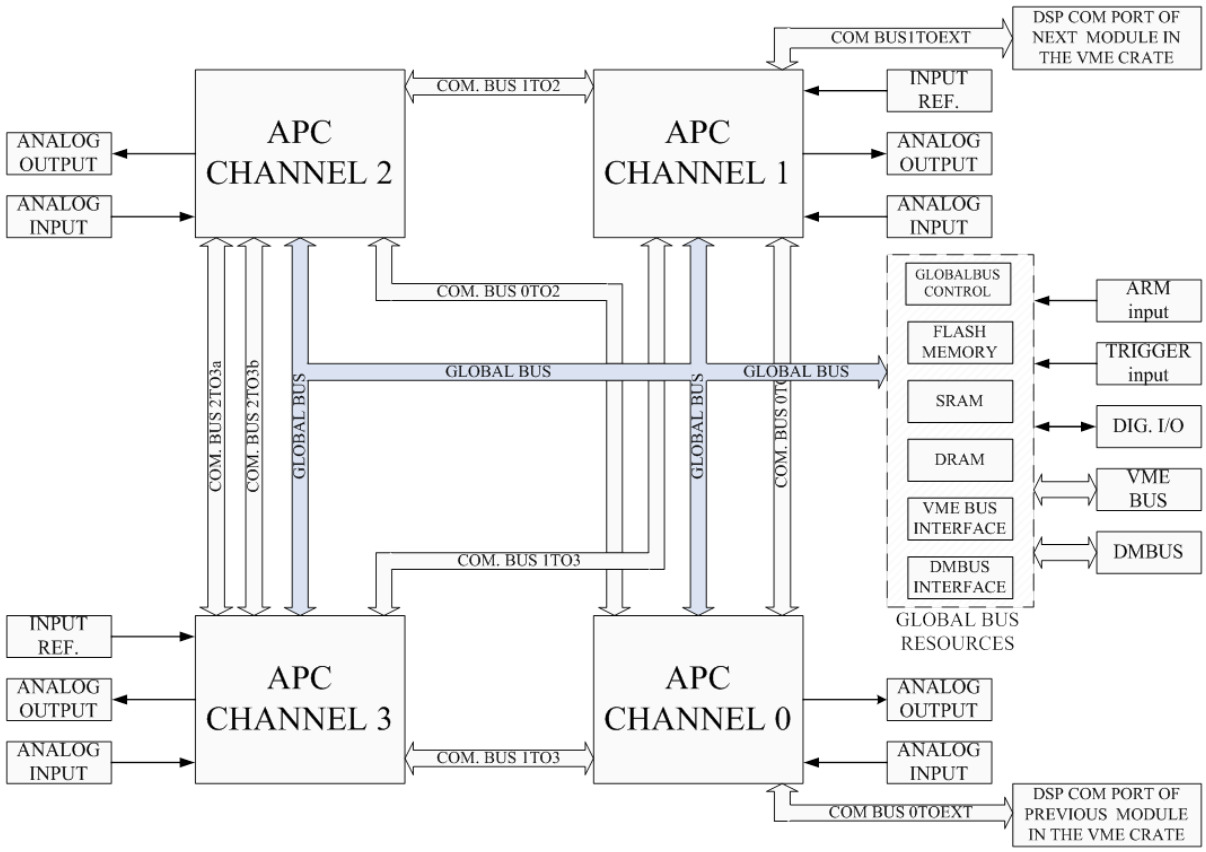

Figure 4.6: Complete intelligent module block diagram, composed of 4 APCC blocks, shared memory and VME Bus access.

faces, in order to have external synchronization (input trigger) and the ability to trigger other modules (output trigger).

The module can generate interrupts to the VME HOST, if needed, and all the configuration of the board, including the VME bus address, is jumper less. The control and set-up of the module is made by the VME HOST, which sends and receives commands through FIFOs to or from the DSPs.

The digital signal processing algorithms ran by the DSPs, can be downloaded by the VME HOST or can reside in its firmware together with the operating system (OS). This firmware is kept in a flash memory with up to 512 kB of memory and is shared by all DSPs. The use of a flash memory to keep the firmware of the module has two great advantages:

- During power on or reset, the module can start and run an application in a stand alone mode, meaning that it does not need the intervention of the VME HOST to download programs or algorithms;

- Since the flash memory can be programmed, it is possible to add or change algorithms or programs to the firmware permanently. It is also possible to keep, in a static way, parameters of an algorithm for later use.

4.3.4 Parallel Processing Software Using DSPs

4.3.4.1 Parallel Computing and Distributed System

The desired flexibility when setting up very complex systems is many times a barrier to the easy use and complete user understanding of what and how to do things. The behavior of such systems must be based on the complete specification of the interactions among its parts. The interface design of the system took these difficulties into account aiming at achieving an abstraction from the hardware implementation when building the physics control algorithm. A suitable interface between the system and the TCV plant enabling the complete integration into the existing scheme running and controlling the TCV was designed and implemented.

In order to build the Control Algorithm (TCV-ALGO) a set of instructions should be available for the high-level programmer in a way that it is both easy to implement and fast to run using as many hardware features as possible. To achieve this goal, a library and software interface were implemented in the low-level DSP software, which can be called from C language or from a high-level graphical language with the appropriate syntax by the use of a graphical interface using a set of logical blocks. The first option was implemented as the first choice for system exploitation and is presented in this document, the second one can be implemented as a Matlab Simulink like application with real-time programming blocks.

This section describes the Message Passing Interface (MPI) and the Real-Time MPI. The principles of the MPI standard were used to help the design and implementation of the Real-Time Data Mover. It is also discussed the Data Mover bus implementation, which is the hardware part of the Real-Time Data Mover. Finally, this section presents the software details of the Data Mover and the Application Programming Interface (API).

4.3.4.2 Message Passing Interface (MPI)

According to the MPI designers [92], the goal is to develop a widely used standard for writing message-passing programs, which is practical, portable, efficient, flexible and most of all a standard that is easy to use by everyone and a reference for all parallel system

developers. MPI provides vendors with a clearly defined base set of routines that can be efficiently implemented, providing a common software standard for several hardware manufacturers.

Instead of selecting one of several existing message passing systems and making it the standard, MPI designers try to make use of the most attractive features of each one and make a better standard that can be used in a wide range of platforms. MPI is then strongly influenced by the work of several other message passing libraries.

Although the complete MPI standard is composed by more than 100 functions, a reduced set of functions can be implemented to use the basic functionality of the MPI standard. The basic MPI library contains the following six functions:

- `MPI_INIT` - Initializes the use of the MPI library.
- `MPI_COMM_SIZE` - Returns the number of processes that are running.
- `MPI_COMM_RANK` - Returns the number of the process that runs this function (identifies the process).
- `MPI_SEND` - Sends a message from one process to another.
- `MPI_RECV` - Receives the message sent by the other process.
- `MPI_FINALIZE` - Terminates the use of the MPI library.

Although these functions are the most basic set, they are already very powerful to write many efficient parallel algorithms.

One function that should be emphasize is `MPI_BCAST`, which broadcasts a message from one process to all the others. The idea of a function that broadcasts some data from one process to all the others is the base of the implementation of the Real-Time Data Mover that will be described in another section. At the hardware level, if the system is built in a star configuration, it is possible to achieve a significant improvement in the system performance if the messages are broadcasted to all processes at the same time instead of sending one independent message for each process. This concept will be exploited and explained in this thesis, because this is a very important idea that was used in the system that is being presented.

4.3.4.3 Real-Time MPI

The Real-Time MPI (MPI/RT) [93] is a standard aiming at designing MPI for real-time programming, defining the components for real-time communication support, targeting embedded, fault-tolerant and real-time systems.

MPI/RT appears as a need to develop a standard way of creating real-time parallel

applications with an abstraction layer from the hardware. Without a standard application developers must become experts on the hardware platform before they can take advantage of the system features. When thinking about applications that require timing constraints and real-time interaction with the environment (a control application) the difficulties are even greater.

The approach has been that the platform designers provide the user with an API and it is up to the application developers to satisfy the final requirements, satisfying the time constraints and the quality of service. With MPI/RT a new approach is being tried. The user provides the timing and data application requirements and the system platform analyses them. After that they are either satisfied and the code is generated accordingly or they are denied due to lack of resources. With this approach application programmers can concentrate on improving algorithms and specific code, letting middleware providers guarantee the best possible performance for the specific hardware.

One of the common difficulties in real-time systems is the scheduling of the several components. When it comes to a real-time parallel processing system with several CPUs, this problem can become even bigger than in one CPU systems. It is very hard (I would say impossible, most of the times.) for the application programmers to coordinate the use of all hardware resources, providing the desired system performance. Even when it was successfully achieved for one platform, the programmer would have to relearn the hardware details for the other platforms making it difficult to port applications from one platform to the other. However, if hardware vendors provide their systems with the standard MPI/RT API code, portability between different systems will be much easier and system performance can greatly improve due to the better knowledge of the platform when building the low-level and middleware software. Moreover, application programmers are provided with a layer of abstraction from the hardware point of view and can easily develop software for different platforms as well as port the code without spending time learning new hardware architectures.

4.3.4.4 Real-Time Data Mover

The Real-Time Data Mover is a complete set of software tools and hardware designed to exchange a pre-programmed data structure across the 32 Digital Signal Processors that permit a real-time control cycle under 25 μs. To achieve this target a broadcast architecture was implemented capable of moving the complete data structure in less than 15 μs, leaving 10 μs free for data processing.

This implementation has a different approach from the MPI/RT philosophy presented. Instead of giving all the functionality using a complete library for message passing, it is made available a set of commands that configure the data transfer process. Although the data to be transferred is configured through the commands, the transfer process is completely managed by the hardware and the in-house specially developed DSP operating system. In this way, the system scheduling is much easier to manage because all processors are synchronized by the operating system code that is not changed by the algorithm developer. Moreover, the algorithm developer doesn't have to worry about how and when the data will be exchanged, he just knows that all data is exchanged and made available to all processors for each algorithm's iteration.

Because there is always a compromise between the standardization and the performance, it is sometimes difficult to make some of the decisions when specifying the system architecture. In this case (because it is a unique system that must achieve very high performance and stability) the final balance pended to the performance. This is why some of the programming concepts may be sometimes difficult to understand, although a great effort was made to simplify the usability of the system by the physicists.

The Real-Time Data Mover is described in the next sections of this thesis.

4.3.4.5 Data Mover Bus Implementation

One of the most important features to permit real-time parallel processing capabilities between several modules in the same crate is the in house developed Data Mover Bus (DMBUS) [94] interface through the VME P2 connector. Each module has an interface to the external DMBUS, an evolution of the Timing and Event Management System previously developed [95][30]. This bus provides high performance connectivity as well as the ability to send events very fast to the Timing and Event Management System generating synchronized triggers to the main data acquisition and control system.

The DMBUS architecture is based on an 18 bit parallel synchronous data bus with the necessary control signals. Each hardware module has an interface to the bus composed of two first-in-first-out (FIFO) memories, one in each direction, for receiving and transmitting data. A Complex Programmable Logic Device (CPLD) produces the bus control signals and manages 8 digital inputs and 8 digital open collector outputs for general purpose application.

The DMBUS data transfer chain follows a fixed pattern based on the initial configuration of the modules. Each module is configured to belong to the transfer chain and one

of the modules must be configured as the DMBUS Master. This module has the function of initiating the data transfer cycle.

In each transfer cycle, all data that is sent to the DMBUS is received by all other modules in the chain, including the module that sent the data. The transmitter and receiver FIFOs are managed by one DSP in each module, which is the only one that puts and gets data from the FIFOs. This master DSP receives the data from all DSPs of the same module, using the intercommunication buses. This data is then sent to the transmitter FIFO organized in a predefined structure, known by every DSP in all modules. The master DSP in the DMBUS Master module starts the transfer process and the data in the transmitter FIFO is sent to the DMBUS data lines and to the receiver FIFOs of all modules in the DMBUS chain, using a 16 MHz synchronized clock. When the Master Module finishes transferring its data, a control signal is sent through the bus and a pulse on the daisy chain is generated to transfer the bus control to the next module in the DMBUS chain. The process of data transfer is repeated for this module, that passes the bus ownership to the next module after it has finished to send its own data. The process repeats until the data of the last module has been transfered. At that point, the DMBUS Master gets the ownership of the bus again and is ready to start a new transfer cycle triggered by the control cycle clock signal.

At the same time the data is being sent, it is being transferred from the receiver FIFOs to the SRAM in the global bus of each module using a Direct Memory Access (DMA) channel, making all the slow control cycle data available to all DSPs in each cycle.

According to timing tests performed, it takes 8 μs for the DMBUS to share 128 words of data among 32 DSPs using the slow control cycle. This test was made previewing the use of one analogue input (1 word, 16 bits), one analogue output (1 word, 16 bits) and one calculated float (2 words, 32 bits) per DSP. The total time (including interrupt change of context and data transfer preparation) from control cycle clock trigger until all data is available for use in all DSPs is less than 13 μs.

4.3.5 APCS Software Structure

4.3.5.1 Introduction

This section presents the software structure that supports the integration of the APCS in TCV. It is presented the host software break down structure into the different layers that give the system the necessary robustness, performance and liability.

The software in the DSPs is also presented, as well as the Application Programming

Interface (API) that can be used by the control algorithms developer. The API software was developed taking into consideration the abstraction from the hardware implementation aiming at simplifying the design and implementation of the physics control algorithm. This method permits the code to be easily upgradeable and reusable to different systems.

4.3.5.2 Host Software Overview

Figure 4.7 depicts the host software structure.

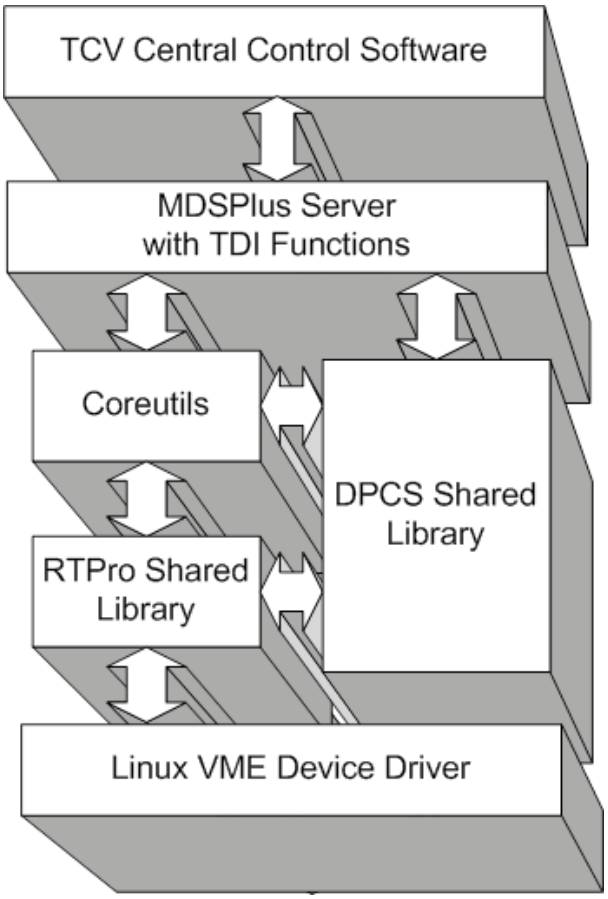

Figure 4.7: The APCS Software Block Diagram.

The host software is built on top of the Linux VME device driver [96]. The hardware access is made using a shared library built for the module (RTPro library) and a set of commands that can be called from the Linux command line (Coreutils). Then a specific shared library was built to deal with the APCS system (DPCS library) that makes calls to the RTPro library but also uses some system commands from the Coreutils. On top of these libraries a set of Tree Data Interface (TDI) functions [97] were developed to interface

the TCV central control software.

4.3.5.3 DSP Programming Interface

To build the TCV-ALGO, a set of instructions should be available for the high-level programmer in a way that it is both easy to implement and fast to run using as many hardware features as possible. To achieve this goal a library and software interface was implemented in the low-level DSP software, which can be called from a high-level language with the appropriate syntax.

This section presents the Digital Signal Processor (DSP) Operating System (OS) Application Programming Interface (API) to develop the TCV control algorithm software in C language.

The DSP Programming Interface appears as a need to develop a simple way of programming the real-time parallel applications with an abstraction layer from the hardware. Without this tool algorithm developers and physicists would have to become experts on the hardware platform before they could take advantage of the system features. Moreover, when applications require timing constraints and real-time interaction with the environment the difficulties are even greater.

The usual approach has been that the system designers provide the user with an API and it is up to the application developers to satisfy the final requirements, checking the time constraints and the quality of service. In this case a different approach is being tried. The user provides the mathematical algorithm while the timing and data transferring requirements are handled by the DSP Operating System. With this approach, application programmers can concentrate on improving the algorithms and mathematical specific code, letting the OS guarantee the best possible performance for the hardware.

One of the common difficulties in real-time systems is the scheduling of the several components. When it comes to a synchronous real-time parallel processing system with several CPUs one CPU systems. It is very hard (impossible, most of the times) for the application programmers to coordinate the use of all hardware resources, providing the desired system performance.

The deeper system designers knowledge when building the low-level software (the OS) is an obvious advantage. Moreover, algorithm developers may be provided with a layer of abstraction from the hardware making it easier to develop the algorithms. In the future, new systems may be designed using the same philosophy for different platforms, providing code portability without spending time learning the new hardware architectures.

Even when this is successfully achieved for one platform, the programmer has to relearn the hardware details for other platforms making it difficult to port applications from one platform to the other.

However, by providing the system with a standard interface code and the implementation of the real-time data transfer capabilities, portability between different systems will be much easier and system performance can greatly improve. The deeper system designers knowledge when building the low-level software is an obvious advantage. Moreover, algorithm developers may be provided with a layer of abstraction from the hardware making it easier to develop the algorithms. In the future, new systems may be designed using the same philosophy for different platforms, providing code portability without spending time learning the new hardware architectures.

4.3.5.4 The Data Mover Software

The DSP OS has two main algorithms when in the control cycle:

- The *Data Mover algorithm* is responsible for reading, formating and broadcasting the data to all DSPs:
  - Normalization and calibration of the DAC data;
  - Trigger detection;
  - Reset ADC FIFO to start acquisition;
  - Write to DAC output;
  - Store local data in local memory for post shot analysis;
  - ADC sample average/calibration and normalization;
  - Transfer DSP1 to 3 local structure to DSP0;
  - Transfer all data channels from DSP0 to DMBUS FIFO on DSP card.
  - DSP0 reads from DMBUS FIFO and send to DSP1 to 3 in the same module.
- The *TCV control algorithm(TCV-ALGO)* is responsible for data processing:
  - Read necessary inputs and software variables from DMBUS data structure;
  - Process data (IIR, FIR, PID, custom algorithm);
  - Write output data into local data structure.

It is the independence between the data transfer (using the Data Mover algorithm) and the TCV control algorithm that permits the desired hardware abstraction. The TCV-ALGO developer knows that the data is available for use without worrying with how it was transferred between DSPs. Therefore all his attention may be put into the control algorithm implementation.

4.3.5.5 Integrating the TCV-ALGO in the DSP Code

A simple method was found to include the algorithm developed by the physicists in the DSP aiming at easily interfacing the DSP OS structure. The tools available from Texas Instruments are the C and Assembler compiler for the TMS320C3X/4X [98]. Therefore, the solution is to include predefined C and H files into the project where the algorithm can be coded.

This approach permits a higher level programming environment such as a visual language (similar to MatLab/Simulink) to be used. The real-time programming blocks are converted into the C and H code files that are included in the DSP project using a precompiler [99].

The linkage of the DSP OS to the TCV algorithm is made by calling three predefined C functions in different determined time slots during the control process:

- `void RT_init(void)` - called when the system is armed, before the first trigger;
- `void RT_loop(void)` - called at each real-time control cycle, triggered by the real-time loop clock;
- `void RT_post(void)` - called at the end of the shot, after last trigger, when the gate closes or on error as a safety procedure.

These functions are coded in a C file named tcvalgo.c and defined in tcvalgo.h. The files are compiled with the DSP OS files using the Texas Instruments (TI) compiler, the Linux scripts using Wine and the DSP API library.

4.3.5.6 DSP Data Structure

The DSP software is composed of several important data structures that must be understood by the algorithm developer to achieve a better system performance. The main data structures are:

- The algorithm data structure;
- The DMBUS data structure;
- The data channels structure;
- The post-processing data storage.

These data structures are depicted in the table 4.2 and in the next subsections.

Algorithm Data Structure

The algorithm data structure is the memory space that can be used by the algorithm developer to store its global variables and all information that shall be available and must

Name	Description	Initial Addr	Final Addr	Size (kw)
Program	Program and software variables - including the data channels structure	400000	407FFF	32
DMBUS	DMBUS data structure	408000	40BFFF	16
TCV-ALGO	TCV-ALGO algorithm data structure	40C000	40FFFF	16
Local Storage	Post-processing local data storage	410000	43FFFF	192

Table 4.2: DSP Local Memory Map (256 kwords - 32 bits).

be kept between different algorithm iteration. For example, to use a standard recursive algorithm that depends on previous calculations, both the parameters and the result from previous iterations must be available for the current calculus. The place to store this data is the algorithm data structure.

The algorithm data structure is managed by the algorithm developer or software developer. It has a fixed size that can be accessed using the definition of its base address ALGO_DATA.

DMBUS Data Structure

The DMBUS data structure is a circular buffer with the previous 32 iterations of the data channels that have been set for the system. The data channels in global DMBUS data structure include channels from all DSPs. To set up this data structure it is necessary to send a set of commands to the DSPs. Appendix A gives an overview of how to configure the DMBUS data structure in each DSP.

To access the data channels information there is an assembler optimized function that can be called from C:

float Get_DMBUS_Data(unsigned int iteration, unsigned int channel, unsigned int type);

The global DMBUS data structure is read-only (from the point of view of TCV-ALGO), because it is the result of the transfer of data from all other DSPs in the matrix. The only channels each DSP has the privilege to administer (change and set the value) are the ones attributed to that DSP when configuring the DMBUS data structure.

```
typedef struct                  /* the order of variables affects assembler  */
{ int adc_data;                 /* adc input data of actual iteration        */
  int dac_data;                 /* dac output data of actual iteration       */
  int status;                   /* processing status: 1-enable or 0-disable  */
  int dspindex;                 /* index id of DSP that process the channel  */
  int type;                     /* channel type: s-software or h-hardware    */
  int procspeed;                /* processing speed ch: f-fast or s-slow     */
  float input_nor_factor;       /* normalisation factor in +/-Volts range of input channel   */
  float output_nor_factor;      /* normalisation _factor in +/-Volts range of output channel */
  float in_data;                /* float input data of actual iteration      */
  float out_data;               /* float output data of actual iteration     */
  char name[MAX_CHAR_OF_NAME];  /* data channel name                         */
}DATA_CH;
```

Figure 4.8: Software data channel structure.

Data Channels Structure

The data channels structure stores locally the DMBUS data channels that will be sent to the DMBUS by the Data Mover algorithm. The current values of this structure are the present iteration values. To access previous iterations it is necessary to access the global DMBUS data using Get_DMBUS_Data() function presented.

This means that the result of an algorithm that must be sent to the DMBUS as a software data channel or to the DAC must be updated in this structure at the end of the algorithm stage. To do that the following function can be called from C.

float Put_DMBUS_Data(unsigned int channel, float data);

Note that this function can only be used for local channels: channels that were configured as belonging to the current DSP.

Although it would be possible to read from the local structure, it is not given any procedure to do so, as the same data can be read from global structure without having to distinguish if it is local or global data.

The structure of one channel is given by the C structure presented in figure 4.8

If the channel is defined as hardware, then the adc_data and dac_data compose a 32 bits word that is broadcasted to all DSPs with the Data Mover function. The values of input_nor_factor and output_nor_factor are set for all channels in all DSPs and are used locally to return the float value when an algorithm calls Get_DMBUS_Data function. These values are set using the commands in Appendix A.

If the data channel is defined as software it is the out_data float value that is broadcasted to all DSPs with the Data Mover function.

Post-processing Data Storage

At the end of each iteration, the data from local channels can be stored for post shot analysis and debugging. This data is stored in the local DSP memory according to the configuration loaded before the shot.

At the end of each discharge, this data is stored in the APCS data tree.

4.3.5.7 Compiling and Loading the DSP Software

Besides the problem of how to integrate the TCV-ALGO into the DSP OS code that was already discussed, another problem had to be solved: how to compile and load the 32 DSP's algorithm code in a clean, fast and easy way.

The TCV-ALGO functions of the previous section are coded in tcvalgo.c and tcvalgo.h in the DSP project. To compile and load the DSPs some problems had to be solved:

- Texas Instruments uses the Code Composer Studio as the standard IDE for software development, without Linux version, and with limited scripting capabilities.
- The DSP operating system source code is different for each DSP in a module. There are 36 tcvalgo.c and tcvalgo.h files to be compiled and linked, each one corresponding to a DSP0, DSP1, DSP2 or DSP3 source code that must be linked to the correct one as they are different from each other.
- The upload of the DSPs code must be fast enough so that it can be made at the arm signal of each TCV shot.

The capability to compile and script under Linux OS was achieved using Wine [100], the Texas Instruments win32 shell version of the compiler and linker tools (TMS320C3x/4x Code Generation Tools) and a set of bash shell scripts developed for the system. The 36 C and H source code files are numbered in a working directory and when the `builddsp.sh` script is called they are compiled and linked against the correct DSP OS files according to its number, producing 36 DSP binary code files ready to upload to the DSPs.

The DSPs can boot from the module flash memory, however uploading the code to the module global memory and making the DSPs boot from there is faster and permits that the code stored in the flash memory is used for testing and fail safe booting. A dual-boot mode was implemented.

4.4 APCS Integration in the Plant Control System

4.4.1 Introduction

The human and programming interface to a complex system is a key issue on its usability, integration and algorithm development speed. Moreover, in fusion research experiments, an effort has been made to structure and ease the integration of new systems not only for data acquisition [101], but also to control systems [102].

A suitable interface between the APCS system and the TCV plant control software enabling the complete integration into the existing TCV Plant Control System (PCS) is presented.

The MDSPlus [97] tools were used to develop the PCS integration software. MDSPlus is a set of software tools for data acquisition and storage and a methodology for management of complex scientific data. The advantages of using a structured integrated tool such as MDSPlus is evaluated, as well as the results on the final performance, usability and stability of the system.

The system state machine implemented to interface the APCS to TCV PCS is also presented.

4.4.2 The MDSPlus Interface

This section presents a justification for the use of MDSPlus [97] to interface the TCV Plant Control System [102].

The MDSPlus programming interface contains the basic commands, simplifying data access even when using complex structures. Using the client/server model it is possible to read or write data at remote sites without file transfers.

For the current application the built-in expression evaluator that extends the capabilities of MDSplus has been used. All interfaces to MDSplus data are based on the evaluation of an expression. These expressions are written in a language called TDI (tree data interface). External routines written in other programming languages can be invoked by calling shareable libraries, providing a huge flexibility for calculus and hardware access [103]. This capability has been widely used in this implementation of the interface.

Another important feature used was the MDSip, a client-server with remote routine execution and automatic machine-binary data translation [103]. MDSip permits that a client on any platform make remote routine calls in the server on another platform, receiving a reply in its own binary format. With MDSip it is possible to run native remote

routine calls without any programming effort from the developer. This approach besides making the client relatively simple (because the server performs all the computation), also permits the remote TCV operator to control the hardware in the APCS system. Because the underlying technology is TCP/IP sockets, the security can be dealt with like in any other TCP/IP service, defining user and IP address access permissions.

4.4.3 System State-Machine

A control state-machine was developed to interface the TCV plant control software to the APCS system. This section presents the state-machine, as well as its implementation.

The APCS state machine (figure 4.9) is integrated into a more complex TCV Plant Control System (PCS) state-machine (figure 4.10) that controls all TCV subsystems during a plasma discharge.

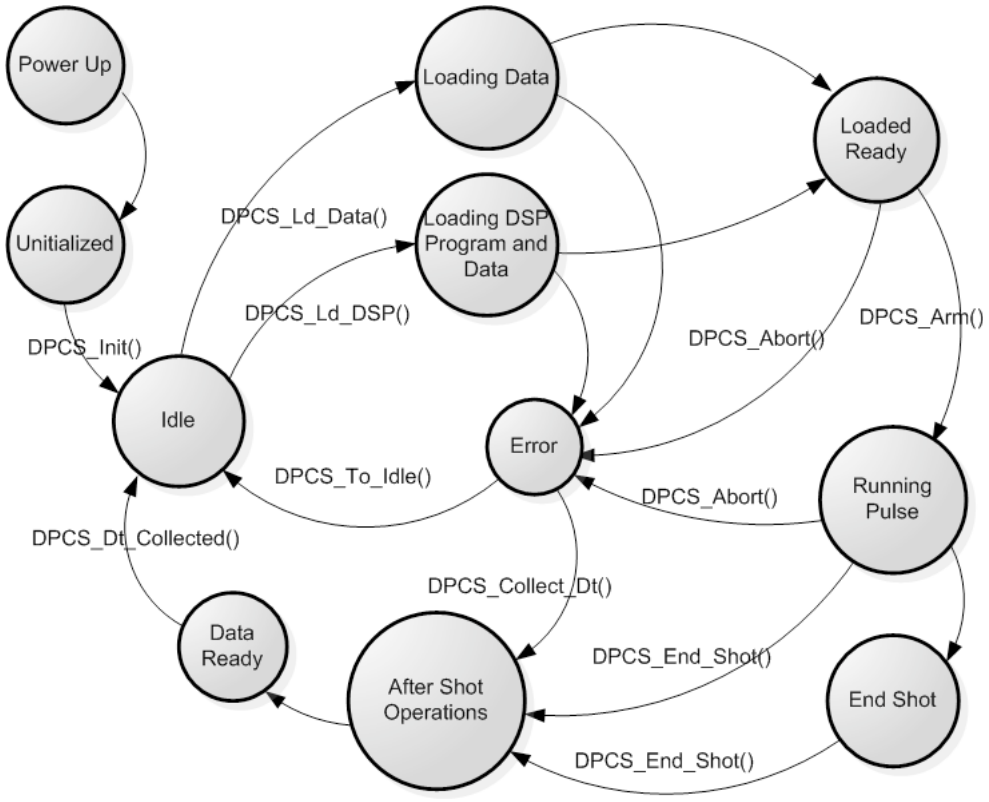

Figure 4.9: APCS interface state-machine.

The following list contains the different states of the APCS state-machine describing its purpose in the system:

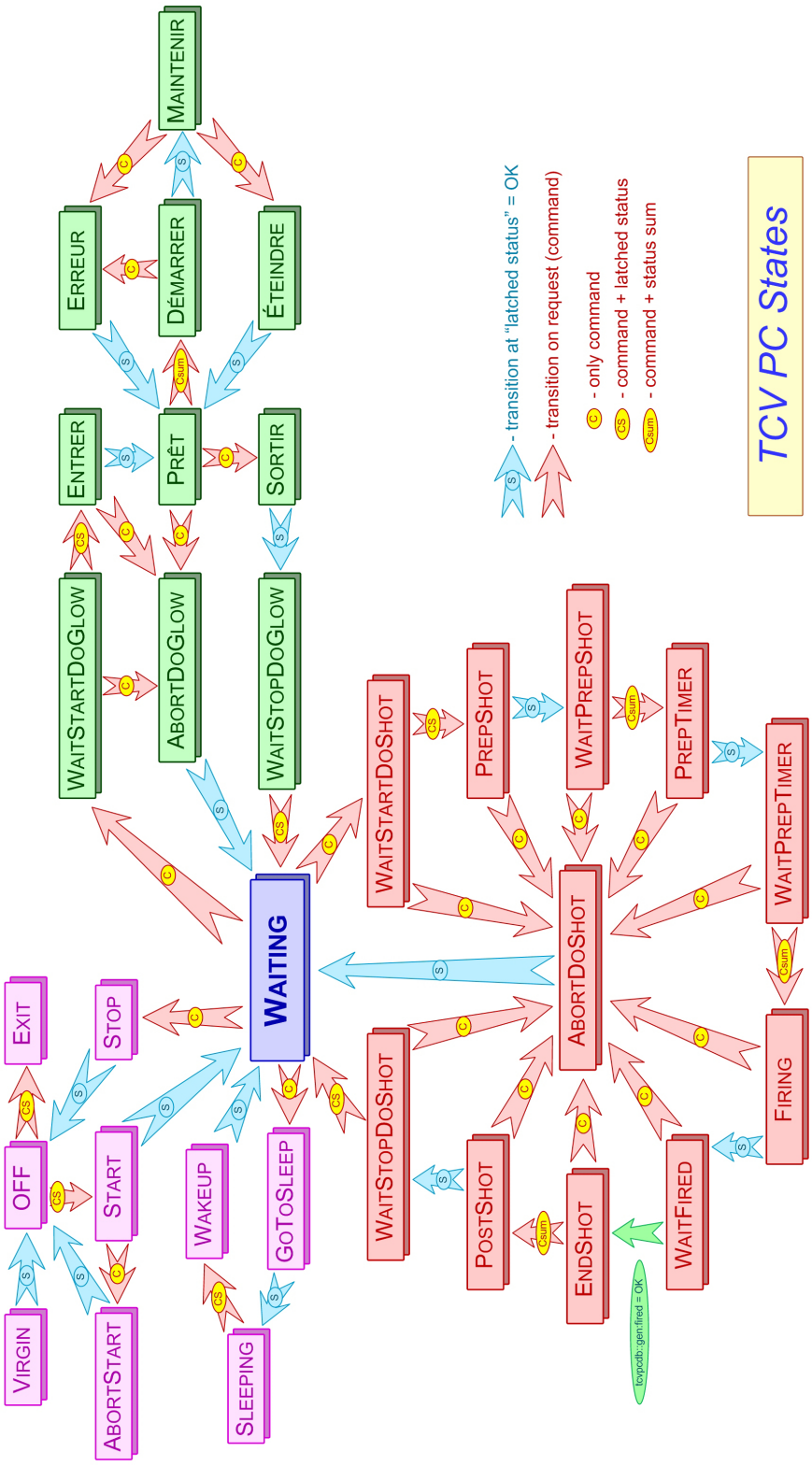

Figure 4.10: TCV Plant Control System state-machine.

- *Not Initialized* - This initial state after a power up is meant to detect undesirable system resets and power ups. The system must be initialized by the operator to go into idle state.
- *Idle* - Between pulses and when initialized after power up, the system is in an idle state waiting for a load command.
- *Loading Data* - After receiving the load command, the system reads the data from tree and prepares the DSPs for pulse. DSPs data is uploaded, but the DSP software is maintained from previous discharge.
- *Loading DSP Program and Data* - After receiving the load DSP program and data command, the system resets all DSPs, reads the data and software from tree and prepares the DSPs for pulse. DSPs are reset, software and data is uploaded.
- *Loaded Ready* - System is ready for pulse after an arm command.
- *Running Pulse* - System has been armed and is pulsing.
- *End Shot* - System can detect the end of a pulse if the hardware gate controlling the software is closed or if the number of programmed iterations is obtained. In this case, system automatically goes from Running Pulse to End Shot state.
- *After Pulse Operations* - When the pulse is over, the system starts collecting data from hardware modules, storing it in the local MDS tree.
- *Data Ready* - After all data is collected and stored, system goes to data ready. Data can now be retrieved from the local tree.
- *Error* - From any state, if a severe system internal error is detected, the system goes into error state. It can also go to error if `DPCS_Abort()` is called externally. The error code can be checked using the `DPCS_Status` TDI function.

A set of TDI functions are the state machine's stimulus. These functions can be called remotely from the central control software using MDSip by connecting to the MDSPlus server installed in the VME crate (figure 4.11). There are two functions (`DPCS_State` and `DPCS_Status`) to check the system state and errors.

The complete list of functions to control the APCS state-machine is:

♢ `DPCS_Init()` - After a power up, the system must be initialized to go to idle state.

♢ `DPCS_Ld_Data()` - Resets the modules to start from safe known state. Reads data from data tree and loads it into DSPs.

♢ `DPCS_Ld_ DSP()` - Resets the modules to start from safe known state. Reads all data from data tree (including the DSP binary code) and loads it into DSP.

♢ `DPCS_Arm()` - Sets the system to receive the hardware trigger to start a pulse.

♢ `DPCS_Abort()` - Resets all modules and enters the Idle state putting all outputs at 0

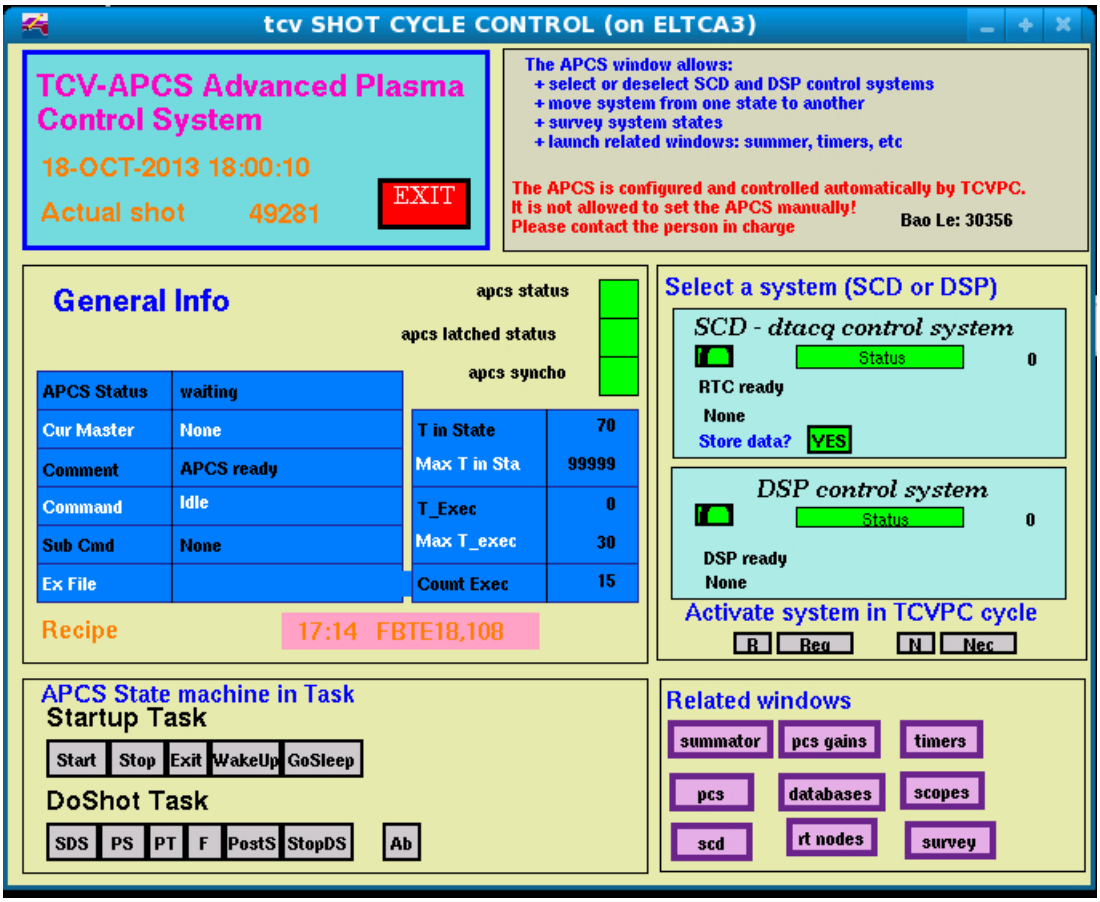

Figure 4.11: The TCV Plant Control System graphic interface window to control the APCS and check its state and status.

Volts.

- ♢ `DPCS_End_Shot()` - Stops the running pulse, putting the outputs at a safe value and starts collecting data from hardware to store in local tree.
- ♢ `DPCS_Collect_Dt()` - If in error state, the operator may want to recover the data for debugging purposes. Using this function the system will try to recover as much valuable data as possible.
- ♢ `DPCS_Dt_Collected()` - After data has been stored in local tree, system can go to idle after being told that data has been collected from the local tree to the global TCV data tree.
- ♢ `DPCS_State()` - Returns the state machine code. This value can also be read directly from the data tree.
- ♢ `DPCS_Status()` - Returns the system error code. This value can also be read directly from the data tree.

4.4.4 DSP Software Compilation State Machine

The same principle was also used to build a compilation state-machine, which reads the source code from the data tree, compiles and links against the DSP OS using the tools described in the previous section and puts the binary code back to the tree.

To start using the compilation state machine, source files must be stored in the APCS data tree under shot number 999 (the compilation shot number). Table 4.3 presents the possible states of the machine.

State Code	Description
1	Idle (Ready to compile)
2	Compiling
3	Compiled with success
32	Error state

Table 4.3: List of States for the Compilation State Machine.

Table 4.4 depicts the TDI functions that can interact with the compilation state machine.

Function	Description
DPCS_Compile_State()	Returns the state of the compilation machine.
DPCS_Compile_Reset()	No matter what the previous state is, this will reset compilation state to 1.
DPCS_Compile()	Compiles the source files in shot 999 and puts the compiled files back on tree (also 999) Returns 2 on error Returns odd number on success
DPCS_Compile_Restart()	After succesfull compilation (from state 3) it is necessary to run this function to restart to idle (state 1)

Table 4.4: List of TDI Functions that interact with the Compilation State Machine.

The system permits to check relevant status in real-time using the system log file. The system sends any errors that may occur (including compilation errors) and any notification or warnings to the system log file. The log file is used as an historical archive of every important events that were acknowledged by the system. The following command can be run from console to view in real-time the messages sent to the log file:

```
tail -n 1 -f /home/tcv_oper/.dpcsdir/dpcs.log
```

At the end of the compilation, it is also possible to check the complete compilation output and the memory map files in the local tree node :

```
\TOP.INPUTS.COMMON:COMP_OUTPUT
\TOP.INPUTS.S_DSP_0xx:COMP_LOG
```

4.4.5 Data Tree

MDSPlus is used to store each discharge's data for algorithm debugging and data analysis.

The system MDSPlus tree has two main branches. Since this is a control system, the first branch is used to store the configuration, algorithm code and initial data to be uploaded to the DSPs before the shot - the control branch. The second branch is the data retrieved from the system after the shot. This data includes the final algorithm DSP memory space and a decimation of iterations of the control cycle's Data Mover data (including ADC, DAC and software data) for debugging purposes.

After defining the data tree structure, the MDSPlus tree was built using Tree Command Language (TCL). Table 4.5 presents an example of the code used to build a part of the tree. This code builds the part of the tree that stores the 9 hardware modules configuration files, data period and start time.

The local tree is used to store the data that will be uploaded to the DSPs before each plasma discharge. After the discharge the data is collected from the hardware modules and stored in the local tree. Between plasma discharges, the tree is synchronized with the central TCV database through the network using standard `rsync` over `ssh` Linux commands.

4.5 APCS Commissioning

4.5.1 Introduction

After preliminary tests in Portugal, the system was installed in TCV. The DSP interface was tested using several algorithms:

- Putting some APCC input into another APCC output;
- Controlling a digital I/O based on an APCC input level;
- Output an IIR low-pass, high-pass or band-pass filter from the corresponding input or from other APCC input.

```
fun public make_apcs_v2()
{
        Tcl("edit/new apcs");

        Tcl("add node .INPUTS");
        Tcl("set default .INPUTS");

        Tcl("set default \\TOP.INPUTS");

        _mods = [".S_MODULE_"//iii(1+ramp(9))];
        for(_i=0; _i<size(_mods); _i++)
        {
                Tcl("add node "//_mods[_i]);
                Tcl("add node/usage=numeric "//_mods[_i]//":CONFIG_FILE");
                Tcl("add node/usage=numeric "//_mods[_i]//":DATA_PERIOD");
                Tcl("add node/usage=numeric "//_mods[_i]//":START_TIME");
        }

        Tcl("write");
        Tcl("close");
}
```

Table 4.5: Example code for the construction of part of the data tree.

These tests revealed that the system is appropriate for the application and performs according to the expectations when properly configured. In the beginning, the lack of some scripting tools capable of automatically create the configuration for the Data Mover created some difficulties with a lot of time being necessary to debug small configuration errors. These difficulties obviate the necessity for the tools developed for APCS integration in TCV.

This section describes the work of commissioning the APCS system in TCV, and depicts how specific problems of the installation of a control system into a complex system such as TCV can be overcome.

4.5.2 ADC and DAC Calibration

To avoid the drift of the ADC and DAC precision during long periods of time in a hostile environment, it was specified that an automatic procedure to check the calibration of the ADCs and DACs should be implemented. If needed the calibration would be integrated in the automatic calculation of the physical values, provided by the DSP software.

The first approach to this problem, would be that before each discharge, in the beginning of the preparation for the next experiment, the DSP would run an automatic acquisition, taking the current value as the zero offset for that experiment. This solution was limited because it only corrects the offset at the input and neither the input gain nor the output offset or gain. Moreover in some cases it was diagnosed that TCV signals were not at zero value during the preparation, misleading the offset correction to create a wrong assumption of the signal offset.

In face of these problems a more complete procedure was developed and implemented for full calibration of all inputs and outputs of the system.

During a dry run discharge that is programmed every morning for a standard test of the Plant Control System, the module inputs are driven by signals provided by calibrated generators that produce predefined signals that cover the ADC scale. The DSPs run a calibration program that uses the DAC outputs to produce a signal that covers the DAC output scale. The analogue inputs of the ADCs and DAC outputs are acquired by the APCS system and by an independent acquisition system and stored in the data tree. In the end a Matlab function reads the data from the tree and by comparing both sets of acquired data, calculates the offset and gain corrections for each ADC and DAC. The calibration correction values are stored in the tree and are uploaded to the DSPs before each discharge to use in every calculation of the ADC input or DAC output.

Figure 4.12 shows the data acquired for the calibration of the system.

4.5.3 From Analogue to Digital Control

4.5.3.1 Using IIR Filters as PID Controllers

To make the first APCS tests with real-time plasma control in a TCV discharge, it was important that a previously tested and validated control algorithm was used. The best known and tested control algorithm would be the PID controller implemented in the analogue control system.

The G-Matrix was replaced by the APCS, receiving the observer signals from the A-Matrix and sending the outputs to the M-Matrix. Digital filters were implemented in APCS with the same transfer functions as the one obtained by combining P, I and D terms, to perform the algorithm substitution.

Figure 4.13 depicts the TCV Hybrid Control System in a simple schematic form and figure 4.14 depicts the TCV Control System with the APCS replacing the analogue PID controller in the G-Matrix.

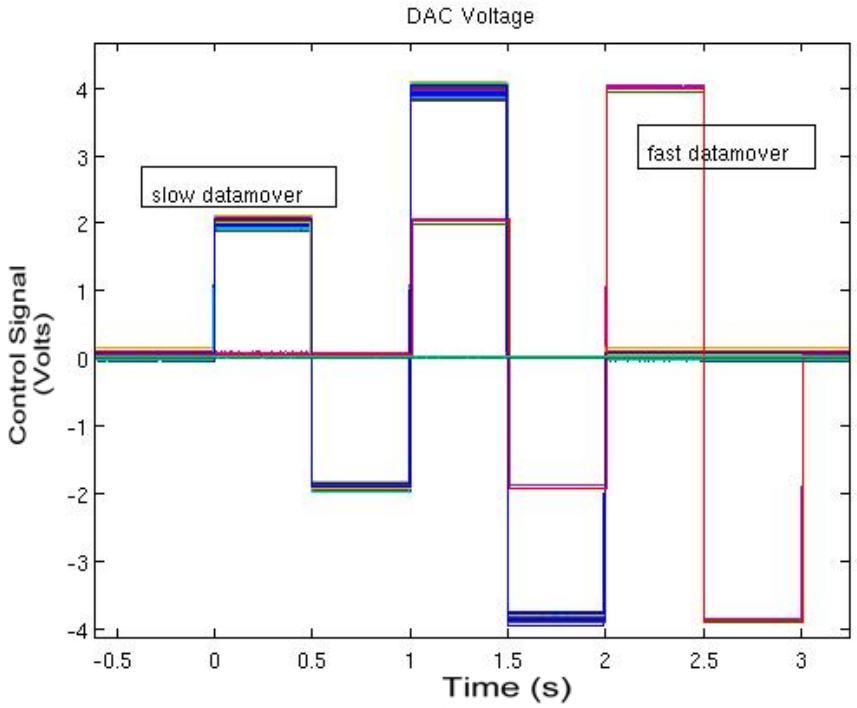

Figure 4.12: DAC acquired data for offset and gain calibration of the APCS system. It is possible to see that the same DAC programmed output voltage produce different signals. The difference between the programmed voltage and the real acquired signal is used to calibrate the system.

To compute the correct parameters for the digital filter running in the DSPs, it is necessary to find the transfer function for the PIDs. This can be derived from the G-Matrix electronics depicted in figure 4.15.

Although the electronic schematic is the same for G1, G2 and G3, the circuit component values are different according to the functionality to implement. Thus different transfer functions can be achieved for this electronic circuit.

Proportional term transfer function

The transfer function for the proportional term is given by

$$H_p = \frac{-G_p}{1 + s\tau_{p1}} \tag{4.2}$$

with $G_p = \frac{R_{p2}}{R_{p1}}$ and $\tau_{p1} = R_{p2}.C_{p2}$.

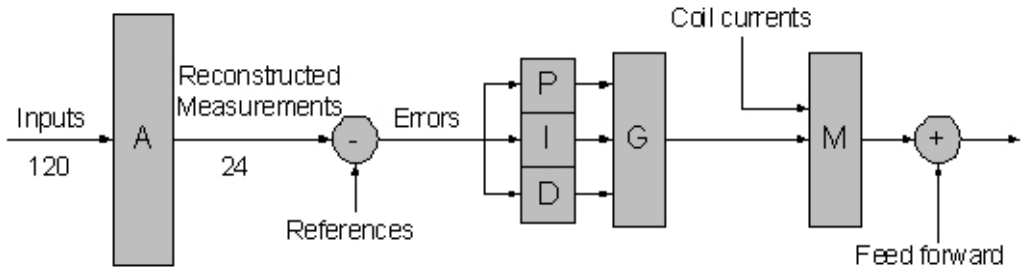

Figure 4.13: TCV Hybrid Control System.

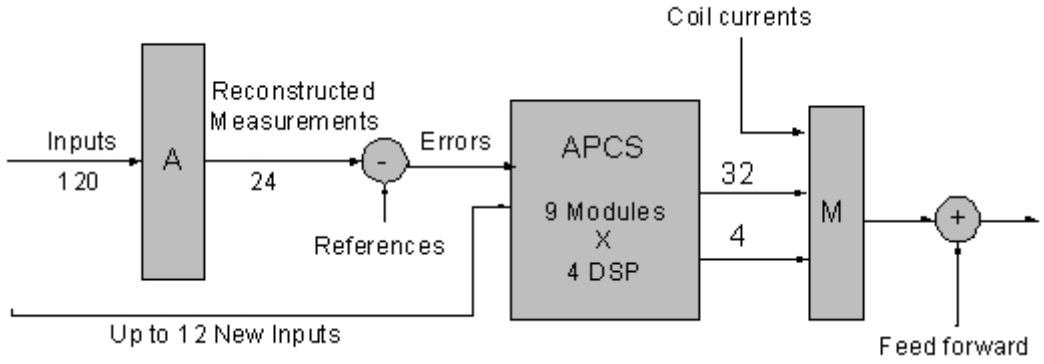

Figure 4.14: TCV digital control scheme with the APCS replacing the PID analogue controller implemented in the G-Matrix.

Integral term transfer function

$$H_I = \frac{-1}{s\tau_I} \tag{4.3}$$

with $\tau_I = R_{I2}.C_{I2}$.

Derivative term transfer function

$$H_D = \frac{-s\tau_D}{(1+s\tau_{D1})(1+s\tau_{D2})} \tag{4.4}$$

with $\tau_D = R_{D1}.C_{D2}$, $\tau_{D1} = R_{D1}.C_{D1}$ and $\tau_{D2} = R_{D2}.C_{D2}$.

Table 4.6 contains the values of the circuit components used to calculate the transfer functions. Channels 23 and 24 have different values and are presented for completeness of information, but they are not used at the moment to control any parameters.

According to the Hybrid controller schematics in figure 4.2, G-Matrix outputs are

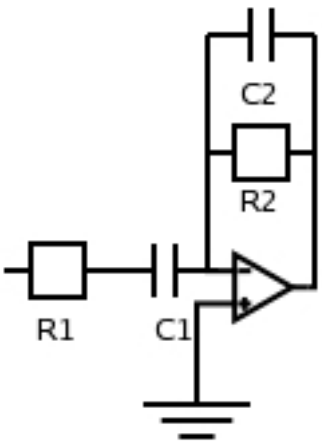

Figure 4.15: Electronic circuit used in the G Matrix hardware.

daisy-chained: G1-Matrix (Integrator) is added to G2-Matrix (Proportional), then to G3-Matrix (Derivative). This means that the final transfer function for the output of each block is given by the following equations:

$$G1_{Output} = H_I.G1_{Input} \tag{4.5}$$

$$G2_{Output} = H_P.G2_{Input} + G1_{Output} \tag{4.6}$$

$$G3_{Output} = H_D.G3_{Input} + G2_{Output} \tag{4.7}$$

From both these equations and the coefficients programmed for the G-Matrix in each discharge, the final transfer functions can be calculated. Using the Tustin's method (also known as bilinear transform)[104], the continuous-time transfer function ($H_{CT}(s)$ - also called an analogue filter) can be converted into a transfer function in the discrete time

	R_1	C_1	R_2	C_2		τ_1	τ_2
Proportional	$10k\Omega$		$100k\Omega$	$680pF$	$G_P = 10$	$68us$	
Integral	$27k\Omega$			$100nF$	$\tau_I = 2.7ms$		
Derivative	100Ω	$1uF$	$68k\Omega$	$1nF$	$\tau_D = 68ms$	$100us$	$102us$
Derivative(23)	$1k\Omega$	$47nF$	$340k\Omega$	$138pF$	$\tau_D = 16ms$	$47us$	$46.92us$
Derivative(24)	100Ω	open	$68k\Omega$	$1nF$	$\tau_D = 0$	0	0

Table 4.6: List of circuit component values to calculate G-Matrix transfer functions.

domain ($H_{DT}(z)$ - also called a digital filter). This digital IIR filter (equation 4.8) are then computed in the APCS DSPs to reproduce the same behavior as the Hybrid Controller. Table 4.7 presents the calculated IIR coefficients for 2 different discretization sampling times.

$$H(z) = \frac{Y(z)}{X(z)} = \frac{\sum_{i=0}^{P} b_i z^{-i}}{\sum_{j=0}^{Q} a_j z^{-j}} \tag{4.8}$$

	b_0	b_1	b_2	a_0	a_1	a_2
$H_P(100us)$	-4.237	-4.237	0	1	-0.1525	0
$H_D(100us)$	-85.1	0	85.1	1	0.06271	9.828e-4
$H_P(50us)$	-2.688	2.688	0	1	-0.4624	0
$H_D(50us)$	-77.25	0	77.25	1	-0.6103	0.09313

Table 4.7: List of coefficients for IIR filters for 100us and 50 us sampling times.

4.5.3.2 Sensitivity to Derivative Action

After the implementation of the Tustin Transforms coefficients in the IIR filters programmed into the DSPs, APCS was tested and the outputs were compared to the outputs of the analogue system for system high level commissioning.

This test was made with success, with all control signals behaving properly except for the APCS module used for the fast plasma vertical stabilization. This signal revealed to be too sensitive to the signal noise that was amplified by the derivative gain used in the controller.

The analysis of the problem is well known on PID digital control implementation as derivative control action is very sensitive to noise, and many times the PI controller is preferable to a more complex PID controller due to this problem.

This problem was solved by the implementation of a new vertical position observer that will be presented in the next chapter.

4.5.4 Test Results and Improvements to the TCV Control

Figure 4.16 shows the APCS system after its integration in TCV. The controller inputs and outputs are cabled respectively from the top and to the bottom of the system. The system timing signals are inputs on the right of the crate using the digital I/O module.

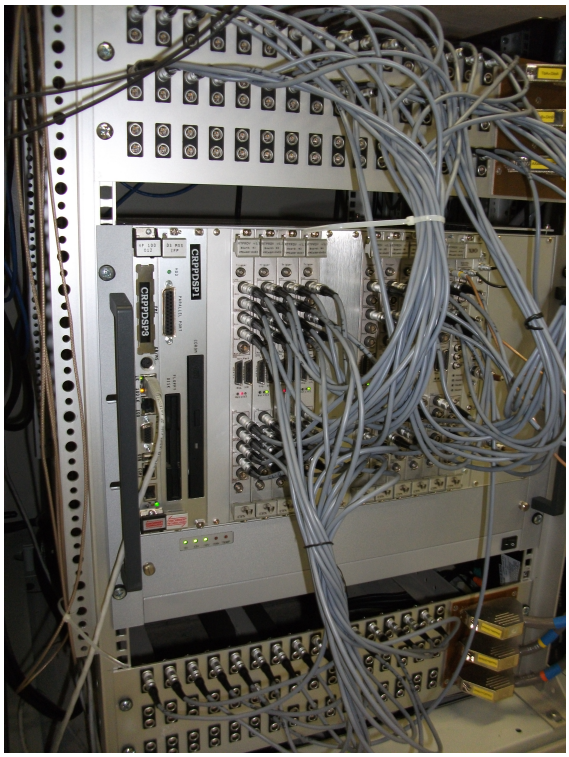

Figure 4.16: APCS system photo taken after its installation at TCV.

The APCS integration into the TCV plant control software was successful. The system was controlled remotely from the control room for several shots. These tests were made using the APCS system in parallel with the PID controllers. The outputs were compared to check the algorithm showing the system behaved correctly, after the correction of some initial typical integration problems such as timing and hardware channel communication configuration as well as IIR filter parameters configuration due to the use of processors that adopt different data endianness[1].

An effective TCV plasma control using the new APCS was first achieved in shot 34313. Figure 4.17 details a comparison of the output (voltage vs time) using the APCS system (red) and the PID controllers (blue). The ripple in the APCS signals when compared to the PID analogue controller signals is due to the the APCS signals having a bigger time resolution both due to (i) the higher acquisition rate used for the digital system and (ii) the higher frequency response of APCS due to its short control cycle. Figure 4.18 depicts

[1]Little Endian and Big Endian refers to the order in which bytes are stored in a digital memory or used in a microprocessor. Because there is no correct order, different data descriptions have been adopted by microchip producers. The term comes from the wars fought between those who thought eggs should be cracked on the Big End and those who insisted on the Little End in the book *Gulliver's Travels*.

one of the signals using the same acquisition time resolution on both control systems. In [105] some results of the system are presented including a signal comparison between the APCS and the previous analogue system.

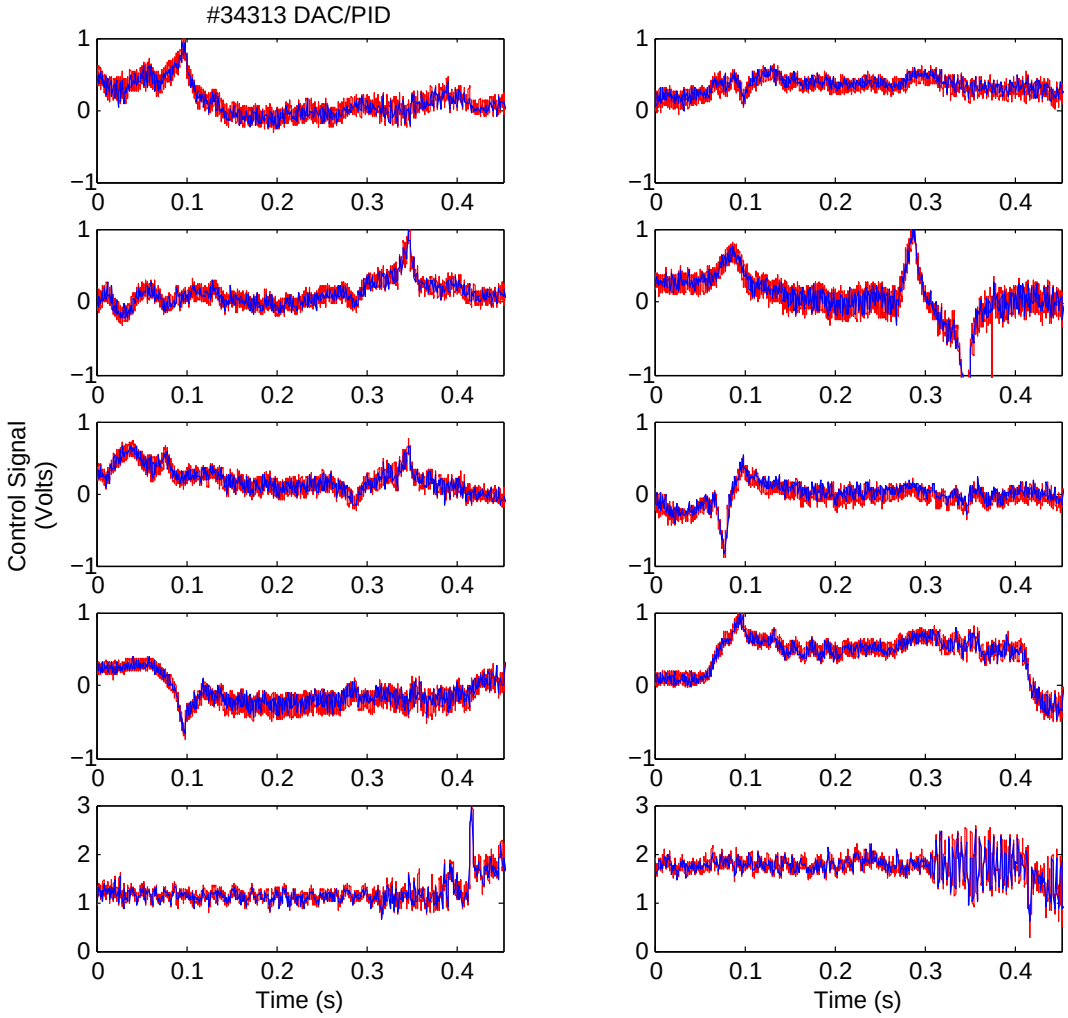

Figure 4.17: The APCS signals (red) and the PID controllers signals (blue) in TCV shot 34313 controlled by the APCS system.

Several TCV discharges have been made with the APCS and analogue control systems in parallel and with only the digital system. The discharges were produced according to the initial control cycle specification of 100 μs of slow control cycle sharing the data between the 32 processing units and 5 μs of fast control cycle sharing the data between the 4 processing units in the same hardware module. The results have shown that APCS

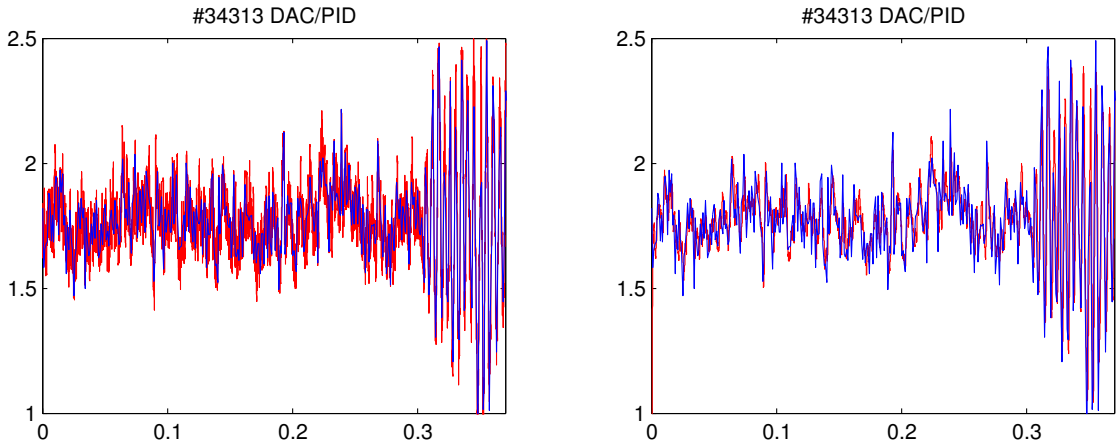

Figure 4.18: The APCS signals (red) and the PID controllers signals (blue): (i) on the left the higher resolution signal of the APCS System; (ii) on the right the signals with the same time resolution.

can control the TCV plasma correctly and contribute to enhance the plasma control performance, provided the appropriate algorithms are developed. One example is the work presented in the next chapter aiming at improving the plasma vertical stability, which could not be implemented using the TCV analogue control system.

The installed APCS provided TCV with a digital, procedural, nonlinear control system as well as a higher number of available control channels [106], with a set of software tools implemented for the development of algorithms and to control the DSPs in the TCV shot cycle [107]. The APCS has been used for the improvement of real time control of plasmas and ECRH systems on TCV [108].

5

Improving the Plasma Vertical Stability

Contents

"Because the shape of the whole universe is most perfect and, in fact, designed by the wisest Creator, nothing in all of the world will occur in which no maximum or minimum rule is somehow shining forth. "

Leonhard Euler, 1744

5.1 Introduction

The plasma vertical instability in modern tokamak devices [20] is a consequence of elongated cross-section plasmas [58][109]. Higher plasma elongation[1] (κ) allow better confinement than the traditional circular plasmas due to:

- larger plasma currents, proportional to $\frac{1+k^2}{2}$ for the same values of the safety factor q, magnetic fields and the major and minor radius [52];
- higher beta values[2] (β), since $\beta < \frac{I_p}{aB_\phi}$ where I_p is the plasma current and B_ϕ is the toroidal magnetic field.

The advantages of such elongated plasma shapes demand an effort to overcome the plasma vertical instabilities. Closed feedback loop control systems have been developed for several tokamaks to accomplish this task [31][55][56].

The *Tokamak à Configuration Variable* (TCV) was specifically designed to accommodate plasmas covering a wide range of shapes and high elongation (up to 3). Higher elongation plasmas make stability margins smaller, demanding more accurate and faster control systems. TCV uses an almost unique shape and vertical control system composed of slow active coils outside the vessel and fast active coils inside the vessel, with sub millisecond response time power supplies [58][110].

The introduction of the new Advanced Plasma Control System (APCS) in TCV requires the development of a new vertical position observer built to optimally exploit the capabilities of the new system and to correct the changes that were detected by the introduction of signal digitizing in the feedback loop. This chapter begins by discussing the need for a new measurement of the plasma vertical position, the method to build the observer and the validation of the measured position and velocity by comparing with the method and observer previously used in TCV.

[1] The plasma elongation (κ) is one of the parameters used to define the plasma cross section. It is defined as the ratio $\kappa = \frac{b}{a}$, where a is the plasma minor radius and b is the height of the plasma.

[2] β is the ratio of the kinetic plasma pressure energy density by the magnetic field energy density, which is a measure of the plasma confinement performance.

As for most control situations, two problems must be solved in vertical plasma position control to obtain the desired performance: (i) the plasma position must be accurately detected in real time (a measurement of the position achieved by the use of an observer); and (ii) a suitable algorithm calculates the best coil currents to be applied to correct any unwanted position deviations (control). In this chapter both problems were tackled to upgrade the TCV vertical plasma stabilization controller performance.

While for the plasma position observer a study of the TCV magnetic diagnostics was made, to understand the best way to improve the position observer, to build and improve the control algorithm, the plasma models that describe the plasma behavior in TCV were analyzed and studied, to find the choice that better suites the application.

From the modeling of the plasma response to the actuators, a state-space model was used to calculate a high order transfer function (TF) of the plasma position response to the voltage applied to the in-vessel control coils. This TF must go through a model reduction algorithm to obtain a lower-order model that is used to establish the bang-bang time-optimal controller. A state-space map of the controllable region and switching points was derived for the calculation of the bang-bang controller. From this map the optimized switching-time that minimizes the time to reach the set point was taken for different pairs of position-velocity.

A simulation tool using Matlab Simulink [111] was built to validate, analyze and improve the controller design. The final controller was implemented in the APCS system and tests of the controller during TCV discharges were performed and analyzed.

A description of the control algorithm development and implementation using the hardware and software tools already presented is depicted and at the end of the chapter the results of the controller performance during real TCV discharges are provided.

5.2 Vertical Plasma Position Observer

The TCV plasma vertical displacement can be measured using three different methods:

- The observer used for real time feedback control of the plasma vertical position using the magnetic measurements available for the control system. Since the magnetic signals from the probes and flux loops are proportional to the plasma current, this observer is the product zI_p;
- The value of the magnetic axis position obtained from the equilibrium reconstruction LIUQE code [112][113]. This code uses the complete set of magnetic measurements;

- The centroid motion of the soft X-ray emissivity using tomographic techniques.

For the purpose of this work the first method was analyzed and improved, because it is readily available in real-time, while the second one was used as a reference to evaluate the quality of the achieved improvements.

To estimate the position of the plasma to be used in the control system, the magnetic probes signals are fed into the A-Matrix (see section 4.2.2) and, using the proper coefficients, a real time observer signal estimates the plasma position as a linear combination of the magnetic measurements (recall figure 3.7). The coefficients used to build the observer are calculated before each TCV discharge, on the basis of the programmed position of the plasma and weighting the probes appropriately.

5.2.1 Plasma Position Observer Requirements

When migrating from the analogue into the digital control system some precautions had to be taken to ensure that the digital system can cope with the demands and specifications of the currently running system.

It became clear that the noise on the measurement of the vertical position of the plasma affects the overall stability of the closed loop control of the plasma. The initial analogue vertical position control loop for the internal fast coils was composed of a zI_p observer (from integrated magnetic probe signals) and a D (derivative) controller [87]. When migrating to the digital control system the derivative algorithm running on the digitized observer signal proved to amplify the noise, rendering the controller unstable. As a consequence the transfer function of the D controller could not be used over the digital data, because the 12 bit ADC resolution of the APCS system would not be enough.

From control theory, it is well known that the utilization of derivative action in a controller is highly sensible to noise. Because of this concern, derivative action is often omitted by the use of PI instead of PID controllers [114].

The original controller for plasma stabilization at TCV used only the D term, with the zI_p observer built based on the integrated signals from the magnetic probes, also called the B-observer. By changing the observer to the non integrated signals from the magnetic probes, a similar control signal can be obtained by the application of a P controller, avoiding the derivative action of the original controller, because the observer signal is already derived.

In TCV both B and $\dot{B}$ measurements are available because magnetic probes intrinsically measure $\dot{B}$. In consequence, the non integrated raw signals from 20 magnetic probes

may be applied for real time measurement by the control system. Using these 20 non integrated magnetic probe signals, a new observer was built for integration with the P controller, also called the Bdot observer.

Since the new observer uses dB/dt as input signals instead of B, it is not a real zI_p observer but a $d(zI_p)/dt$ observer that measures the plasma displacement velocity instead of the position. The new observer is applied for plasma vertical stabilization control, using the internal G coils. This method is often employed in tokamaks that have migrated to digital controllers [31].

5.2.2 Vertical Position Observer Design

The vertical position observer uses a linear combination of magnetic field probe signals. The A-Matrix coefficients of the probes signals are calculated before each plasma discharge, accounting for plasma parameters such as shape and position. This means that, although the real-time vertical position observer is independent of these plasma parameters, the contribution of each probe to the observer has in account the pre-planned plasma parameters. For example, when the experiment aims at creating a plasma in the upper part of the vacuum vessel, the probes closer to the predicted plasma will be more efficient estimating its position, thus being given more weight in the observer.

The coefficients calculated are the zI_p observer. From a finite element set of plasma current filaments, using Green's functions, the magnetic field produced in the probes by the filaments is calculated. A-matrix is built with the probes that are going to be used, which are inverted to obtain the observer coefficients [110].

The plasma current density is decomposed into m_h by n_h vertically bilinear finite elements evenly distributed in a two dimensional poloidal cut of the vessel. This defines a rectangle with boundaries $[a, b] \times [c, d]$ set to include the plasma inside it according to the pre programmed equilibria defined in the discharge preparation, storing its values in the matrix T_{xh} according to [113]:

$$h_{ij}(r,z) = \left(1 - \frac{|r - r_i|}{\Delta r}\right)\left(1 - \frac{|z - z_j|}{\Delta z}\right)[|r - r_i| \leq \Delta r][|z - z_j| \leq \Delta z], \\ i = 1 \ldots m_h,\ j = 1 \ldots n_h \quad (5.1)$$

where

$$\Delta r = \frac{b-a}{m_h + 1},\ \Delta z = \frac{d-c}{n_h + 1},\ r_i = a + i\Delta r,\ z_j = c + j\Delta z$$

and the square brackets represent the Iverson brackets with value 1 for a true condition and 0 otherwise. The current density can thus be written as a linear combination with coefficients a_h[113]:

$$j_\varphi(r_x, z_x)\Delta r\Delta z = I_x = T_{xh} \cdot a_h \tag{5.2}$$

Using this geometry and introducing the weights w_m that permit to give more relevance to some measures over others, the magnetic field probe measurements can be related to the current density by:

$$w_m B_m = w_m(B_{mc}I_c + B_{mx}T_{xh}a_h) \tag{5.3}$$

where B_m is the vector of the measured quantities in the magnetic probes, B_{mc} is the matrix of the Green functions between the coils and the magnetic probes, I_c is the vector of the poloidal field coil currents, B_{mx} is the matrix with the Green functions to link the current in the plasma filaments with the magnetic field measured by the probes.

The weighted coefficients can be obtained taking the term with the current density from equation 5.3:

$$w_m B_{mx} T_{xh} a_h = w_m B_m - w_m B_{mc} I_c \tag{5.4}$$

and solving in order to a_h:

$$a_h = A_h^{-1}(A_{hT} w_m B_m - A_{hT} w_m B_{mc} I_c) \tag{5.5}$$

with A_h and A_{hT} given by:

$$A_h = T_{xh}^T B_{mx}^T w_m^T w_m B_{mx} T_{xh} \tag{5.6}$$

$$A_{hT} = T_{xh}^T B_{mx}^T w_m^T \tag{5.7}$$

Using the Einstein notation and replacing I_x according to 5.2, the observer is defined as [115]:

$$zI_p = (z_x^T - z_a).I_x = Z_x^T A_m B_m - Z_x^T A_c I_c \tag{5.8}$$

where z is the position of the plasma column, z_x is the position of the filaments of the plasma column and z_a is the reference position of the plasma axis. Z_x is the vector of relative positions given by $Z_x = z_x - z_a$. A_m and A_c are given by:

$$A_m = T_{xh} A_h^{-1} A_{hT} w_m \tag{5.9}$$

$$A_c = T_{xh} A_h^{-1} A_{hT} w_m B_{mc} \tag{5.10}$$

The plasma velocity observer ($d(zI_p)/dt$) uses the same method. Since the time derivative of I_c has slow variation compared to vertical position growth rate, it is not relevant for the control system. In consequence, the following reduced equations define the Bdot observer:

$$\frac{dI_x}{dt} = A_m . \frac{dB_m}{dt} \tag{5.11}$$

$$\frac{d(zI_p)}{dt} = Z_x^T \frac{dI_x}{dt} \tag{5.12}$$

The correction due to the coil currents in this case is added to the reference signal in the controller, which makes the output error signal completely consistent. Another difference between the two algorithms that build both observers is the set of probes that can be used. Although the TCV control system can use 38 probes with integrated signals, only 20 non-integrated signals are available at the moment as inputs to the control system, due to the initial plasma control design and availability of input channels at the observer matrix.

When building the observer, attention was given to the fact that some probes are close to the internal active coils. As a consequence, the plasma measurement is hidden by the effect of the coils and therefore the weights of those probes are set to zero to avoid coupling between the observer and the actuators.

Figure 5.2 depicts the time derivative of the magnetic field as measured by the magnetic probes and the coefficients of the new observer while figure 5.1 shows the magnetic field (integrated probe signals) and the standard plasma vertical observer coefficients. In each observer, the matrix of measurements (top plot) is multiplied by the vector of coefficients (bottom plot) to obtain the plasma position (B observer) or velocity (Bdot observer) time vector. The magnetic field probes are mounted inside the vessel on the wall of the vacuum vessel, roughly equidistant in the poloidal plane. They are numbered clockwise, starting from the inboard midplane (recall figure 3.7).

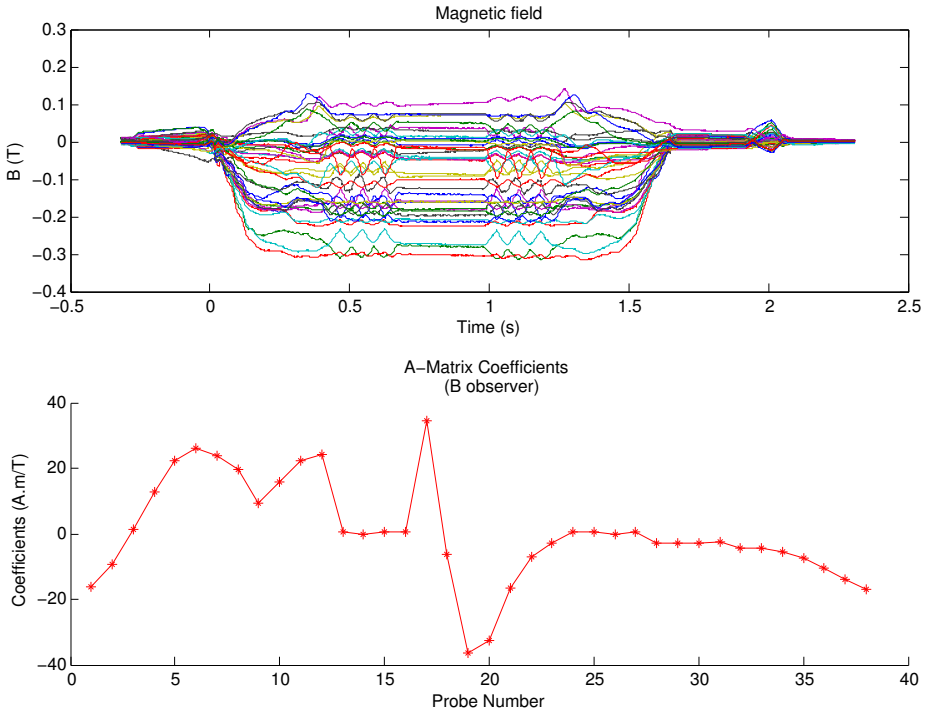

Figure 5.1: The magnetic field measured by the probes and the standard plasma vertical observer coefficients.

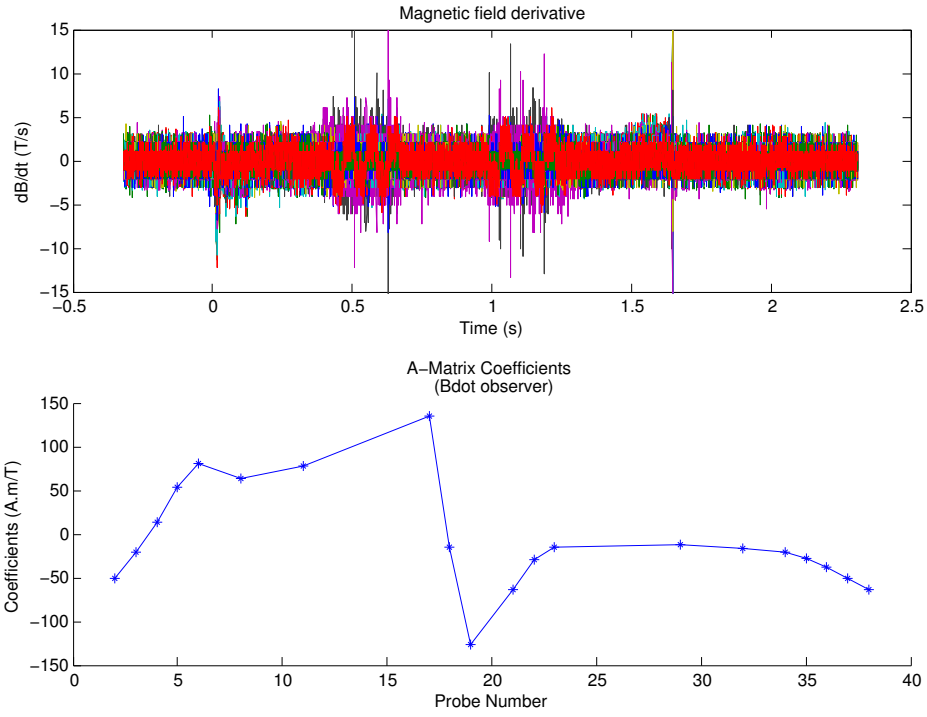

Figure 5.2: The derivative of magnetic field as seen by the magnetic probes and the coefficients of the new Bdot observer using probe numbers $[2:6,\ 8,\ 11,\ 17:19,\ 21:23,\ 29,\ 32,\ 34:38]$.

5.2.3 Observer Validation

The validation of the observers and of the method used to find the coefficients was performed by evaluating and comparing the plasma position obtained using different methods. Figure 5.3 presents the observer signals and the control output voltages for both control loops during a TCV discharge with the plasma under the influence of a small preprogrammed vertical oscillation.

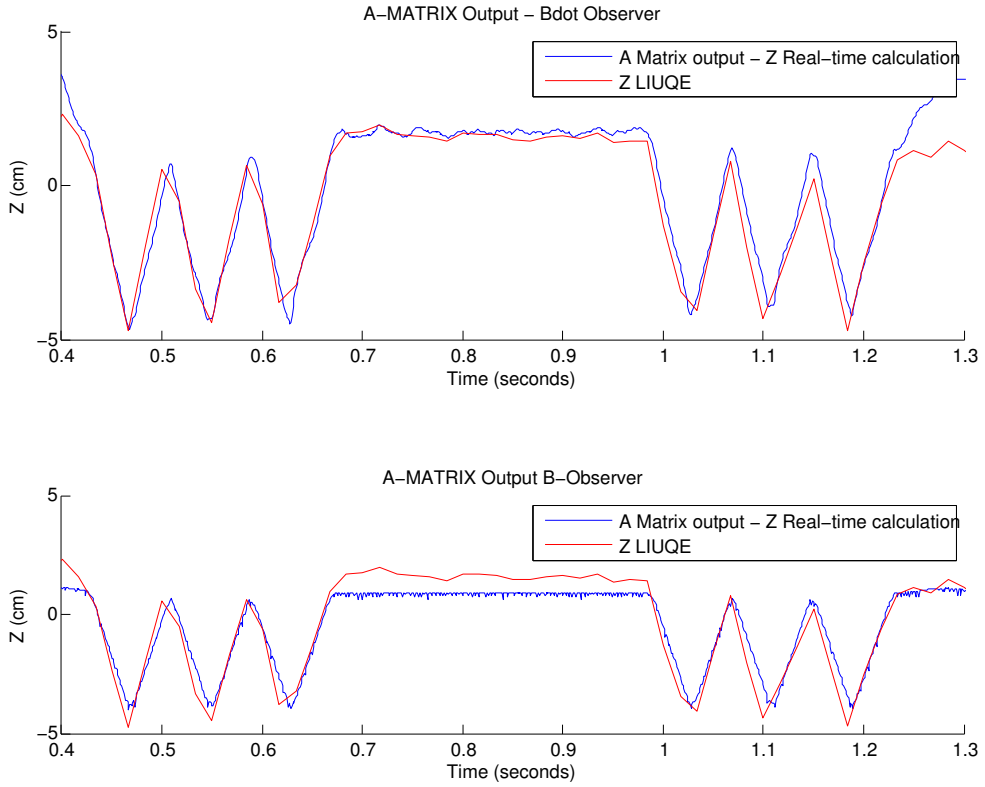

Figure 5.3: Verification of the observer signals during TCV discharge 39082 where the plasma had a small "yo-yo" movement (vertical oscillation).

The observer measurement in the first plot (Bdot observer) had to be integrated to give the plasma position since the observer is in reality a plasma velocity observer. The initial known plasma position is used as the constant of integration. Both observers are compared to the plasma position given by LIUQE equilibrium plasma reconstruction code.

Note that the Bdot observer estimates the plasma position more accurately than the B observer, which has a slightly smaller value as the plasma position deviates from the zero position. The better accuracy in the measurement of the plasma position with this observer is due to the way some coefficients are set to zero because of the probes vicinity

to the fast control coils. While in the case of the velocity observer these probes are not taken into account when calculating the coefficients, in the B observer the coefficients were only set to zero at the end of the calculation, causing a slight inconsistency. This fact was compensated by a higher gain in the D term. With the Bdot observer this gain was recalculated because the compensation is not needed anymore, but as a result the observer is fully self-consistent.

Figure 5.4 depicts the comparison between the control signals for both observers and digital/analogue systems. Figure 5.4.B allows to see the improvement in signal to noise ratio of digital system over the PID analogue system when using the new Bdot observer. On the other hand, figure 5.4.D shows the bad performance of the digital system (blue line) when compared to the analogue PID (red line), for the original B observer. The digital control output using the B observer amplifies the input signal noise too much justifying the implementation of the new dB/dt observer.

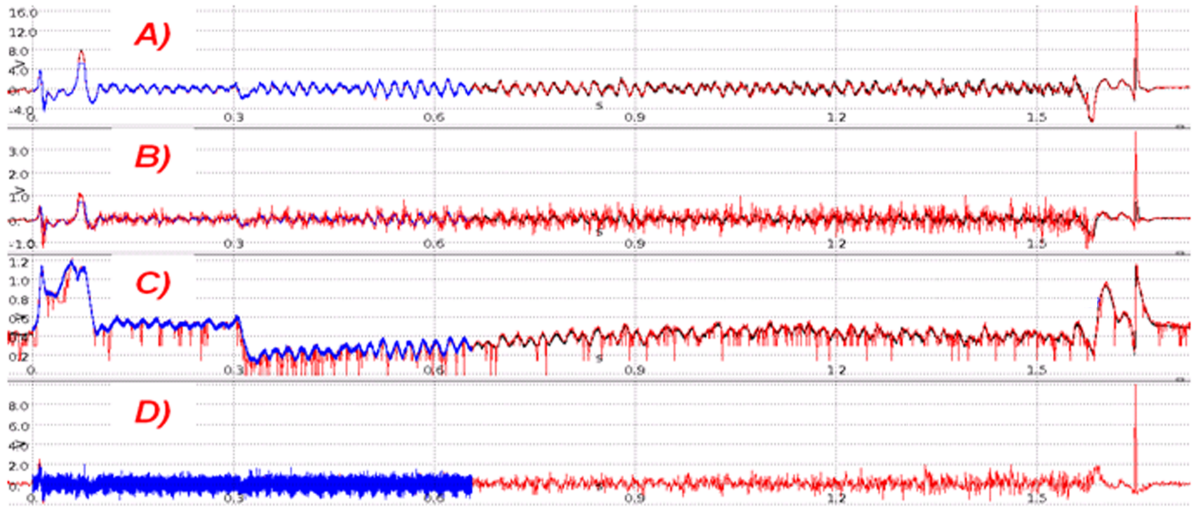

Figure 5.4: Comparison between the control signals for both observers and digital/analogue systems (discharge 40122) - A) dB/dt observer signal as input to analogue (red) and digital (blue for APCS and black for data acquisition system) control systems; B) Digital control output (blue and black) and analogue output (red); C) B observer signal input to analogue (red) and digital (blue and black) control systems; D) Digital control output (blue) using B observer.

5.3 TCV Plasma Actuators for Vertical Stabilization

5.3.1 Fast Internal Controller Coils

Aiming at achieving the control of highly elongated plasmas, TCV is equipped with a set of 6 internal coils. As it was already said, high elongated plasmas are vertically unstable, with growth rates up to $\lambda = 4000s^{-1}$. Due to the shielding effect produced by the vessel, the outer coils, equipped with power supplies with relative slow responses (0,8 ms), are limited to control plasmas with growth rates up to $\lambda = 1000s^{-1}$.

Following the design and the study of trade off between the mechanical constraints and wall separation, to reduce the screening by image currents in the vessel, the position of G coils is set according to the figure 3.7, in the outer corners of the vacuum vessel.

The coils are connected in series, with opposite currents, with a maximum current of 2 kA. The maximum current can be achieved in up to 250 μs, to be faster than the vertical instability growth rate. The series connections permit the controller to be a SISO controller. Table 5.1 presents the main parameters of the coils together with the main fast power supply parameters [116] that act together as a system to control the plasma vertical instability.

5.3.2 Fast Power Supply

A Fast Power Supply (FPS) is used to drive the current in the fast controller coils. Since the coils are connected in series, although with opposite current directions, only one power supply is needed to drive the coils. Table 5.1 also presents the relevant parameters for the FPS. The data on this table was used to build a model of the behaviour of the FPS to be introduced in the controller simulations.

5.3.3 FPS Transfer Function

5.3.3.1 From Control Signal Voltage to Current in the Coils

The information from the fast power supply and internal poloidal coils was used to build a transfer function that would permit to preview the current in the coils given the control signal sent to the power supply. This transfer function is important for use with plasma models that use the coils current as inputs[3].

[3]The model that is used to describe the plasma in this thesis uses the voltage of the control coils as inputs. This section is part of the document for future work using different type of plasma models and

Parameter	Value
Coil Impedance (frequency dependent)	$40uH$ to $100uH$ $10m\Omega$ to $100m\Omega$
FPS Output Current	$\pm 2000A$
FPS Output Voltage (no load)	$\pm 566V$
Current rise time (FPS + Coil)	$0.25ms$
Current Controlability (FPS + Coil)	$\pm 100A$ at $\pm 2000A$ $\pm 40A$ at $\pm 50A$
FPS Voltage reaction time	$5us$
FPS Switching frequency	$10KHz$ (typical) $25KHz$ (maximum)

Table 5.1: Main TCV internal coils and fast power supply parameters .

The transfer function is an integrator with gain (k) and integration time (τ), which is also a low-pass filter, given by the equation:

$$G(s) = \frac{k}{\tau s + 1} \tag{5.13}$$

The value used for the gain k is -499.5, including the gain at the output of the control signal, and the integration time τ is $1/(6.75 \times 10^6)$ seconds. Figure 5.5 reproduces the evaluated coil current following the measured values after the application of the transfer function to estimate the coil current from the control signal that was sent to the power supply.

5.3.3.2 From Control Signal to the Input Voltage in the Coils

The transfer function from the control signal to the input voltage of the coils is used for the simulation of the controller that is presented in this chapter. The plasma model uses the voltage in the coils as actuators or inputs to the plasma parameters. Moreover, the output of the digital control system uses the FPS to drive that voltage. The transfer function between the output of the control signal and the voltage in the FPS input is a simplification of the one presented in the previous section.

The transfer function from the control signal to the input voltage of the coils considered for simulation purposes is a gain with a delay. The latter may be neglected, based in the fact that the transfer function integration time presented in the previous section is much

as an example of a more generic method than the one presented in section 5.3.3.2

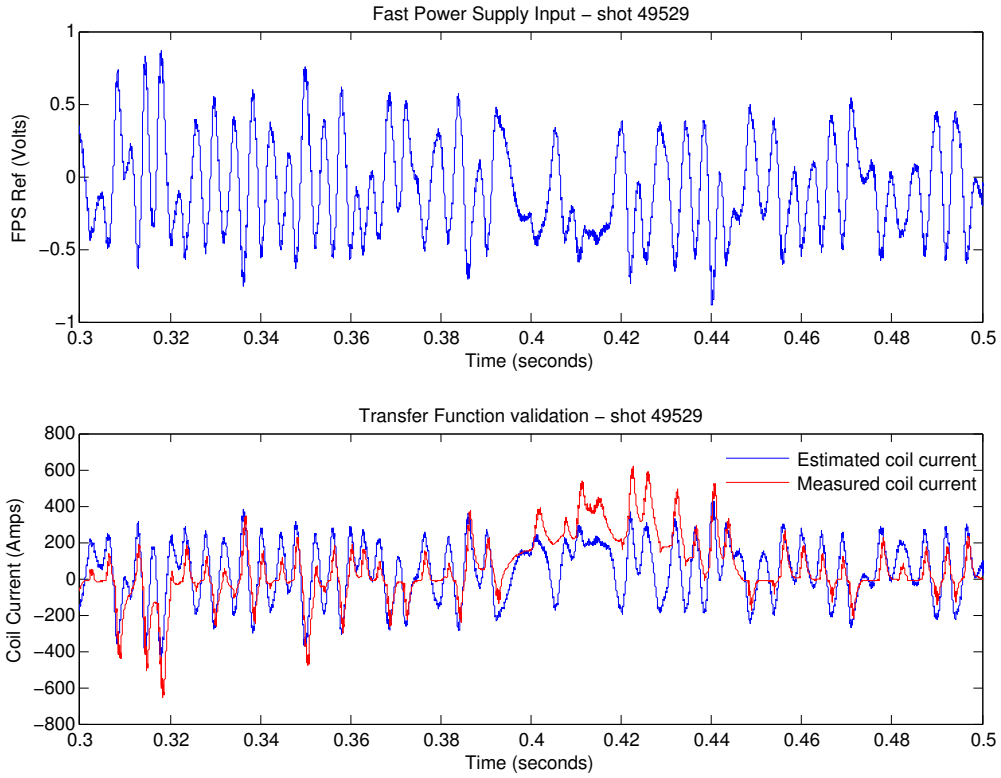

Figure 5.5: Estimated coil current using the transfer function over the FPS control signal.

smaller than the control cycle that is used.

5.4 Plasma Model

5.4.1 Introduction

As it was already said, a tokamak is a very complex system that consists of different components that interact between them. Therefore, a system model must be developed aiming at:

- Simulating the plasma behavior;
- Predicting the plasma behavior;
- Confirming our understanding of the plasma behavior;
- Improving, in the end, the vertical plasma stabilization controller algorithm.

The simulation tools to enhance the control of tokamak algorithms are particular important because expensive devices are involved (both for the device cost and for the operations cost), to avoid putting in danger the hardware while testing new algorithms

and to permit faster controller evaluation without spending machine time.

Depending on the purpose of the plasma model that is being designed, different degrees of mathematical complexity may be acceptable. While for some physics studies of plasma phenomena detailed description of the processes involved may be necessary, in tokamak control the challenge is to use simplifying physical assumptions and numerical approximations that permit the development of a model that describes the processes involved with enough precision, but maintaining the necessary mathematical simplicity to permit the design of a controller.

Plasma models for control should be good enough models, that can be compensated by the control algorithm itself that is used exactly to correct plasma instabilities but can also correct the modeling inaccuracies of the physics system model, due to physical knowledge limitations, mathematical difficulties or system complexity.

Three types of modeling are referenced in control literature, where the mathematical models are built based on:

- The physical laws of the system, *Whitebox model*;
- The system response, without any knowledge of the internal physical processes, *Blackbox model*. In this case, experimental data is used to determine the mathematical model that describes the process;
- The physical knowledge of the system, but some parameters are left to be tuned based on the experimental data, *Greybox model*.

This section presents the method used to build a model of the plasma response to the poloidal field control coils in a tokamak. The main parameters of interest are the plasma positions, current and shape. The model is linear and time invariant. With this model it should be possible to predict the behavior of the plasma position, aiming at the upgrade of the plasma vertical stabilization algorithm.

Figure 5.6 depicts a schematic of the control cycle simulator where the plasma model will be introduced to verify the plasma response to the actuator signals from the controller.

5.4.2 TCV RZIP Plasma Model

The RZIP[4] model [117][118][119][120][121][78] is a rigid current displacement model that gets its name from the simplifications assumed to build the circuit equations, with the following characteristics:

[4](R, Z, I_p) from the model state variables radial position (R), vertical position (z) and total toroidal plasma current (I_p)

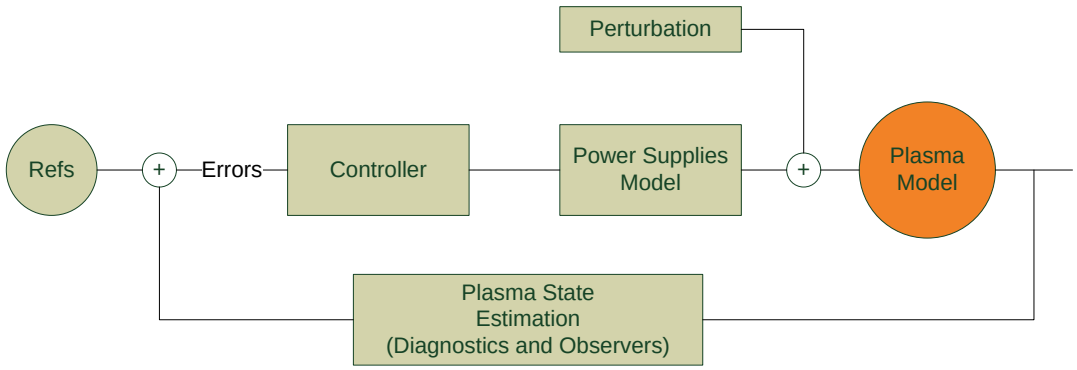

Figure 5.6: Schematic of the control cycle simulator where the plasma model will be introduced.

- The current has constant distribution, rigid model, as the plasma shape is assumed not to change;
- The vertical position of the plasma centroid can change: plasma is free to move vertically;
- The radial position of the plasma centroid can change: plasma is free to move radially;
- The integral of the plasma filaments current can change: the total plasma current is free to change.

Moreover, some more general considerations are also assumed [121]:

- All quantities are independent of the toroidal angle, toroidal symmetry is assumed;
- The mass of the plasma is negligible, reaching the equilibrium instantaneously;
- The system may be perturbed around the equilibrium;
- All poloidal currents are ignored, including plasma and conducting structures ;
- The tokamak structure and plasma are represented by a finite set of axisymmetric toroidal filaments with (i) variable current over time; (ii) finite resistance that is assumed to be constant;
- Plasma transport effects are ignored;
- The equilibrium PF coil currents are constant.

These simplifications to some more complex plasma models bring important advantages, maintaining an overall accuracy of the model. Main advantages are:

- A simple model that is easier to implement;
- No need to calculate the complete plasma equilibrium;
- More explicit model to the quantities that define plasma response to the control variables (a better control model).

The RZIP model can be derived [78][121] from: (i) the equilibrium equation of the vertical forces in the plasma (equation 5.22); (ii) the equilibrium equation of the radial forces in the plasma (equation 5.23); (iii) the plasma current and structure circuit equations (equations 5.24 and 5.25 respectively).

Some quantities that are used in these equations must be defined. I_p and I_s are the total plasma current and the vector of currents in the structure elements, both passive and active elements. V_s is the voltage applied to the active elements of the structure.

The plasma radial position R and similarly the plasma vertical position z are defined by the weighted average of the plasma current density j:

$$R = \frac{\int_{\mathrm{plasma}} jr\mathrm{dS}}{\int_{\mathrm{plasma}} j\mathrm{dS}} \tag{5.14}$$

with S the plasma cross-section and r the major radial coordinate.

The effective plasma self-inductance L_p is found using the equivalent energy of the total current distribution:

$$\frac{1}{2}L_p I_p^2 = \frac{1}{2}\sum_i \sum_k j_i M_{ik} j_k \tag{5.15}$$

with M_{ik} the mutual inductance between elements i and k or the self-inductance of the element i when $i = k$.

The effective mutual inductance matrix between the plasma and the structure M_{ps} is given by:

$$I_p M_{ps} I_s = \sum_i j_i M_{is} I_s \tag{5.16}$$

with M_{is} the mutual inductance between an element i and the structure element currents vector.

The set of system generalized coordinates are (Q_s, Q_p, R, z) that represent the charge flow in the structure and the plasma, Q_s and Q_p respectively, and the variables already defined as the plasma radial position (R) and vertical position (z).

System Lagrangian

The Lagrangian of the system (L) is given by:

$$L = \frac{1}{2}I_s^T L_s I_s + \frac{1}{2}L_p I_p^2 + I_p M_{ps} I_s + Q_s^T V_s + W_T \tag{5.17}$$

where W_T is the thermal energy of the plasma, L_s the self-inductance and V_s the electric potential difference of the structure components (including the control coils). This equation is a consequence of the Lagrangian definition ($L = T - V$) using the system generalized kinetic energy (T) and the system generalized potential energy (V) given by:

$$T = \frac{1}{2} I_s^T L_s I_s + \frac{1}{2} L_p I_p^2 + I_p M_{ps} I_s \tag{5.18}$$

$$V = -Q_s^T V_s - W_T \tag{5.19}$$

The Euler-Lagrange Equation

$$\frac{d}{dt}\left(\frac{\partial L}{\partial \dot{q}_i}\right) - \frac{\partial L}{\partial q_i} = \frac{\partial P}{\partial \dot{q}_i}, i = 1, 2, \ldots, n \tag{5.20}$$

is applied to the system Lagrangian for each generalized coordinate (q_i), with the power dissipation (P) due to the resistances of the plasma (Ω_p) and structure (Ω_s) given by:

$$P = -\frac{1}{2}(\Omega_p I_p^2 + I_s^T \Omega_s I_s) \tag{5.21}$$

The equations for each of the generalized coordinates are obtained.

Vertical Force Equation (z)

$$\frac{\partial L_p}{\partial z}\frac{I_p^2}{2} + \frac{\partial I_p M_{ps} I_s}{\partial z} = 0 \tag{5.22}$$

Radial Force Equation (R)

$$\frac{1}{2}\frac{\partial L_p I_p^2}{\partial R} + \frac{\partial I_p M_{ps} I_s}{\partial R} + \frac{\partial W_T}{\partial R} = 0 \tag{5.23}$$

Plasma Circuit Equation (I_p)

$$\begin{aligned} &\frac{d(M_{ps}I_s)}{dt} + \frac{d(L_pI_p)}{dt} + \Omega_p I_p + \frac{d}{dt}\left(\frac{\partial W_T}{\partial I_\mathrm{p}}\right) = 0 \\ &\qquad\qquad\qquad\qquad\qquad\qquad\qquad\qquad \Leftrightarrow \\ &\dot{M}_{ps}I_s + M_{ps}\dot{I}_s + \dot{L}_pI_p + L_p\dot{I}_p + \Omega_p I_p + \frac{d}{dt}\left(\frac{\partial W_T}{\partial I_\mathrm{p}}\right) = 0 \end{aligned} \tag{5.24}$$

Structure Circuit Equation

$$\begin{aligned} &\frac{d(M_{sp}I_p)}{dt} + \frac{d(L_sI_s)}{dt} + \Omega_s I_s = V_s \\ &\qquad\qquad\qquad\qquad\qquad\qquad\qquad\qquad \Leftrightarrow \\ &\dot{M}_{sp}I_p + M_{sp}\dot{I}_p + \dot{L}_sI_s + L_s\dot{I}_s + \Omega_s I_s = V_s \end{aligned} \tag{5.25}$$

Linearization of the Equations

To linearize the equations around a fixed point to obtain the plasma model that includes the power supplies, the control coils and the TCV plasma, the following notation is used for a generic variable α, that is a fuction of a generic variable ϵ:

- $\delta\alpha$ represents a small variation in α from the static equilibrium α^0 and $\alpha = \alpha^0 + \delta\alpha$;
- The continuous time derivative of α ($\frac{d}{dt}$) may also be represented by $\dot{\alpha}$, as already used in this thesis;
- $\frac{\partial\alpha}{\partial\epsilon}|_0$ is the partial derivative $\frac{\partial\alpha}{\partial\epsilon}$ evaluated at equilibrium.

The state vector x for the linearized model is:

$$x = \begin{bmatrix} I_s - I_s^0 \\ (z - z^0)I_p^0 \\ (R - R^0)I_p^0 \\ I_p - I_p^0 \end{bmatrix} = \begin{bmatrix} \delta I_s \\ (\delta z)I_p^0 \\ (\delta R)I_p^0 \\ \delta I_p \end{bmatrix} \tag{5.26}$$

Plasma Model

After the linearization of each equation [53], they can be put in matrix form to describe the plasma:

$$\mathbf{M}\dot{x} + \mathbf{\Omega}x = u \tag{5.27}$$

where the $\mathbf{M}$ and $\mathbf{\Omega}$ matrices are given by:

$$\mathbf{M} = \begin{bmatrix} \mathbf{L}_s & \frac{\partial M_{sp}}{\partial z}|_0 & \frac{\partial M_{sp}}{\partial R}|_0 & M^0_{sp} \\ \frac{\partial M_{ps}}{\partial z}|_0 & \left(\frac{\partial^2 M_{ps}}{\partial^2 z}|_0 \frac{I^0_s}{I^0_p}\right) & \left(\frac{\partial^2 M_{ps}}{\partial z \partial R}|_0 \frac{I^0_s}{I^0_p}\right) & 0 \\ \frac{\partial M_{ps}}{\partial R}|_0 & \left(\frac{\partial^2 M_{ps}}{\partial z \partial R}|_0 \frac{I^0_s}{I^0_p}\right) & M_{33} & M_{34} \\ M^0_{ps} & 0 & M_{43} & L^0_p + \frac{\partial^2 W_T}{\partial I^2_p} \end{bmatrix} \tag{5.28}$$

with the values in the Mutual matrix given by:

$$M_{33} = \frac{1}{2}\frac{\partial^2 L_p}{\partial R^2}|_0 + \frac{\partial^2 M_{ps}}{\partial^2 R}|_0 \frac{I^0_s}{I^0_p} \tag{5.29}$$

$$M_{34} = M_{43} = \frac{1}{2}\frac{\partial L_p}{\partial R}|_0 + \frac{\partial M_{ps}}{\partial R}|_0 \frac{I^0_s}{I^0_p} + \frac{\partial^2 W_T}{\partial I_p \partial R}\frac{1}{I^0_p} \tag{5.30}$$

$$\mathbf{\Omega} = \begin{bmatrix} \Omega^0_s & 0 & 0 & 0 \\ 0 & 0 & 0 & 0 \\ 0 & 0 & 0 & \frac{\partial \Omega_p}{\partial R}|_0 \\ 0 & 0 & \frac{\partial \Omega_p}{\partial R}|_0 & \Omega^0_p \end{bmatrix} \tag{5.31}$$

The input vector u is given by:

$$u = \begin{bmatrix} \delta \boldsymbol{V_s} \\ 0 \\ \frac{\partial^2 W_T}{\partial R \partial \alpha}\dot{\alpha} \\ \frac{\partial^2 W_T}{\partial I_p \partial \alpha}\dot{\alpha} \end{bmatrix} \tag{5.32}$$

The variable α is introduced in the input vector to allow the independent variation of the thermal energy of the plasma (W_T) independently of the states.

Equation 5.27 may be put in the state-space form:

$$\begin{aligned} \dot{x} &= Ax + Bu \\ y &= Cx + Du \end{aligned} \tag{5.33}$$

with

$$A = -M^{-1}\Omega, \tag{5.34}$$

$$B = M^{-1} \tag{5.35}$$

The output vector (y) agree with the state vector (x) as a consequence of the coincidence between the measurements and the state variables, yielding the values of C and D:

$$C = 1 \tag{5.36}$$

$$D = 0 \tag{5.37}$$

Moreover, this model is further simplified by applying the remaining assumptions already presented, but that were not taken into account until this step of the deduction.

As a consequence of the rigid current displacement the normalized current profile can not change for plasma movements on R or z directions nor due to changes to the total plasma current, leading to a simplification in the plasma mutual and self inductance derivatives, the thermal energy of the plasma [121]:

- The radial derivative of the mutual inductance between two plasma elements f and g is

$$\frac{\partial M_{fg}}{\partial R} = \frac{\partial M_{fg}}{\partial R_f}\frac{\partial R_f}{\partial R} + \frac{\partial M_{fg}}{\partial R_g}\frac{\partial R_g}{\partial R}. \tag{5.38}$$

  The relation between the two radius relation with rigid current displacement is

$$\frac{\partial R_f}{\partial R} = \frac{\partial R_g}{\partial R} = 1 \tag{5.39}$$

  with the following consequences:

$$\frac{\partial L_p}{\partial z} = 0 \tag{5.40}$$

$$\frac{\partial W_T}{\partial z} = 0 \tag{5.41}$$

- The poloidal beta is the ratio between the average of the kinetic pressure ($\overline{P}_K$) and magnetic pressure ($\overline{P}_B$):

$$\beta_p = \frac{\overline{P}_K}{\overline{P}_B} \tag{5.42}$$

  with

$$\overline{P}_K = \frac{\int_{plasma} p dV}{\int_{plasma} dV} \tag{5.43}$$

$$\overline{P}_B = \frac{B_a^2}{2\mu_0} \tag{5.44}$$

and

$$B_a = \frac{\mu_0 I_p}{l}, \tag{5.45}$$

where p is the plasma pressure, S is the plasma cross-section and l is the poloidal circumference (or perimeter) of the plasma. Considering the thermal plasma energy for a volume V and substituting β_p:

$$W_T = \int_{plasma} pdV = \int_{plasma} p2\pi RdS = \pi\mu_0 \frac{S}{l^2}\beta_p R I_p^2 \tag{5.46}$$

This equation gives the value of $\alpha = \beta_p$ that appears in the input vector u. Note that B_ϕ term was neglected as the model ignores all poloidal currents.

- The model uses the following approximation to the plasma self-inductance that was earlier defined in 5.15. This approximation gives identical values with considerable less computational effort [121]:

$$L_p = \mu_0 R(4\pi R\frac{\overline{B}_v}{\mu_0 I_p} - \beta_p - \frac{1}{2}) \tag{5.47}$$

The line over the quantities means the average over the plasma current distribution and $\overline{B}_v S = \overline{M_{ps} I_s}$. Note that if the internal inductance l_i was used as an independent variable the current profile would be allowed to change, violating the assumption of a rigid current distribution.

These assumptions permit to obtain a simpler state space model by simplifying the matrices in equation 5.27. The model implemented in Matlab [122] use the following streamlined matrices [78]:

$$\mathbf{M} = \begin{bmatrix} \mathbf{L}_s & \frac{\partial M_{sp}}{\partial z}|_0 & \frac{\partial M_{sp}}{\partial R}|_0 & M_{sp}^0 \\ \frac{\partial M_{ps}}{\partial z}|_0 & \left(\frac{\partial^2 M_{ps}}{\partial^2 z}|_0 \frac{I_s^0}{I_p^0}\right) & 0 & 0 \\ \frac{\partial M_{ps}}{\partial R}|_0 & 0 & M_{33} & M_{34} \\ M_{ps}^0 & 0 & M_{43} & L_p^0 \end{bmatrix} \tag{5.48}$$

$$\mathbf{\Omega} = \begin{bmatrix} \Omega_s^0 & 0 & 0 & 0 \\ 0 & 0 & 0 & 0 \\ 0 & 0 & 0 & 0 \\ 0 & 0 & 0 & \Omega_p^0 \end{bmatrix} \tag{5.49}$$

The plasma control is limited to the voltages of the control coils and the input vector is given by:

$$u = \begin{bmatrix} \delta \boldsymbol{V_s} \\ 0 \\ \frac{\partial^2 W_T}{\partial R \partial \alpha} \dot{\alpha} \\ 0 \end{bmatrix} \tag{5.50}$$

The Matlab function reads the plasma equilibrium details from the TCV database based on the discharge number and time, as well as the tokamak structure parameters, used to build the state-space model for specific plasma elongations. This function also calculates a plasmaless model that permits the verification of the model with the envisaged advantage of verifying the magnetic tokamak mathematical description.

As a final note on the RZIP plasma model, it is important to emphasize that the simplifications assume that the current distribution may only be displaced vertically or radially, neglecting any changes to the plasma cross section area or current profile, changes to the force due to the toroidal field (that is set to zero in this model approximation), the induction and dissipation of currents in the poloidal plane. However, this simpler model has been compared with more detailed models and the agreement is enough to compensate the simplifications presented [121].

5.4.3 Transfer Function of the Voltage in the Fast Coils on the Plasma Vertical Position

This section aims at obtaining the independent transfer function that describes the influence of the poloidal field coils internal to the TCV structure close to the plasma on the plasma vertical position. From the complete RZIP model described with several state variables that are not necessary to the vertical stabilization problem, the model is simplified to find the transfer function from the fast vertical coils to the plasma vertical position. That is to say, the mathematical method that describes the influence of the input voltage on the fast coils in the plasma vertical position. This is a necessary simplification of the full plasma model obtained before, for the particular case of the plasma vertical stability using the in-vessel fast coils. The complexity of this simplification comes from the fact that the MIMO[5] system that is obtained from the plasma model must be diagonalized to obtain a SISO system with independent input and output from the remain system inputs

[5]See section 2.1.3 for the definitions of MIMO and SISO systems

and outputs. This is not always possible and some constraints must be analyzed to make the variables independent from each other.

This simplification assumes that vertical stabilization is independent from the remaining plasma control variables such as shape or current and operates in a different time scale from the other plasma parameters. Although the actuators for the control are the same, one can separate mathematically their influence because the time scale of the plasma vertical stabilization is much shorter then the one for the current and shape control [123]. Moreover the vertical position that is also controlled by the poloidal coils outside the vessel can be considered independent of the internal poloidal coils, due to the same reason. While the poloidal coils outside the vessel control the slow vertical displacement of the plasma, the in-vessel coils act on a much faster time-scale, reacting to fast plasma disturbances.

The state space system is diagonalized to obtain the independent influence of the in-vessel poloidal field coils voltage over the plasma vertical position, neglecting the influence of the other coils. The accuracy of this implementation is only possible due to the already mentioned different response time of the actuation of the coils. A 52^{nd} order transfer function is obtained with one positive pole that represents the plasma vertical instability. Figure 5.8 depicts the pole zero plot for three transfer functions obtained for a circular, a standard elongated and an extremely elongated TCV plasma respectively (figure 5.7). The vertical instability can be confirmed as the real positive pole that can be seen for the elongated plasmas, but is not present in the top plot that represents the circular plasma transfer function.

As a first approach to the evaluation of this method, a simple qualitative verification was made by comparing the value of the plasma vertical instability growth rates for different plasmas with the transfer function unstable pole. Figure 5.8 permits to immediately check that higher elongation correspond to higher instability. Values for some discharges were compared with the growth rate measurements in TCV [120]. Table 5.2 presents some data for different plasma configurations relative to elongation (figure 5.9). This data is not a complete validation but it shows the correspondence between the growth rate of the plasma and the instability pole in the transfer function for different plasma discharges.

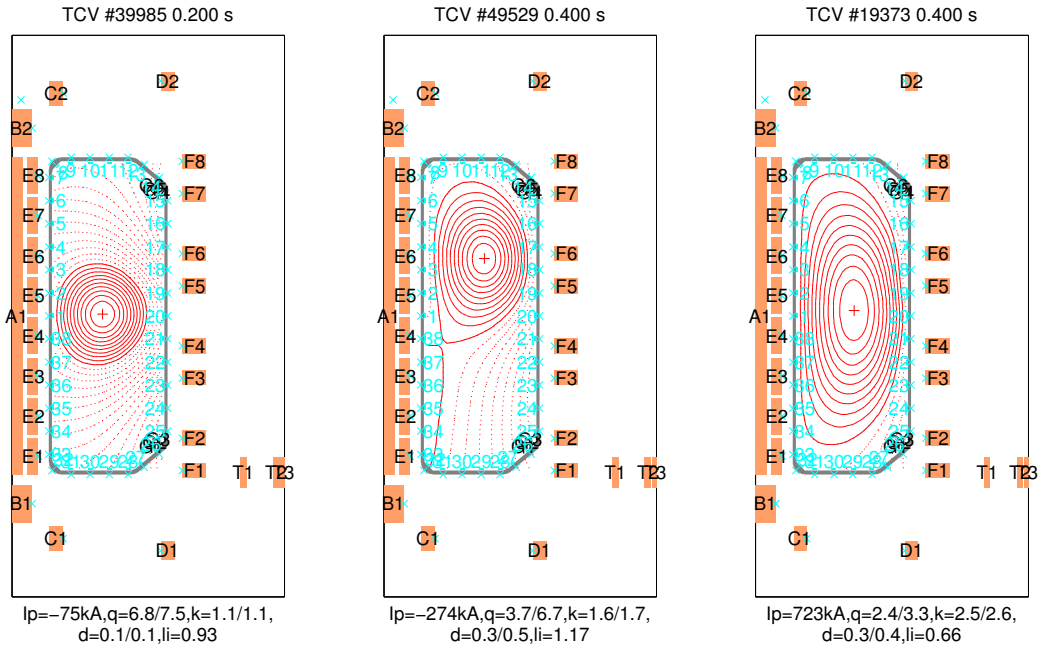

Figure 5.7: Some plasma configurations used for validation of the plasma response to the voltage change in the fast coil.

Discharge Number	Plasma Elongation	Measured Growth Rate (s^{-1})	Positive Pole Instability (s^{-1})
7613@.40s	1.7	approx. 740	841
7615@.40s	1.6	approx. 460	642
7453@.45s	1.4	approx. 70	33

Table 5.2: Measured TCV growth rates (estimated from the data presented in [120]) and the values of the instability pole given by the model transfer function.

5.5 Application of Optimal Control Theory

5.5.1 Model Reduction and Validation

The best model in control engineering is not always the most accurate, but the one that permits the construction of a robust stable controller, according to the necessary performance and specifications.

For the application of optimal control theory to the obtained plasma model, a reduction was necessary to permit the mathematical treatment presented in the next subsections. The transfer function obtained in the previous section is of too high order for the application of optimal control theory, that is only applicable to systems not higher than second

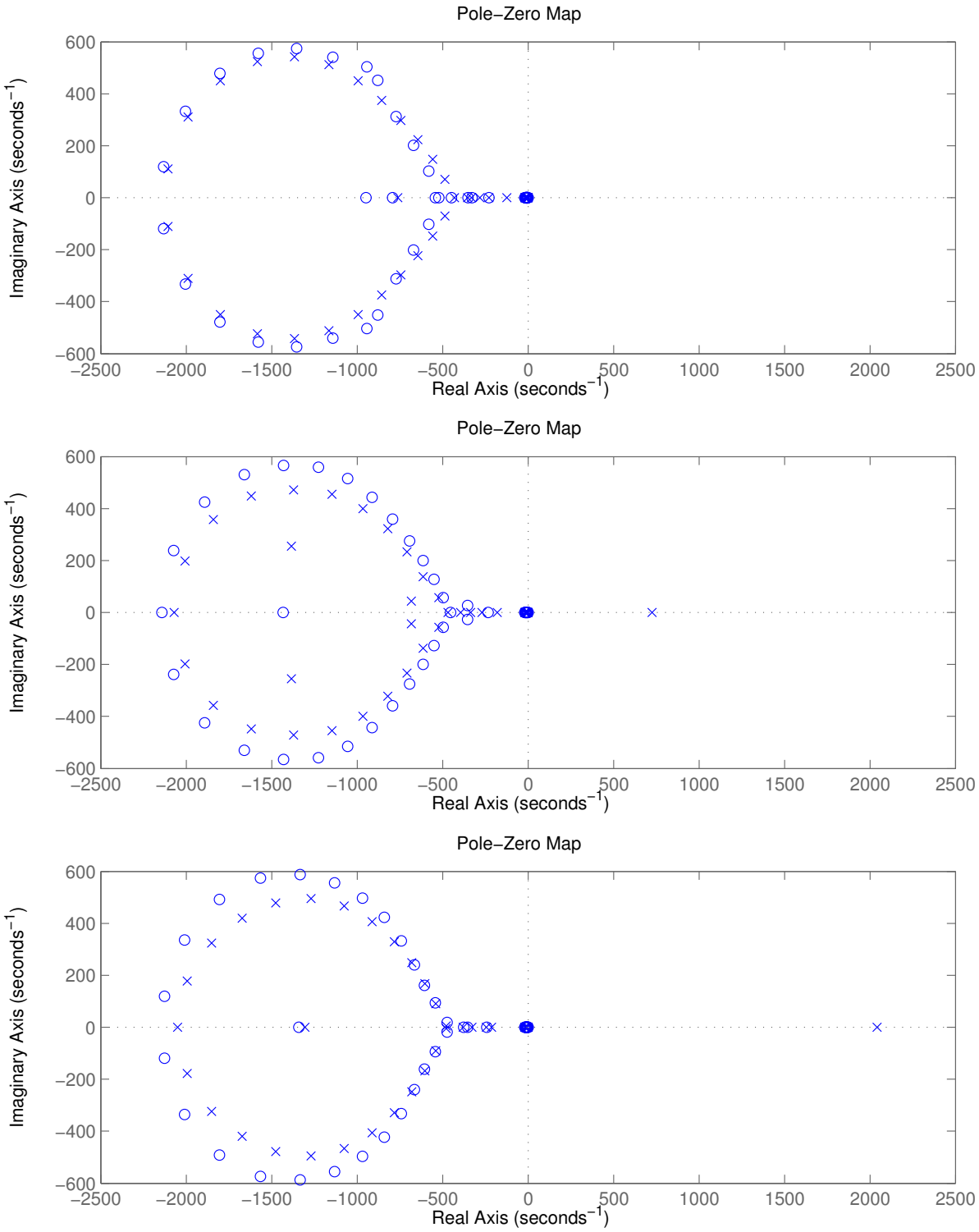

Figure 5.8: Pole-Zero plot of 52^{nd} order transfer function of a circular TCV plasma (top) standard elongated plasma (middle) and extremely elongated plasma. The poles are plotted as x's and the zeros as o's.

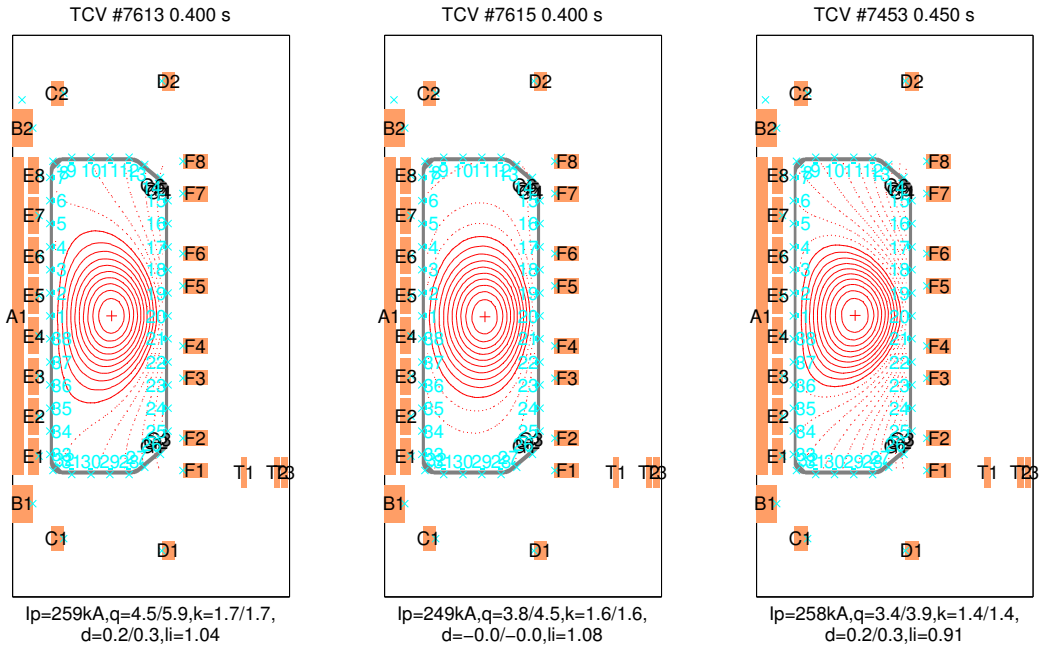

Figure 5.9: Some plasma configurations with different elongation for preliminary verification of transfer function instability.

or third order. This led to the application of model reduction techniques to the complete model.

Model reduction techniques are a powerful tool that uses methods based on the idea of projecting the state space to a much lower dimension, obtaining a reduced system that may be solved more efficiently. For control design purposes, it is possible to approximate the model with another model of reduced order that preserves the original transfer function as much as possible.

The method applied consists of first calculating a balanced realization of the transfer function [124]. This step returns the state space balanced realization of the input transfer function. For the case of the system with an unstable pole, the stable part is isolated before applying the balanced realization, that is added to the unstable part of the system. On the second step the system in balanced form is reduced by eliminating the states with small Gramians (σ_i), i.e. with small influence in the behavior of the transfer function.

Two methods were evaluated for the model reduction: truncation and matching DC gains. The first method simply deletes the chosen states from the state vector. On the other hand the second method sets the reduced state vector (X_r) to be:

$$X_r = X_1 + T\, X_2 \tag{5.51}$$

where X_2 is the part of the state vector to be discarded, X_1 the remaining part of the state vector and T is a matrix chosen to enforce the matching of DC gains between the reduced and the full model.

From the evaluation of the reduced transfer functions bode plot resulting from both methods, the choice was to use the truncation method, as it presented better results for the approximation with the original transfer function. Figure 5.10 shows the bode plot for the original transfer function (right) and the reduced transfer function using matching DC gains (center) and truncation (right) methods. Note that using the matching DC gains the bode plot doesn't even resemble the original one, to the point that the same axis can not be used. Moreover, the controller uses the time derivative as the input, making the DC gain a characteristic that is not important to maintain.

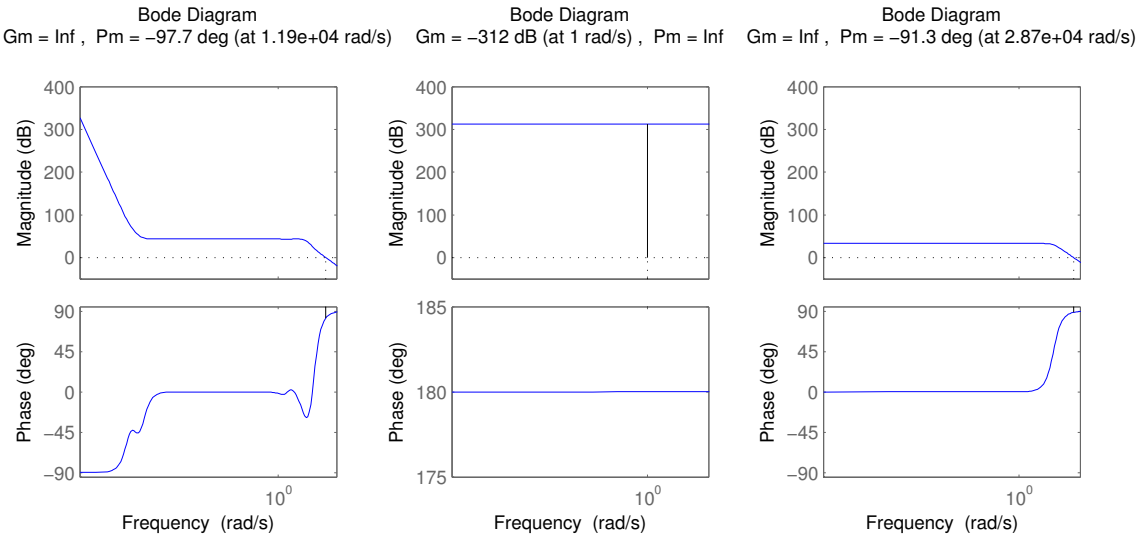

Figure 5.10: Bode plot for the original 52^{nd} order transfer function (left) and the reduced to a 2^{nd} order using matching DC gains (center) and truncation (right) methods. The model reduction using matching DC gains (center) maintains the gain at extremely low frequencies, with no application for higher frequency control systems.

The aim of the application of the method is to obtain a reduction from the 52^{nd} order transfer function to a 2^{nd} order that could not be achieved by the standard method that was presented until this point. The application of the method, truncating the values of σ_i minor then 10^{-3} reduces the model up to the 15^{th} order. To achieve the 2^{nd} order system another truncation is applied living only the most influent values of σ_i that result in a 2^{nd} order transfer function.

The reduction of the model to the aimed order transfer function using a non standard method demands the verification of the reduced model for different plasmas aiming at

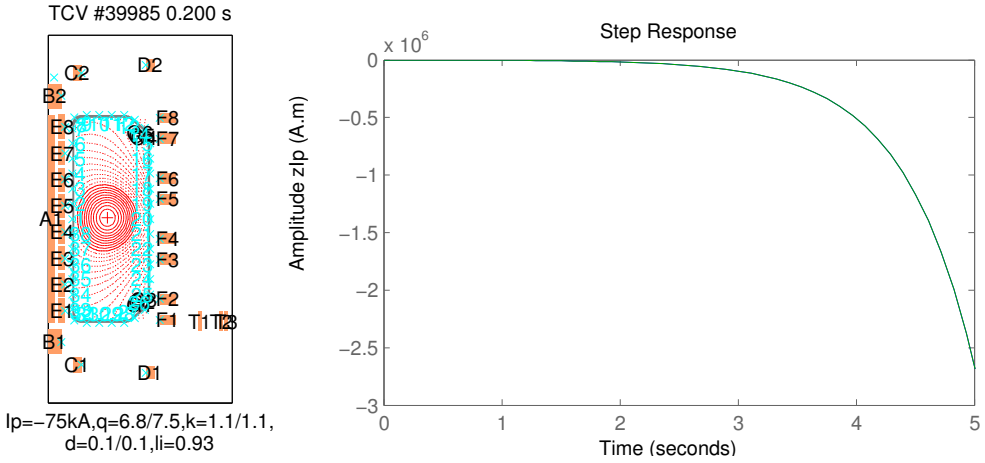

(a)

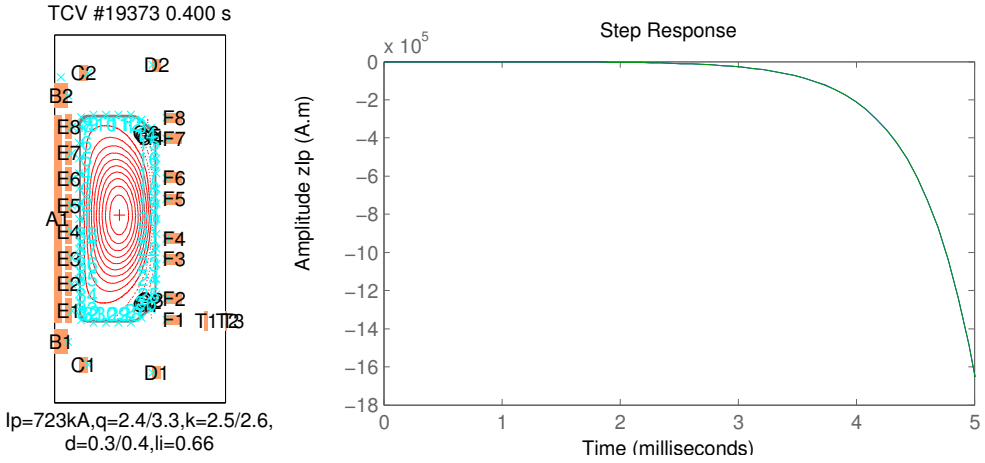

(b)

Figure 5.11: Model reduction for two different TCV plasmas: **(a)** a circular plasma and **(b)** a very elongated plasma. The step responses of complete and reduced models completely overlap.

the validation of the method. Results are now presented with differences that could not be detected by the plot of the step response. Figure 5.11a depicts the step response for a model using a circular plasma and figure 5.11b presents the step response for a very elongated plasma. Note that the lines of the step response of the complete model and the reduced model completely overlap.

Figure 5.12 depicts a more detailed analysis with bode diagrams of both transfer functions. The diagram on the left represents the complete model and the one on the right represents the reduced model, for a circular plasma (5.12a) and a very elongated plasma (5.12b). These plots show the difference in magnitude and phase response for complete

and reduced models. Nevertheless these differences are only present for slower frequencies that are not relevant for the fast process involved in the plasma vertical stability control.

5.5.2 Reduction of the Plasmaless Model

The same reduction algorithm was applied to the plasmaless model for verification of the reduced transfer function in the representation of the vessel and in-vessel control coils time response characteristics.

Figure 5.13 details the complete model characteristics on the left and the reduced model on the right. Figure 5.13a depicts the pole zero plot, while 5.13b reproduces the bode diagram of both transfer functions. The results show that the reduction maintains the characteristic behavior of the vessel properties. Moreover, the pole zero plot shows the stabilizing behavior of the vessel. The only noticed difference refers to the phase shift that rotates 180°.

Figures 5.14 and 5.15 detail the pole zero plot of the complete and reduced model of two different plasma elongations for comparison with the plasmaless plot in figure 5.13a. It was not found the numeric relation between negative poles and zeros, that contribute to the stabilization of the plasma, and the ones on the plasmaless model. Moreover, these values may vary depending on the plasma elongation. However if one such relation is established, the reduced plasmaless model could be used for all plasma discharges, by the introduction of the unstable pole into the plasmaless model and changing the stabilizing pole and zero accordingly. One indication towards this direction is the similarity between the stabilizing components in figures 5.14 and 5.15.

5.5.3 From System Model to Control Parameters

This section contains the application of optimal time control to the second order model obtained from the reduction in the previous section to obtain the switching and final time of the bang-bang controller. This work was based in optimal control theory work that derive the control law for first and second-order systems [47][125][126][127].

The second order transfer-function that describes the plasma model has the form:

$$\frac{X_s(s)}{U(s)} = \frac{n_1 s + n_2}{s^2 + d_1 s + d_2} \tag{5.52}$$

From this definition transfer function, it is possible to define the following controllable

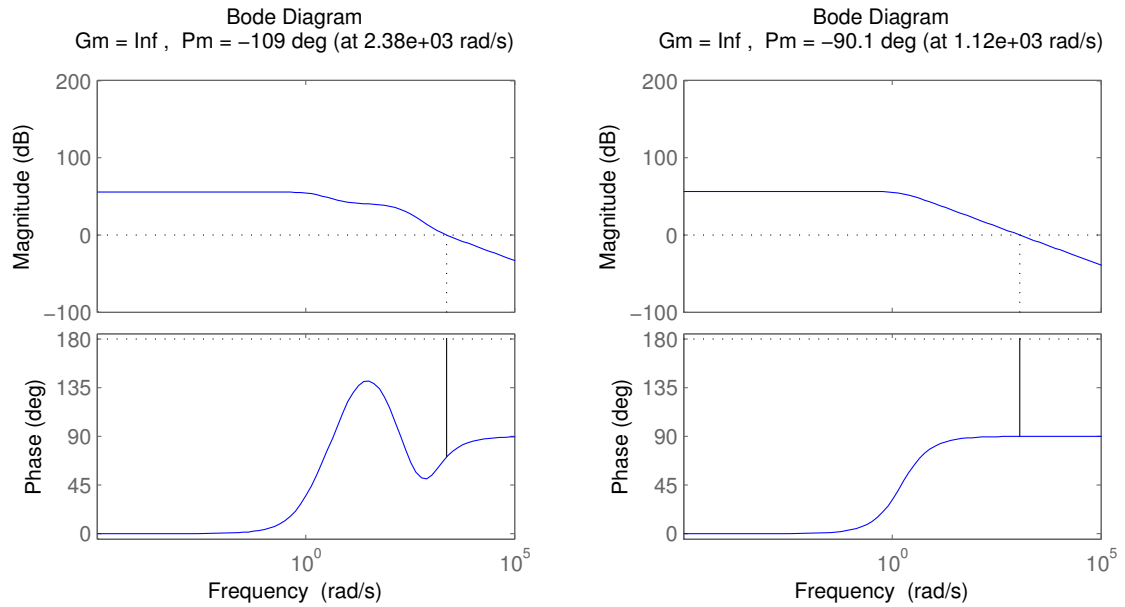

(a)

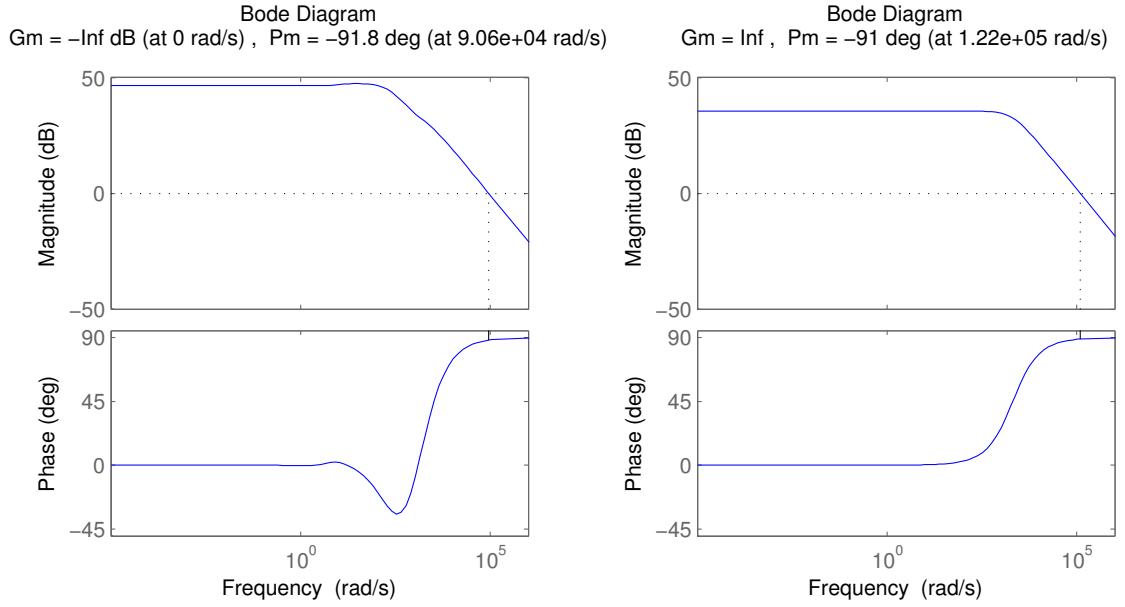

(b)

Figure 5.12: Model reduction for two different TCV plasmas: **(a)** a circular plasma and **(b)** a very elongated plasma. In each figure: (i) On the left the bode diagram of the complete model; (ii) On the right the bode diagram of the reduced model.

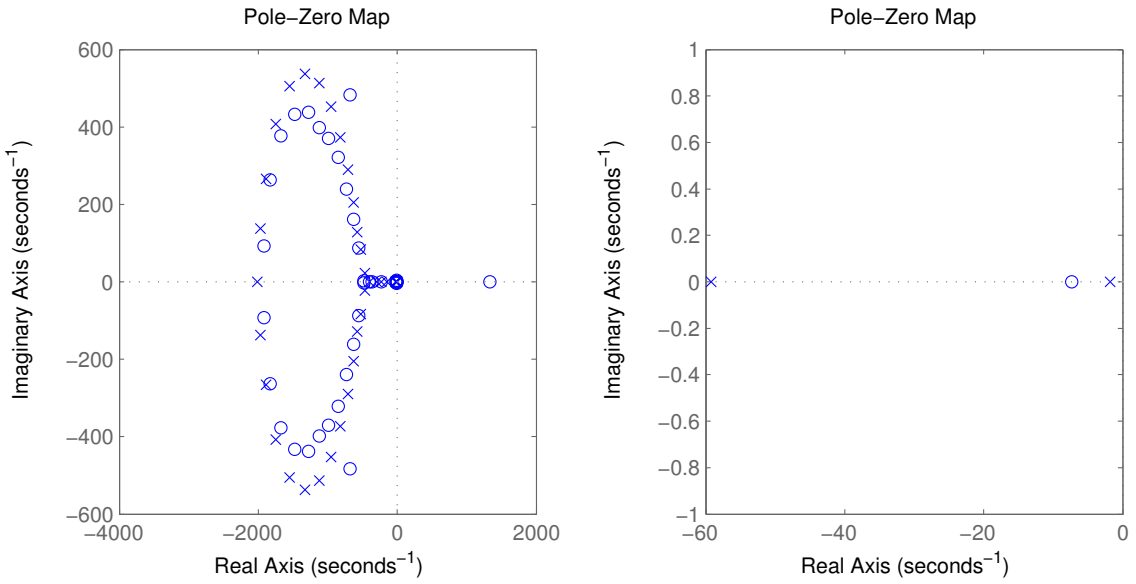

(a)

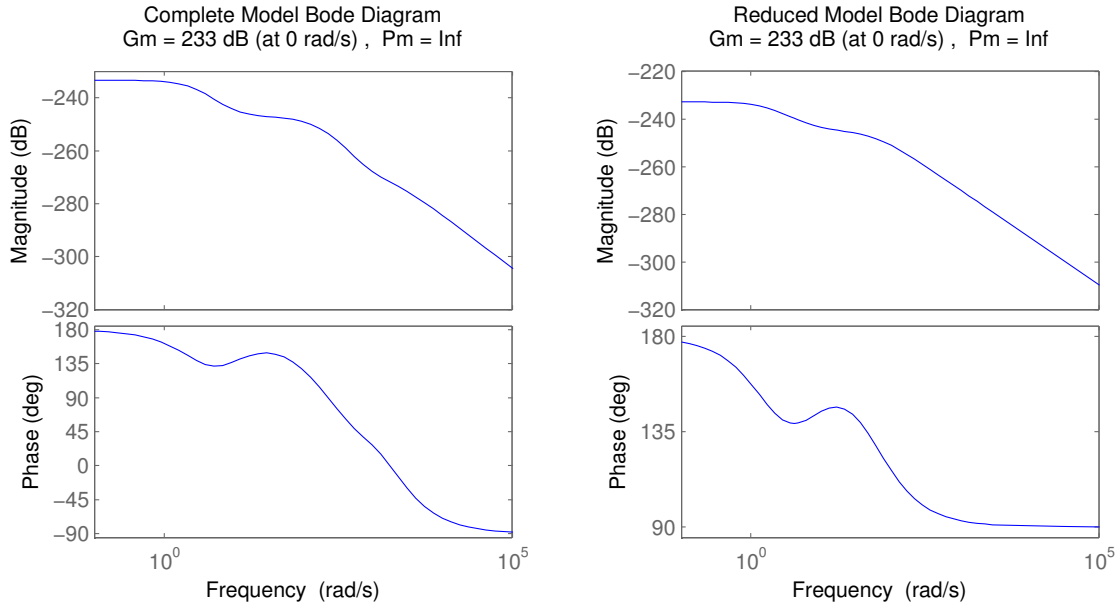

(b)

Figure 5.13: Model reduction of plasmaless model: **(a)** Pole-Zero map; and **(b)** Bode diagram for the complete model (on the left) and for the reduced model (on the right)

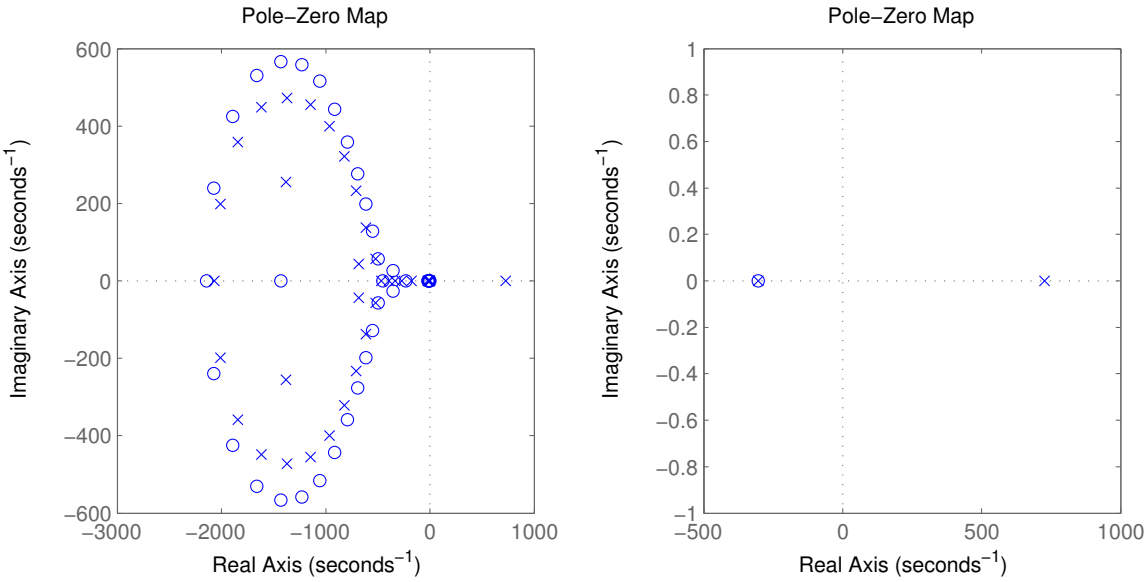

Figure 5.14: Pole zero plot for the complete model (on the right) and for the reduced plasma model for plasma discharge 49529.

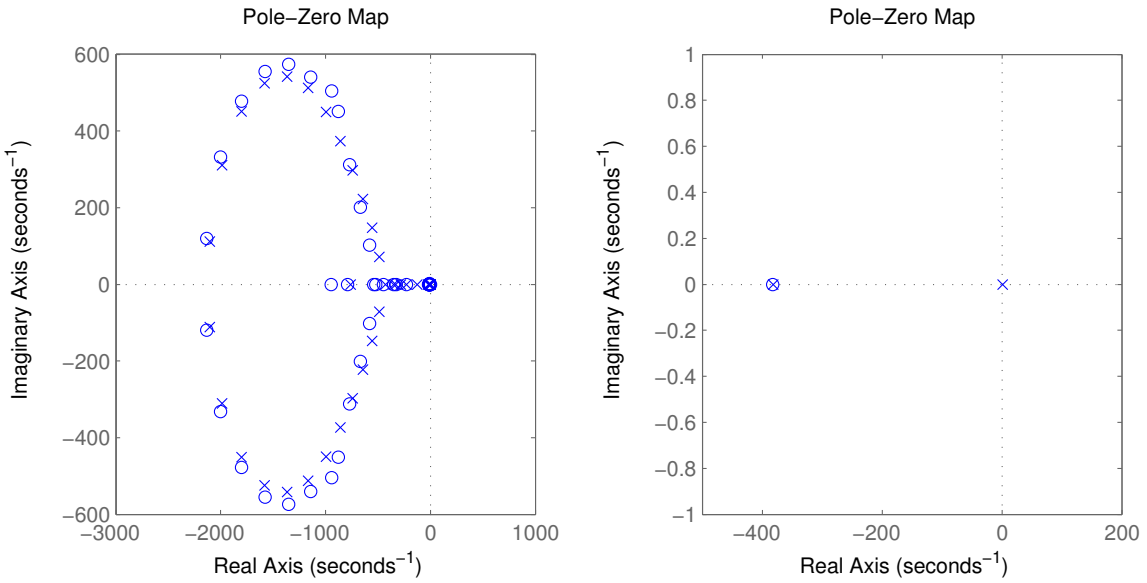

Figure 5.15: Pole zero plot for the complete model (on the right) and for the reduced plasma model for plasma discharge 39985.

state space model:

$$\dot{X} = AX + Bu \tag{5.53}$$

with $X = \begin{bmatrix} x_1 \\ x_2 \end{bmatrix}$, $A = \begin{bmatrix} 0 & 1 \\ -d_2 & -d_1 \end{bmatrix}$, $B = \begin{bmatrix} b_1 \\ b_2 \end{bmatrix}$, where

$$x_1 = x_s \tag{5.54}$$

and

$$x_2 = \dot{x}_1 = x_1 + b_1 u \tag{5.55}$$

are the system variables when b_i is given by

$$\begin{bmatrix} 0 \\ n_1 \\ n_2 \end{bmatrix} = \begin{bmatrix} 1 & 0 & 0 \\ d_1 & 1 & 0 \\ d_2 & d_1 & 1 \end{bmatrix} \begin{bmatrix} b_0 \\ b_1 \\ b_2 \end{bmatrix} \tag{5.56}$$

The eigenvalues of A are thus, given by

$$\lambda_1 = -\frac{d_1}{2} + i\sqrt{4d_2 - d_1^2} \tag{5.57}$$

$$\lambda_2 = -\frac{d_1}{2} - i\sqrt{4d_2 - d_1^2} \tag{5.58}$$

and the eigenvectors are given by

$$P = \begin{bmatrix} 1 & 1 \\ \lambda_1 & \lambda_2 \end{bmatrix} \tag{5.59}$$

Having defined the system model and given the initial system state X_0, the aim is finding the control law and parameters that take the system from the initial state X_0 to a target state X_1, minimizing the time to target.

5.5.4 Control Law

The problem of finding the control law that drives the plasma position from an initial position X_0 to a final position X_1 in the minimum time, can be easily understood with the help of the definition of a new system state X_N, and the redefinition of the state system equations:

$$X_N = X - X_1 \tag{5.60}$$

$$\dot{X}_N = AX_N + Bu + AX_1 \tag{5.61}$$

$$X_{N0} = X_0 - X_1 \tag{5.62}$$

In this new state system with changed variable the set point becomes the origin, thus simplifying the problem.

The Pontryagin Minimum Principle (PMP) is used aiming at minimizing the cost function given by the time to achieve the set point:

$$J = \int_0^{t_f} dt \tag{5.63}$$

According to PMP the control must minimize the optimal control theory Hamiltonian of the system that is given by:

$$H = 1 + \lambda^T (AX_N + Bu + AX_1) \tag{5.64}$$

where λ is the state of the adjoint system, representing the system as a linear transformation using the vector space defined by the eigenvectors.

The combined system is thus given by:

$$\dot{X}_N = \frac{\partial H}{\partial \lambda} = AX_N + Bu + AX_1 \tag{5.65}$$

$$\dot{\lambda} = -\frac{\partial H}{\partial X_N} = -A^T \lambda \tag{5.66}$$

The minimization of the Hamiltonian yields $H(t) = 0$ for all the time and in particular for t_f:

$$H(t_f) = 0 \Rightarrow 1 + \lambda(t_f)^T (AX_N(t_f) + Bu(t_f) + AX_1) = 0 \tag{5.67}$$

Moreover, using the information that $X_N(t_f) = 0$ because the target state is the origin, the previous equation may be simplified to

$$1 + \lambda(t_f)^T (Bu(t_f) + AX_1) = 0 \tag{5.68}$$

In the particular case where the set point $X_1 = 0$, the equation may be further simplified. The optimal time control law is then given by:

$$\begin{aligned} \lambda^T B > 0 &\Rightarrow \dot{u} = u_{min} \\ \lambda^T B < 0 &\Rightarrow \dot{u} = u_{max} \end{aligned} \tag{5.69}$$

The bang-bang control law is complete with an arbitrary value of u for $\lambda^T B = 0$. This may also be completed by applying a small dead zone where no control is applied to avoid unnecessary switching due to hysteresis.

Although the desired control law was found, the explicit switching time and final time are still missing. Next subsection highlights the advantages of knowing this values and finds a path to calculate them.

5.5.5 Predictive Control and Construction of Switching Curves

This section presents a method to predict the action ahead, preventing situations when the observer becomes temporarily unavailable, for example in the presence of edge localized modes (ELMs). By the use of this method, it is possible to keep the system stable, by predicting the control action needed, provided the time the observer is not available is shorter than the final control time calculated and no other major unpredicted disturbance affects the system. Moreover the FPS has a minimum "on-time" of 10 μs that renders impossible the change of control under that time. Using this method it is possible to verify if the control should be applied immediately or if it is more efficient to wait before applying the action.

This method is based on the a-priori calculation of the switching time and final time for the optimal time control law of the system. According to the demonstration in [127], we can get the second order system from one state to another using one control switch, and that is the time optimal control. In [127] is also presented a graphical solution to the problem of finding the switching and final times, as well as the state transition matrix.

The deduction and results presented in [127] were initially adopted to find an optimal controller, but a new simpler and more generic algorithm was then developed and implemented. The idea is to find the cross point of two paths. The first path from the initial system state when is applied the maximum control possible in the direction of the set point and the second path that is traced when the opposite control is applied backward from the set point. The state-space point where these two paths cross is the state where

the controller should switch the control.

Based on the idea presented an algorithm was developed and implemented. Figure 5.16 depicts the algorithm flowchart that is detailed in the following description:

Step 1 Define what path control (u_{max}/u_{min}) should the system travel first in the direction of the set point, based on the initial system state.

Step 2 Build the trace of the path that the system travels from initial position, when the maximum/minimum control is applied u_{max}/u_{min}. The path is an array with system state and time information.

Step 3 Build the back trace in time that the system travels, when the maximum/minimum control is applied. This path includes a negative time array that counts the time from t_f backward.

Step 4 Calculate the intersection of both paths, leading to the calculation of the desired values. The system state intersection time in the first array gives the switching time t_s, that can be added to the time in the system state of the second array to give the final time t_f.

Step 5 Store the data and repeat the same procedure to a different initial system state, building a matrix of initial system states versus switching and final times.

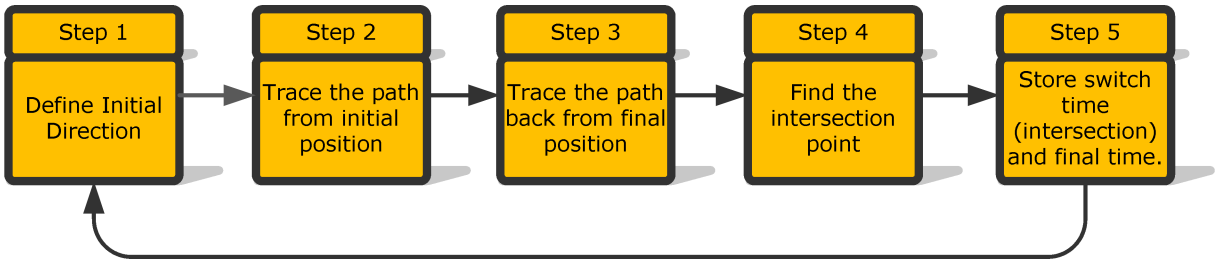

Figure 5.16: Computer algorithm flowchart to find the switch control and final time of an optimal control path.

To first validate the algorithm the same function and values presented in [127] were used. The results can be depicted in figure 5.17a and compared with the similar figure based on a graphical calculation presented in figure 5.17b [127].

5.5.6 Application to the Reduced Plasma Model

The method of calculation with no human interference can be applied to a set of admissible system states, to drive the system to the desired set point. A table is built in offline mode, that is implemented in the APCS system.

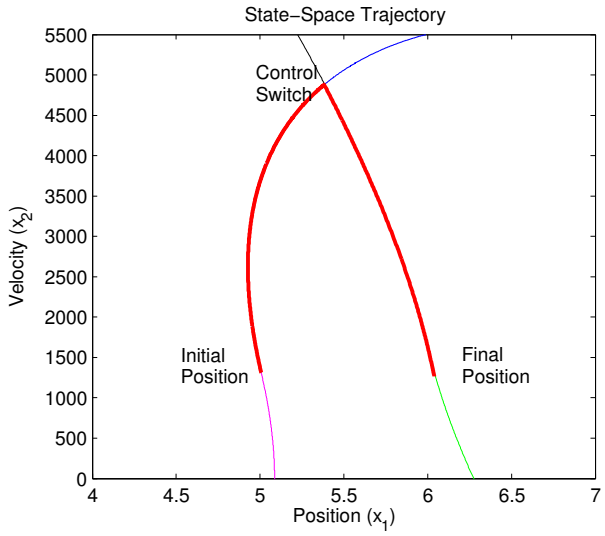

(a) Simulation of the trajectory in state space from initial position to the set point using the new method described. The blue line represents u_{max} control from the initial position, magenta is u_{min} from the initial position. The green is the application of u_{max} until the target final position, while the black is the application of u_{min} until the final position. The red line is the optimal control path between initial and final position.

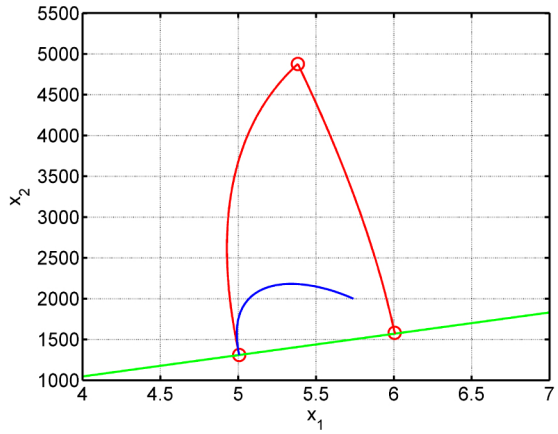

(b) The same trajectory under step and bang-bang control signal. Both state trajectories start from the initial state. The bang-bang trajectory (red) gets to the target state before the step trajectory (blue) does [127].

Figure 5.17: Comparison of bang-bang control trajectories using two different plot methods.

Figure 5.18 depicts several possible trajectories for different initial plasma positions to the target position velocity pair (0,0) showing an uncontrollable position in the negative side, going through a set of controllable initial positions and finding at the end the uncontrollable position at the positive side.

Figure 5.19 reproduces the time: (i) to cross the zero position; (ii) to switch the control; (iii) to the set point position velocity pair (0,0). The simulation used a fixed initial velocity for different initial positions, applied to the same discharge. The values obtained are used to build and optimize the controller. Moreover, it is possible to check once again the uncontrollable zones on the left and on the right of the graphics. This method defines the controllable zone of the plasma given its initial position and velocity, permitting the simulation of the plasma parameter limits and the design of new control systems.

Figure 5.20 depicts the different trajectories from the same initial position, scanning several different initial plasma velocities. It is also possible to confirm that the initial velocity may render the plasma uncontrollable, although the initial position was inside the controllable zone for zero initial velocity.

5.6 Simulator Tool

The plasma model was used to build a system simulation tool using Matlab Simulink [111]. Figure 5.21 depicts the block diagram design of the simulation implemented. The simulator was used to test different controllers improving the fine tuning of any parameters and the device protection before the use in tokamak real discharges.

The plasma model includes the transfer function from the voltage in the internal poloidal field coils and the plasma position, but lacks the transfer function of the fast power supplies that were also taken into account using a different simulation block. The stabilization controller has two inputs: the plasma velocity and plasma position error. From the inputs this block builds the controller signal to be sent to the fast power supplies. A disturbance generator is used to simulate unpredictable influences in the plasma. The complete plasma model is used for the simulation, for accuracy, because there is no need to use a reduced model except for the fact of faster computational simulations. Finally, the plasma model outputs the plasma position and a derivative block is used to simulate the plasma velocity measurements.

This Matlab Simulink model was used to obtain preliminary results.

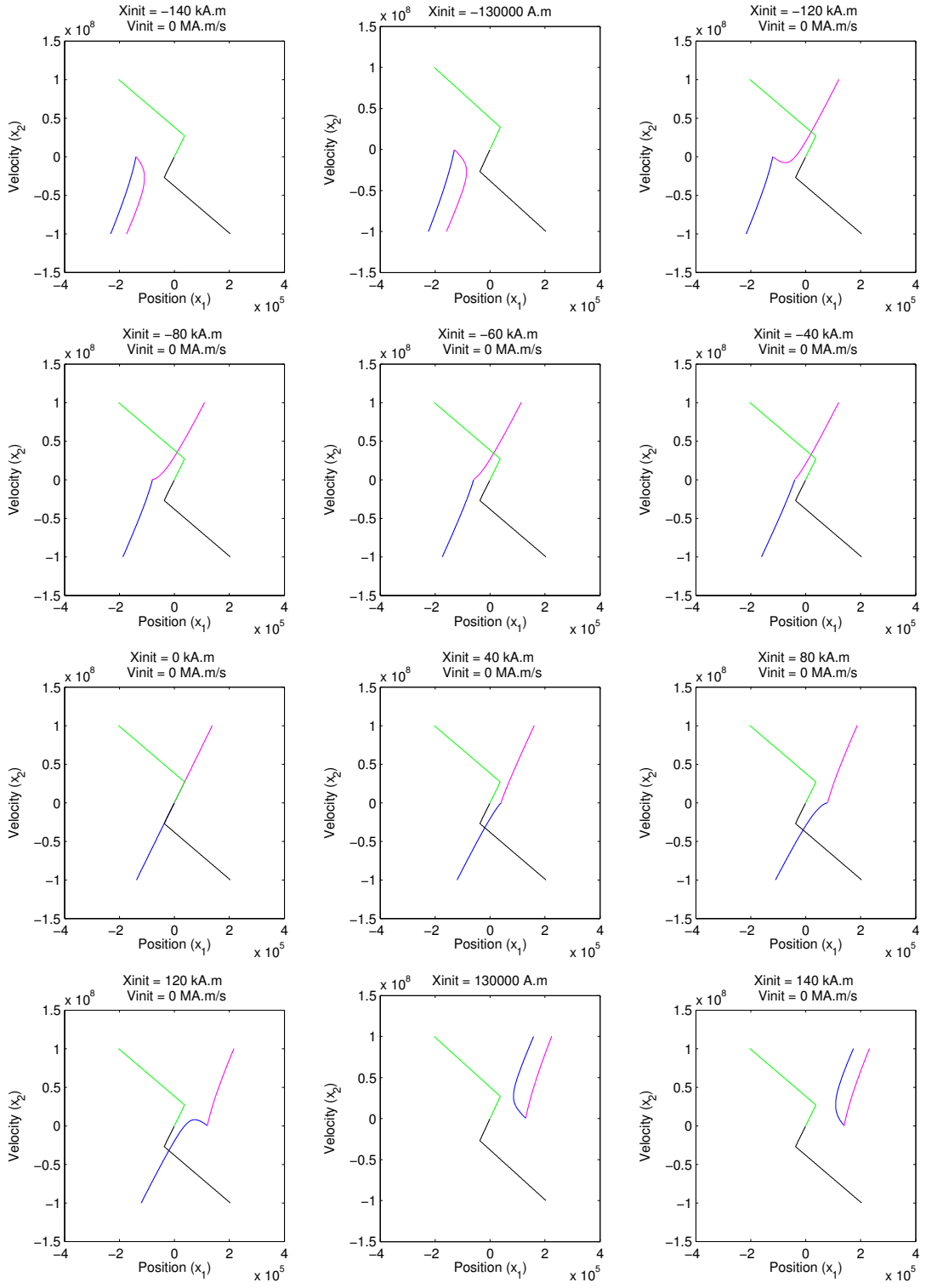

Figure 5.18: Prediction of state trajectories for different initial positions (X_{init}) using reduced model from discharge 49529@.4s. The blue line represents u_{max} control (600V) from X_{init}, magenta is u_{min} (-600V) from X_{init}. The green is the application of u_{max} until the target X_{tar}, while the black is the application of u_{min} until X_{tar}.

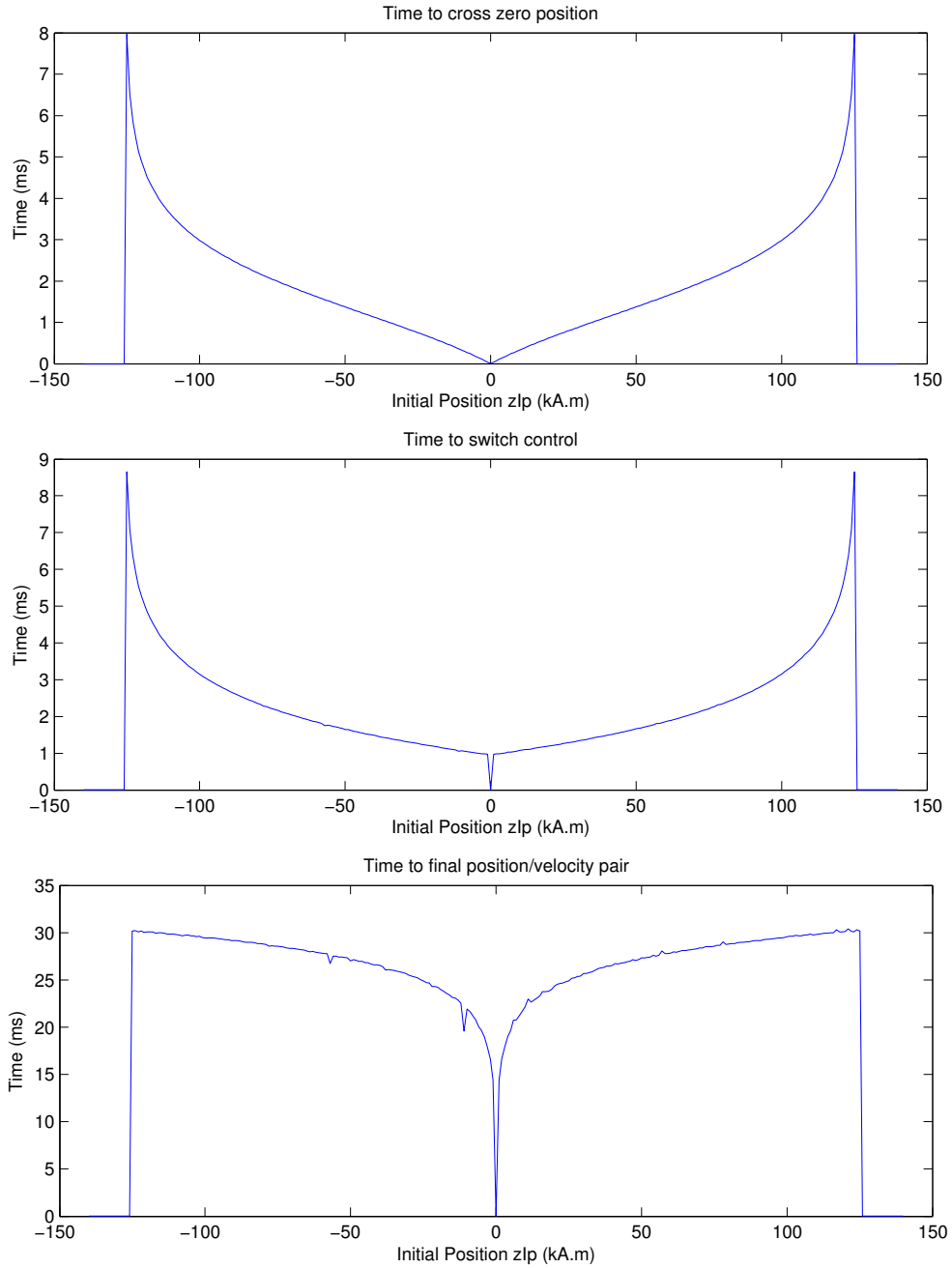

Figure 5.19: Representation of the simulated time:(i) to cross the zero position (top); (ii) to switch the control (middle); (iii) to the set point position velocity pair (0,0) (bottom) versus the initial position using the model for discharge 49529.

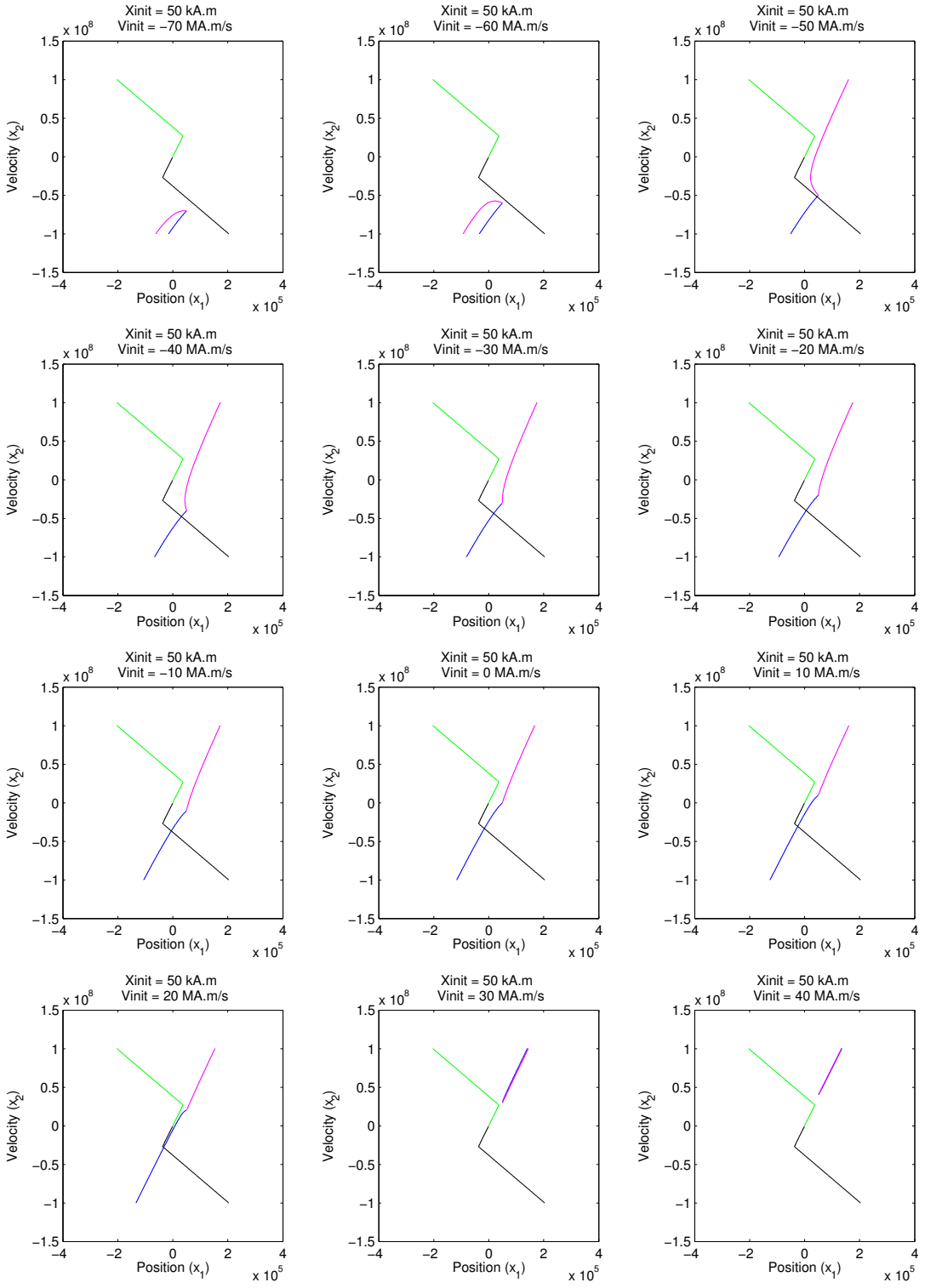

Figure 5.20: Prediction of state trajectories for different initial velocities, maintaining the same initial position using reduced model from discharge 49529@0.4s. The blue line represents u_{max} control (600V) from X_{init}, magenta is u_{min} (-600V) from X_{init}. The green is the application of u_{max} until the target X_{tar}, while the black is the application of u_{min} until X_{tar}.

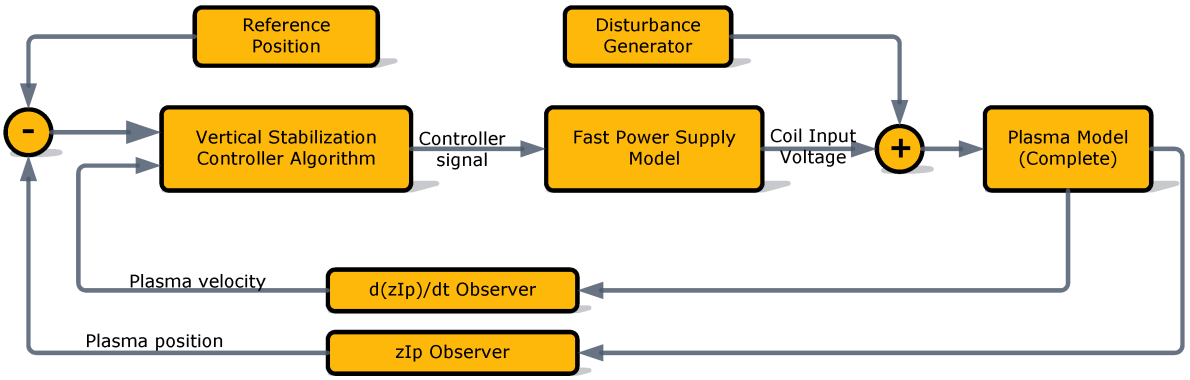

Figure 5.21: Block diagram of the simulation tool to analyze controller performance before implementation in real plasma discharges.

5.6.1 Controller Simulations

The controller algorithm was tested and tuned based on simulation analysis. The decision for the best controller based on these analysis, resulted in a controller that adapts its force to the initial velocity detected.

A true bang-bang controller that always applies the maximum restore signal would exhibit a big oscillation in the plasma position. On the opposite side, a bang-bang controller that was limited to use a small control signal avoiding to exhibit oscillations, would be limited to the control of small perturbations. Thus, a weighted bang-bang controller that increases its restore signal according to the initial plasma velocity demonstrated to be much more efficient, resulting in a more stable controller.

Figures 5.22 and 5.23 support the use of a weighted bang-bang controller.

In these simulations it is possible to see a bang-bang controller with maximum possible strength that was tested against a high level of disturbances (fig. 5.22) with the plasma position under good control. However, using a variable bang-bang controller that changes state according to the distance of the plasma to the set point (fig. 5.23), also on the presence of big disturbances, the coil voltages needed to stabilize the plasma are lower, as well as the plasma position error. The analysis of further simulations show that big disturbances can be controlled using a high control signal for higher displacements and smaller control signal for smaller displacements.

Figure 5.24 presents a diagram with the controller state-machine. The controller is a weighted bang-bang controller, that is similar to use an adaptive bang-bang controller that reconfigures based on system state position and velocity limits. This controller option improves stability by introducing a linear component to the classical nonlinear bang-bang

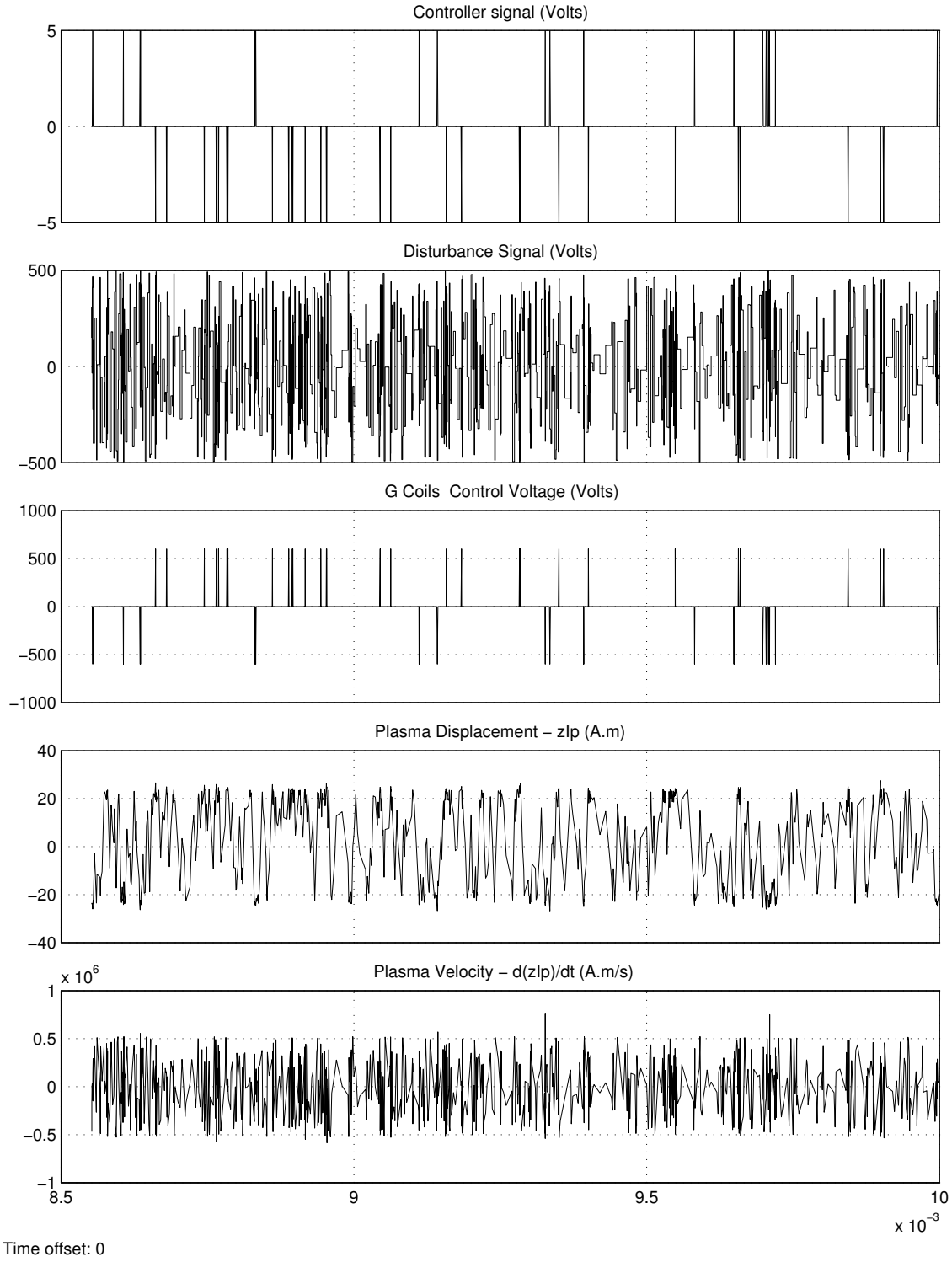

Figure 5.22: Simulation results of the bang-bang controller.

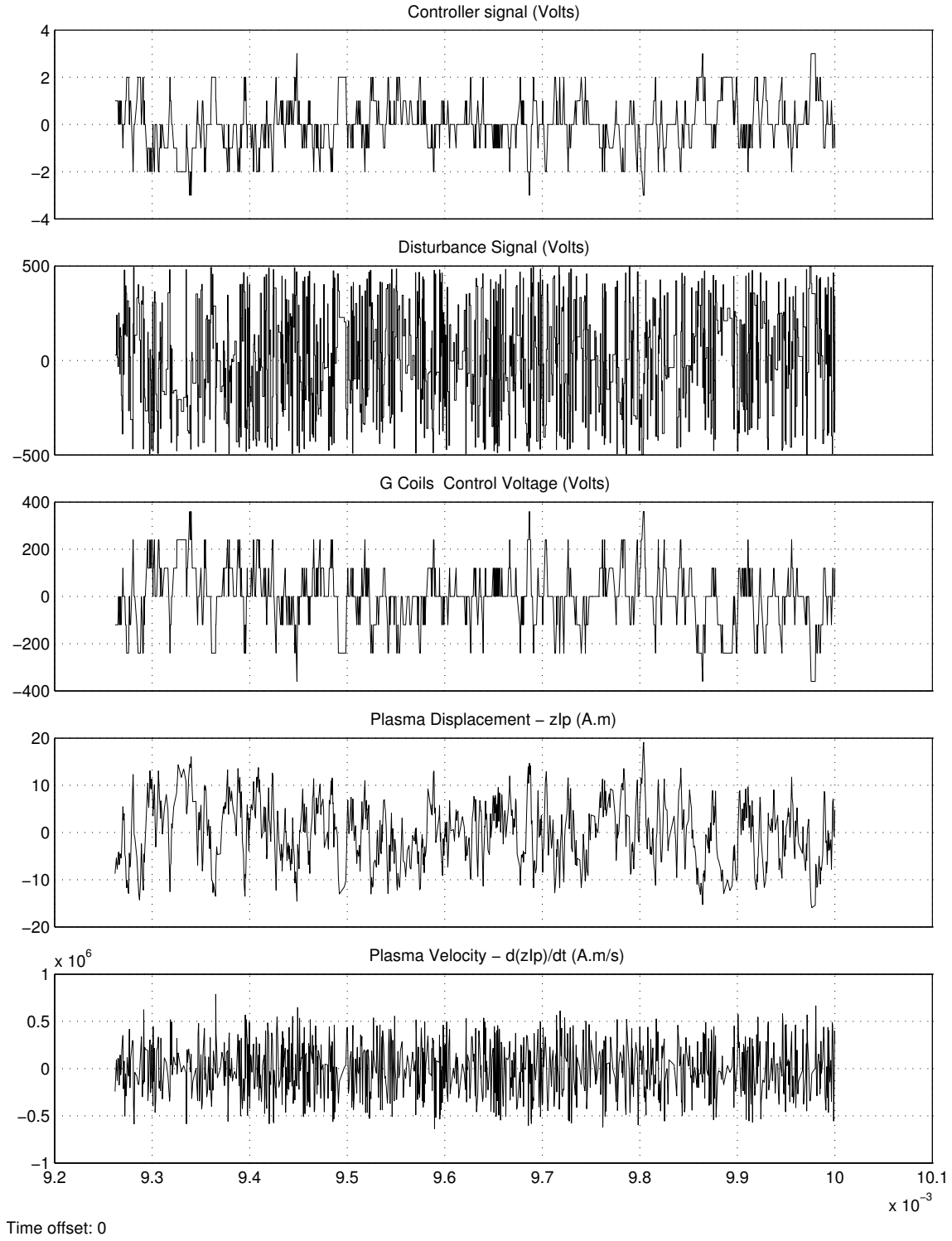

Figure 5.23: Simulation results of the variable bang-bang controller.

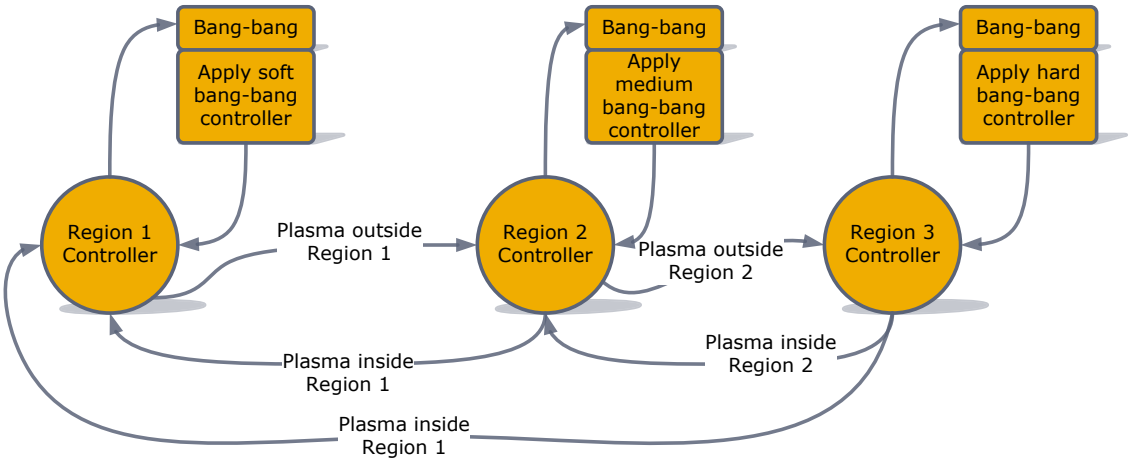

Figure 5.24: Diagram of the controller state machine.

controller.

Table 5.3 depicts the controller regions defined and the maximum applied control voltage for that region during the plasma experiments.

	zIp (kA.m)	Coils Control Voltage (V)
Zone 1	<4.8	No Control
Zone 2	4.8 to 12	24
Zone 3	12 to 24	60
Zone 4	24 to 48	120
Zone 5	48 to 72	240
Zone 6	72 to 96	360
Zone 7	>96	600

Table 5.3: Plasma postition region and corresponding maximum applied voltage (positive or negative) by the bang-bang controller.

5.7 Controller Validation and Results

The vertical stabilization controller was implemented and tested [128][129] using one hardware module with parallel digital signal processing capabilities of the Advanced Plasma Control System [107]. The controller implementation based on the simulation results was tested during plasma discharges at TCV, with improvement in the overall stability of the

plasma. Figures 5.25 and 5.26 depict the stability improvement using the new controller. The plasma discharges were designed to test the limits of the controllers by increasing the plasma elongation from 0.5 seconds, which can be seen at the top of each figure. These plots already confirm the higher elongation achieved using the bang-bang controller.

The increased instability limit using the new controller can also be confirmed by the improvement in discharge time for the same conditions. The current PID controller was not able to cope with the vertical instability finishing the discharge with a vertical disruption at approximately 0.65 s (0.15 s after starting the linear increase in plasma elongation). On the other hand the new bang-bang controller maintained the plasma discharge up to approximately 0.8 s (0.3 s after starting the linear increase in plasma elongation).

Figures 5.25 and 5.26 also show a smaller deviation for the plasma position and velocity during the discharge. Figures 5.27 and 5.28 depict a better use of the coil currents. The plasma position and velocity are more stable during the complete discharge without the continuous fast up-down movement that can be seen using the PID controller.

In conclusion, the stabilization of the axisymmetric MHD instability of highly elongated plasmas requires very fast responses that can not be provided by reconstruction algorithms, some of which presented in Chapter 3. The internal stabilization coils of TCV are designed to counter growth rates of up to 3000 s^{-1}. The bang-bang controller developed was an effort to improve even further over the performance of the analogue Plant Control System (PCS). This was implemented in the APCS digital signal processors and tested successfully on TCV discharges featuring an elongation ramp: the higher elongation achieved by the new bang-bang controller than by the standard PID one will be exploited to improve the TCV plasma stability during the future campaigns of TCV Tokamak Science Program [130].

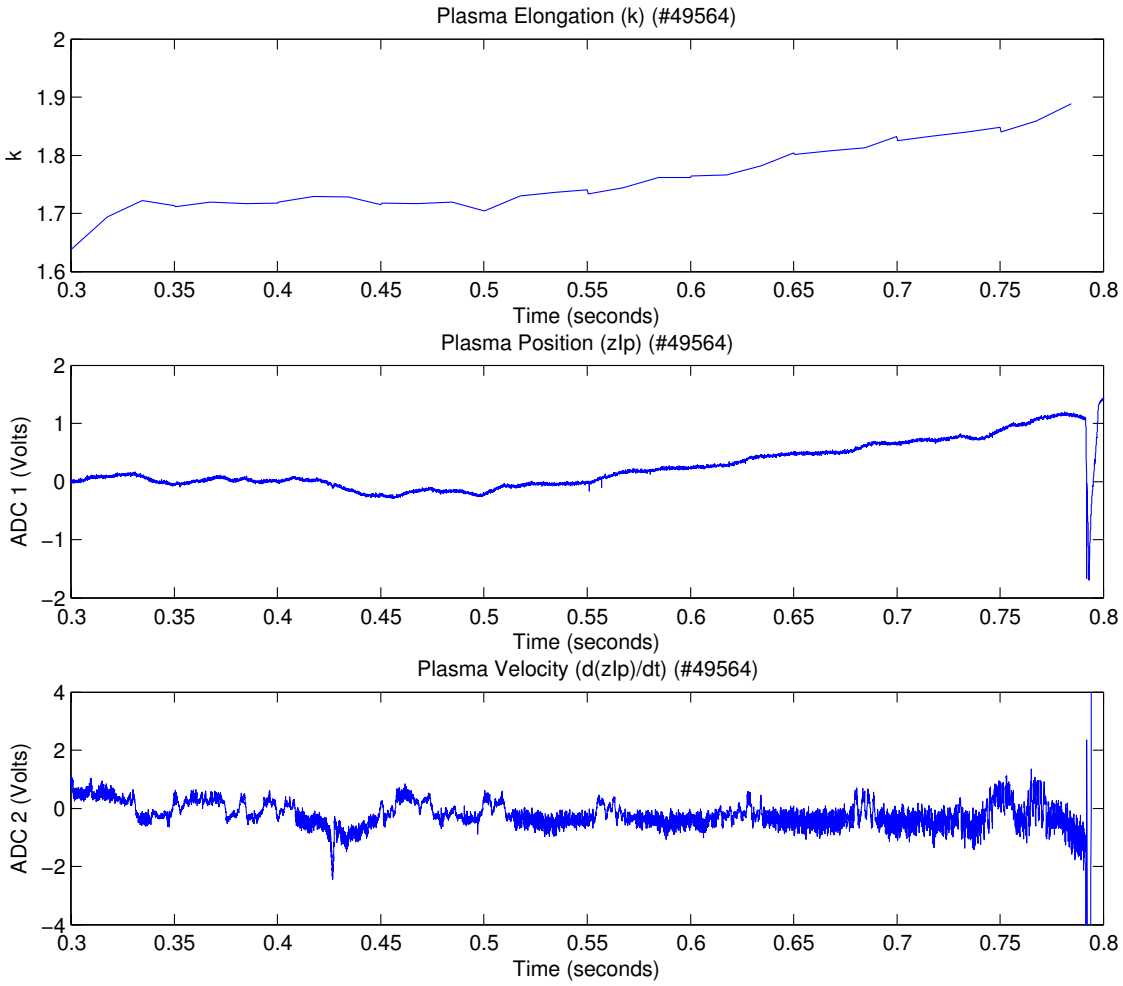

Figure 5.25: Plasma position and velocity for shot 49564 using the new bang-bang controller.

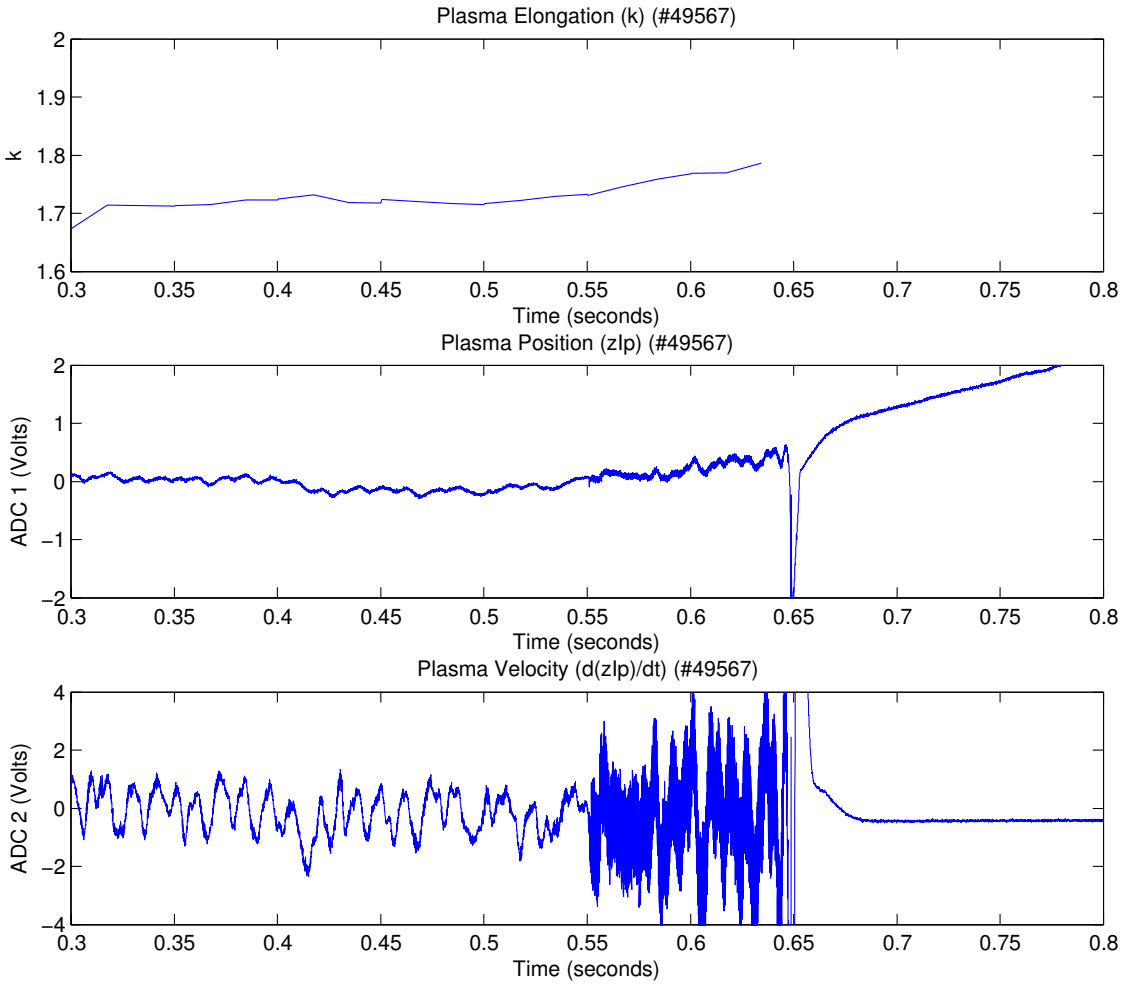

Figure 5.26: Plasma position and velocity for reference shot 49567 using the PID controller in the same plasma conditions as discharge 49564.

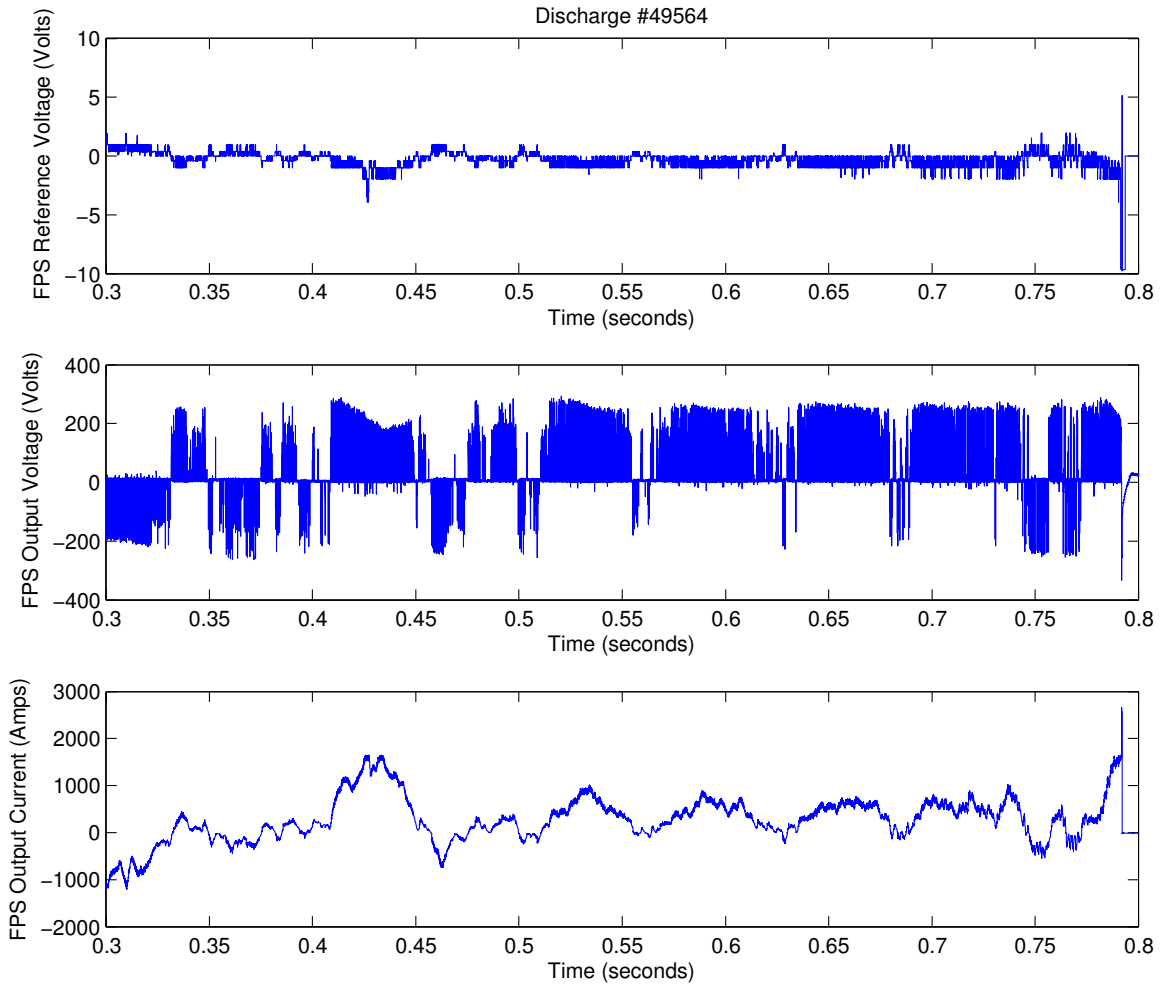

Figure 5.27: Control signal and coil current for discharge 49564 using the new bang-bang controller.

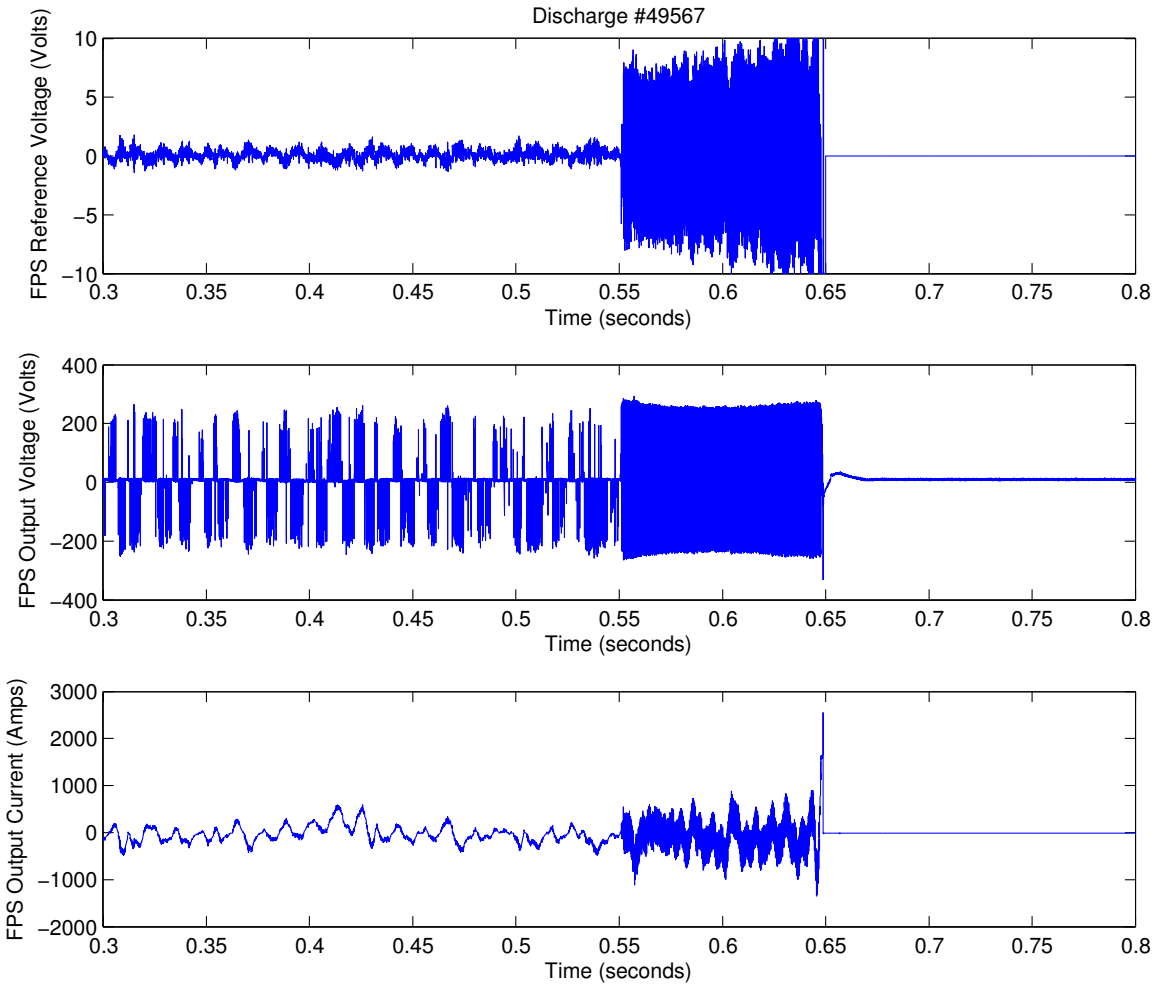

Figure 5.28: Control signal and coil current for reference discharge 49567 using the PID controller in the same plasma conditions as discharge 49564.

6

Conclusion and Future Work

Contents

"As a child, I merely knew this; now I can explain it."
David Deutsch (The Fabric of Reality)

"If you can't explain it to a six year old, you don't understand it yourself."
Albert Einstein

6.1 Introduction

This thesis presents an important part of the work carried out jointly by "Instituto Superior Técnico" (IST) and "Centre de Recherches en Physique des Plasmas" (CRPP), concerning the development of an Advanced Plasma Control System (APCS) [106][107] for real-time control of the TCV plasma shape, position, current and density. This system uses a VME module [30], specially developed by IST for a TCV real-time pulse height analysis X-ray diagnostic [29], based on Digital Signal Processors providing high efficiency parallel processing.

The author of this thesis has collaborated on the APCS conceptual design and has been in charge for: (i) the adaptation of the initial VME module operating software to the APCS requirements; (ii) the development of the software for the integration of APCS in the TCV control system; (iii) the development of the control algorithms; (iv) the APCS tests, calibration, operation; and (v) the application of APCS to the vertical stabilization of the TCV plasma column.

There is a point during the development of a PhD thesis in the frame of a more general research project in which a decision about where to stop must be made. After several achievements and contributions, one can feel that several other breakthroughs could be accomplished if more time would be given. Nevertheless, the idea that the work presented is not the end of an adventure, but a succession of doors that were opened for future work and for others to come gives me the feeling of joy for an accomplished mission.

The next two sections contain not only the main achievements and contributions of this thesis, but also several other relevant questions and new paths that this work may have opened for future work.

6.2 Achievements and Contributions

The main research goals that were achieved during the development of this thesis are the following:

- An Advanced Plasma Control System, capable of improving the capacity of control of highly configurable plasmas by the introduction of nonlinear digital controllers, was developed, integrated and tested at the *Tokamak à Configuration Variable*
- An adaptive near optimal bang-bang controller for control of vertical instabilities on tokamak plasmas was implemented.
- A mathematical simulator based on a plasma model, that can be used as a tool for future improvements of control algorithms for plasma vertical stabilization was developed.
- The proposed method for optimal controller design permits the calculation of the switching time and the final time, which allows the use of predictive control, enabling the control system to maintain its performance with temporary lost of the plasma position and velocity observer, provided the time of "blindness" is smaller than the vertical instability growth rate.
- The TCV plasma vertical stability was enhanced with advantages to the operation capabilities of the tokamak.
- The work presented can also be used to define the controllable zone of the plasma given its initial position and velocity, giving important information on the limits of the plasma parameters and to the design of new control systems.

These achievements were presented and published in the following international peer reviewed journals:

♢ N. Cruz, A.P. Rodrigues, B. Santos, C.A.F. Varandas, B.P. Duval, J.-M. Moret, J. Berrino, Y. Martin, X. Llobet, *The integration of the new advanced digital plasma control system in TCV*, Fusion Engineering and Design 83 (2008) 215-219.

♢ A.P. Rodrigues, N. Cruz, B. Santos, C.A.F. Varandas, J.-M. Moret, J. Berrino, B.P. Duval, *TCV Advanced Plasma Control System Software Architecture and Preliminary Results*, IEEE Transactions On Nuclear Science, vol. 55, pages 316-321 (2008).

♢ J.I.Paley, F.Felici, J.Berrino, S.Coda, N.Cruz, B.P.Duval, T.P.Goodman, Y.Martin, J.M.Moret, F.Piras, A.P.Rodrigues, B.Santos, C.A.F.Varandas and the TCV team, *Real Time Control of Plasmas and ECRH Systems on TCV*, Nuclear Fusion, Volume: 49 Issue: 8, 2009.

♢ N. Cruz, J.-M. Moret, S. Coda, J. I. Paley, B.P. Duval, A. P. Rodrigues, F. Piras, F. Felici, C. M. B. A. Correia, C. A. F. Varandas, *Using APCS for Plasma Vertical Control at TCV*, IEEE Transactions on Nuclear Science, 58 Issue 4, 1570-1575, 2011.

♢ S. Coda for the TCV team, *Progress and scientific results in the TCV tokamak*,

Nuclear Fusion, 51, 094017, 2011.

- ♢ S. Coda for the TCV team, *Overview of recent and current research on the TCV tokamak*, Nuclear Fusion, 53, 104011, 2013.
- ♢ N. Cruz, J.-M. Moret, S. Coda, B.P. Duval, H.B. Le, A.P. Rodrigues, C.A.F. Varandas, C.M.B.A. Correia and B. Gonçalves, *An optimal real-time controller for vertical plasma stabilization*, submitted to IEEE Transactions on Nuclear Science for publication.

as well as the following international meetings and conferences:

- N. Cruz, A.P. Rodrigues, B. Santos, C.A.F. Varandas, B.P. Duval, J.-M. Moret, J. Berrino, Y. Martin, X. Llobet, *The Integration of the New Advanced Digital Plasma Control System in TCV*, Sixth IAEA Technical Meeting on Control, Data Acquisition, and Remote Participation for Fusion Research, 4 - 8 June 2007, Inuyama, Japan.
- A.P. Rodrigues, N. Cruz, B. Santos, C.A.F. Varandas, J.-M. Moret, J. Berrino, B.P. Duval, *TCV Advanced Plasma Control System Software Architecture and Preliminary Results*, IEEE NPSS, 15th Real Time Conference (Fermilab, Batavia, Illinois, USA, April 29 - May 4, 2007).
- J.I. Paley, F. Felici, J. Berrino, S. Coda, N. Cruz, B.P. Duval, T.P. Goodman, Y. Martin, J.M. Moret, F. Piras, A.P. Rodrigues, B. Santos, C.A.F. Varandas and the TCV team, *Real Time Control of Plasmas and ECRH Systems on TCV*, 22nd IAEA Fusion Energy Conference (FEC), Geneva, Switzerland, October 13 to 18, 2008.
- N. Cruz, J.-M. Moret, S. Coda, J.I. Paley, B.P. Duval, A.P. Rodrigues, F. Piras, F. Felici, C.M.B.A. Correia, C.A.F. Varandas, *Using APCS for Plasma Vertical Control at TCV*, 17th IEEE NPSS Real Time Conference, Lisbon, Portugal, May 24th to May 28th, 2010.
- N. Cruz, A.P. Rodrigues, J.-M. Moret, S. Coda, F. Felici, F. Piras, C.A.F. Varandas, *Integration and application of TCV Advanced Plasma Control System*, 2011 Joint Annual Meeting of SPS, OPG, SSAA and OGAA, June 15 -17, 2011, EPFL, Lausanne, Switzerland.
- N. Cruz, J.-M. Moret, S. Coda, B.P. Duval, A.P. Rodrigues, C.A.F. Varandas, *Application of optimal control theory to the vertical plasma stabilization at TCV*, oral presentation, 54th Annual Meeting of the APS Division of Plasma Physics, October 29 - November 2, 2012, Providence, RI, USA.
- N. Cruz, J.-M. Moret, S. Coda, B.P. Duval, H.B. Le, A.P. Rodrigues, C.A.F. Varandas, C.M.B.A. Correia and B. Gonçalves, *An optimal real-time controller for vertical*

plasma stabilization, oral presentation, 19th IEEE Real-Time Conference, May 26th to 30th 2014, Nara, Japan.

- Hoang-Bao Le, B.P. Duval, J.-M. Moret, N. Cruz and the TCV team, *New Developments for Real-Time Plasma Control System of TCV Tokamak based on FPGA*, 19th IEEE Real-Time Conference, May 26th to 30th 2014, Nara, Japan.
- S. Coda for the TCV team, *The Science Program of the TCV Tokamak: Exploring Fusion Reactor and Power Plant Concepts*, 25th IAEA FEC - Fusion Energy Conference in St-Petersburg, Russia, October 2014.

6.3 Other Contributions During the Ph.D. Programme

During the time frame planned for the development of his Ph.D. Programme, the author participated in other projects with scientific, educational and technical relevance. The main work includes:

- Participation in the elaboration of the curriculum of the MSc. on Physics Engineering course "Complementos de Electrónica". The author of this thesis was responsible for the chapter on "Data Structures and Storage Methods" during 2013/2014 and 2014/2015 in the Department of Physics of the University of Coimbra.
- Participation in the development of an ATCA hotplug and hotswap PCI Express implementation aiming at high reliability and high availability data acquisition systems for ITER CODAC. This work has been presented at the 28th Symposium on Fusion Technology [131] and submitted for publication [132].
- Participation in the ATCA shelf-manager device support implementation for ITER CODAC core system. This work has also been presented at the 28th Symposium on Fusion Technology [133] and submitted for publication [134].
- Participation in the on-going project for the Radial Neutron Camera (RNC) for ITER as an Electronics and CODAC Expert, co-responsible for the specification and design of the high speed, high resolution ATCA based control and data acquisition system. The RNC is being developed for the ITER Organization and Fusion for Energy[1] in Consortium, including under the head institution ENEA-Frascati the following partners: IST-IPFN, CNR, UNIMIB, UU, IPPLM, IFJPAN, PTB and CREATE.

[1]Fusion for Energy is the European Domestic Agency for the ITER Project.

Other scientific work developed by the author of this thesis prior to the beginning of the work presented in this document is briefly described in Appendix B.

6.4 Future Work

Following promising results in the implementation and test in TCV of the new time optimal controller (bang-bang controller) for plasma vertical stability, some important improvements and analysis are foreseen to prepare this type of controllers to be used in future devices such as ITER. A more complete test of the controller for ELM and Beta collapse resilience, by application of predictive control based on the developed work, is foreseen.

The following main activities are envisaged:

- ♢ Improvement of the optimal controller algorithm.
- ♢ Simulation of the controller using the mathematical test bench that includes the plasma and actuators model.
- ♢ Adaptation of the test bench for other tokamaks.
- ♢ Evaluation of different hardware systems in terms of calculation performances, bigger memory for table allocation, and integration in the TCV control system for implementation of the improved controller.
- ♢ Validation of the controller in TCV plasma discharges in the presence of ELMs and other possible perturbative events.

Part IV

Appendices

A

APCS Low-Level System Configuration

Contents

A.1 Introduction

To configure the way DataMover handles data channels, it is necessary to build the command files that set the system to understand which channels are used, which DSPs are managing them, etc... Each hardware module has an ascii cmd file that is built according to the rules described in this section.

Each line in the cmd file is a command for a DSP to run, setting the values that are passed as parameters. As each command is an action to be performed by a DSP, all messages sent must have a source and destination address. DSPs are addressed from 0 to 3 in each VME module, and the VME host has address 4. A typical command line would be:

```
[destiny, source [command type, command: par 1, par 2,..., par n]]
```

Each command has its own parameters to be set, that can be any value or definition passed as text. Due to DSP0 being the distributor of each module messages, the commands should be sent in descending order, in the following sequence:

- `[3,4[command...]]`
- `[2,4[command...]]`
- `[1,4[command...]]`
- `[0,4[command...]]`

A.2 Initializing and Retrieving Algorithm Data Structure

The TCV algorithm is programmed in the DSPs using the tcvalgo.c and tcvalgo.h described in the next section. This means that a change in the algorithm demands recompiling, linking and reloading the DSP software into the module. However, most of the times the algorithm can be reused with different startup data without the need of recompilation. To permit this feature an algorithm data structure may be uploaded into the module to the predefined place in DSP memory map. The source of this data is a binary file that can be stored in the DPCS tree described in the MDSPLUS interface to TCV section.

It is the responsibility of the algorithm developer to arrange and initialize the data in a way the algorithm will "understand" the data that is being sent. Some important notes must be taken into account:

- Texas Instrument DSP Float format is different from IEEE float format. Depending on the way Algo Data Structure is built, you might consider the need of using *double toieee(double)* and *double frieee(double)* functions defined in intrin.h header file. This functions should be used in the pre and post shot functions of the *tcvalgo.c*.
- *char, short, int* and *long* data formats are all 32 bits in size in TMS320C4x DSP family. When building the data structures this information must be taken into account with the risk of loosing data and context by overlapping variables .

After the shot the Algorithm Data Structure is retrieved from the DSP memory and stored back into the DPCS MDSPlus tree for analyzing and debugging purposes.

A.3 Commands and Command File

A.3.1 Implementation Rules

The command file for each module defines the DMBUS data structure to be exchanged between modules in real-time. To get the best performance possible out of the hardware, a compromise between fast transfers and usability had to be made, that ended in some important rules to have in mind. Some of these rules will be highlighted near the commands that use them. Nevertheless, they are listed bellow for clarity and ease of use:

- The number of data channels to transfer must be even.
- All modules in the slow data mover DMBUS must have at least one data channel configured on DSP3.
- Data channels and DSP numbers must be in consecutive ascending order. The DSP numbering is consecutive ascendant inside a module and from one module to the next in the chain. No gaps or jumps are permitted.
- All the DSPs in the chain must be initialized with a DSPCFG command, even if the DSP doesn't manage any channels.
- Virtual channels that are not moved by the data bus must be numbered higher than the number of data channels to be moved. As these channels are only seen by the manager DSP, several DSPs can use the same virtual channel numbers.
- Commands should be sent in descending order to DSPs inside a module because DSP0 is the manager of the module. If a command is sent to DSP0 that takes long to process, messages will not pass from VME to destination DSPs 1, 2 and 3, until the command has been executed. If messages are sent in descending order, messages will be delivered to all DSPs at almost the same time, and executed in parallel.

- APCS, RTS or RTF commands must be the last command issued as it changes the DSP state from configuration state to real-time control cycle. The command must be sent to DSP 3, 2, 1 and finally 0 by this order. These are the commands that will start the DataMover and Algo processes in the DSP, so all DSPs must receive these commands to start. All DSPs in the same module must receive the same command.

Module number	Module DSP number	Global DSP number	Data Channel number
1	0	0	0,1
1	1	1	2,3
1	2	2	
1	3	3	4 (must have)
2	0	4	5
2	1	5	6,7
2	2	6	8
2	3	7	9 (must have)
- Number of data channels is even (10) *- All DSPs and data channels are in consecutive ascending order* *- All DSP3 in all modules have a data channel*			

Table A.1: Example of DMBUS data channels structure

Table A.1 give a simple example of the DMBUS

A.3.2 List of Main Commands

In this section a list of the main commands to configure the data channels and the data mover is presented.

Name: DATACH

Description: Sets a data channel

Syntax: *[destiny, source [A,DATACH: data_ch_index, name, st, dspindex, type, procspeed, input_range, output_range, init_in_data]*

Parameters:

data_ch_index – data channel index – integer between 0 and 69

name – data channel name – ascii array

st – status enable or disable – integer 1-enable 0-disable.

dspindex – DSP index that manages the data channel – integer between 0 and 31

type – defines if the data channel is hardware type or software type – char 'h' or 's'

procspeed – defines if the data channel is part of the fast or slow process datamover – char 'f' or 's'

input_range – hardware ADC input range – only used when the data channel type is hardware – float value

output_range – hardware DAC output range – only used when the data channel type is hardware – float value

init_out_data – initial data output value

Example: *[0,4[A,DATACH:0,a,1,0,h,s,5,5,0]*

Note: Channels must be indexed in sequential ascending order

Note: To simplify the algorithm channels should be indexed after the corresponding hardware channel.

Name: ACQPAR

Description: Configures the hardware data channel ADC acquisition parameters

Syntax: *[destiny,source[A,ACQPAR:adc_data_ch_id,avg_words, div_factor, adc_gain,adc_offset]*

Parameters:

adc_data_ch_id – data channel index – integer between 0 and 69

avg_words – number of words to do the ADC average – power of 2 integer

div_factor – division factor, number of binary rotation to obtain the average – the integer exponent of the power of 2.

adc_gain – gain correction to calculate the ADC input – float value

adc_offset – offset correction to calculate ADC input – integer

Example: *[0,4[A,ACQPAR:0,4,2,1,0]*

Note: If you want to do a media of 8 values, you can use *avg_words* = 8 and *div_factor* = 3, getting a 12bit value of the average. It is also possible to do *avg_words* = 8 and *div_factor* = 0, getting a 15 bit value of the sum of 8 12bit values.

Algorithm can be described as:

SUM(ADC DATA *avg_words* times) –> BITSHIFT(*div_factor*)
-> MULTIPLY(*adc_gain*) -> SUM(*adc_offset*)

Name: CTLPAR
Description: Configures the hardware data channel DAC control parameters
Syntax: *[destiny, source [A, CTLPAR:dac_data_ch_id,dac_gain,dac_offset]*
Parameters:
dac_data_ch_id – the data channel index – integer between 0 and 69
dac_gain – gain correction to calculate the DAC output – float value
dac_offset – offset correction to calculate DAC output – integer
Example: *[0,4[A,CTLPAR:0,1,0]*

Name: DSPCFG
Description: Configures the DSP as the manager of its data channels
Syntax: *[destiny,source[A,DSPCFG:dspindex,nb_ch_to_proc,id_ch1,id_ch2,...,id_chN]*
Parameters:
Dspindex – the DSP index that manages the data channel – integer between 0 and 31
nb_ch_to_proc – number of channels to manage (0 to 4)
id_ch1, id_ch2,...,id_chN – the data channel index – integer between 0 and 69
Example: *[0,4[A,DSPCFG:0,2,0,1]*

Name: DMCFG
Description: Configures the DMBUS hardware parameters
Syntax: *[destiny, source [A,DMCFG:ON/OFF,FBOARD,USO_EN,CLKSRC]*
Parameters:
ON/OFF – turns the DMBUS functionality on/off – integer 1-on 0-off
FBOARD – first board defines if this is the board that begins the transfer cycle – integer 1-first board 0-another board
USO_EN – if DMBUS is off, enables to connect the token pass control line from previous module to the next – integer 0-backplane has physical jumper connecting the lines 1-backplane doesn't have physical jumper
CLKSRC – hardware digital input clock source - integer 0- external dmbus clk, 1 internal dmbus clk

Example: *[0,4[A,DMCFG:1,1,1,0]*

Important Note: If more than one module is set as first board there will be bus collisions in DMBUS and Datamover algorithm will stall.

Important Note: It is possible to take out a module from the data mover setting *ON/OFF* to 0 and *FBOARD* to 0. If not, the module must have at least the hardware data channel enabled in DSP 3.

Important Note: Taking out a module from data mover (like taking out a channel) demands a reconstruction of all modules configuration files, because channels must be numbered in ascending order with no gaps in numbering.

Name: APCS

Description: Changes the DSP state to real-time control TEST cycle

Syntax: *[destiny, source [A, APCS: nb_ of_ data_ ch, nb_ iterations, watch_ dog_ timer]*

Parameters:

nb_ of_ data_ ch – number of data channels – integer between 0 and 69

nb_ iterations – number of iterations to execute – integer 0-infinite or hardware controlled *n*-pre-programmed number of iterations

watch_ dog_ timer – not used at the moment

Example: *[3,4[A,APCS:64,0,5]*

Name: RTS

Description: Changes the DSP state to real-time slow control cycle

Syntax: *[destiny, source [R,RTS: nb_ of_ data_ ch, nb_ iterations, watch_ dog_ timer]*

Parameters:

nb_ of_ data_ ch – number of data channels – integer between 0 and 69

nb_ iterations – number of iterations to execute – integer 0-infinite or hardware controlled *n*-pre-programmed number of iterations

watch_ dog_ timer – not used at the moment

Example: *[3,4[R,RTS:64,0,5]*

Name: RTF

Description: Changes the DSP state to real-time fast control cycle

Syntax: *[destiny, source [R,RTF: nb_ of_ data_ ch, nb_ iterations, watch_ dog_ timer]*

Parameters:

nb_ of_ data_ ch – number of data channels – integer between 0 and 69

nb_ iterations – number of iterations to execute – integer 0-infinite or hardware controlled *n*-pre-programmed number of iterations

watch_ dog_ timer – not used at the moment

Example: *[3,4[R,RTF:64,0,5]*

Note: APCS, RTS and RTF commands must be the last command issued as it changes the DSP state from configuration state to real-time control cycle. The command must be sent to DSP 3, 2, 1 and finally 0 by this order.

Name: SAVE_DATA

Description: Save local data

Syntax: *[destiny, source [A,SAVE_ DATA:start_ iter,final_ iter,save_ step]*

Parameters:

start_ iter – start iteration – integer

final_ iter – final iteration _ integer 0 to n < start_iter + 192k * step/number of local data channels < 192k

save_ step – iteration step to save local data – integer must be power of two

Example: *[3,4[A,* SAVE_DATA*:10,65535,4]*

B

Participation in Research Projects

Contents

B.1 Introduction

The author of this thesis has participated in several research, development and innovation projects prior to the beginning of the work presented in this document. This appendix presents a resume of the main activities of the author, including a brief description of the project highlights, the candidate contributions and the main scientific outputs to peer reviewed journals and conferences.

From 1998 to 2008, the author of this thesis worked in the following projects, having had responsibilities in specification of control and data acquisition systems, software design and implementation, test and final integration in fusion devices:

- Control and data acquisition system for the JET laser in-vessel viewing system prototype;
- Control and data acquisition system for the ITER laser in-vessel viewing system prototype;
- Control and data acquisition system for the JET correlation reflectometer upgrade;
- Data acquisition system for the Jet Heterodyne Radiometer Upgrade;
- Low-Cost Galvanic Isolated Fast PCI Transient Recorder with Signal Processing Capabilities;
- JET magnetic proton recoil neutron spectrometer upgrade (MPRu);
- JET time-of-flight neutron spectrometer (TOFOR);
- JET Real-Time Test-Bench System;

B.2 Prototype of the Laser In-Vessel Viewing Systems (LIVVS) for JET and ITER[1]

B.2.1 Highlights

IPFN was responsible for the the design and implementation of the laser beam deflection control system for in-vessel scanning, with the image acquisition and storing (18 Bytes per pixel acquired every 10 μs). The system also included an interlocking safety control system to avoid damaging the head of the scanning probe and the step motors due to the excessive load when high accelerations are demanded.

Figure B.1 shows the VME hardware modules used for the control and data acquisition

[1]Project developed in collaboration with ENEA-Frascati.

on the left and for safety monitoring (motor temperature and position) on the right.

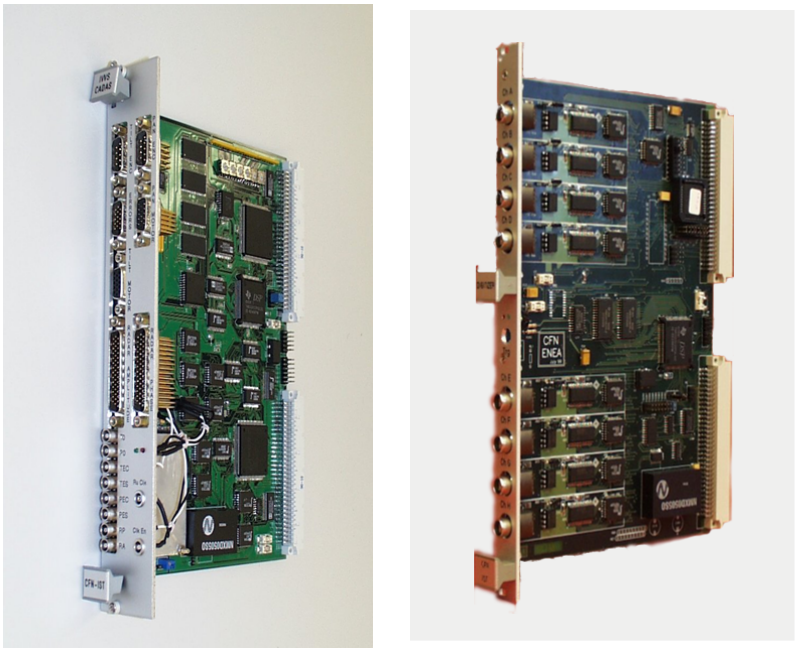

Figure B.1: Control and data acquisition hardware modules for the laser in-vessel viewing system prototype.

B.2.2 Author Contribution

The author participated in the hardware specification and system testing and was responsible for the software design and development. His main contributions were:

- ⋆ DSP TMS320C31 motors and timing control software;
- ⋆ OS-9 and LynxOS real time TCP-IP server software and VME drivers;
- ⋆ Unix station client software;
- ⋆ Hardware and system testing.

Figure B.2 depicts the client/server software structure implemented in three levels and the communication between the different software and hardware parts.

B.2.3 Publications in Peer Reviewed Journals

♢ R. Pereira, N. Cruz, C. Neri, M. Riva, C. Correia e C.A.F. Varandas, *The Control And Data Acquisition System Of A Laser In-Vessel Viewing System*, Fusion Engineering and Design, vol. 48, No 1, pp. 205-212, August 2000.

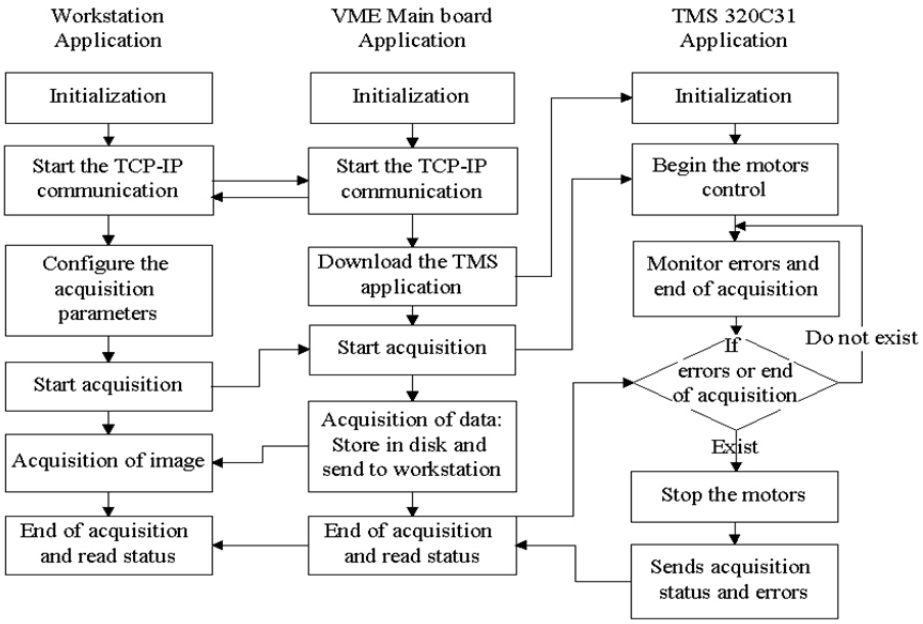

Figure B.2: The client/server software structure implementation for the LIVVS prototype.

♢ R. Pereira, N. Cruz, C. Neri, C. Correia and C. Varandas, *A high-data-transfer-rate VME system for TCP-IP remote real-time control of the ITER in-vessel vision system*, Fusion Engineering and Design, 60, (3), 253, 2002.

B.2.4 Contributions to Conferences

♢ Rita Pereira, Nuno Cruz, Carlos Correia, Carlo Neri, Marco Riva, Alberto Coletti, Carlos Varandas, *Control and data acquisition on a laser in-vessel viewing system*, 20th Symposium on Fusion Tecnhology, Marseille, France, June 1998.

♢ Rita Pereira, Nuno Cruz, C. Neri, M. Riva, C. Correia and C.A.F. Varandas, *The Control And Data Acquisition System Of A Laser In-Vessel Viewing System*, 2nd IAEA (International Atomic Energy Agency) Technical Committee Meeting On Control, Data Acquisition And Remote Participation On Fusion Research, Lisboa, Portugal, 19-21 July 1999.

♢ Nuno Cruz, R.C.Pereira, C.A.F.Varandas , C.Correia, *Software Structure of a Control and Data Acquisition System for a Laser In-Vessel Viewing System*, ICSPAT (International Conference on Signal Processing Applications & Technology), Orlando, Florida, EUA, 1-4 November 1999.

♢ R.C.Pereira, Nuno Cruz, C.A.F.Varandas , C.Correia, *Control And Data Acquisition System For A Laser In-Vessel Viewing System For Big Fusion Machines*, ICSPAT

(International Conference on Signal Processing Applications & Technology), Orlando, Florida, EUA, 1-4 November 1999.

♢ Rita Pereira, Nuno Cruz, Carlo Neri, Carlos Correia,Carlos Varandas, *A High Data Transfer Rate VME System For TCP-IP Remote Real-Time Control Of The ITER In-Vessel Vision System*, 3rd IAEA Technical Committee Meeting on Control, Data Acquisition, and Remote Participation for Fusion Research, Padova, Italy, July 2001.

B.3 JET Correlation Reflectometer

B.3.1 Highlights

IPFN developed a correlation reflectometer system for JET [135], which included the design and implementation of the control and data acquisition system with real time signal processing. This system combines 16 slow acquisition channels with real-time DSP capability with 16 fast acquisition channels (3 MSPS). The system was installed in JET and is running since May 2002.

Figure B.3 shows the control and data acquisition hardware modules, as well as the system installed in the JET diagnostic cubicle during commissioning. The intelligent module on the left features a Texas Instruments Digital Signal Processor (DSP) used for the implementation of the timing control and the real time digital filter. The fast acquisition module at the center features 8 acquisition channels to acquire the reflectometer signals at predetermined time windows.

B.3.2 Author Contribution

The author was responsible for the design and implementation of the control and data acquisition system and performed the following main activities:

⋆ Integration in CODAS through Level-1 HTTP based interface;
⋆ Linux VME module device drivers;
⋆ Real time DSP filter processing software and acquisition timing control;
⋆ Programme reflectometers sweep frequency using RS232;
⋆ Hardware and system integration testing;
⋆ System commissioning and data validation.

Figure B.4 outlines the author design of the control and data acquisition system to interface the reflectometer channels and the JET timing, network and file system.

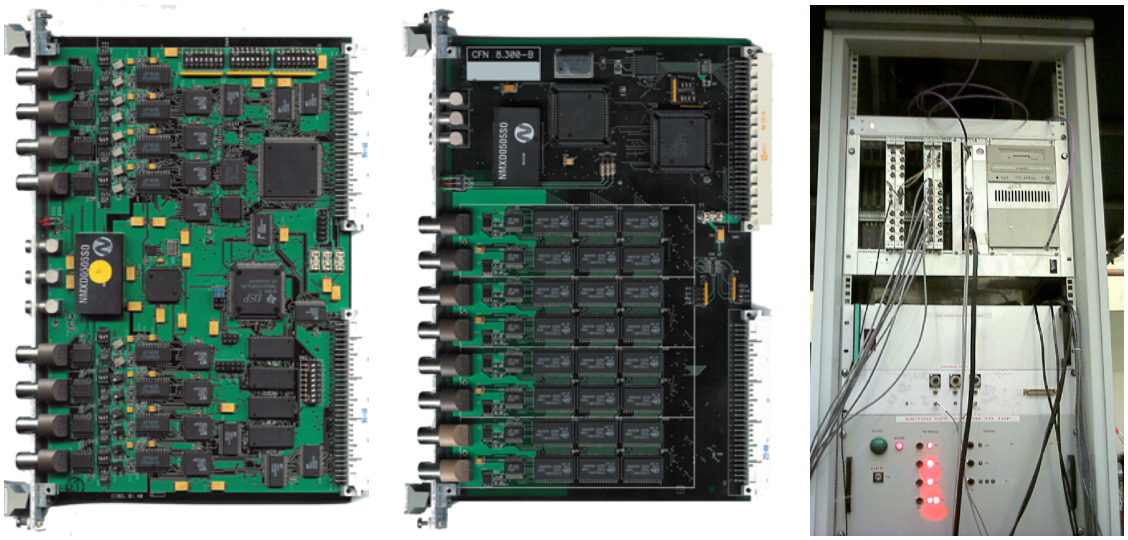

Figure B.3: Control and data acquisition hardware modules and diagnostic cubicle installed in JET.

Figure B.5 depicts the real time digital filter algorithm implemented in the DSP.

B.3.3 Publications in Peer Reviewed Journals

- ♢ N. Cruz, R. Pereira, M. Correia, L. Cupido, C. Correia and C. Varandas, "A large memory, high transfer rate VME data acquisition system for the JET correlation reflectometer", Fusion Engineering and Design, 60, (3), 273, 2002.
- ♢ S. Hacquin, L. Meneses, L. Cupido, N. Cruz, L. Kokonchev, R. Prentice, C. Gowers, "Upgrade of the X-mode reflectometry diagnostic for radial correlation measurements in the Joint European Torus", Review of Scientific Instruments, 75, (10), 3834, 2004.

B.3.4 Contributions to Conferences

- ♢ Nuno Cruz, Rita Pereira, Miguel Correia, Luis Cupido, Carlos Correia, Carlos Varandas, "A Large Memory, High Transfer Rate Vme Data Acquisition System For The Jet Correlation Reflectometer", 3rd IAEA Technical Committee Meeting on Control, Data Acquisition, and Remote Participation for Fusion Research, Padova, Italy, July 2001.
- ♢ Meneses L, Cupido L, Cruz N, Kokonchev L, Mazzucato E, Prentice R, "Upgrade of the JET multichannel fluctuation and correlation reflectometer diagnostic", 44th

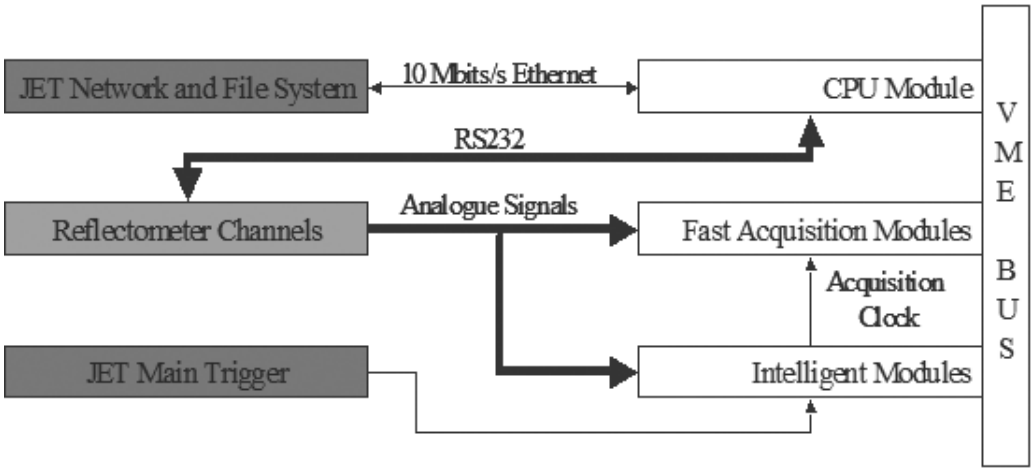

Figure B.4: Correlation reflectometer control and data acquisition system design.

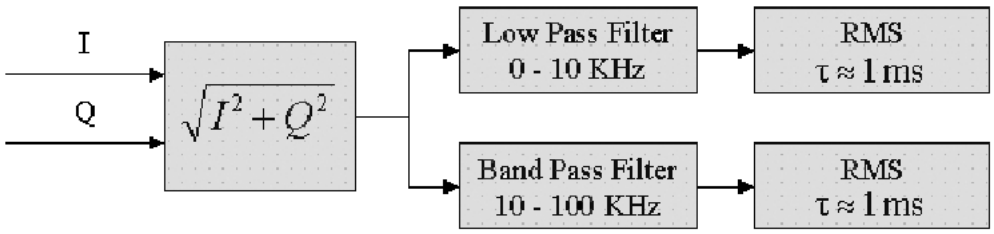

Figure B.5: Correlation reflectometer algorithm implemented using real time digital filtering.

Annual Meeting of The American Physical Society, Division of Plasma Physics, Orlando, Florida, November 11-15, 2002, abstract in Bulletin of The American Physical Society 47, 238 (2002).

♢ S. Hacquin, L. Meneses, I. Nunes, N. Cruz, L. Cupido, R. Prentice and JET-EFDA Contributors, "Possibilities of X-mode Correlation Reflectometry Measurements from the Upgraded KG8b Diagnostic on JET", 15th Topical Conference on High Temperature Plasma Diagnostics, 19-22 of April, 2004, San Diego, USA.

♢ A. Fonseca, A.C.A. Figueiredo, J. Fessey, L. Cupido, B. Alper, N. Cruz, L. Meneses, A. Sirinelli, M.E. Manso, M. Walsh and JET EFDA contributors, "In-Situ Calibration of the Correlation Reflectometry Systems on the Joint European Torus Tokamak", 17th High Temperature Plasma Diagnostics (HTPD) Conference, Albuquerque, New Mexico, 11th May 2008 - 15th May 2008.

B.4 JET Heterodyne Radiometer Upgrade[2]

B.4.1 Highlights

IPFN developed the data acquisition system for the JET heterodyne radiometer upgrade, with the following main technical characteristics:

- 48 channels DAQ system for the KK3 diagnostic;
- 6 modules with eight 12-bit differential channels each, sampling up to 3 MSPS 6 MSample per channel of memory;

This system is running in JET since January 2003.

Figure B.6 shows the hardware module used for data acquisition on the left and the complete data acquisition system on the right.

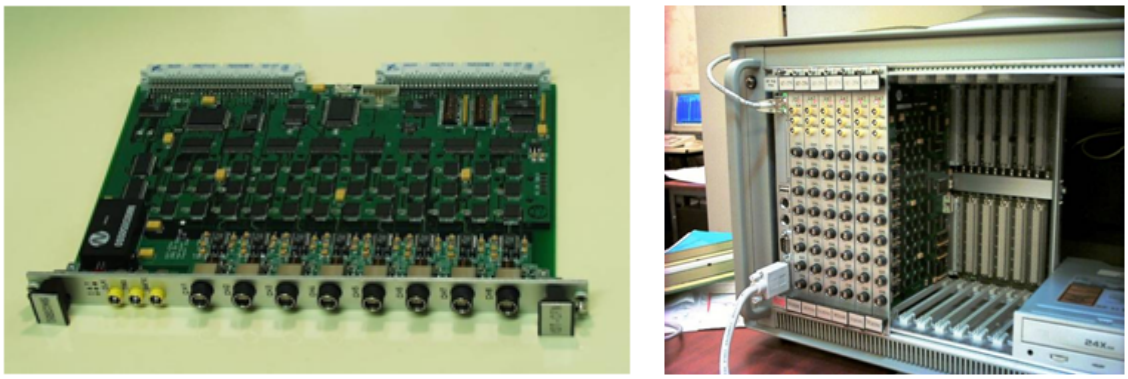

Figure B.6: Data acquisition hardware module for the JET Heterodyne Radiometer Upgrade (on the left) and the complete data acquisition system (on the right).

B.4.2 Author Contribution

The author was responsible for the software design and development and for the hardware testing and compliance verification. The main tasks included:

- ⋆ Integration in CODAS through Level-1 HTTP based interface;
- ⋆ Linux device driver development;
- ⋆ Memory test software design and implementation;
- ⋆ Hardware testing and verification.

[2]Project developed in collaboration with UKAEA Fusion Association.

B.4.3 Publications in Peer Reviewed Journals

♢ Nuno Cruz, Jorge Sousa, Rita Pereira, Álvaro Combo, C.A.F. Varandas, Misha Beldishevski, Simon Dorling, Barry Alper and contributors to the EFDA-JET work programme, "A Large Memory VME Data Acquisition System for the Jet Heterodyne Radiometer Upgrade", Fusion Engineering and Design, vol. 71, 167-173, 2004.

B.4.4 Contributions to Conferences

♢ N. Cruz, Jorge Sousa, Rita Pereira, Álvaro Combo, C.A.F. Varandas, Misha Beldishevski, Simon Dorling, Barry Alper and contributors to the EFDA-JET work programme, "A Large Memory VME Data Acquisition System for the Jet Heterodyne Radiometer Upgrade", 4th IAEA TCM on Control Data Acquisition and Remote participation for Fusion Research, San Diego, USA, July 21-23, 2003.

B.5 JET Magnetic Proton Recoil Neutron Spectrometer Upgrade (MPRu)[3]

B.5.1 Highlights

IPFN developed the control and data acquisition system for the JET MPRu [136][137], with the following main technical characteristics:

- 32 channels DAQ system;
- Four 8-bit, 200 MSPS ADCs p/ module;
- Variable memory per channnel up to 512 Mbytes of total data;
- Time stamp with 5 ns resolution;

Figures B.7 and B.8 depict the hardware module block diagram and picture respectively.

B.5.2 Author Contribution

The author was responsible for the software design and implementation, including the following parts:

⋆ Linux PCI module driver and API;

[3]Project developed in collaboration with Uppsala University and UKAEA Fusion Association.

- ⋆ DSP real-time data transfer from FPGA to local memory (up to 300 Mbytes/s);
- ⋆ Data management software;
- ⋆ Hardware testing.

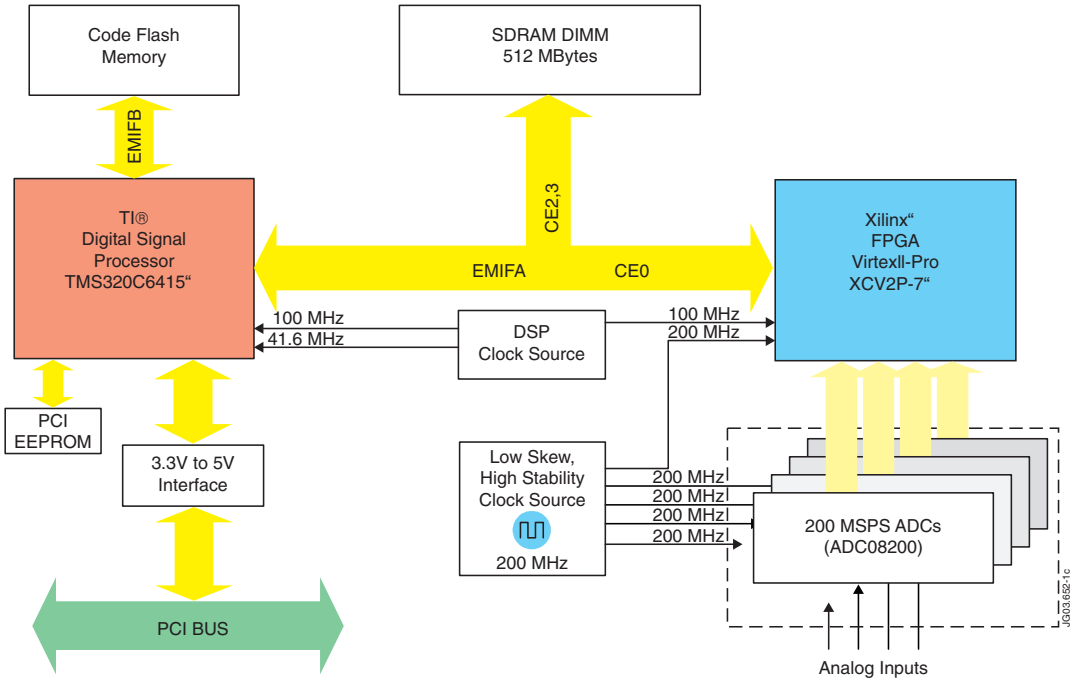

Figure B.7: PCI data acquisition module block diagram for JET MPRu project.

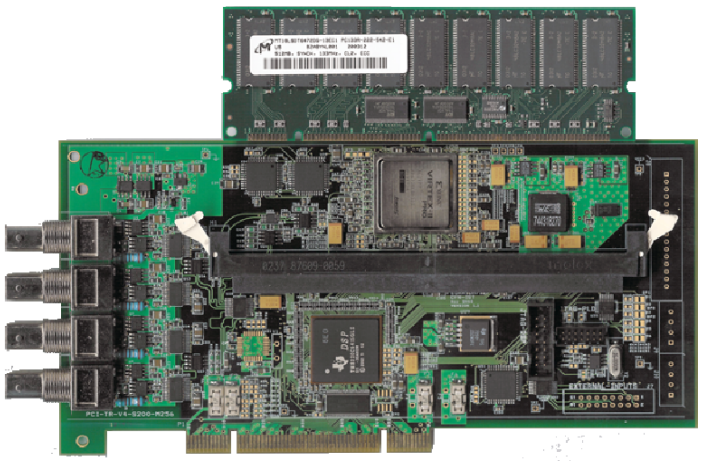

Figure B.8: Picture of the PCI data acquisition module for JET MPRu project.

Figure B.9 illustrates the software developed for hardware module testing and verification.

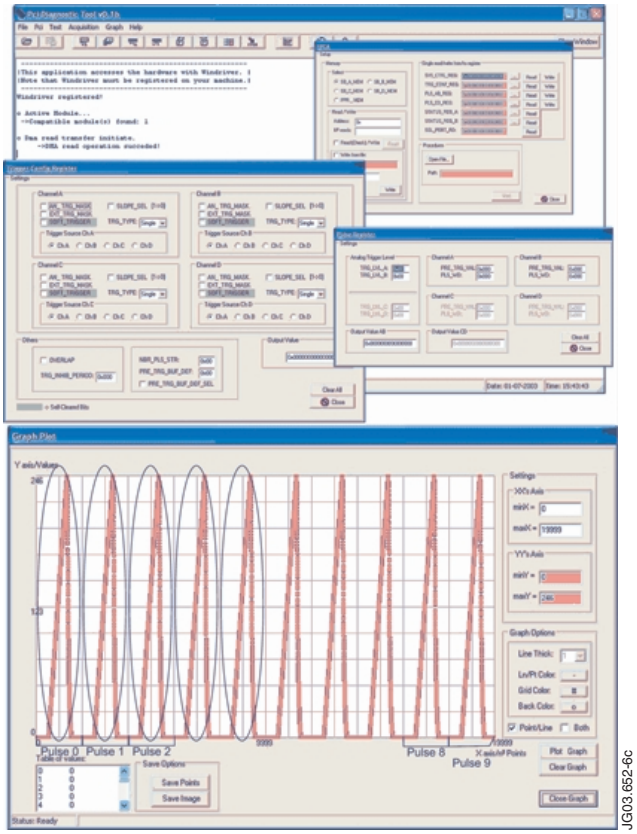

Figure B.9: Test software for the data acquisition hardware module used in MPRu project.

B.5.3 Publications in Peer Reviewed Journals

- ♢ A. Combo, R. Pereira, J. Sousa, N. Cruz, P. Carvalho, C.A.F. Varandas, S. Conroy, J. Kallne and M. Weiszflog, "A PCI transient recorder module for the JET magnetic proton recoil neutron spectrometer", Fusion Engineering and Design, vol. 71, 151-157, 2004.
- ♢ J.M. Cardoso, J.B. Simões, C.M.B.A. Correia, A. Combo, R. Pereira, J.Sousa, N. Cruz, P. Carvalho, C.A.F. Varandas, "A High Performance Reconfigurable Hardware Platform for Digital Pulse Processing", IEEE Transactions on Nuclear Science, vol 51, Issue 3, 921 - 925, 2004.

- ♢ L. Giacomelli, E. Andersson Sundén, S. Conroy, G. Ericsson, M. Gatu Johnson, C. Hellesen, A. Hjalmarsson, J. Källne, E. Ronchi, H. Sjöstrand, M. Weiszflog, G. Gorini, M. Tardocchi , A. Murari S. Popovichev, J. Sousa, R. C. Pereira, A. Combo, N. Cruz and JET EFDA contributors, "Development and characterization of the proton recoil detector for the MPRu neutron spectrometer", Review of Scientific Instruments 77 (10): 10E708 (2006).
- ♢ H. Sjostrand, L. Giacomelli, E. Andersson Sunden, S. Conroy, G. Ericsson, M. Gatu Johnson, C. Hellesen, A. Hjalmarsson, J. Kallne, E. Ronchi, M. Weiszflog, G. Wikstrom, G. Gorini, M. Tardocchi, A. Murari, G. Kaveney, S. Popovichev, J. Sousa, R. C. Pereira, A. Combo, N. Cruz and JET-EFDA Contributors, "New MPRu instrument for neutron emission spectroscopy at JET", Review of Scientific Instruments 77 (10): 10E717 (2006).
- ♢ E. Andersson Sunden, H. Sjostrand, S. Conroy, G. Ericsson, M. Gatu Johnson, L. Giacomelli, C. Hellesen, A. Hjalmarsson, E. Ronchi, M. Weiszflog, J. Kallne, G. Gorini, M. Tardocchi, A. Combo, N. Cruz, A. Batista, R. Pereira, R. Fortuna, J. Sousa, S. Popovichev, "The thin-foil magnetic proton recoil neutron spectrometer MPRu at JET", Nuclear Instruments and Methods in Physics Research, A610 (2009) 682-699.

B.5.4 Contributions to Conferences

- ♢ A. Combo, R. Pereira, J. Sousa, N. Cruz, P. Carvalho, C.A.F. Varandas, S. Conroy, J. Kallne and M. Weiszflog, "A PCI transient recorder module for the JET magnetic proton recoil neutron spectrometer", 4th IAEA TCM on Control Data Acquisition and Remote participation for Fusion Research, San Diego, USA, July 21-23, 2003.
- ♢ L. Giacomelli, E. Andersson Sunden, S. Conroy, G. Ericsson, M. Gatu Johnson, C. Hellesen, A. Hjalmarsson, J. Kallne, E. Ronchi, H. Sjostrand, M. Weiszflog, G. Gorini, M. Tardocchi , A. Murari S. Popovichev, J. Sousa, R. C. Pereira, A. Combo, N. Cruz and JET EFDA contributors, "Development and characterization of the proton recoil detector for the MPRu neutron spectrometer", 16th Topical Conference on High-Temperature Plasma Diagnostics, MAY 07-11, 2006.
- ♢ H. Sjostrand, L. Giacomelli, E. Andersson Sunden, S. Conroy, G. Ericsson, M. Gatu Johnson, C. Hellesen, A. Hjalmarsson, J. Kallne, E. Ronchi, M. Weiszflog, G. Wikstrom, G. Gorini, M. Tardocchi, A. Murari, G. Kaveney, S. Popovichev, J. Sousa, R. C. Pereira, A. Combo, N. Cruz and JET-EFDA Contributors, "New MPRu in-

strument for neutron emission spectroscopy at JET", 16th Topical Conference on High-Temperature Plasma Diagnostics, MAY 07-11, 2006.

B.6 JET Time-of-flight Neutron Spectrometer (TOFOR)[4]

B.6.1 Highlights

IPFN developed the data acquisition system for the JET TOFOR [138], with the following main technical characteristics:

- 8 independent Time to Digital Converter (TDC) channels per module with 0.4 ns resolution;
- Variable memory per channel up to 512 Mbytes of total data;
- Peak event rate of 1.25 Gevents/s;
- Sustained pulse rate of 5 Mevents/s;

Picture B.10 depicts the TDC hardware module developed for the JET TOFOR project.

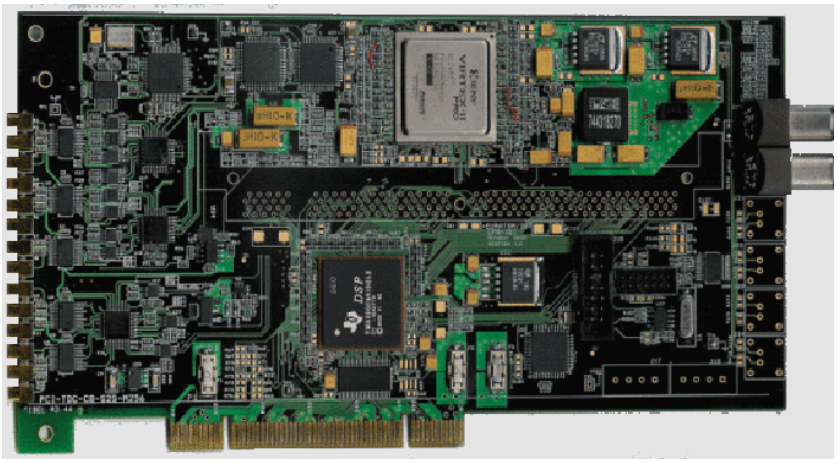

Figure B.10: Picture of the PCI TDC module for JET TOFOR project.

B.6.2 Author Contribution

The author was responsible for the software design and implementation. The first task included some unique features to cope with the variable channel memory and high data transfer rates needed. The main developments were:

[4]Project developed in collaboration with Uppsala University and UKAEA Fusion Association.

- ⋆ Linux PCI module driver and API;
- ⋆ DSP real time data transfer from FPGA to local memory using DMA;
- ⋆ Manipulation of event interruptions to trigger the data transfer of different channels in the same module;
- ⋆ Time constrains validation and error reporting;
- ⋆ TCP/IP module synchronization between several PCs;
- ⋆ Data management for real time size regulation of the channels memory.

B.6.3 Publications in Peer Reviewed Journals

- ♢ J.Sousa, A.J.N. Batista, A. Combo, R. Pereira, N. Cruz, P. Carvalho, C.A.F. Varandas, S. Conroy, G. Ericsson and J. Kallne, "A PCI time digitizer for the new JET time-of-flight neutron spectrometer", Fusion Engineering and Design, vol. 71, 101-107, 2004.
- ♢ R.C. Pereira, A. Combo, N. Cruz, J. Sousa, C. Correia, C. Varandas, S. Conroy and J. Kallne, "Enhanced Neutron Diagnostics Data Acquisition System based on a Time Digitizer and Transient Recorder Hybrid Module", Fusion Engineering and Design 81, Issues 15-17, Pages 1873-1877, July 2006.
- ♢ M.Gatu Johnson, L.Giacomelli, A.Hjalmarsson, M.Weiszflog, E.Andersson Sunden, S.Conroy, G.Ericsson, C.Hellesen, J.Kallne, E.Ronchi, H.Sjostrand, G.Gorini, M.Tardocchi, A.Murari, S.Popovichev, J.Sousa, R.C.Pereira, A.Combo, N.Cruz and JET EFDA contributors, "The TOFOR neutron spectrometer and its first use at JET", Review of Scientific Instruments 77, 10E702 (2006).
- ♢ M. Gatu Johnson, L. Giacomelli, A. Hjalmarsson, J. Kallne, M. Weiszflog, E. Andersson Sunden, S. Conroy, G. Ericsson, C. Hellesen, E. Ronchi, H. Sjostrand, G. Gorini, M. Tardocchi, A. Combo, N. Cruz, J. Sousa, S. Popovichev, JET-EFDA contributors, "The 2.5-MeV neutron time-of-flight spectrometer TOFOR for experiments at JET", Nuclear Instruments and Methods in Physics Research A, 591 (2): 417-430, June 21st 2008.

B.6.4 Contributions to Conferences

- ♢ J. Sousa, A.J.N. Batista, A. Combo, R. Pereira, N. Cruz, P. Carvalho, C.A.F. Varandas, S. Conroy, G. Ericsson and J. Kallne, "A PCI time digitizer for the new JET time-of-flight neutron spectrometer", 4th IAEA TCM on Control Data

Acquisition and Remote participation for Fusion Research, San Diego, USA, July 21-23, 2003.

♢ R. C. Pereira, A. Combo, N. Cruz, Jorge Sousa, C. Correia, C. Varandas, S. Conroy and J. Källne, "Enhanced Neutron Diagnostics Data Acquisition System based on a Time Digitizer and Transient Recorder Hybrid Module", 5th IAEA TM on Control, Data Acquisition and Remote Participation for Fusion Research, 12-15 of July 2005, Budapest, Hungary.

♢ M. Gatu Johnson, L. Giacomelli, A. Hjalmarsson, M. Weiszflog, E. Andersson Sunden, S. Conroy, G. Ericsson, C. Hellesen, J. Kallne, E. Ronchi, H. Sjostrand, G. Gorini, M. Tardocchi, A. Murari, S. Popovichev, J. Sousa, R.C. Pereira, A. Combo, N. Cruz and JET EFDA contributors, "The TOFOR neutron spectrometer and its first use at JET", 16th Topical Conference on High-Temperature Plasma Diagnostics, MAY 07-11, 2006.

B.7 JET Real Time Test Bench

B.7.1 Highlights

IPFN developed the JET Real Time Test Bench [139], which aims at simulating the JET signal environment to test new real time systems. The implementation of this system included the development and integration of:

- 32 DAC channels - 16 bit, 2 MSPS;
- 8 ADC channels - 14 bit, 2 MSPS;
- Real time ATM interface.

Figure B.11 depicts the JET Real Time Test Bench System installed at Culham Science Centre.

B.7.2 Author Contribution

The mains responsibilities of the author were:

⋆ Integration into JET environment;

⋆ Interface JET signals using MDSPlus and feed them into the signal generator;

⋆ DSP real-time data transfer from local memory to FPGA (up to 300 Mbytes/s);

⋆ Linux PCI module drivers and API.

Figure B.12 depicts the software structure designed and implemented by the author.

Figure B.11: Picture of the JET Real Time Test Bench System.

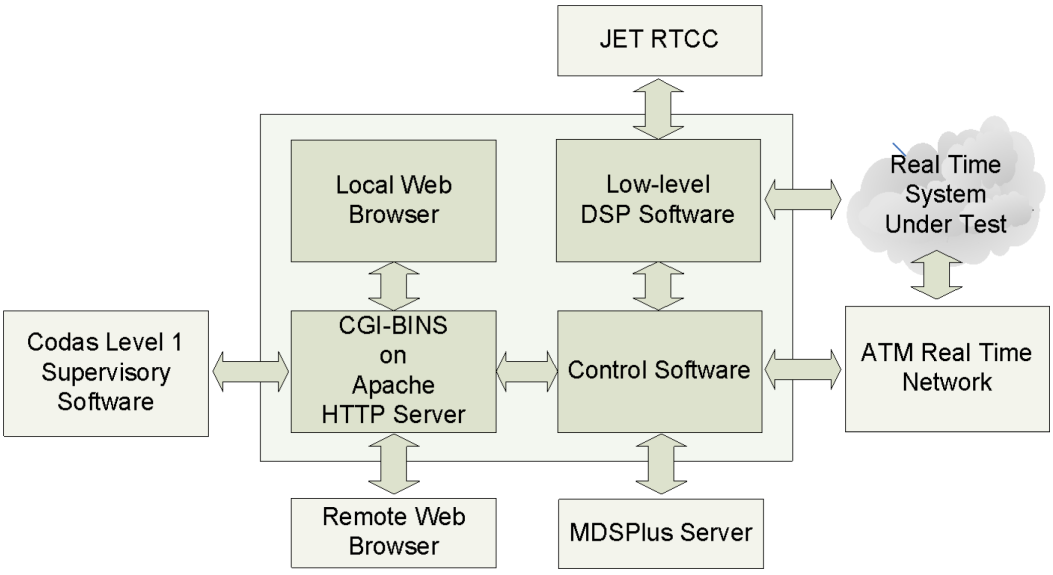

Figure B.12: Picture of the JET Real Time Test Bench System software and communications structure.

B.7.3 Publications in Peer Reviewed Journals

- ♢ M. Correia, A. J. N. Batista, A. Combo, N. Cruz, P. Carvalho, C. Correia, J. Sousa, "A Low-Cost Galvanic Isolated Fast PCI Transient Recorder with Signal Processing Capabilities", Fusion Engineering and Design, vol. 71, 159, 2004.
- ♢ J. Sousa, A.J.N. Batista, A. Combo, R. Pereira, M. Correia, N. Cruz, P. Carvalho, C. Correia and C.A.F. Varandas, "PCI data acquisition and signal processing hardware modules for long pulse operation", Review of Scientific Instruments, 75, (10), 4271, 2004.
- ♢ A. J. N. Batista, D. Alves, N. Cruz, J. Sousa, C. A. F. Varandas, E. Joffrin, R. Felton, J. Farthing and JET-EFDA Contributors, "A FPGA-Based Multi-Rate Interpolator with Real-Time Rate Change for a JET Test-Bench System", IEEE Transactions On Nuclear Science 53 (3): 756-760 Part 1, Jun 2006.
- ♢ N. Cruz, A. J. N. Batista, D. Alves, J. Sousa,C. A. F. Varandas, E. Joffrin, R. Felton, J. W. Farthing and JET-EFDA Contributors, "JET Real Time Project Test-Bench Software Structure", Fusion Engineering and Design, 81, Issues 15-17, Pages 1933-1937, July 2006.

B.7.4 Contributions to Conferences

- ♢ M. Correia, A. J. N. Batista, A. Combo, N. Cruz, P. Carvalho, Carlos Correia, J. Sousa, "A Low-Cost Galvanic Isolated Fast PCI Transient Recorder with Signal Processing Capabilities", 4th IAEA TCM on Control Data Acquisition and Remote participation for Fusion Research, San Diego, USA, July 21-23, 2003.
- ♢ J. Sousa, A. J. N. Batista, A. Combo, R. Pereira, Miguel Correia, N. Cruz, P. Carvalho, Carlos Correia and C.A.F. Varandas, "PCI Data Acquisition and Signal Processing Hardware Modules for Long Pulse Operation", 15th Topical Conference on High Temperature Plasma Diagnostics, 19-22 of April, 2004, San Diego, USA.
- ♢ A. J. N. Batista, D. Alves, N. Cruz, J. Sousa, C. A. F. Varandas, E. Joffrin, R. Felton, J. Farthing and JET-EFDA Contributors, "A FPGA-Based Multi-Rate Interpolator with Real-Time Rate Change for a JET Test-Bench System", 14th IEEE Real Time Conference 2005, 4-10 of June 2005, Stockholm, Sweden.
- ♢ N. Cruz, A. J. N. Batista, D. Alves, J. Sousa,C. A. F. Varandas, E. Joffrin, R. Felton, J. W. Farthing and JET-EFDA Contributors, "JET Real Time Project Test-Bench Software Structure", 5th IAEA TM on Control, Data Acquisition and Remote Participation for Fusion Research, 12-15 of July 2005, Budapest, Hungary.

Bibliography

[1] David Rutledge, *Estimating long-term world coal production with logit and probit transforms*, International Journal of Coal Geology 85, 23-33, (2011).

[2] Carlos Varandas , Aníbal Traça de Almeida, António Vallera, Eduardo Oliveira Fernandes, Manuel Collares Pereira, Pedro Coelho, *As Energias do Presente e do Futuro*, Gazeta da Física, Sociedade Portuguesa de Física, Vol. 29, Novembro de 2005.

[3] Francis F. Chen, *An Indispensable Truth - How Fusion Power Can Save the Planet*, Springer, New York (2011).

[4] Ralph F. Keeling, *Recording Earth's vital signs*, Science, v. 319, no. 5871, p. 1771-1772 (2008).

[5] J. R. Petit et al, *Climate and atmospheric history of the past 420 000 years from the Vostok ice core, Antarctica*, Nature 399, 429-436 (3 June 1999).

[6] Intergovernmental Panel on Climate Change (IPCC), *Climate Change 2007: Synthesis Report - An Assessment of the Intergovernmental Panel on Climate Change*, IPCC Plenary XXVII (Valencia, Spain, 12-17 November 2007).

[7] European Environment Agency, *The European environment - state and outlook 2010: assessment of global megatrends*, EEA, Copenhagen, (2011).

[8] Garry McCracken and Peter Stott, *Fusion (Second Edition), The Energy of the Universe*, Elsevier Inc., (2012).

[9] Richard Fitzpatrick, *Plasma Physics*, The University of Texas at Austin, University Reprints (2012).

[10] Atkinson, R. and Houtermans, F., *Aufbaumoglichkeit in Sternen*, Z. fur Physik 54, 656-665, (1929).

[11] Bethe, H. A., *Energy Production in Stars*, Physical Reviews 55, 5, p. 434-456 (1939).

[12] https://www.llnl.gov/

[13] O. A. Hurricane, D. A. Callahan, D. T. Casey, P. M. Celliers, C. Cerjan, E. L. Dewald, T. R. Dittrich, T. Doppner, D. E. Hinkel, L. F. Berzak Hopkins, J. L. Kline, S. Le Pape, T. Ma, A. G. MacPhee, J. L. Milovich, A. Pak, H.-S. Park, P. K. Patel, B. A. Remington, J. D. Salmonson, P. T. Springer and R. Tommasini, *Fuel gain exceeding unity in an inertially confined fusion implosion*, Nature 506, 343-348, (20 February 2014).

[14] http://www-lmj.cea.fr/

[15] M. Seki, *ITER activities and fusion technology*, Nuclear Fusion, Vol. 47, Issue 10, S489-S500, (2007).

[16] J. D. Lawson, *Some Criteria for a Power Producing Thermonuclear Reactor*, Proceedings of the Physical Society. Section B Volume 70 Number 1 (1957).

[17] M. Keilhacker, et al., *High fusion performance from deuterium-tritium plasmas in JET*, Nuclear Fusion, Vol. 39, 209, (1999).

[18] S. Ishida, K. Abe, A. Ando, T. Cho, T. Fujii, T. Fujita, S. Goto, K. Hanada, A. Hatayama, T. Hino, H. Horiike, N. Hosogane, M. Ichimura, S. Tsuji-Iio, S. Itoh, Y. Kamada, M. Katsurai, M. Kikuchi, A. Kitsunezaki, A. Kohyama, H. Kubo, M. Kuriyama, M. Matsukawa, M. Matsuoka, Y. Miura, Y.M. Miura, N. Miya, T. Mizuuchi, Y. Murakami, K. Nagasaki, H. Ninomiya, N. Nishino, Y. Ogawa, K. Okano, T. Ozeki, M. Saigusa, M. Sakamoto, A. Sakasai, M. Satoh, M. Shimada, R. Shimada, M. Shimizu, T. Takagi, Y. Takase, S. Takeji, T. Tanabe, K. Toi, Y. Ueda, Y. Uesugi, K. Ushigusa, M. Wakatani, Y. Yagi, K. Yamaguchi, T. Yamamoto, K. Yatsu and K. Yoshikawa, *Objectives and design of the JT-60 superconducting tokamak*, Nuclear Fusion, Vol. 43, Issue 7, pp. 606, (2003).

[19] K. Ikeda, et al., *Progress in the ITER Physics Basis*, Nuclear Fusion, Vol. 47, Number 6, (2007).

[20] J. Wesson, *Tokamaks*, Oxford University Press (2004).

[21] Atul S. Sharma, David J. N. Limebeer, Imad M. Jaimoukha and Jonathan B. Lister, *Modeling and Control of TCV*, IEEE Transactions on Control Systems Technology, Vol. 13, No. 3, (2005).

[22] B.J.D. Tubbing, N.A.C. Gottardi, B.J. Green, J.A. How, M. Huart, R. Konig, C.G. Lowry, P.J. Lomas, P. Noll, J.J. O'Rourke, P.H. Rebut, D. Stork, A. Tanga, A. Taroni and D.J. Ward, *AC plasma current operation in the JET tokamak*, Nuclear Fusion, Vol. 32, Issue 6, pp. 967, (1992).

[23] Fernandes, H.; Varandas, C. A F; Cabral, J. A C; Figueiredo, H.; Galvao, R.; Batista, A.J., *Engineering aspects of the ISTTOK operation in a multicycle alternating flat-top plasma current regime*, Fusion Engineering, 17th IEEE/NPSS Symposium , vol.1, pp.576-580, 6-10 Oct 1997.

[24] E Bertolini and the JET Team, *Current engineering issues and further upgrading of the JET tokamak*, Fusion Engineering, 17th IEEE/NPSS Symposium (Volume:1), pp. 81-87, 6-10 Oct 1997.

[25] Y. Gribov, D. Humphreys, K. Kajiwara, E.A. Lazarus, J.B. Lister, T. Ozeki, A. Portone, M. Shimada, A.C.C. Sips and J.C. Wesley, *Progress in the ITER Physics Basis - Chapter 8: Plasma operation and control*, Nuclear Fusion, Vol. 47, Number 6, pp. 385-403, (2007).

[26] http://www.efda.org/jet/

[27] http://www.iter.org

[28] R.A.Pitts, R.Chavan and J.-M.Moret, *The design of central column protection tiles for the TCV tokamak*, Nuclear Fusion, Vol. 39, pp. 1433, (1999).

[29] T.I. Madeira, A.P. Rodrigues, C.A.F. Varandas, P. Amorim, B.P. Duval, *Real-time signal analysis on the TCV PHA diagnostic*, Review of Scientific Instruments, Vol.74, Number 3, pp. 2004-2006, March 2003.

[30] A.P. Rodrigues, C.M.B Correia and C.A.F. Varandas, *A High Performance Real-Time Plasma Control and Event Detection DSP Based VME System*, Fusion Engineering and Design, Vol. 60, Number 3, pp. 435-441, (2002).

[31] F. Sartori, A. Barbalace, A.J.N. Batista, T. Bellizio, P. Card, G. De Tommasi, P. Mc Cullen, A. Neto, F. Piccolo, R. Vitelli, L. Zabeo and JET-EFDA contributors,

The PCU JET plasma vertical stabilization control system, Fusion Engineering and Design, Volume 85, Issues 3-4, Proceedings of the 7th IAEA Technical Meeting on Control, Data Acquisition, and Remote Participation for Fusion Research, pp. 438-442, July 2010.

[32] A.J.N. Batista, J. Sousa, and C.A.F. Varandas, *ATCA digital controller hardware for vertical stabilization of plasmas in tokamaks*, Review of Scientific Instruments, Vol. 77, pp. 10F527, (2006).

[33] A.J.N. Batista, A. Neto, M. Correia, A.M. Fernandes, B.B. Carvalho, J.C. Fortunato, J. Sousa, C.A.F. Varandas, F. Sartori, M. Jennison, and JET-EFDA contributors, *ATCA Control System Hardware for the Plasma Vertical Stabilization in the JET Tokamak*, IEEE Transactions on Nuclear Science, Vol. 57, pp. 583-588, (2010).

[34] A.C. Neto, F. Sartori, F. Piccolo, R. Vitelli, G. De Tommasi, L. Zabeo, A. Barbalace, H. Fernandes, D.F. Valcarcel, A.J.N. Batista and JET-EFDA Contributors, *MARTe: A Multiplatform Real-Time Framework*, IEEE Transactions On Nuclear Science 57, 2,(2010).

[35] T.Bellizio, G. De Tommasi, P. Mc Cullen, A. Neto, F. Piccolo, F. Sartori, R. Vitelli, L. Zabeo and JET-EFDA Contributors, *The Software Architecture of the new Vertical Stabilization System for the JET tokamak*, IEEE Transactions On Plasma Science 38, 9, (2010).

[36] T. Bellizio, G. De Tommasi, N. Risoli, R. Albanese, A. Neto, *A MARTe based simulator for Vertical Stabilization System*, 26th Symposium on Fusion Technology (SOFT), Porto, Portugal.

[37] N. Cruz, A.J.N. Batista, D. Alves, J. Sousa,C.A.F. Varandas, E. Joffrin, R. Felton, J.W. Farthing and JET-EFDA Contributors, *JET Real Time Project Test-Bench Software Structure*, Fusion Engineering and Design, 81, Issues 15-17, pp. 1933-1937, (2006).

[38] A.J.N. Batista, D. Alves, N. Cruz, J. Sousa, C.A.F. Varandas, E. Joffrin, R. Felton, J. Farthing and JET-EFDA Contributors, *A FPGA-Based Multi-Rate Interpolator with Real-Time Rate Change for a JET Test-Bench System*, IEEE Transactions On Nuclear Science 53 (3): 756-760 Part 1, (2006).

[39] Richard C. Dorf and Robert H. Bishop, *Modern Control Systems - 11th Edition*, Pearson Education International, (2008).

[40] R.E. Bellman and S.E. Dreyfus, *Applied Dynamic Programming*, Princeton University Press, (1962).

[41] R.E. Bellman and R.E. Kalaba, *Dynamic Programming and Modern Control Theory*, New York Academic Press, (1965).

[42] L.S. Pontryagin, V.G. Boltyanskii, R.V. Gamkrelidze and E.F. Mischenko, *The Mathematical Theory of Optimal Processes*, New York: Interscience Publishers, Inc., (1962).

[43] V.G. Boltyanskii, R.V. Gamkrelidze. L.S. Pontryagin, *Towards a theory of optimal processes*, (Russian), Reports Acad. Sci. USSR, vol.110(1), (1956).

[44] D.E. Kirk, *Optimal Control Theory, An Introduction*, Prentice Hall, (1970), in the republished version of 2004.

[45] L.E. Elsgolc, *calculus of variations*, Addison-Wesley. (1962)

[46] Dimitri P. Bertsekas, *Dynamic Programming and Optimal Control*, Volume I, Athena Scientific, Belmont, Massachusetts, (1995).

[47] M. Athans and P. L. Falb, *Optimal Control: An Introduction to the Theory and its Applications*, McGraw-Hill, New York, (1966).

[48] A. E. Bryson and Y. C. Ho, *Applied Optimal Control*, Blaisdell, Waltham, Mass., (1969).

[49] A. P. Rodrigues, *Sistema de Multiprocessamento para Controlo em Tempo Real em Experiências de Fusão Nuclear*, PhD Thesis, Instituto Superior Técnico, Portugal (2005).

[50] A. J. Baptista, *Sistema ATCA de Controlo em Tempo Real de Tokamaks com Descargas de Longa Duração*, PhD Thesis, Instituto Superior Técnico, Portugal (2010).

[51] A. Neto, *The JET Vertical Stabilisation Controller Framework*, PhD Thesis, Instituto Superior Técnico, Portugal (2011).

[52] J-Y. Favez, *Enhancing the Control of Tokamaks Via a Continuous Nonlinear Control Law*, PhD thesis no.3034, École Polytechnique Fédérale de Lausanne (EPFL), Switzerland (2004).

[53] A Sharma, *Tokamak Modelling and Control*, PhD Thesis, Imperial College of Sciences Technology and Medicine, UK (2002)

[54] F. Felici, *Real-time control of tokamak plasmas: from control of physics to physics-based control*, PhD thesis no.5203, École Polytechnique Fédérale de Lausanne (EPFL), Switzerland, October 2011.

[55] P. Vyas, D. Mustafa and A.W. Morris, *Vertical position control on COMPASS-D*, Fusion Technology, 33(2), 97-105 (1998)

[56] M.L. Walker, D.A. Humphreys, *On feedback stabilization of the tokamak plasma vertical instability*, Automatica, Volume 45, Issue 3, pp.665-674, March 2009.

[57] A. Neto et al., *Exploitation of modularity in the JET tokamak vertical stabilization system*, Control Engineering Practice, Vol 20, Issue 9, 846-856, (2012).

[58] M. Ariola and A. Pironti, *Magnetic control of tokamak plasmas*, Springer-Verlag (2008).

[59] M. Ariola, A. Pironti, *Basic issues on tokamak plasma magnetic control*, Proceedings of the 47th IEEE Conference on Decision and Control, Cancun, Mexico, Dec. 9-11 (2008).

[60] J-Y. Favez, Ph. Mullhaupt, B. Srinivasan and D. Bonvin, *A globally stabilising controller under saturated input for linear planar systems with one unstable pole*, American Control Conference, Boston, USA (2004).

[61] V. D. Shafranov, *Equilibrium of a Toroidal Plasma in a Magnetic Field*, Plasma Physics (Journal of Nuclear Energy Part C) Vol. 5, pp. 251 to 258 (1963).

[62] V. D. Shafranov, *Plasma equilibrium in a magnetic field*, Reviews of Plasma Physics, Vol. 2, p. 103, New York: Consultants Bureau (1966).

[63] H. J. de Blank, *Plasma Equilibrium in Tokamaks*, Fusion Science and Technology, Volume 61, Number 2T, Pages 89-95, February (2012).

[64] G. Ambrosino and R. Albanese. *Magnetic control of plasma current, position, and shape in tokamaks*, IEEE Control Systems Magazine, vol. 25, no. 5, pp. 76-92, October (2005).

[65] S. I. Braginskii, *Transport Processes in a Plasma*, Reviews of Plasma Physics, Vol 1, p.205, Consultants Bureau, New York (1965).

[66] J. D. Callen, C. C. Hegna, A. J. Cole, *Transport equations in tokamak plasmas*, Physics of Plasmas, 17, 056113 (2010).

[67] Aitor J. Garrido, Izaskun Garrido, M. Goretti Sevillano, Mikel Alberdi, Modesto Amundarain, Oscar Barambones, Manuel De La Sen, *Nuclear fusion control-oriented plasma current linear models*, ICS'10 Proceedings of the 14th WSEAS international conference on Systems: part of the 14th WSEAS CSCC multiconference - Volume I, Pages 145-150, July (2010).

[68] S.A. Galkin, A.A. Ivanov, S.Yu. Medvedev and Yu.Yu. Poshekhonov, *Comparison of tokamak axisymmetric mode growth rates from linear MHD and equilibrium evolution approaches*, Nuclear Fusion, Vol. 37, 1455, (1997).

[69] G.V. Pereverzev, P.N. Yushmanov, *ASTRA - Automated System for TRansport Analysis*, Max-Planck-Institut Fur Plasmaphysik, IPP-Report, IPP 5/98, February (2002).

[70] S. C. Jardin , N. Pomphrey and J. De Lucia, *Dynamic Modeling of Transport and Positional Control of Tokamaks*, Journal of Computational Physics, 66, 481-507, (1986).

[71] L.L. Lao, J.R. Ferron, R.J. Groebner, W. Howl, H. St. John, E.J. Strait and T.S. Taylor, *Equilibrium analysis of current profiles in tokamaks*, Nuclear Fusion, Vol. 30, 1035, (1990).

[72] F. Hofmann, G. Tonetti, *Tokamak equilibrium reconstruction using faraday-rotation measurements*, Nuclear Fusion, Vol. 28, 1871, (1988).

[73] F. Hofmann, *FBT - a free-boundary tokamak equilibrium code for highly elongated and shaped plasmas*, Computer Physics Communications, Volume 48, Issue 2, p. 207-221, (1988).

[74] R. Albanese, J. Blum, and O. De Barbieri, *Numerical studies of the NEXT European Torus via the PROTEUS Code*, Proceedings of the 12th Conference on the Numerical Simulation of Plasmas, San Francisco CA (USA), (1987).

[75] . R. Albanese and F. Villone *The linearized CREATE-L plasma response model for the control of current, position and shape in tokamaks*, Nuclear Fusion, Vol. 38, 723, (1998).

[76] P. Vyas, F. Villone, J.B. Lister, and R. Albanese. *The separatrix response of diverted TCV plasmas compared with the predictions of the CREATE-L model*, Nuclear Fusion, Vol. 38, no. 7, pp. 1043-1053, (1998).

[77] R. Khayrutdinov, *Studies of Plasma Equilibrium and Transport in a Tokamak Fusion Device with the Inverse-Variable Technique*, Journal of Computational Physics, vol. 109, pp. 193-201, (1993).

[78] A. Coutlis, I. Bandyopadhyay, J.B. Lister, P. Vyas, R. Albanese, D.J.N. Limebeer, F. Villone and J.P. Wainwright, *Measurement of the open loop plasma equilibrium response in TCV*, Nuclear Fusion, Vol. 39, 663, (1999).

[79] J. Santos, L. Guimarais, M. Zilker, W. Treutterer, M. Manso and the ASDEX Upgrade Team, *Reflectometry-based plasma position feedback control demonstration at ASDEX Upgrade*, Nuclear Fusion, Vol. 52, no. 3, March (2012).

[80] I.H. Hutchinson, *Principles of Plasma Diagnostics*, Second edition, Cambridge University Press, (2002).

[81] Alan Wootton, *Magnetic Fields and Magnetic Diagnostics for Tokamak Plasmas*, University of Texas, (2008).

[82] The JET ELM Coil Study Team, *JET ELM Control Coil Feasibility Study*, Report for the EFDA Steering Committee, (2010).

[83] W. Suttrop, et al., *In-vessel saddle coils for MHD control in ASDEX Upgrade*, Fusion Engineering and Design 84, 290-294, (2009).

[84] H.K. Kim, H.L. Yang, G.H. Kim, Jin-Yong Kim, Hogun Jhang, J.S. Bak, G.S. Lee, *Design features of the KSTAR in-vessel control coils*, Fusion Engineering and Design 84, 1029-1032, (2009).

[85] P. Titus, et al., *ELM and In-Vessel Coil Programs at PPPL for ITER, DIII-D, and JET*, Proceedings of the 23rd IAEA Fusion Energy Conference, Daejon, Republic of Korea, (10th October 2010 - 16th October 2010).

[86] G.A. Navratil, et al., *Active Control of MHD Modes in DIII-D*, American Physical Society Meeting, Philadelphia, (April 2003).

[87] J.-M. Moret, F. Buhlmann, D. Fasel, F. Hofmann and G. Tonetti, *Magnetic measurements on the TCV tokamak*, Review of Scientific Instruments, 69, 2333 (1998).

[88] Francesco Piras, *Extremely Shaped Plasmas to Improve the Tokamak Concept*, PhD thesis no.5015,École Polytechnique Fédérale de Lausanne (EPFL), Switzerland, March (2011).

[89] P.F. Isoz, J.B. Lister and Ph. Marmillod, *A hybrid matrix multiplier for control of the TCV tokamak*, Proc. 16Ih Symp. On Fusion Technology, pp. 1264-1267, London (3rd-7th September 1990).

[90] J.B. Lister, F. Hofmann, J.M. Moret, F. Buhlmann, M.J. Dutch, D. Fasel, A. Favre, P.F. Isoz, B. Marletaz, P. Marmillod, Y. Martin, A. Perez and D.J. Ward, *The Control of TCV Plasmas*, Fusion Technology, vol 31, number 7 (1997).

[91] James Kohout and Alan D. George, *A high-performance communication service for parallel computing on distributed DSP systems*, Parallel Computing 29, 851-878, (2003).

[92] Message Passing Interface Forum (www.mpi-forum.org), *MPI: A Message-Passing Interface Standard, Version 3.0*, University of Tennessee, Knoxville, Tennessee, (2012).

[93] Anthony Skjellum, Arkady Kanevsky, Yoginder S. Dandass, Jerrell Watts, Steve Paavola, Dennis Cottel, Greg Henley, L. Shane Hebert, Zhenqian Cui, Anna Rounbehler and The Real-Time Message Passing Interface (MPI/RT) Forum, *The Real-Time Message Passing Interface Standard*, Concurrency and Computation: Practice and Experience, 16 S1-S332, (2004).

[94] A.P. Rodriguesa, L. Pereira, J.-M. Moret, B.P. Duval, C.A.F. Varandas, *Real-time data transfer in the TCV advanced plasma control system*, Fusion Engineering and Design 81 (2006) 1939-1943.

[95] J. Sousa, A. Combo, A. Batista, C. Correia, C.A.F. Varandas, D. Trotman, J. Waterhouse, *The 32 bit timing unit of a real-time event-based control system for a nuclear fusion experiment*, IEEE Transactions on Nuclear Science, 45 (4)(1998) 2052.

[96] http://www.vmelinux.org/

[97] http://www.mdsplus.org

[98] http://www.ti.com

[99] J.-M. Moret, *A software package to manipulate space dependencies and geometry in magnetic confinement fusion*, Review of Scientific Instruments, 76, pp 073507 (2005).

[100] http://www.winehq.org/

[101] C. Hogben, S. Griph, *Interfacing to JET plant equipment using the HTTP protocol*, JDN/H(02)11, CODAS Documentation Centre, http://www.iop.org/Jet/article?EFDR02004, (2002).

[102] Y. R. Martin, S. Coda, B. P. Duval, X. Llobet, J-M. Moret, *A new plant control software for the TCV tokamak*, ICALEPCS 2005, Tenth International Conference on Accelerator and Large Experimental Physics Control Systems, Geneva, (October 2005).

[103] B.P. Duval, X. Llobet, P.F. Isoz, J.B. Lister, B. Marletaz, Ph. Marmillod, J.-M. Moret, *Evolution not revolution in the TCV tokamak control and acquisition system*, Fusion Engineering and Design 56-57 (2001) 1023-1028.

[104] Alan Oppenheim, *Discrete Time Signal Processing, Third Edition*, Pearson Higher Education, (2010).

[105] A.P. Rodrigues, N. Cruz, B. Santos, C.A.F. Varandas, J-M. Moret, J. Berrino, B. P. Duval, *TCV Advanced Plasma Control System Software Architecture and Results*, IEEE NPSS, 15th Real Time Conference (Fermilab, Batavia, Illinois, USA, April 29 - May 4, 2007)

[106] A.P. Rodrigues, N. Cruz, B. Santos, C.A.F. Varandas, J.-M. Moret, J. Berrino, B.P. Duval, *TCV advanced plasma control system software architecture and preliminary results*, IEEE Transactions On Nuclear Science, vol. 55, pages 316-321 (2008).

[107] N. Cruz, A.P. Rodrigues, B. Santos, C.A.F. Varandas, B.P. Duval, J.-M. Moret, J. Berrino, Y. Martin, X. Llobet, *The integration of the new advanced digital plasma control system in TCV*, Fusion Engineering and Design 83, 215-219, (2008).

[108] J.I. Paley, J. Berrino, S. Coda, N. Cruz, B.P. Duval,F. Felici, T.P. Goodman, Y. Martin, J.M. Moret, F. Piras, A.P. Rodriques, B. Santos, C.A.F. Varandas and the TCV Team, *Real time control of plasmas and ECRH systems on TCV*, Nuclear Fusion, Vol 49, Issue 8, (2009).

[109] G. Ambrosino and R. Albanese, *Magnetic control of plasma current, position, and shape in tokamaks - A survey of modeling and control approaches*, IEEE Control Systems Magazine, vol.25, no.5, pp. 76- 92, Oct. 2005.

[110] F. Hofmann , M.J. Dutch , A. Favre , Y. Martin , J.-M. Moret and D.J. Ward, *Feedback stabilization of axisymmetric modes in the TCV tokamak using active coils inside and outside the vacuum vessel*, Nuclear Fusion, Vol. 38, 399, (1998).

[111] SIMULINK version 7.9 (R2012a), Natick, Massachusetts: The MathWorks Inc., 2012.

[112] F. Hofmann, I. Furno, S. Gerasimov, Y. Martin, F. Milani, M.F.F. Nave, H. Reimerdes, F. Sartori, O. Sauter, *Effect of ELMs on the measurement of vertical plasma position in TCV and JET*, Nuclear Fusion, Vol. 42, 59-65, (2002).

[113] J.-M. Moret, B.P. Duval, H.B. Le, S. Coda, F. Felici, H. Reimerdes, *Tokamak equilibrium reconstruction code LIUQE and its real time implementation*, accepted for publication in Fusion Engineering and Design, July 28th, 2014.

[114] B. Kristiansson, B. Lennartson, *Robust tuning of PI and PID controllers: using derivative action despite sensor noise*, Control Systems, IEEE, Vol. 26 Issue:1, 55-69, (2006).

[115] N. Cruz, J.-M. Moret, S. Coda, J. I. Paley, B.P. Duval, A. P. Rodrigues, F. Piras, F. Felici, C. M. B. A. Correia, C. A. F. Varandas, *Using APCS for Plasma Vertical Control at TCV*, IEEE Transactions on Nuclear Science, 58 Issue 4, 1570-1575, 2011.

[116] A. Favre, J-M. Moret, R. Chavan, A. Elkjaer, D. Fasel, F. Hofmann, J.B. Lister, J-M. Mayor, A. Perez, *Control of Highly Vertically Unstable Plasmas in TCV with*

Internal Coils and Fast Power Supply, 19th Symposium on Fusion Technology, SOFT, September 16-20, Lisbon, Portugal, (1996).

[117] E.A. Lazarus, J.B. Lister, G.H. Neilson, *Control of the vertical instability in Tokamaks*, Nuclear Fusion, Vol. 30, 111, (1990).

[118] J.B. Lister, et al., *Experimental study of the vertical stability of high decay index plasmas in the DIII-D Tokamak*, Nuclear Fusion, Vol. 30, 2349, (1990).

[119] J.B. Lister, Y. Martin, J-M. Moret, *On locating the poloidal field coils for tokamak vertical position control*, Nuclear Fusion, Vol. 36, 1547, (1996).

[120] F. Hofmann, et al., *Vertical instability in TCV: comparison of experimental and theoretical growth rates*, Nuclear Fusion, Vol. 37, 681, (1997).

[121] J.B. Lister, A. Sharma, D.J.N. Limebeer, Y. Nakamura, J.P. Wainwright and R. Yoshino, *Plasma equilibrium response modelling and validation on JT-60U*, Nuclear Fusion, Vol. 42, 708-724, (2002).

[122] MATLAB version 7.14 (R2012a), Natick, Massachusetts: The MathWorks Inc., 2012.

[123] A. Portone, *Design of the ITER-FEAT plasma control system by a frequency separation approach*, Fusion Engineering and Design, 56-57, 789-794, (2001).

[124] A.J. Laub, M.T. Heath, C.C. Paige and R.C. Ward, *Computation of System Balancing Transformations and Other Applications of Simultaneous Diagonalization Algorithms*, IEEE Trans. Automatic Control, vol. 32, pp. 115-122, (1987).

[125] I. Vakilzadeh, *Bang-bang control of a plant with one positive and one negative real pole* J. Optim. Theory Appl. 24, 2, 315-324, (1978).

[126] I. Vakilzadeh, A. A. Keshavarz, *Bang-bang control of a second-order non-linear stable plant with second-order nonlinearity*, Kybernetika- Volume 18, Number 1, (1982).

[127] Z. Shen and S.B. Andersson, *Minimum Time Control of A Second-Order System* 49th IEEE Conference on Decision and Control, Hilton Atlanta Hotel, Atlanta, GA, USA, December 15-17, (2010).

[128] N. Cruz, J.-M. Moret, S. Coda, B.P. Duval, H.B. Le, A.P. Rodrigues, C.A.F. Varandas, C.M.B.A. Correia and B. Gonçalves, *An optimal real-time controller for vertical plasma stabilization*, submitted to IEEE Transactions on Nuclear Science for publication.

[129] N. Cruz, J.-M. Moret, S. Coda, B.P. Duval, H.B. Le, A.P. Rodrigues, C.A.F. Varandas, C.M.B.A. Correia and B. Gonçalves, *An optimal real-time controller for vertical plasma stabilization*, Proceedings of the 19th IEEE Real-Time Conference, May 26th to 30th 2014, Nara, Japan.

[130] S. Coda for the TCV team, *The Science Program of the TCV Tokamak: Exploring Fusion Reactor and Power Plant Concepts*, 25th IAEA FEC - Fusion Energy Conference in St-Petersburg, Russia, October 2014.

[131] P.F. Carvalho, B. Santos, M. Correia, A.M. Combo, A.P. Rodrigues, R.C. Pereira, A. Fernandes, N. Cruz, J. Sousa, B.B. Carvalho, A.J.N. Batista, C.M.B.A. Correia, B. Gonçalves, *PCI Express Hotplug Implementation for ATCA based Instrumentation*, 28th Symposium on Fusion Technology, San Sebastian, Spain, October 2014.

[132] P.F. Carvalho, B. Santos, M. Correia, A.M. Combo, A.P. Rodrigues, R.C. Pereira, A. Fernandes, N. Cruz, J. Sousa, B.B. Carvalho, A.J.N. Batista, C.M.B.A. Correia, B. Gonçalves, *PCI Express Hotplug Implementation for ATCA based Instrumentation*, submitted to Fusion Engineering and Design.

[133] B. Santos, P.F. Carvalho, A.P. Rodrigues, B.B. Carvalho, J. Sousaa, A.J.N. Batista, M. Correia, A.M. Combo, N. Cruz, C.M.B. A. Correia, B. Gonçalves, *ATCA Shelf Manager EPICS Device Support for ITER CODAC Core System*, 28th Symposium on Fusion Technology, San Sebastian, Spain, October 2014.

[134] B. Santos, P.F. Carvalho, A.P. Rodrigues, B.B. Carvalho, J. Sousaa, A.J.N. Batista, M. Correia, A.M. Combo, N. Cruz, C.M.B. A. Correia, B. Gonçalves, *ATCA Shelf Manager EPICS Device Support for ITER CODAC Core System*, submitted to Fusion Engineering and Design.

[135] S. Hacquin, L. Meneses, L. Cupido, N. Cruz, L. Kokonchev, R. Prentice, C. Gowers, *Upgrade of the X-mode reflectometry diagnostic for radial correlation measurements in the Joint European Torus*, Review of Scientific Instruments, 75, (10), 3834, 2004.

[136] G. Ericsson, S. Conroy, G. Gorini, H. Henriksson, A. Hjalmarsson, J. Kallne, M. Tardocchi, *Proposed Magnetic Proton Recoil Neutron Spectrometer Upgrade (MPRU)*, in Advanced Diagnostics for Magnetic and Inertial Fusion, pp 121-124, Springer US, (2002).

[137] H. Sjostrand, L. Giacomelli, E. Andersson Sunden, S. Conroy, G. Ericsson, M. Gatu Johnson, C. Hellesen, A. Hjalmarsson, J. Kallne, E. Ronchi, M. Weiszflog, G. Wikstrom, G. Gorini, M. Tardocchi, A. Murari, G. Kaveney, S. Popovichev, J. Sousa, R. C. Pereira, A. Combo, N. Cruz and JET-EFDA Contributors, *New MPRu instrument for neutron emission spectroscopy at JET*, Review of Scientific Instruments 77 (10): 10E717 (2006).

[138] M. Gatu Johnson, L. Giacomelli, A. Hjalmarsson, J. Kallne, M. Weiszflog, E. Andersson Sunden, S. Conroy, G. Ericsson, C. Hellesen, E. Ronchi, H. Sjostrand, G. Gorini, M. Tardocchi, A. Combo, N. Cruz, J. Sousa, S. Popovichev, JET-EFDA contributors, *The 2.5-MeV neutron time-of-flight spectrometer TOFOR for experiments at JET*, Nuclear Instruments and Methods in Physics Research A, 591 (2): 417-430, June 21st 2008.

[139] N. Cruz, A. J. N. Batista, D. Alves, J. Sousa,C. A. F. Varandas, E. Joffrin, R. Felton, J. W. Farthing and JET-EFDA Contributors, *JET Real Time Project Test-Bench Software Structure*, Fusion Engineering and Design, 81, Issues 15-17, Pages 1933-1937, July 2006.